Programa de Doctorado en Ciencias Biomédicas y Salud

Escuela de Doctorado de la Universitat Jaume I

Evaluation of bioactive coatings for titanium surfaces: a proteomic approach

Memoria presentada por Andreia Filipa Lages Cerqueira para optar al grado de doctor/a por la Universitat Jaume I

Author

Andreia Filipa Lages Cerqueira

Firmado por ANDREIA FILIPA LAGES CERQUEIRA - NIF:Y6447463W el día 22/02/2022 con un certificado emitido por ACCVCA-120

Directed by

Julio José Suay Antón

SUAY ANTON JULIO JOSE - 22698197A

Firmado digitalmente por SUAY ANTON JULIO JOSE - 22698197A
Fecha: 2022.02.21 23:00:28 +01'00'

José Javier Martín de Llano

JOSE JAVIER|MARTIN|DE LLANO

Firmado digitalmente por JOSE JAVIER|MARTIN|DE LLANO
Nombre de reconocimiento (DN): cn=JOSE JAVIER|MARTIN|DE LLANO, serialNumber=50698273V, givenName=JOSE JAVIER, sn=MARTIN DE LLANO, ou=CIUDADANOS, o=ACCV, c=ES
Fecha: 2022.02.16 18:06:48 +01'00'

Castellón de la Plana, February 2022

FUNDING

Generalitat Valenciana funded this doctoral thesis through the Santiago Grisolía program (GRISOLIAP/2018/091) and a financial help for an international research stay (BEFPI/2021/043). The Ministry of Economy and Competitiveness (MINECO) (MAT2017-86043-R; RTC-2017-6147-1) and Generalitat Valenciana (PROMETEO/2020/069) financed the projects that allowed the experimental work to be carried out. The Helmholtz-Zentrum Hereon (Geesthacht, Germany) financed the experimental work carried out during the research stay.

THESIS BY COMPENDIUM OF PUBLICATIONS

This thesis is a compendium of the following publications:

- **Cerqueira, A.**, Romero-Gavilán, F., Araújo-Gomes, N., García-Arnáez, I., Martinez-Ramos, C., Ozturan, S., Azkargorta, M., Elortza, F., Gurruchaga, M., Suay, J., Goñi, I. (2020). A possible use of melatonin in the dental field: Protein adsorption and in vitro cell response on coated titanium. Materials Science and Engineering: C - Materials for Biological Applications, 116, 111262. https://doi.org/10.1016/j.msec.2020.111262. Impact factor: 7.328 (Q1).

- **Cerqueira, A.**, Romero-Gavilán, F., García-Arnáez, I., Martinez-Ramos, C., Ozturan, S., Iloro, I., Azkargorta, M., Elortza, F., Izquierdo, R., Gurruchaga, M., Goñi, I., Suay, J. (2021). Bioactive zinc-doped sol-gel coating modulates protein adsorption patterns and in vitro cell responses. Materials Science and Engineering: C - Materials for Biological Applications, 121, 111839. https://doi.org/10.1016/j.msec.2020.111839. Impact factor: 7.328 (Q1).

- **Cerqueira, A.**, Romero-Gavilán, F., García-Arnáez, I., Martinez-Ramos, C., Ozturan, S., Izquierdo, R., Azkargorta, M., Elortza, F., Gurruchaga, M., Suay, J., Goñi, I. (2021). Characterization of magnesium doped sol-gel biomaterial for bone tissue regeneration: The effect of Mg ion in protein adsorption. Materials Science and Engineering: C - Materials for Biological Applications, 125, 112114. https://doi.org/10.1016/j.msec.2021.112114. Impact factor: 7.328 (Q1).

This thesis has been accepted by the co-authors of the publications listed above that have waved the right to present them as a part of another PhD thesis.

"Faz essa viagem, meu bem

Tudo o que se perde ganha asas

Anjos que caminham lado a lado

Vozes que nos guiam as palavras"

Viagem de Tiago Bettencourt

Ao pai Tunes

ACKNOWLEDGMENTS

À minha família, o maior de todos os agradecimentos. Vocês são a minha base e o meu motivo. Obrigada pelo amor, pelo carinho, pelo apoio. Por não me deixarem desistir, nunca. Ao meu pai, a minha estrela mais brilhante, espero que estejas orgulhoso.

A mi director de tesis, Julio Suay, por la oportunidad de llevar a cabo esta tesis doctoral, así como la confianza mostrada al largo de estos 3 años. A Javier Martín de Llano por las correcciones de la tesis.

A Fran, muchas gracias por tu apoyo y por todo lo que me has enseñado. Por la paciencia, por la amistad y por mostrarme el camino cuando me sentía perdida. Ao Nuno, por tudo o que me ensinaste, que se revelou essencial para todo o trabalho que faço até hoje, pelo apoio que me deste na minha chegada a Espanha e pela amizade. Sin vosotros esto no sería posible.

Muchas gracias a todas las personas que me acogieron en España. Al grupo de investigación PIMA, Pepe, Raquel, Luís, José, Jorge, Lourdes, Braulio, Raúl y Maria José por vuestra simpatía desde del primer día. A Estefanía, por la amistad y los cafés. A Patricia, José, Anna y Kerly por los planes de finde, por ensañarme las maravillas de la gastronomía española y por las noches de juegos.

A Maria Muriach y Pablo Baliño del departamento de Medicina de la Universitat Jaume I por dejarme *invadir* vuestro laboratorio y hacer el trabajo experimental de esta tesis. A Ricard por mostrarse siempre disponible para ayudarme.

A Isabel Goñi y Mariló Gurruchaga de la Universidad del País Vasco por vuestra ayuda en la redacción de los artículos y proyectos que tornaran esta tesis posible. A Felix y Mikel del CICbioGUNE por todo el apoyo en la realización de la proteómica aquí presentada.

Thank you to Regine Willumeit-Römer and Berengere Luthringer for accepting me at the Institut für Metallische Biomaterialien for my short research stay. To Heike Helmholz for your supervision during this period. To Anke for everything you have taught me and all colleagues at the Biological Characterization lab for your kindness and sympathy.

À Bárbara, Cláudia, Filipa, Gracinha, Natacha e Vanessa, as melhores amigas que tive a sorte de conhecer. Obrigada pelo apoio, por ouvirem os meus desabafos, por estarem sempre lá, não importa o dia e a hora, por serem a família que a vida me deu. Obrigada ao Alexandre, Helder, Micael e Rita pela amizade e carinho.

ABSTRACT

At present, biologically protheses represent the current gold-standard treatments for clinical treatment of bone defects. Titanium and its alloys are among the most used metals in bone implants due to their excellent bulk properties; however, they are relatively bioinert. Surface modifications are useful to improve its bioactivity via the delivery of tissue regeneration enhancer components, such as biomolecules and ions. The sol-gel process is one of many techniques that allow this modification and design control release vehicles for bioactive compounds that can potentiate tissue regeneration. Moreover, the ever-increasing demand for better biomaterials has led to the need to improve current *in vitro* test methods to be more predictive and representative of the *in vivo* outcomes. With this purpose, the application of proteomics presents an interesting alternative to be explored. On the one hand, upon implementation, a layer of proteins immediately adheres to the material surface, consequently modulating the following biological responses. On the other hand, the characterization of the proteomic profile of cells in contact with a material can give us an insight into the cellular responses to a biomaterial. Thus, this thesis aimed to develop sol-gel coatings doped with melatonin, zinc, magnesium, and calcium-magnesium mixtures and its *in vitro* characterization with osteoblasts and macrophages. Then, two experimental designs employing proteomics were performed. First, the serum protein adsorption patterns onto the material surface were analyzed. Secondly, the proteomic profile of osteoblasts in contact with the material with the best *in vitro* response was also analyzed. The results showed that materials specific properties conditioned the proteomic profile found. For example, materials with more osteogenic potential had a greater affinity with VTNC. At the same time, the inflammatory response was associated with a higher affinity with regulators of inflammation (CLUS, IC1, CFAH, and VTNC), and an increment in cell adhesion was associated with higher affinity with DSG1, FILA2, and DESP. The analysis of the proteomic profile of cells showed that the sol-gel coatings regulated early osteoblast differentiation, insulin metabolism, cell adhesion, and oxidative stress. These results show that the effects of the material on the cells are rather complex, affecting the whole cellular machinery. Thus, the application of proteomics allowed the identification of specific markers associated with distinct biological processes such as adhesion, inflammation, coagulation, and regeneration. From the identification of the proteins adhered to the material surface and the study of the proteomic profiles of the cells exposed to it, it was possible to establish a direct relationship with the *in vitro* results. This opens a door to the determination of biomarkers involved in the tissue regeneration processes and possible correlation with *in vivo* results.

RESUMEN

Actualmente se utilizan prótesis (mayormente de titanio) como tratamiento estándar ante problemas clínicos donde haya implicados defectos en la estructura ósea. El titanio y sus aleaciones se encuentran entre los metales más utilizados en implantes óseos debido a sus excelentes propiedades mecánicas y de biocompatibilidad, a pesar de que son relativamente bioinertes. Se necesitan modificaciones de la superficie para mejorar su bioactividad a partir de la incorporación de moléculas e iones potenciadores de la regeneración de tejidos. El proceso sol-gel es una de las muchas técnicas que permiten esta modificación de la superficie al poder desarrollar recubrimientos bioactivos gracias a la liberación controlada de los compuestos bioactivos que pueden potenciar la regeneración tisular. Además, la demanda creciente biomateriales con mejores prestaciones ha traído consigo la necesidad de desarrollar nuevas técnicas de evaluación *in vitro* para que sean más predictivos y representativos de los resultados *in vivo*. Con este propósito, la aplicación de la proteómica representa una interesante alternativa que puede ser explorada. Tras la implantación de una prótesis, una capa de proteínas se adhiere inmediatamente a la superficie del material, modulando las siguientes respuestas biológicas. La caracterización del perfil proteómico de las células en contacto con la superficie de los materiales puede darnos una idea de la respuesta celular a estos. Así, esta tesis tuvo como objetivo desarrollar recubrimientos sol-gel dopados con melatonina, zinc, magnesio y mezclas de calcio-magnesio; su caracterización *in vitro* con osteoblastos y macrófagos; así como ensayos de proteómica con dos tipos de desarrollo experimental. En primer lugar, se analizaron los patrones de adsorción de proteínas séricas sobre la superficie de los materiales. Por otro lado, se analizó el perfil proteómico de los osteoblastos expuestos al material con mejor respuesta *in vitro*. Los resultados mostraron que las propiedades específicas de los materiales condicionaron el perfil proteómico encontrado. Los resultados mostraron que los materiales con un potencial osteogénico más significativo tenían una mayor afinidad por VTNC. Al mismo tiempo, la regulación de las respuestas inflamatorias se asoció con una mayor adsorción de proteínas reguladoras de las respuestas inflamatorias (CLUS, IC1, CFAH y VTNC) y un incremento en la adhesión celular se asoció con una mayor afinidad con DSG1, FILA2 y DESP. El análisis del perfil proteómico de las células mostró que los recubrimientos sol-gel regularon la diferenciación temprana de los osteoblastos, el metabolismo de la insulina, la adhesión celular y el estrés oxidativo. Estos resultados muestran que los efectos del material sobre la célula son bastante complejos y afectan a toda la maquinaria celular. Así pues, la aplicación del análisis proteómico permitió la identificación de marcadores específicos asociados a distintos procesos biológicos

como la adhesión, inflamación, coagulación y regeneración. A partir de la caracterización de proteínas adsorbidas en la superficie del material o estudiando los perfiles proteómicos de las células expuestas al material esta tesis establece una relación directa con los resultados obtenidos mediante cultivos celulares y abre una puerta para la posible correlación con los resultados de experimentación *in vivo* al establecer biomarcadores de cada uno de los procesos biológicos involucrados en el proceso de regeneración.

GRAPHICAL ABSTRACT

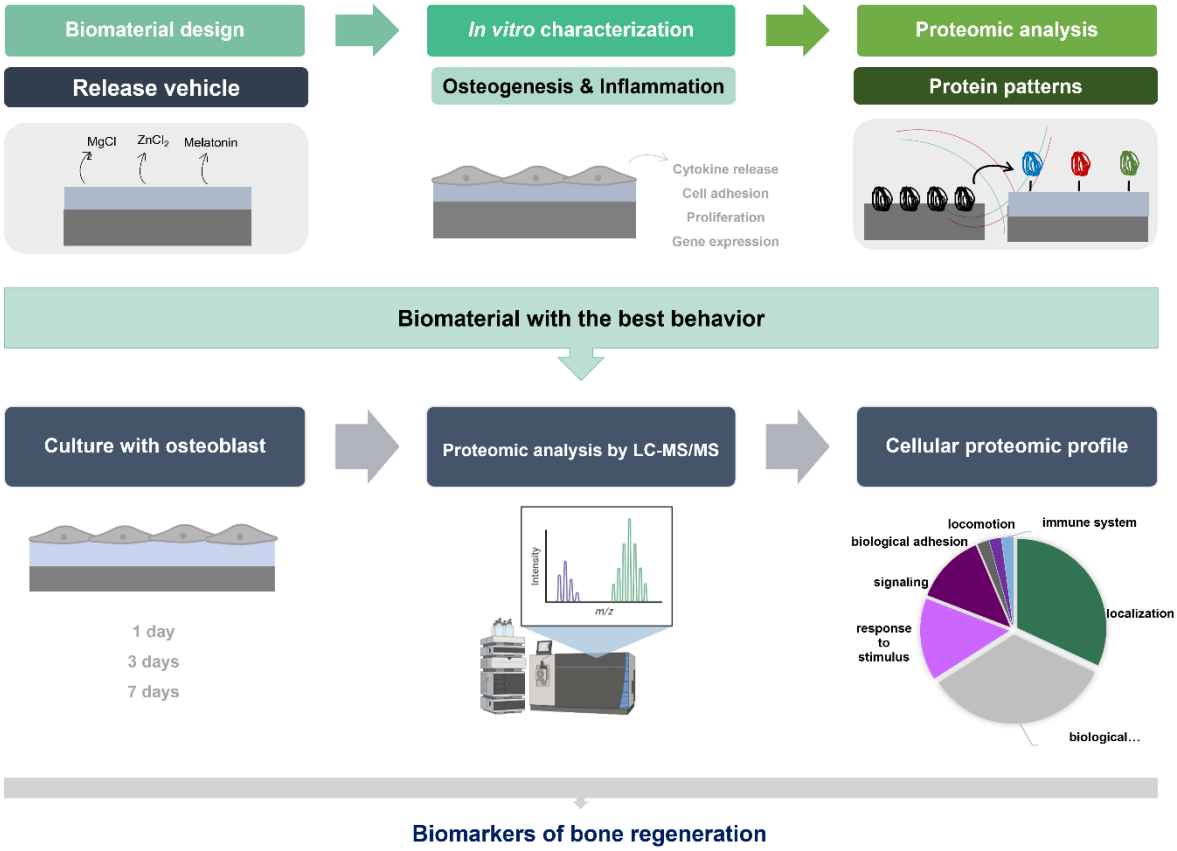

INDEX

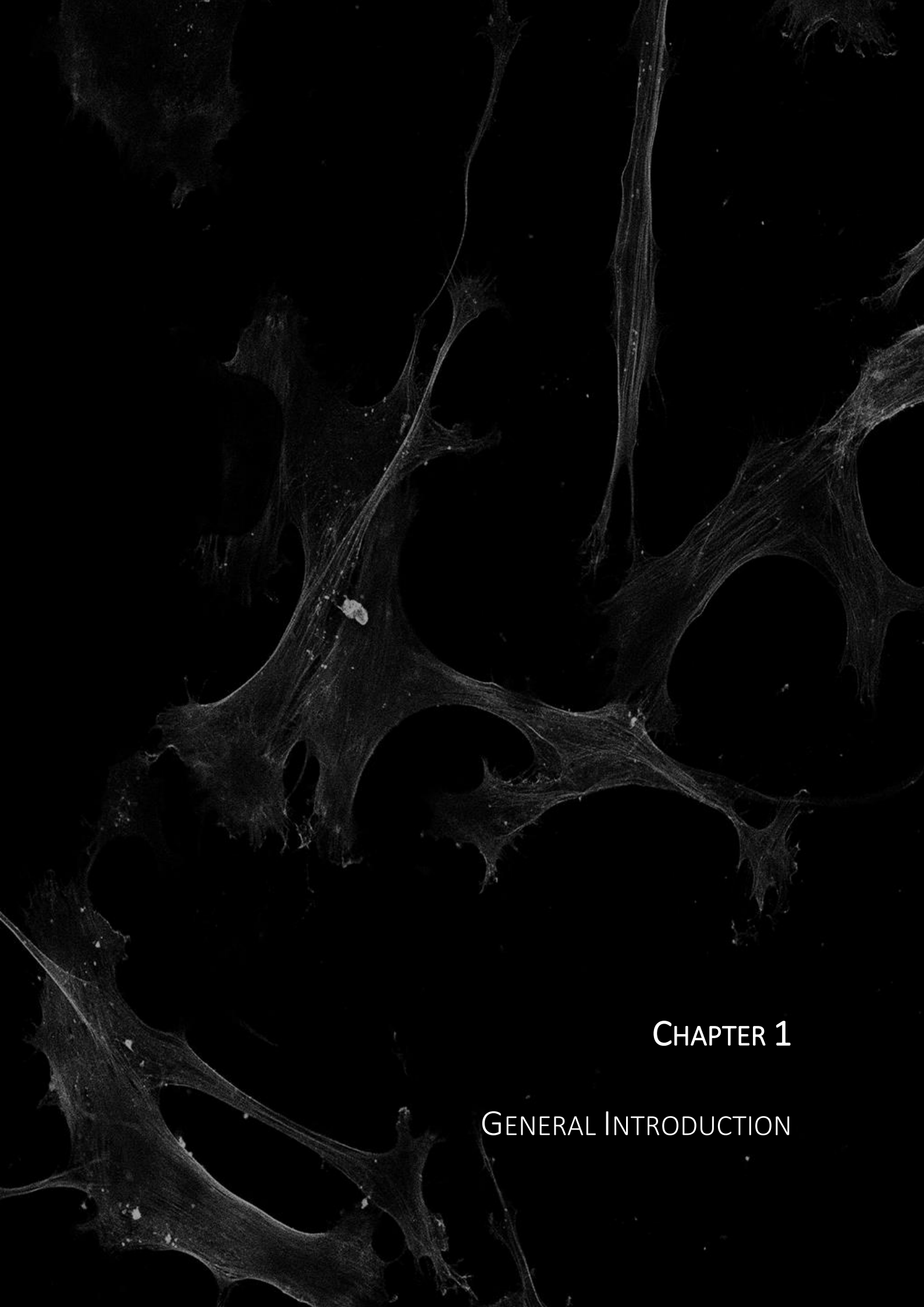

Chapter 1

General Introduction

CHAPTER 1

GENERAL INTRODUCTION

1.1. THEORETICAL FRAMEWORK

1.1.1. BONE STRUCTURE AND PHYSIOLOGY

Bone is a specialized connective tissue featuring organic proteins, inorganic minerals, and more than 30 different cell types [1]. Bone presents vital functions such as locomotion, support and protection of internal organs and structures, blood production, mineral storage and homeostasis, growth factors and cytokines reservoir, and harboring progenitor cells (mesenchymal, hemopoietic) and bone marrow [2,3].

Bone is a complex organ comprising mineralized osseous tissue, marrow, endosteum and periosteum, nerves, blood vessels, and cartilage [3]. It is organized into cancellous and cortical bone. Cancellous bone (also known as trabecular or spongy bone) is porous, consists of plates (trabeculae), and supports the bone marrow [1]. On the other hand, cortical bone is compact, surrounds the marrow space, confers mechanical strength, and accounts for 80% the total mass [1,3].

Natural bone is a mineralized composite arranged into organic and inorganic phases. In the organic matrix, type I collagen is the most abundant component (about 90%), being organized into microfibrils. Another constituent of said matrix is fibronectin, which plays an important role in collagen aggregation. Additionally, non-collagenous proteins (*e.g.*, osteopontin, osteocalcin, osteonectin) account for 10% of the extracellular matrix (ECM) and are extremely important in mineralization, cell signaling, and tissue metabolism. The inorganic matrix or mineral phase is mainly composed of hydroxyapatite ($Ca_{10}(PO_4)_6(OH)_2$), which has a central role in bone stiffness and stress-bearing capacity [4].

1.1.2. BONE REMODELING

Bone is a highly dynamic tissue undergoing constant remodeling through a lifetime [3]. About 10% of the total bone content of an adult is replaced per year [5] in a process known as bone remodeling (**Figure 1.1**). This process is dependent on the dynamic balance between bone formation and resorption and is carried out by temporary clusters of osteoblasts and osteoclasts named basic multicellular unit (BMU) [6,7]. Bone formation is performed by osteoprogenitor cells differentiated into osteoblasts that produce the organic bone matrix and regulate mineralization through the expression of proteins such as osteocalcin (BGLAP) and alkaline phosphatase (ALP) [3,8]. Bone resorption is coordinated by osteoclasts derived from myeloid cells that are uniquely adapted to degrade bone minerals and the ECM proteins [8,9]. During bone formation, a subpopulation of osteoblasts undergoes terminal differentiation to osteocytes and is buried into the osteoid (the unmineralized, organic portion of the bone matrix). These cells can control bone mechano-physiology as well as resorbing and deposing bone [6,9].

The cycle of bone remodeling consists of 4 phases: latent, resorption, reversal, and formation [6]. The first stage of bone remodeling involves the detection of a signal that triggers the beginning of the process. The signal can be a structural damage or hormone (*e.g.*, estrogen) action on bone cells [9]. It will be sensed by osteocytes that translate it into biological signs to initiate bone remodeling. Then, the resorption phase begins with the differentiation of preosteoclasts to multinucleated osteoclasts, which will degrade the bone and prepare the surface for osteoblasts to form new bone. The formation phase follows with macrophage-like cells cleaning osteoclasts' debris and providing osteoblast differentiation and migration signals. Finally, osteoblasts lay down new bone in the formation phase until it completely replaces the resorbed bone; this is the most prolonged phase lasting up to 6 months. When it is complete, the surface is covered by bone lining cells and a prolonged resting period begins until a new remodeling cycle is initiated [7].

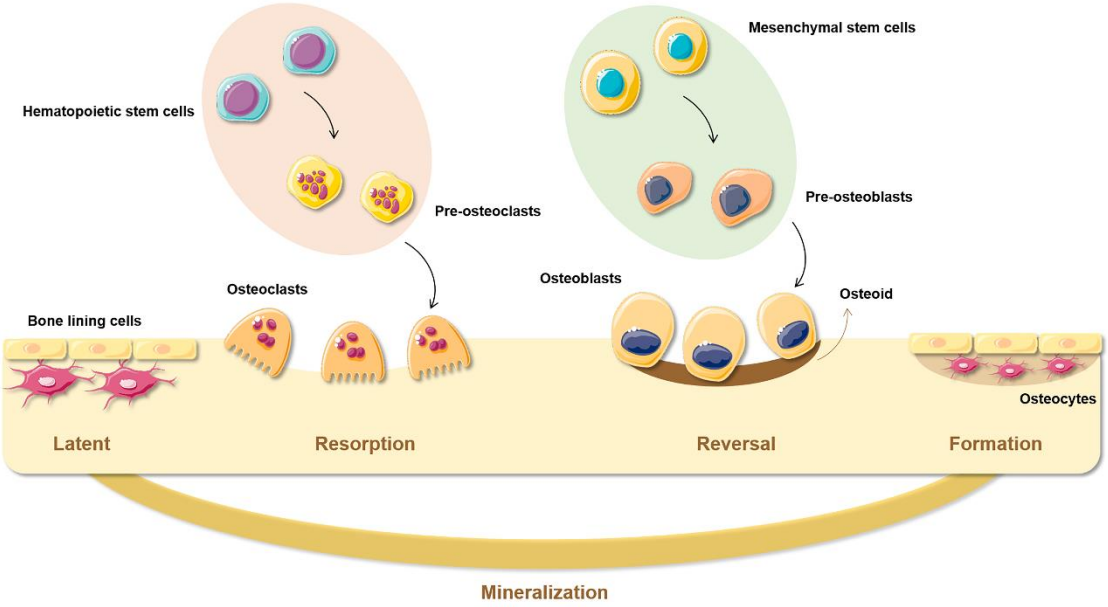

Figure 1.1. Bone remodeling.

1.1.3. BONE REGENERATION UPON BIOMATERIAL IMPLANTATION

Brånemark first described bone-implant osseointegration in 1962 as a direct structural and functional connection between bone and a metallic substrate [10]. The implantation process results in injury to the bone by disturbing its homeostasis, leading to the activation of wound healing cascades [11]. Tissue regeneration around a biomaterial is carried out in a similar way to fracture healing. It is a complex mechanism that involves a cross-talk between several cell types and soluble factors, and it can be broadly classified into three phases: inflammation, proliferation, and remodeling [12].

Upon surgical implantation, the first event to occur is blood protein adsorption onto the biomaterial. This protein-modified surface is what other host components (*e.g.*, cells) will encounter and use as adhesion substrate. Then, platelets and the mechanisms of hemostasis lead to fibrin polymerization and blood clot formation, which serves as a base for neoangiogenesis, ECM deposition, and bone-forming cells [10]. The inflammatory phase is initiated immediately after recruitment and activation of inflammatory cells (*e.g.*, macrophages) upon detection of damage-associated molecular patterns (DAMPs), pro-inflammatory cytokines, and chemokines from the damaged cells [12]. This step is critical in bone regeneration since immune cell depletion can impact fracture healing efficacy and kinetics [12]. Then, a range of bone morphogenic proteins (BMPs), fibroblast growth factors (FGF), platelet-derived growth factors (PDGF), and insulin-like growth factors (IGF) are released by immune cells, promoting the recruitment and differentiation of osteoprogenitor and mesenchymal cells [13]. The increased

levels of interleukin (IL)-1β, IL-6, IL-8, interferon (IFN)-ϒ, and chemokine monocyte chemoattractant protein (MCP-1), macrophage inflammatory protein (MIP)-1α, MIP-1β, RANTES, and vascular endothelial growth factor (VEGF) are also characteristic from this phase [13]. With this, immune cells can regulate the early phases of wound healing and vascularization by promoting the recruitment and differentiation of endothelial cells, fibroblasts, and osteoblasts [12]. The proliferative phase starts with the resorption of necrotic bone resorption by osteoclasts and the formation of ECM and new blood vessels. At the same time, the fibrinolytic system degrades the fibrin clot, which allows tissue remodeling. Connective tissue and fibroblast-derived soft callus are formed, and the new blood vessels deliver the necessary nutrients to form new (woven) bone [13]. The remodeling is the last phase of this process. The callus either mineralizes and forms bone or exuberant fibrotic tissue and scarring if the remodeling is too prolonged [14].

1.1.3.1. *Growth factors in bone regeneration: a brief overview*

Bone regeneration is a well-orchestrated process with various growth factors (GF) controlling the cell migration, proliferation, and differentiation in a spatiotemporal manner [15]. The binding of GFs to tyrosine kinase leads to the initiation of a signaling cascade that will trigger the genetic apparatus and induce different cell responses [16]. As of now, BMP, PDGF, IGF, FGF, and VEGF are the most broadly described GF in the field of bone regeneration. Belonging to the transforming growth factor (TGF)-β superfamily, BMPs were first described in 1965 by Marshal Urist. Osteoblasts and chondrocytes primarily secrete these proteins. They are essential for fracture healing and bone/cartilage formation by interacting with serine/threonine kinase receptors and kicking off the BMP/TGF-β pathway. More than 20 BMPs are known, of which BMP-2, BMP-4, and BMP-7 are the most investigated due to their notable osteogenic activity [17,18].

Angiogenesis and vascular organization are essential in bone regeneration by providing a vascular network able to supply nutrients and oxygen [15]. These processes are regulated by PDGFs, IGFs, FGFs, and VEGF. Stored in the alpha granules of platelets, PDGFs regulate numerous cell functions via mitogenic, angiogenic, and proliferative activities [19]. Their effects are observed by incrementing mesenchymal stem cells (MSC) number and consequent differentiation into osteoblasts. In addition, they play a role in the chemotaxis and activation of macrophages, which are essential for the wound site cleaning and serve as a source of second phase growth factors that will stimulate the following bone repair and regeneration [20]. The IGF family has an essential role in the proliferation and differentiation of osteoblastic cells. IGF-1 and IGF-2 are both expressed in osteoblasts and are local regulators of bone matrix composition and remodeling by

mediating the actions of hormones, growth factors, cytokines, and morphogenes [21]. Among the multiple roles of IGFs are the induction of collagen synthesis and inhibition of its degradation, cell proliferation, differentiation stimulation, and bone matrix deposition [17]. Also involved in osteogenesis, the FGF signaling presents roles in angiogenesis and wound healing [17]. FGFs exhibit strong mitogen activity and roles in endocrine, regulatory and morphological signaling in response to injury [16]. FGFs control the proliferation of osteoblasts and fibroblasts, the maturation of chondrocytes and osteoblasts, and enhance the expression of the osteogenic markers BMP-2, TGF-β, and runt-related transcription factor 2 (RUNX2) [16,17]. VEGFs are signal peptides essential for the recruitment, survival, and activity of endothelial cells, osteoblasts, and osteoclasts, playing a critical role in inducing vascular genesis. In addition, VEGFs are vital in regulating inflammation and endochondral ossification during tissue repair [22] and often act combined with BMPs.

1.1.3.2. *Signaling pathways in bone regeneration*

Numerous key signaling pathways are involved in bone development and fracture healing, including Wnt/β-catenin, Notch, mitogen-activated protein kinase (MAPK), and phosphoinositide 3-kinase/protein kinase b (PI3K/Akt)/mTOR. The Wnt family comprises many conserved genes implicated in cellular processes that determine cell proliferation, adhesion, differentiation, and growth [23]. Commonly referred to as the canonical Wnt pathway, the Wnt/β-catenin pathway is involved in the promotion of osteoblastogenesis and osteoblast function. During bone regeneration, this pathway is induced and has a critical role in promoting osteogenic differentiation of MSCs, osteoblast proliferation, and maturation [24]. The Notch signaling is also involved in bone regeneration, directly affecting the BMP/Smad and TGF-β/MAPK pathways and suppressing bone resorption by acting on osteocytes and osteoclasts differentiation [17,24,25].

Moreover, MAPK pathways are pivotal in bone formation since they link the cell surface and nucleus and regulate all molecular pathways involved [17]. Specifically, extracellular signal-regulated kinase (ERK) and p38 have been implicated in said processes. They have been shown to control cell proliferation, differentiation, senescence, and apoptosis. ERK and p38 can regulate TGF-β, BMP-2, RUNX2, Wnt/ β-catenin expression, and their interaction with growth factors and adhesion molecules (*e.g.*, integrins) are obligatory for bone healing post-facture [26,27]. PI3K/Akt/mTOR is an important signaling pathway activated by extracellular stimuli and with roles in cell growth, survival, proliferation, and cell cycle progression. Several studies have shown the involvement of PI3K/Akt/mTOR on osteogenesis via Akt and mTOR phosphorylation

[28,29]. In addition, other signaling pathways (*e.g.*, FGF and IGF) can promote the expression of several osteogenic markers via PI3K/Akt.

1.1.4. BIOMATERIALS FOR BONE REGENERATION

Currently, biologically inert metallic devices represent the current gold-standard treatments for bone defects [1]. The most commonly used metals in bone implants are stainless steel, cobalt-chromium alloys, and titanium (Ti) and its alloys [30]. All of them present advantages such as high tensile strength and fatigue resistance compared to ceramics and polymers [30]. However, the application of these materials for long-term use is still hampered by some physical limitations, such as low fatigue strength, high Young's modulus/elasticity, low wear and corrosion resistance or lack of biocompatibility. With this, researchers worldwide are working to develop materials for long-life implantation in the human body [31].

1.1.4.1. *Metallic materials: titanium and alloys*

Since 1970, Ti and its alloys have been used extensively in hard tissue replacements and dental implants. These metals present excellent bulk properties, such as high mechanical strength, corrosion resistance, low density, and generally high biocompatibility [32], excellent for biomedical applications. Commercially available pure Ti comes in four grades (I-IV) [30], and the standard procedure for manufacturing Ti materials usually forms an oxidized layer on the material surface. On the one hand, said layer protects against the corrosion that naturally occurs *in vivo*; on the other hand, it will inevitably influence how the biological response to the material is carried out. Over the years, it has become more evident that such surfaces are unsuitable for biomedical applications, and surface treatments must be performed [32,33].

Titanium surface modifications techniques can be broadly classified as mechanical, physical, and chemical methods [33]. The mechanical methods encompass machining, grinding, polishing, and blasting, and the main goal is to obtain specific surface topographies and roughness and remove surface contamination. The physical methods employ thermal, kinetic, and electrical energy to modify the surface, including thermal spraying, physical vapor deposition (PVD), ion implantation and deposition, and glow discharge plasma treatment. Finally, chemical methods involve reactions at the interface of Ti and a solution and include chemical treatment, anodic oxidation, chemical vapor deposition (CVD), and the sol-gel method [34–36].

In the doctoral thesis presented here, the selected technique for surface modification was the sol-gel, which is described briefly in the following section.

1.1.4.2. *The sol-gel method*

Silica-based bioactive glasses have been successfully applied in the biomedical fields in the past decades. In 1969, Larry Hench developed the first bioactive glasses (Bioglass®) and employed them as implantable material [37,38]. Since then, many glasses with added biomedical value have been developed and provided exciting results. These materials can bond and integrate with bone without forming fibrous tissue around them or promoting toxicity [39]. Later, in the 90s, the sol-gel route was employed to prepare bioactive glasses for the first time, allowing the development of porous bioglasses from metal hydroxides, alkoxides, and inorganic salts [39]. Alkoxides are the class of precursors most widely employed in sol-gel research. In the present doctoral thesis, alkoxysilanes were employed based on the properties of silicon (Si) on bone regeneration (reviewed in [40]).

The sol-gel process involves the preparation of inorganic polymers or ceramics through the transformation of liquid precursors into a sol (colloidal suspension of solid particles) and then into a gel (interconnected network of solid-phase particles that forms a continuous entity throughout a secondary phase (usually liquid) [41,42]. These phases converse through the chemical reactions that occur during the gel evolution and can be manipulated in various ways (*e.g.*, altering initial precursors, time for gelation) [41,43]. The sol-gel process can be divided into two main steps: hydrolysis and condensation (**Figure 1.2**), which are strongly affected by process parameters such as the nature of the R-group, the ratio of water to alkoxide, and the catalysts (acid or base). In the first step, the alkoxysilane precursor is hydrolyzed by the water to form silanol groups (**Equation 1.1**). The precursor can only be partially hydrolyzed depending on the amount of water or catalyst present during condensation. The two partially hydrolyzed molecules can link together in a condensation reaction (**Equation 1.2** or **Equation 1.3**) and liberate a small molecule of water or alcohol [44].

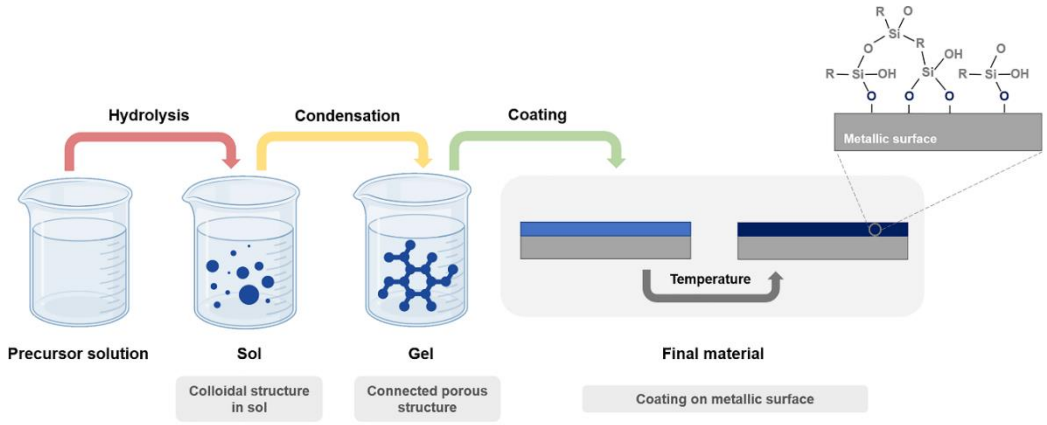

Figure 1.2. The sol-gel route.

1. $Si(OR)_4 + nH_2O \rightarrow Si(OR)_{4-n}(OH)_n + nR(OH)$
2. $R_3SiOH + HOSiR'_3 \rightarrow R_3Si - O - SiR'_3 + H_2O$
3. $R_3SiOH + ROSiR'_3 \rightarrow R_3Si - O - SiR'_3 + R(OH)$

Equation 1. Hydrolysis-condensation reactions in the sol-gel process [44].

The sol-gel route offers many advantages, such as low-temperature processing, easy fabrication, and microstructural and chemical control. Additionally, the sol-gel process is inexpensive, and the coatings obtained present molecular homogeneity, high purity, reasonably good adhesion, durability, and high uniformity [32,45,46]. The sol-gel coatings show a good degree of biocompatibility, high specific surface area, allowing the synthesis of drug-carrier, and potential for surface functionalization employing biomolecules of interest [41]. As porosity and degradation of these materials can be controlled, it is possible to design drug delivery systems employing a wide range of bioactive compositions that can aid tissue regeneration [47].

In the past decades, sol-gel silica-based materials have been successfully applied to the biomedical field. Hybrid organic-inorganic coatings with the ability to induce the formation of hydroxyapatite crystals in simulated body fluid (SBF) and promote new bone formation have been developed [48], while others improved *in vitro* cell response and the osseointegration properties *in vivo* [49]. Martínez-Ibañez *et al*. [50] developed and characterized a sol-gel material with tetraethyl orthosilicate (TEOS) and methyltrimethoxysilane (MTMOS) in a proportion of 7:3 that revealed good *in vitro* cell responses and accelerated growth of new bone *in vivo*.

The materials have also been applied as release vehicles of strontium (Sr) [51,52], Ca [53], and boron (B) [54] that induced osteogenic responses *in vitro*. Also, chitosan [55], octenidine dihydrochloride, chlorhexidine diacetate [56], and silver (Ag) [57] incorporated in sol-gel coatings showed antimicrobial activity, frequently required in biomedical applications. With these, it is possible

to understand the broad applicability of the sol-gel technology and how it allows synthesizing materials with powerful osteoinductive properties.

1.1.4.3. *Sol-gel coatings as release vehicles: biomolecules and ions*

Implantable drug delivery systems are among the most promising therapeutic concepts in bone disease treatments, orthopedic surgery, and dentistry. Biomolecules (*e.g.,* hormones) and inorganic ions (*e.g.,* zinc, magnesium, calcium) influence cellular functions and tissue homeostasis, and their role in the bone regeneration process is well described [58,59]. Considering that sol-gel networks allow the functionalization or release of these compounds from metallic surfaces such as Ti, these hybrids present themselves as an interesting alternative to design biomaterials to incite different biological responses.

The present doctoral thesis selected melatonin, zinc, magnesium, and calcium based on the literature review to be incorporated into the sol-gel coatings. A brief description of each one based on their properties on bone regeneration and inflammatory responses follows.

1.1.4.3.1. Melatonin

Mainly produced by the pineal gland, the indoleamine hormone melatonin (*N*-acetyl-5-metoxy-tryptamine; MLT) is a widely known regulator of the circadian cycles, sleep, aging, and immune defense [60,61]. In tissue regeneration, this hormone is regarded as a relevant mediator of angiogenesis and bone formation [62,63]. *In vitro* studies with MC3T3-E1 preosteoblasts, rat osteoblast-like osteosarcoma [64], human bone cells [65], human osteoblasts [66], and bone marrow mesenchymal stem cells (MSCs) [67,68] showed that MLT promotes osteoblast proliferation, mineralization, and type I collagen synthesis. The osteoblastic genes RUNX2, BMP-2, BMP-6, and BGLAP display a circadian rhythm coincident with MLT levels [63] and are associated with MLT cell receptors [64,67]. Park *et al.* [69] showed that MLT controls bone cell differentiation by activating BMP/ERK/Wnt pathways, thus regulating osteoblast differentiation and bone formation.

On the other hand, the free radical scavenger action of MLT acts directly on osteoclasts and thereby inhibits bone resorption via the downregulation of receptor activator of NF-κB ligand (RANKL)-mediated osteoclast formation and activation [70]. Also, MLT downregulates the expression of pro-inflammatory nitric oxide synthase (iNOS), cyclooxygenase (COX)-2, and nuclear factor kappa-light-chain-enhancer of activated B cells (NF-κB), and the production of tumor necrosis factor (TNF)-α, IL-1β, and IL-6 [71]. However, the action of MLT is dependent on the concentration applied and mode of exposure (continuous or intermittent). Liu *et al*. [72] showed that MLT delayed osteoblast proliferation *in vitro* at a concentration of 1 mM, while

MLT significantly promoted cell proliferation at 1 nM–100 µM. Moreover, Sethi *et al.* [67] reported that MLT must be administered continuously to positively affect ALP activity and calcium deposition in MSCs.

1.1.4.3.2. Zinc

Zinc (Zn) is a ubiquitous trace element present in all body tissues, being the second most abundant micronutrient in living organisms [73,74]. Fundamental to cell biology and physiology, Zn is necessary for hundreds of enzymatic reactions [74]. At the cellular level, transcription factors often bind to DNA through zinc-finger binding domains, which require Zn to function correctly and regulate hormone receptors (*e.g.,* estrogen) and vitamin D actions, among others [75]. In bone, Zn directly affects apatite nucleation and tissue mineralization and the activity of matrix metalloproteinases responsible for the bone collagenous ECM remodeling [76,77]. Also, as an enzymatic cofactor, Zn induces ALP activity on in vitro cell culture, organ culture, and *in vivo* [78], prompting the mineralization process. Two master osteogenic regulators (RUNX2 and Osterix/SP7) along with essential constituents of bone ECM such as collagen type I alpha 1 chain (Col1A1), osteopontin (OPN), and fibronectin are positively regulated by Zn [79]. Zn affects insulin-like factor-1 (IGF-1) [78], MAPK [80], and TGF-β/SMAD [81] pathways, involved in osteogenic differentiation regulation. Park *et al.* [82] described the enhancement of osteogenic differentiation by the cAMP-PKA-CREB signaling pathway in MSCs treated with increasing amounts of Zn.

On the other hand, Zn also has an essential role in regulating osteoclastogenesis and bone resorption. Yamaguchi & Weitzmann [83] found that increasing Zn concentration inhibited RANKL induced osteoclast differentiation and NF-κB regulated osteoclastogenesis in RAW264.7 cells. Zn was found to inhibit tartrate-resistant acid phosphatase (TRAP) activity [84], which is expressed in early osteoclast differentiation and maturation. Nonetheless, the Zn concentration plays an important role in the observed cellular effects. Positive effects occur in a narrow range (1–50 µM). Dosages above this can inhibit the osteogenic activity, while too low concentrations can have no measurable effects. Conversely, only very high doses (600 and 900 µM) are cytotoxic [78].

1.1.4.3.3. Magnesium

Magnesium (Mg) is the fourth most abundant element in the human body, with about 60% residing in bones as an integral part of the hydroxyapatite [58,85]. Usually found as a divalent cation (Mg^{2+}), salt, or mineral form, Mg has several well-known roles in physiology, acting as an enzymatic cofactor, signal modulator, transporter, and mediator of energy metabolism and cell proliferation [86]. In addition, Mg has roles in protein and nucleic acid synthesis, mitochondrial integrity, ion channel modulation, membrane stabilization, and translational processes [86].

Castiglioni *et al.* [87] described a correlation between osteoporosis and Mg deficiency that leads to a decrease in bone formation and a bone resorption increment from an augmented production of TNF-α, IL-1β, and RANKL. In MSCs, Mg^{2+} enhances matrix mineralization and the expression of collagen type X and VEGF [88], stimulates osteoblastic differentiation, ALP activity, and mineral deposition in human fetal osteoblastic cells (hFOB1.19), and decreases osteoclast differentiation of RAW264.7 cells [89]. Mg^{2+} selectively activates the MAPK/ERK pathway, which is associated with the signaling pathways governing the osteogenic differentiation of stem cells. Recently, Huang *et al*. [90] described that Mg^{2+} activates the canonical Wnt signaling pathway and significantly upregulates β-catenin expression, leading to differentiation of MSCs to the osteoblast lineage and inducing an osteogenic effect. Also, Mg is well known for enhancing cell adhesion, primarily mediated by membrane-associated adhesion receptors (*i.e.,* integrins), which is crucial for successfully implanting a biomaterial. As studied by Zreiqat and colleagues [91], the adhesion of human bone-derived cells (HBDCs) grown on Mg^{2+}-modified surfaces enhanced the expression of the integrin receptors α5β1, β1, and α3β1.

Similarly, Jin-Woo *et al.* [92] found that Mg significantly increased the attachment of MC3T3-E1 cells to Ti materials. Mg affects immune responses by promoting macrophage polarization to an anti-inflammatory phenotype (M2) and regulating the pro-inflammatory factors TNF-α, IL-1β, and IL-6 [93,94]**.** Even though pure Mg has been applied in orthopedic applications, it corrodes too quickly (1 to 4 months) and generates harmful hydrogen gas [74]. Consequently, surface modifications with Mg^{2+} have been developed to increase cellular response in vitro and enhance osseointegration *in vivo* [58].

1.1.4.3.4. Calcium

Calcium (Ca) is an essential molecule in cell biology. It is an essential part of cellular signaling cascades in its divalent cation form (Ca^{2+}), which allows the cell to interpret and respond to different external stimuli [85]. In bone biology, this ion is particularly relevant, as it is one of the two most essential components of the mineralized matrix along with phosphate [58]. Around 99% of the Ca in the body is stored in bone hydroxyapatite, which acts as a reservoir for this element [58,85]. Moreover, Ca^{2+} is key in bone formation and repair, acting as a signaling molecule between osteoclasts and osteoblasts and stimulating pathways associated with bone synthesis [95]. In MSCs, Ca^{2+} enhances cell differentiation through the regulation of BGLAP, BMP-2, bone sialoprotein (BSP), OPN, RUNX2, type I collagen, and ALP expression [96]. Ca signaling also stimulates MSC and mature bone cell proliferation in a process dependent on nitric oxide (NO) [97,98] and the activation of the ERK 1/2 pathway.

Additionally, PI3K/Akt activation, essential for the survival of osteoblasts, is a downstream effect of Ca signaling. In osteoclasts, Ca is involved in osteoclastogenesis, cell motility, and resorption regulation [85]. In addition, Ca affects other important processes associated with tissue regeneration, such as coagulation and angiogenesis [99]. In blood coagulation, Ca^{2+} promotes and accelerates the formation of the prothrombinase complex and mediates factor IXa and factor Xa binding and platelet activation, required for the formation of cloths [100]. The shape and function of the blood cloth are essential in the implant-surface interaction as it mediates cell adhesion, proliferation, and differentiation[101]. Nevertheless, it is important to remark that *in vitro* studies have shown that Ca concentrations need to be moderate for optimal tissue regeneration and ECM mineralization [53,102].

1.1.5. PROTEOMICS AS A TOOL TO PREDICT A BIOMATERIAL OUTCOME

The selection of the ideal material for bone implants and prostheses is an intense topic of debate due to difficulties in translating *in vitro* results into *in vivo* patient outcome [12]. The inadequacies of *in vitro* current methods and the growing number of biomaterials in development increased the interest in developing alternative early-stage assays predictive of *in vivo* outcomes to optimize the biomaterial testing [103]. However, understanding and improving the study of the biomaterial-biological interface is not a trivial task. Many factors, such as material physicochemical properties or type of structure, may hamper this effort and hinder the comprehension of a correlation between properties and biological responses.

A potent tool to describe the interactions between cells/tissues and materials is proteomics [104]. On the one hand, and as mentioned in section 1.1.3, when a material is implanted, protein adsorption takes place onto the surface. These proteins are derived from the biological fluids (*i.e.*, blood plasma), and said adsorption significantly affects the following biological mechanisms that take place at the biomaterial/biological fluids interface [105]. When cells arrive at the material surface, they will encounter it coated in a monolayer of proteins; therefore, the host does not sense the material itself but the dynamic protein layer instead [106]. Considering this, it is not surprising to verify that said protein layer affects the biological response to biomaterials to a great extent. For example, cell adhesion is mediated/guided by adsorbed proteins on the material surface and is a crucial step for the successful outcome of a medical implant [105]. Hence, understand, predict, and control protein adsorption onto material surfaces is essential for the successful development and applications of biomaterials; however, it is a rather complex process, not completely understood thus far [105].

Earlier studies employed fetal bovine serum (FBS) to simulate protein adsorption after material implementation [105,107]. Recently, human serum has been used instead as a better approximation to what happens in the human body. Magnani *et al*. [108] analyzed human serum protein adsorption dynamics onto four surfaces, identifying that high-density lipoproteins (HDL) can play an important role in biomaterial biocompatibility. Romero-Gavilán *et al*. [109] showed that materials with lower biocompatibility *in vivo* presented a higher affinity for proteins associated with the complement system, even though the *in vitro* cell assays did not present significant differences. Similarly, Araújo-Gomes *et al.* [110] showed a correlation between the deposition of complement system proteins and a higher inflammatory response *in vitro* in materials with poorer biocompatibility *in vivo*. Wang *et al.* [111] showed that reduced adsorption of vitronectin, thrombin, fibrinogen, and complement component C3 in hydrogels correlated with a lower number of monocytes on poly(ethylene glycol) hydrogels. Other studies analyzed the effects of adding Ca [53] and Sr [52] to a biomaterial on protein adsorption. These studied highlight a strong correlation between *in vitro* cellular responses and the proteomic analysis, once again proving the potential of proteomics to predict a biomaterial outcome.

Moreover, when cells are in contact with the biomaterial, they express unique protein profiles, and the description of said profiles results useful in understanding cell-material interactions [104]. However, only a few studies have been done to date exploring the relationship between cell proteomic profiles and biomaterial properties. To better understand the effects of surface topography on cellular behavior, Kim *et al*. [112] analyzed the protein production of MG-63 osteosarcoma cells when seeded onto Ti with different superficial surfaces (smooth, grit-blasted, acid-etched, and hydroxyapatite-coated). It was demonstrated that grit-blasted, acid-etched, and hydroxyapatite-coated surfaces triggered the production of proteins associated with relevant roles on cell adhesion, proliferation, differentiation, and cell-cell contact, which may explain the different clinical behaviors of these materials. In another study, Henrionnet *et al.* [113] quantified the secreted proteins by human MSCs undergoing chondrogenic differentiation inside collagen-based scaffolds. This study made it possible to validate the quantification of secreted proteins as a non-invasive testing/validation tool for *in vitro* biomaterial evaluation. Other work by Zhang and colleagues [114] demonstrated the crucial role of the ERK1/2 and MAPK/JNK pathways in the osteogenic differentiation of MSCs when cultured in natural hydroxyapatite ceramics. Yang *et al.* [115] applied cell proteomic analysis in fibroblasts cultured on silk fibroin-modified biopolymers, concluding that the material improved cell adhesion by inducing the expression of CD44. Recently, Othman *et al*. [116] studied the proteomic profile of human mesenchymal stromal cells seeded on calcium phosphate ceramics, identifying the

overexpression of proteins associated with wound healing, cell proliferation, and the production of ECM on the cells seeded on the materials. Omidi *et al*. [117] compared the cellular responses of osteoblasts to Ti-based and Mg-based implants employing liquid chromatography-tandem mass spectrometry (LC-MS/MS), allowing the identification of several proteins associated with ECM maturation and tissue remodeling associated with the exposure to the materials.

While the number of studies is still limited, it has been demonstrated that proteomics is a useful tool to predict the outcome of a biomaterial. With proper material design, proteomic profiling can give insights into the relationship between the biomaterial and biological system. This knowledge can be used as an important parameter for designing new biomaterials with specific bioactivity and will allow to design and develop improved biomaterials for regenerative therapies.

1.2. AIMS

This doctoral thesis intends to study the effects of biomolecules and ions contained in a release vehicle for bone regeneration and understand how the presence of these elements in a biomaterial affects the *in vitro* cell responses, modulates protein adsorption patterns and cellular proteomic profile.

For that, specific aims were established:

1. Development of different sol-gel coatings doped with a selected biomolecule (melatonin) and ions (Zn, Mg, and Ca).

- Sol-gel coating: promotion of osteogenesis by Si release
- Melatonin: regulation of inflammation
- Zn: regulation of osteoclastogenesis
- Mg: promotion of cell adhesion
- Ca and Mg mixtures: promotion of coagulation and cell adhesion

2. Characterization of *in vitro* responses of the materials employing osteoblasts and macrophages.

3. Analysis serum protein adsorption patterns onto the material surface by LC-MS/MS.

4. Evaluation of the proteomic profile of osteoblasts exposed to the material with the best *in vitro* response.

5. Study the *in vitro* and proteomic results and define biomarkers for bone regeneration around a biomaterial.

1.3. Experimental Design

To attain the aims outlined for the present doctoral thesis, a stepwise experimental design was established logically and sequentially (**Figure 1.3**). The first experimental phase involves the synthesis of different sol-gel coating formulations doped with selected bioactive agents. A biomolecule (melatonin) and three salts (zinc, magnesium, and calcium chloride) were selected based on bibliographic research. In the case of calcium, it will be employed in a mixture with magnesium. Then, the materials will be incubated *in vitro* with osteoblasts and macrophages to evaluate theirs effects on osteogenesis and immune responses. The protein adsorption of the materials after the incubation with human serum will also be performed. With these results, it will be possible to understand the effects on these bioactive agents when applied in a coating in the *in vitro* responses and correlate the kind of proteins adsorbed with the cellular responses observed.

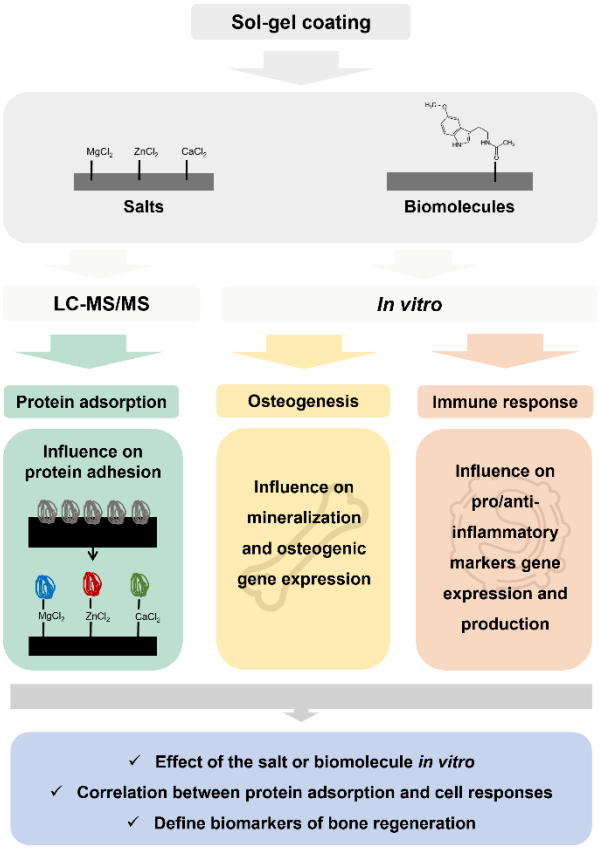

Figure 1.3. Experimental design of the present doctoral thesis.

In the second phase, the material with the most promising results will be selected and the proteomic profile of osteoblasts seeded on said material will be evaluated (**Figure 1.4**). The proteomic analysis will be carried out by nLC-MS/MS and will allow us to understand if a biomaterial activates specific cascades on osteoblasts responsible for osteogenesis.

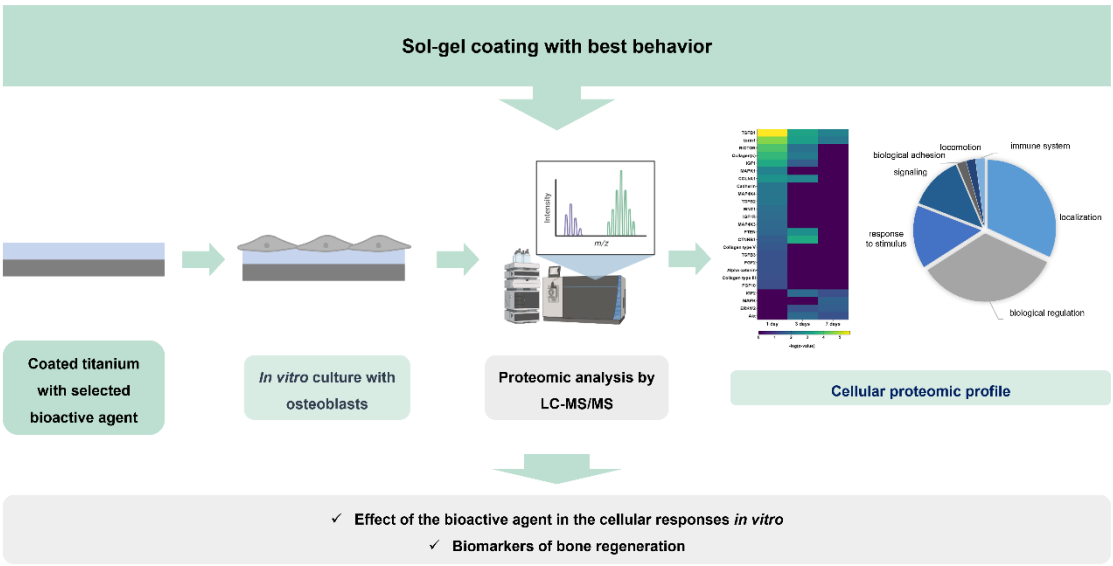

Figure 1.4. Experimental design of the present doctoral thesis.

1.4. REFERENCES

1. Koons, G. L., Diba, M. & Mikos, A. G. Materials design for bone-tissue engineering. *Nat. Rev. Mater.* **5**, 584–603 (2020).
2. Rinaldo Florencio-Silva, G., Rodrigues da Silva Sasso, E. S.-C., Simões, M. J. & Cerri, P. S. Structure, Function, and Factors That Influence Bone Cells. *Biomed Res. Int.* **2015**, 1–11 (2015).
3. Porter, J. R., Ruckh, T. T. & Popat, K. C. Bone tissue engineering: A review in bone biomimetics and drug delivery strategies. *Biotechnol. Prog.* **25**, 1539–1560 (2009).
4. Hu, C., Ashok, D., Nisbet, D. R. & Gautam, V. Bioinspired surface modification of orthopedic implants for bone tissue engineering. *Biomaterials* **219**, 119366 (2019).
5. Tsukasaki, M. & Takayanagi, H. Osteoimmunology: evolving concepts in bone–immune interactions in health and disease. *Nat. Rev. Immunol.* **19**, 626–642 (2019).
6. Ponzetti, M. & Rucci, N. Updates on osteoimmunology: What's new on the cross-talk between bone and immune system. *Front. Endocrinol. (Lausanne).* **10**, 236 (2019).
7. Hadjidakis, D. J. & Androulakis, I. I. Bone Remodeling. *Ann. N. Y. Acad. Sci.* **1092**, 385–396 (2006).
8. Crockett, J. C., Rogers, M. J., Coxon, F. P., Hocking, L. J. & Helfrich, M. H. Bone remodelling at a glance. *J. Cell Sci.* **124**, 991–998 (2011).
9. Raggatt, L. J. & Partridge, N. C. Cellular and molecular mechanisms of bone remodeling. *J. Biol. Chem.* **285**, 25103–25108 (2010).
10. Smeets, R. *et al.* Impact of Dental Implant Surface Modifications on Osseointegration. *Biomed Res. Int.* **2016**, 1–16 (2016).
11. Anderson, J. M. Biological responses to materials. *Annu. Rev. Mater. Sci.* **31**, 81–110 (2001).
12. Armiento, A. R., Hatt, L. P., Sanchez Rosenberg, G., Thompson, K. & Stoddart, M. J. Functional Biomaterials for Bone Regeneration: A Lesson in Complex Biology. *Adv. Funct. Mater.* **30**, 1909874 (2020).
13. Oryan, A., Monazzah, S. & Bigham-sadegh, A. Bone Injury and Fracture Healing Biology. *Biomed. Environ. Sci.* **28**, 57–71 (2015).
14. Sheikh, Z., Brooks, P. J., Barzilay, O., Fine, N. & Glogauer, M. Macrophages, foreign body giant cells and their response to implantable biomaterials. *Materials (Basel).* **8**, 5671–5701 (2015).
15. Chen, R., Wang, J. & Liu, C. Biomaterials Act as Enhancers of Growth Factors in Bone Regeneration. *Adv. Funct. Mater.* **26**, 8810–8823 (2016).
16. Toosi, S. & Behravan, J. Osteogenesis and bone remodeling: A focus on growth factors and bioactive peptides. *BioFactors* **46**, 326–340 (2020).

17. Majidinia, M., Sadeghpour, A. & Yousefi, B. The roles of signaling pathways in bone repair and regeneration. *J. Cell. Physiol.* **233**, 2937–2948 (2018).

18. Wang, R. N. *et al.* Bone Morphogenetic Protein (BMP) signaling in development and human diseases. *Genes Dis.* **1**, 87–105 (2014).

19. Davies, O. G., Grover, L. M., Lewis, M. P. & Liu, Y. PDGF is a potent initiator of bone formation in a tissue engineered model of pathological ossification. *J. Tissue Eng. Regen. Med.* **12**, e355–e367 (2018).

20. Shah, P., Keppler, L. & Rutkowski, J. A Review of Platelet Derived Growth Factor Playing Pivotal Role in Bone Regeneration. *J. Oral Implantol.* **40**, 330–340 (2014).

21. Wirth, T. & Yla-Herttuala, S. Gene transfer vectors (DNA vehicles) and their incorporation into biomaterials for bone repair. *Biomater. Bone Regen. Nov. Tech. Appl.* 374–405 (2014). doi:10.1533/9780857098104.3.374

22. Hu, K. & Olsen, B. R. The roles of vascular endothelial growth factor in bone repair and regeneration. *Bone* **91**, 30–38 (2016).

23. Houschyar, K. S. *et al.* Wnt Pathway in Bone Repair and Regeneration – What Do We Know So Far. *Front. Cell Dev. Biol.* **6**, 170 (2019).

24. Hayrapetyan, A., Jansen, J. A. & Van Den Beucken, J. J. J. P. Signaling pathways involved in osteogenesis and their application for bone regenerative medicine. *Tissue Eng. - Part B Rev.* **21**, 75–87 (2015).

25. Luo, Z. *et al.* Notch Signaling in Osteogenesis, Osteoclastogenesis, and Angiogenesis. *Am. J. Pathol.* **189**, 1495–1500 (2019).

26. Thouverey, C. & Caverzasio, J. Focus on the p38 MAPK signaling pathway in bone development and maintenance. *Bonekey Rep.* **4**, 1–8 (2015).

27. Kim, J. *et al.* The ERK MAPK Pathway Is Essential for Skeletal Development and Homeostasis. *Int. J. Mol. Sci.* **20**, 1803 (2019).

28. Tong, Y. *et al.* Mechano-growth factor accelerates the proliferation and osteogenic differentiation of rabbit mesenchymal stem cells through the PI3K/AKT pathway. *BMC Biochem.* **16**, 1–6 (2015).

29. Zhou, H. *et al.* Orthosilicic Acid Accelerates Bone Formation in Human Osteoblast-Like Cells Through the PI3K-Akt-mTOR Pathway. *Biol. Trace Elem. Res.* **190**, 327–335 (2011).

30. Priyadarshini, B., Rama, M., Chetan & Vijayalakshmi, U. Bioactive coating as a surface modification technique for biocompatible metallic implants: a review. *J. Asian Ceram. Soc.* **7**, 397–406 (2019).

31. Abdel-Hady Gepreel, M. & Niinomi, M. Biocompatibility of Ti-alloys for long-term implantation. *J. Mech. Behav. Biomed. Mater.* **20**, 407–415 (2013).

32. Liu, X., Chu, P. K. & Ding, C. Surface modification of titanium, titanium alloys, and related materials for biomedical applications. *Materials Science and Engineering R: Reports* **47**,

49–121 (2004).

33. Zhang, L. C., Chen, L. Y. & Wang, L. Surface Modification of Titanium and Titanium Alloys: Technologies, Developments, and Future Interests. *Adv. Eng. Mater.* **22**, 1–37 (2020).

34. Zhang, L.-C., Chen, L.-Y. & Wang, L. Surface Modification of Titanium and Titanium Alloys: Technologies, Developments, and Future Interests. *Adv. Eng. Mater.* **22**, 1901258 (2020).

35. Sasikumar, Y., Indira, K. & Rajendran, N. Surface Modification Methods for Titanium and Its Alloys and Their Corrosion Behavior in Biological Environment: A Review. *J. Bio- Tribo-Corrosion* **5**, 1–25 (2019).

36. Chouirfa, H., Bouloussa, H., Migonney, V. & Falentin-Daudré, C. Review of titanium surface modification techniques and coatings for antibacterial applications. *Acta Biomater.* **83**, 37–54 (2019).

37. Jones, J. R. Review of bioactive glass: From Hench to hybrids. *Acta Biomater.* **23**, S53–S82 (2015).

38. Hench, L. L., Splinter, R. J., Allen, W. C. & Greenlee, T. K. Bonding mechanisms at the interface of ceramic prosthetic materials. *J. Biomed. Mater. Res.* **5**, 117–141 (1971).

39. Arcos, D. & Vallet-Regí, M. Sol-gel silica-based biomaterials and bone tissue regeneration. *Acta Biomaterialia* **6**, 2874–2888 (2010).

40. Arora, M. & Arora, E. The Promise of Silicon: bone regeneration and increased bone density. *J. Arthrosc. Jt. Surg.* **4**, 103–105 (2017).

41. Owens, G. J. *et al.* Sol-gel based materials for biomedical applications. *Progress in Materials Science* **77**, 1–79 (2016).

42. Danks, A. E., Hall, S. R. & Schnepp, Z. The evolution of 'sol-gel' chemistry as a technique for materials synthesis. *Mater. Horizons* **3**, 91–112 (2016).

43. Xue, T. *et al.* Surface Modification Techniques of Titanium and its Alloys to Functionally Optimize Their Biomedical Properties: Thematic Review. *Front. Bioeng. Biotechnol.* **8**, 1261 (2020).

44. Brinker, C. J. & Scherer, G. W. *Sol-Gel Science: The Physics and Chemistry of Sol-Gel Processing*. (Academic Press Inc., 1990).

45. Asri, R. I. M., Harun, W. S. W., Hassan, M. A., Ghani, S. A. C. & Buyong, Z. A review of hydroxyapatite-based coating techniques: Sol-gel and electrochemical depositions on biocompatible metals. *J. Mech. Behav. Biomed. Mater.* **57**, 95–108 (2016).

46. Chernev, G. *et al.* Sol-gel silica hybrid biomaterials for application in biodegradation of toxic compounds. *J. Sol-Gel Sci. Technol.* **58**, 619–624 (2011).

47. Avnir, D., Coradin, T., Lev, O. & Livage, J. Recent bio-applications of sol-gel materials. *J. Mater. Chem. B* **16**, 1013–1030 (2006).

48. Ballarre, J. *et al.* Improving the osteointegration and bone-implant interface by incorporation of bioactive particles in sol-gel coatings of stainless steel implants. *Acta*

Biomater. **6**, 1601–1609 (2010).

49. Catauro, M., Bollino, F., Papale, F., Gallicchio, M. & Pacifico, S. Influence of the polymer amount on bioactivity and biocompatibility of SiO2/PEG hybrid materials synthesized by sol-gel technique. *Mater. Sci. Eng. C* **48**, 548–555 (2015).

50. Martinez-Ibañez, M. *et al.* Biological characterization of a new silicon based coating developed for dental implants. *J. Mater. Sci. Mater. Med.* **27**, (2016).

51. Almeida, J. C. *et al.* A biocompatible hybrid material with simultaneous calcium and strontium release capability for bone tissue repair. *Mater. Sci. Eng. C* **62**, 429–438 (2016).

52. Romero-Gavilán, F. *et al.* The effect of strontium incorporation into sol-gel biomaterials on their protein adsorption and cell interactions. *Colloids Surfaces B Biointerfaces* **174**, 9–16 (2019).

53. Romero-Gavilán, F. *et al.* Proteomic analysis of calcium-enriched sol–gel biomaterials. *JBIC J. Biol. Inorg. Chem.* **24**, 563–574 (2019).

54. Coelho, S. A. R. *et al.* Cellular Response to Sol-Gel Hybrid Materials Releasing Boron and Calcium Ions. *ACS Biomater. Sci. Eng.* **7**, 491–506 (2021).

55. Palla-Rubio, B. *et al.* Synthesis and characterization of silica-chitosan hybrid materials as antibacterial coatings for titanium implants. *Carbohydr. Polym.* **203**, 331–341 (2019).

56. García-Arnáez, I. *et al.* A single coating with antibacterial properties for prevention of medical device-associated infections. *Eur. Polym. J.* **113**, 289–296 (2019).

57. Kawashita, M. *et al.* Antibacterial silver-containing silica glass prepared by sol-gel method. *Biomaterials* **21**, 393–398 (2000).

58. O'Neill, E., Awale, G., Daneshmandi, L., Umerah, O. & Lo, K. W. H. The roles of ions on bone regeneration. *Drug Discovery Today* **23**, 879–890 (2018).

59. Cardinali, D. P., Ladizesky, M. G., Boggio, V., Cutrera, R. A. & Mautalen, C. Melatonin effects on bone: experimental facts and clinical perspectives. *J. Pineal Res.* **34**, 81–87 (2003).

60. Cardinali, D. P. & Pévet, P. Basic aspects of melatonin action. *Sleep Medicine Reviews* **2**, 175–190 (1998).

61. Zhang, L. *et al.* Sustained release of melatonin from poly (lactic-co-glycolic acid) (PLGA) microspheres to induce osteogenesis of human mesenchymal stem cells in vitro. *J. Pineal Res.* **54**, 24–32 (2013).

62. Ramírez-Fernández, M. P. *et al.* Melatonin promotes angiogenesis during repair of bone defects: a radiological and histomorphometric study in rabbit tibiae. *Clin. Oral Investig.* **17**, 147–158 (2013).

63. Maria, S., Witt-Enderby, P, A. & Witt-Enderby, P. A. Melatonin effects on bone: Potential use for the prevention and treatment for osteopenia, osteoporosis, and periodontal disease and for use in bone-grafting procedures. *J. Pineal Res.* **56**, 115–125 (2014).

64. Roth, J. A., Kim, B. G., Lin, W. L. & Cho, M. I. Melatonin promotes osteoblast differentiation and bone formation. *J. Biol. Chem.* **274**, 22041–22047 (1999).

65. Nakade, O., Koyama, H., Ariji, H., Yajima, A. & Kaku, T. Melatonin stimulates proliferation and type I collagen synthesis in human bone cells in vitro. *J. Pineal Res.* **27**, 106–110 (1999).

66. Satomura, K. *et al.* Melatonin at pharmacological doses enhances human osteoblastic differentiation in vitro and promotes mouse cortical bone formation in vivo. *J. Pineal Res.* **42**, 231–239 (2007).

67. Sethi, S. *et al.* Determination of the minimal melatonin exposure required to induce osteoblast differentiation from human mesenchymal stem cells and these effects on downstream signaling pathways. *J. Pineal Res.* **49**, 222–238 (2010).

68. Zhang, L. *et al.* Melatonin inhibits adipogenesis and enhances osteogenesis of human mesenchymal stem cells by suppressing PPARγ expression and enhancing Runx2 expression. *J. Pineal Res.* **49**, 364–372 (2010).

69. Park, K. H. *et al.* Melatonin promotes osteoblastic differentiation through the BMP/ERK/Wnt signaling pathways. *J. Pineal Res.* **51**, 187–194 (2011).

70. Koyama, H., Nakade, O., Takada, Y., Kaku, T. & Lau, K. H. W. Melatonin at pharmacologic doses increases bone mass by suppressing resorption through down-regulation of the RANKL-mediated osteoclast formation and activation. *J. Bone Miner. Res.* **17**, 1219–1229 (2002).

71. Xia, Y. *et al.* Melatonin in macrophage biology: Current understanding and future perspectives. *J. Pineal Res.* **66**, 1–21 (2019).

72. Liu, L., Zhu, Y., Xu, Y. & Reiter, R. J. Melatonin delays cell proliferation by inducing G1 and G2/M phase arrest in a human osteoblastic cell line hFOB 1.19. *J. Pineal Res.* **50**, no-no (2010).

73. Chasapis, C. T., Spiliopoulou, C. A., Loutsidou, A. C. & Stefanidou, M. E. Zinc and human health: An update. *Arch. Toxicol.* **86**, 521–534 (2012).

74. Su, Y. *et al.* Zinc-Based Biomaterials for Regeneration and Therapy. *Trends Biotechnol.* **37**, 428–441 (2019).

75. Brokesh, A. M. & Gaharwar, A. K. Inorganic Biomaterials for Regenerative Medicine. *ACS Appl. Mater. Interfaces* **12**, 5319–5344 (2020).

76. Yusa, K. *et al.* In vitro prominent bone regeneration by release zinc ion from Zn-modified implant. *Biochem. Biophys. Res. Commun.* **412**, 273–278 (2011).

77. Nosrati, R., Kheirouri, S., Ghodsi, R. & Ojaghi, H. The effects of zinc treatment on matrix metalloproteinases: A systematic review. *J. Trace Elem. Med. Biol.* **56**, 107–115 (2019).

78. Patrick O'Connor, J., Kanjilal, D., Teitelbaum, M., Lin, S. S. & Cottrell, J. A. Zinc as a Therapeutic Agent in Bone Regeneration. *Materials (Basel).* **13**, 2211 (2020).

79. Fu, X. *et al.* Runx2/Osterix and Zinc Uptake Synergize to Orchestrate Osteogenic Differentiation and Citrate Containing Bone Apatite Formation. *Adv. Sci.* **5**, 1700755 (2018).

80. Liang, D. *et al.* Zinc Inhibits H2O2-Induced MC3T3-E1 Cells Apoptosis via MAPK and PI3K/AKT Pathways. *Biol. Trace Elem. Res.* **3**, 420–429 (2012).

81. Yu, J. *et al.* Zinc-modified Calcium Silicate Coatings Promote Osteogenic Differentiation through TGF-β/Smad Pathway and Osseointegration in Osteopenic Rabbits. *Sci. Rep.* **7**, 1–13 (2017).

82. Park, K. H. *et al.* Zinc Promotes Osteoblast Differentiation in Human Mesenchymal Stem Cells Via Activation of the cAMP-PKA-CREB Signaling Pathway. *Stem Cells Dev.* **27**, 1125–1135 (2018).

83. Yamaguchi, M. & Weitzmann, M. N. Zinc stimulates osteoblastogenesis and suppresses osteoclastogenesis by antagonizing NF-κB activation. *Mol. Cell. Biochem.* **355**, 179–186 (2011).

84. Roy, M., Fielding, G., Bandyopadhyay, A., Bose, S. & Keck, M. Effects of Zinc and Strontium Substitution in Tricalcium Phosphate on Osteoclast Differentiation and Resorption. *Biomater. Sci.* **1**, 74–82 (2013).

85. Lakhkar, N. J. *et al.* Bone formation controlled by biologically relevant inorganic ions: Role and controlled delivery from phosphate-based glasses. *Adv. Drug Deliv. Rev.* **65**, 405–420 (2013).

86. Walker, J., Shadanbaz, S., Woodfield, T. B. F., Staiger, M. P. & Dias, G. J. Magnesium biomaterials for orthopedic application: A review from a biological perspective. *J. Biomed. Mater. Res. Part B Appl. Biomater.* **102**, 1316–1331 (2014).

87. Castiglioni, S., Cazzaniga, A., Albisetti, W. & Maier, J. Magnesium and Osteoporosis: Current State of Knowledge and Future Research Directions. *Nutrients* **5**, 3022–3033 (2013).

88. Yoshizawa, S., Brown, A., Barchowsky, A. & Sfeir, C. Magnesium ion stimulation of bone marrow stromal cells enhances osteogenic activity, simulating the effect of magnesium alloy degradation. *Acta Biomater.* **10**, 2834–2842 (2014).

89. Kim, H.-K. *et al.* Comprehensive study on the roles of released ions from biodegradable Mg-5 wt% Ca-1 wt% Zn alloy in bone regeneration. *J. Tissue Eng. Regen. Med.* **11**, 2710–2724 (2017).

90. Hung, C. C., Chaya, A., Liu, K., Verdelis, K. & Sfeir, C. The role of magnesium ions in bone regeneration involves the canonical Wnt signaling pathway. *Acta Biomater.* **98**, 246–255 (2019).

91. Zreiqat, H. *et al.* Mechanisms of magnesium-stimulated adhesion of osteoblastic cells to commonly used orthopaedic implants. *J. Biomed. Mater. Res.* **62**, 175–184 (2002).

92. Park, J. W., Kim, Y. J., Jang, J. H. & Song, H. Osteoblast response to magnesium ion-

incorporated nanoporous titanium oxide surfaces. *Clin. Oral Implants Res.* **21**, 1278–1287 (2010).

93. Li, B. *et al.* In vitro and in vivo responses of macrophages to magnesium-doped titanium. *Sci. Rep.* **7**, 42707 (2017).

94. Wang, M. *et al.* Improved osteogenesis and angiogenesis of magnesium-doped calcium phosphate cement: Via macrophage immunomodulation. *Biomater. Sci.* **4**, 1574–1583 (2016).

95. Liu, D. *et al.* Activation of extracellular-signal regulated kinase (ERK1/2) by fluid shear is Ca2+- and ATP-dependent in MC3T3-E1 osteoblasts. *Bone* **42**, 644–652 (2008).

96. Lorenzo, J., Horowitz, M. & Choi, Y. Osteoimmunology: Interactions of the bone and immune system. *Endocr. Rev.* **29**, 403–440 (2008).

97. Riddle, R. C., Taylor, A. F., Genetos, D. C. & Donahue, H. J. MAP kinase and calcium signaling mediate fluid flow-induced human mesenchymal stem cell proliferation. *Am. J. Physiol. - Cell Physiol.* **290**, C776–C784 (2006).

98. Foreman, M. A., Gu, Y., Howl, J. D., Jones, S. & Publicover, S. J. Group III metabotropic glutamate receptor activation inhibits Ca2+ influx and nitric oxide synthase activity in bone marrow stromal cells. *J. Cell. Physiol.* **204**, 704–713 (2005).

99. Malhotra, A. & Habibovic, P. Calcium Phosphates and Angiogenesis: Implications and Advances for Bone Regeneration. *Trends Biotechnol.* **34**, 983–992 (2016).

100. Anitua, E., Tejero, R., Alkhraisat, M. H. & Orive, G. Platelet-Rich plasma to improve the bio-functionality of Biomaterials. *BioDrugs* **27**, 97–111 (2012).

101. Shiu, H. T., Goss, B., Lutton, C., Crawford, R. & Xiao, Y. Formation of Blood Clot on Biomaterial Implants Influences Bone Healing. *Tissue Eng. Part B Rev.* **20**, 697–712 (2014).

102. Maeno, S. *et al.* The effect of calcium ion concentration on osteoblast viability, proliferation and differentiation in monolayer and 3D culture. *Biomaterials* **26**, 4847–4855 (2005).

103. Hulsart-Billström, G. *et al.* A surprisingly poor correlation between in vitro and in vivo testing of biomaterials for bone regeneration: Results of a multicentre analysis. *Eur. Cells Mater.* **31**, 312–322 (2016).

104. Othman, Z., Cillero Pastor, B., van Rijt, S. & Habibovic, P. Understanding interactions between biomaterials and biological systems using proteomics. *Biomaterials* **167**, 191–204 (2018).

105. Zheng, K., Kapp, M. & Boccaccini, A. R. Protein interactions with bioactive glass surfaces: A review. *Appl. Mater. Today* **15**, 350–371 (2019).

106. Schmidt, D. R., Waldeck, H. & Kao, W. J. Protein Adsorption to Biomaterials. in *Biological Interactions on Materials Surfaces* (eds. Puleo, D. A. & Bizios, R.) 1–18 (Springer, 2009). doi:10.1007/978-0-387-98161-1

107. Swartzlander, M. D. *et al.* Linking the foreign body response and protein adsorption to PEG-based hydrogels using proteomics. *Biomaterials* **41**, 26–36 (2015).

108. Magnani, A. *et al.* Two-step elution of human serum proteins from different glass-modified bioactive surfaces: A comparative proteomic analysis of adsorption patterns. *Electrophoresis* **25**, 2413–2424 (2004).

109. Romero-Gavilan, F. *et al.* Proteomic analysis of silica hybrid sol-gel coatings: a potential tool for predicting the biocompatibility of implants *in vivo*. *Biofouling* **33**, 676–689 (2017).

110. Araújo Gomes, N. *et al.* Complement proteins regulating macrophage polarisation on biomaterials. *Colloids Surfaces B Biointerfaces* **181**, 125–133 (2019).

111. Wang, X., Schmidt, D. R., Joyce, E. J. & Kao, W. J. Application of MS-Based Proteomics to Study Serum Protein Adsorption/Absorption and Complement C3 Activation on Poly(ethylene glycol) Hydrogels. *J Biomater Sci Polym Ed.* **22**, 1343–1362 (2016).

112. Kim, C. S. *et al.* Proteomic analysis of the biological response of MG63 osteoblast-like cells to titanium implants. *Odontology* **102**, 241–248 (2014).

113. Henrionnet, C., Gillet, P., Mainard, D., Vincourt, J. B. & Pinzano, A. Label-free relative quantification of secreted proteins as a non-invasive method for the quality control of chondrogenesis in bioengineered substitutes for cartilage repair. *J. Tissue Eng. Regen. Med.* **12**, e1757–e1766 (2018).

114. Zhang, Z., Wang, J. & Lü, X. An integrated study of natural hydroxyapatite-induced osteogenic differentiation of mesenchymal stem cells using transcriptomics, proteomics and microRNA analyses. *Biomed. Mater.* **9**, (2014).

115. Yang, M. H. *et al.* Characterization of silk fibroin modified surface: A proteomic view of cellular response proteins induced by biomaterials. *Biomed Res. Int.* **2014**, (2014).

116. Othman, Z. *et al.* Comparative proteomic analysis of human mesenchymal stromal cell behavior on calcium phosphate ceramics with different osteoinductive potential. *Mater. Today Bio* **7**, 100066 (2020).

117. Omidi, M. *et al.* Investigation of the impact of magnesium: Versus titanium implants on protein composition in osteoblast by label free quantification. *Metallomics* **12**, 916–934 (2020).

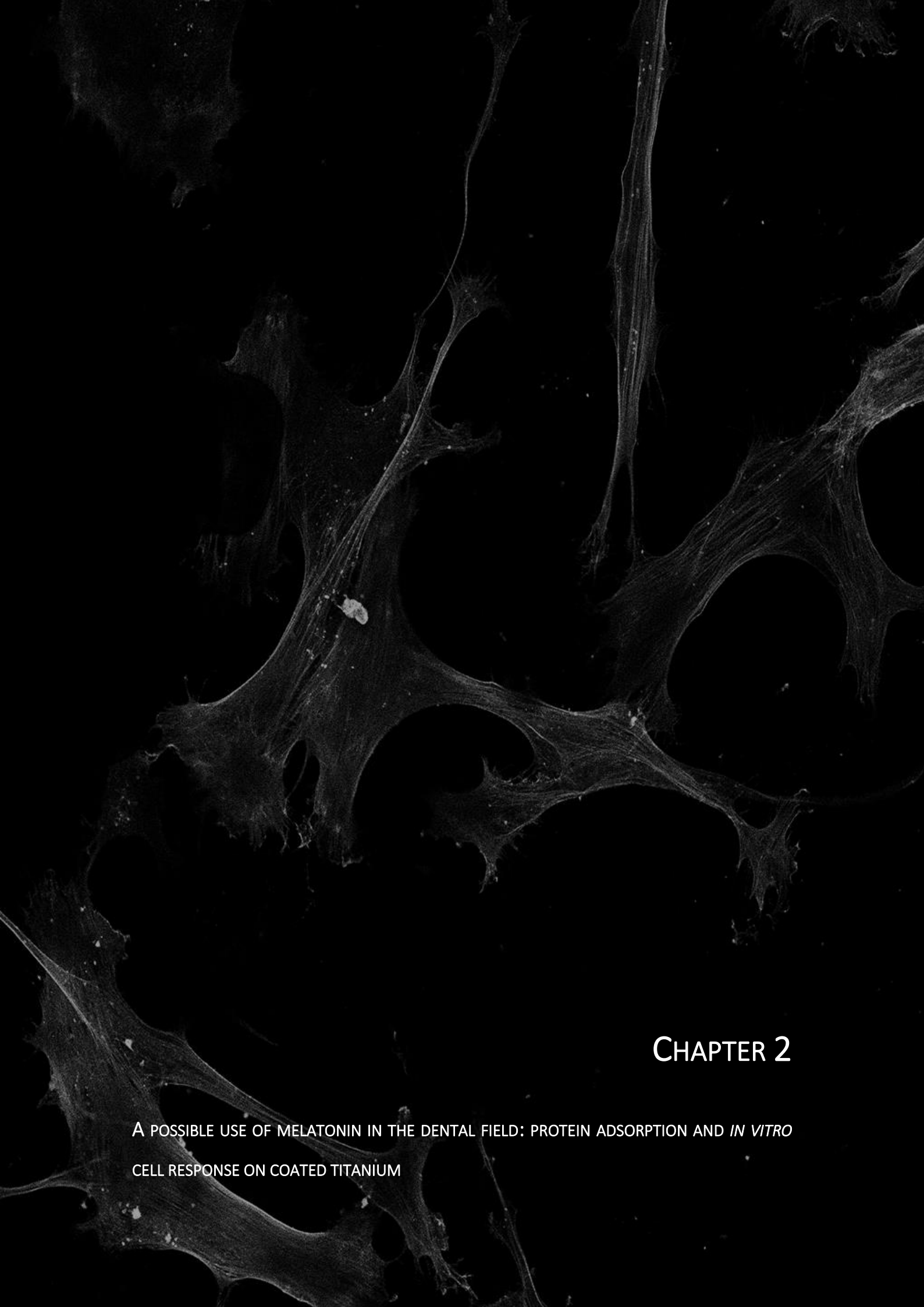

CHAPTER 2

A POSSIBLE USE OF MELATONIN IN THE DENTAL FIELD: PROTEIN ADSORPTION AND *IN VITRO* CELL RESPONSE ON COATED TITANIUM

CHAPTER 2

A POSSIBLE USE OF MELATONIN IN THE DENTAL FIELD: PROTEIN ADSORPTION AND *IN VITRO* CELL RESPONSE ON COATED TITANIUM

ARTICLE 1

Andreia Cerqueira[1], Francisco Romero-Gavilán[1], Nuno Araújo-Gomes[2], Iñaki García-Arnáez[3], Cristina Martinez-Ramos[4], Seda Ozturan[5], Mikel Azkargorta[6], Félix Elortza[6], Mariló Gurruchaga[3], Julio Suay[1], Isabel Goñi[3]

[1]Department of Industrial Systems Engineering and Design, Universitat Jaume I, Av. Vicent Sos Baynat s/n, 12071 Castellón de la Plana, Spain

[2]Department of Developmental Bioengineering, University of Twente, Faculty of Science and Technology, 7522LW, Enschede, The Netherlands

[3]Facultad de Ciencias Químicas, Universidad del País Vasco, P. M. de Lardizábal, 3, 20018 San Sebastián, Spain

[4]Center for Biomaterials and Tissue Engineering, Universitat Politècnica de Valencia, Camino de Vera, s/n 46022 Valencia, Spain

[5]Department of Periodontology, Faculty of Dentristy, Istambul Medeniyet University, Istanbul, Turkey

[6]Proteomics Platform, CIC bioGUNE, CIBERehd, ProteoRed-ISCIII, Bizkaia Science and Technology Park, 48160 Derio, Spain

Published at Materials Science and Engineering: C

Volume 116, November 2020, 111262

ABSTRACT

Melatonin (MLT) is widely known for regulating the circadian cycles and has been studied for its role in bone regeneration and inflammation. Its application as a coating for dental implants can condition the local microenvironment, affecting protein deposition on its surface and the cellular and tissue response. Using sol-gel coatings as a release vehicle for MLT, the aim of this work was to assess the potential of this molecule in improving the osseointegration and inflammatory responses of a titanium substrate. The materials obtained were physicochemically characterized (scanning electron microscopy, contact angle, roughness, Fourier-transform infrared spectroscopy, nuclear magnetic resonance, Si release, MLT liberation, and degradation) and studied *in vitro* with MC3T3-E1 osteoblastic cells and RAW264.7 macrophage cells. Although MLT application led to an increased gene expression of *RUNX2* and *BMP2* in 10MTL, it did not improve ALP activity. On the other hand, MLT-enriched sol-gel materials presented potential effects in the adsorption of proteins related to inflammation, coagulation and angiogenesis pathways depending on the dosage used. Using LC-MS/MS, protein adsorption patterns were studied after incubation with human serum. Proteins related to the complement systems (CO7, IC1, CO5, CO8A, and CO9) were less adsorbed in materials with MLT; on the other hand, proteins with functions in the coagulation and angiogenesis pathways, such as A2GL and PLMN, showed a significant adsorption pattern.

KEYWORDS

Osseointegration, hybrid sol-gel, inflammation, proteomics, coating, *N*-acetyl-5-metoxy-tryptamine

GRAPHICAL ABSTRACT

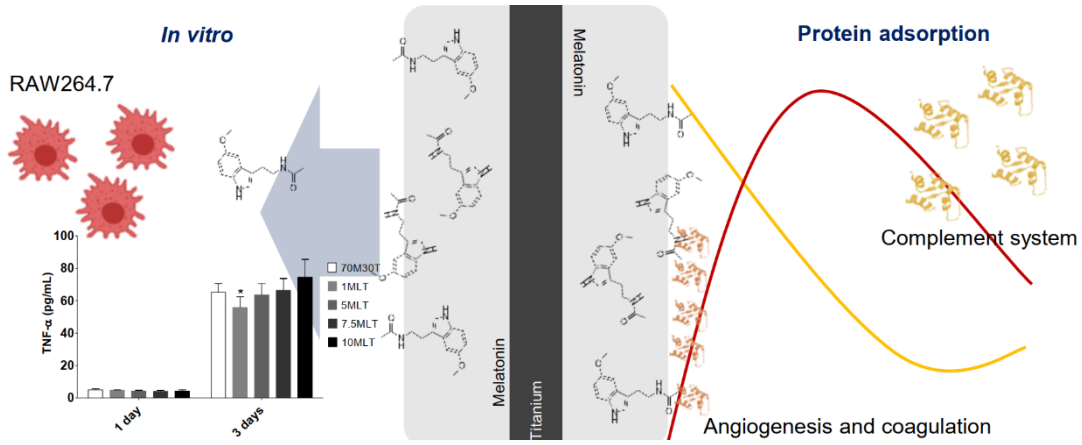

Figure 2.1. Graphical abstract of the paper "A possible use of melatonin in the dental field: protein adsorption and *in vitro* cell response on coated titanium"

2.1. INTRODUCTION

Dental implantations have become a standard procedure in oral rehabilitation, representing a reliable treatment with many advantages. However, implant failure still occurs, particularly in patients with poor osseointegration capability (*e.g.*, patients with osteoporosis), prompting the need for bioactive surfaces that accelerate this process [1].

Titanium (Ti) and its alloys are commonly used in dental implants due to their high degree of biocompatibility. However, these materials have the limitation of being relatively bioinert, and various methodologies are being studied to confer them bioactive properties. The sol-gel technique allows the synthesis of coatings to metal surfaces with a variety of functions, being an attractive method due to the use of mild reaction conditions, easily available precursors, and their potential as controlled release vehicles for ions and biomolecules [2]. Using modified alkoxysilanes as precursors, Martínez-Ibáñez et al. [3] obtained a sol-gel material by the mixture of methyltrimetoxisilane (MTMOS) and tetraethyl orthosilicate (TEOS), in a proportion of 70% MTMOS to 30% TEOS, presenting promising cellular *in vitro* behavior, with the improvement of the osseointegrative properties regarding the non-coated sand-blasted acid-etched titanium.

Melatonin (*N*-acetyl-5-metoxy-tryptamine; MLT), a widely known regulator of the circadian cycles produced by the pineal gland, has been described to play a major role on bone physiology through dual actions on osteoblasts and osteoclasts [4]. Previous studies [5–8] show that MLT upregulates the gene expression of *RUNX2*, *BMP2*, *BMP6*, and *OCN*, which have a pivotal role in osteoblast function and bone mineralization. On the other hand, MLT downregulates the expression of *RANKL* and upregulates *OPG*, leading to a restriction of osteoclast formation and increment of bone regeneration [9]. Additionally, MLT has been studied for its anti-inflammatory potential leading to the downregulation of *TNF-α*, *IL-1β*, *IL-6* [10,11], and *iNOS* [11,12], can either stimulate or inhibit angiogenesis [13,14], and it has an antioxidant potential [15]. Considering the effects of this molecule in bone and inflammatory responses, MLT has become a particularly attractive molecule to use in implants.

Upon implantation, blood/implant interactions lead to immediate protein adsorption onto the implant surface and consequently developing a provisional matrix on and around the biomaterial. The type, level, and surface conformation of the adsorbed proteins will determine the biological response and the ultimate implant outcome [16]. This adsorption is dependent on the surface properties of the material, such as wettability, roughness, and charge [17,18]. Thus, these parameters can ultimately have a determining role not only in the initial immune

responses but also in other processes, such as coagulation, fibrinolysis, and the earlier stages of osteogenesis [19].

In this work, a new sol-gel material doped with several percentages of MLT (1%, 5%, 7.5%, and 10%) to be applied as a coating onto titanium substrates was developed. Then, we proceeded to perform its physiochemical study, *in vitro* characterization with MC3T3-E1 osteoblasts and RAW 264.7 macrophages, and protein adsorption patterns evaluation using proteomics. The main goal was to evaluate the potential of MLT when applied to titanium substrates for future dental field use.

2.2. Materials and methods

2.2.1. Sol-gel synthesis and sample preparation

The sol-gel route was used to obtain hybrid coatings with different percentages of MLT (1%, 5%, 7.5%, and 10%) using MTMOS and TEOS (Sigma–Aldrich, Merck KGaA, Darmstadt, Germany) as precursors. The maximum concentration of MLT was based on preliminary studies, where it was verified that melatonin showed solubility problems in concentrations higher than 10%. The network contained 70 and 30% (molar percentages) of these precursors, respectively. Melatonin was dissolved in 2-Propanol (Sigma-Aldrich) and mixed with the precursors in a volume ratio (alcohol:siloxane) of 1:1. The hydrolysis of alkoxysilanes was carried out by adding (at a rate of 1-drop s^{-1}) the corresponding stoichiometric amount of aqueous solution of 0.1N HCl (Sigma-Aldrich). The preparations were kept under stirring for 1 h and then 1 h at rest. Afterward, grade-4 Ti discs (12-mm diameter, 1-mm thick) with a sandblasted acid-etched treatment as described by Romero-Gavilán et al. [19] were used as a coating substrate. SAE-titanium discs were coated with a dip-coater (KSV DC; KSV NIMA, Espoo, Finland). The discs were immersed in the sol-gel solutions at a speed of 60 cm min^{-1}, left immersed for one minute, and removed at a 100 cm min^{-1}. To measure hydrolytic degradation and silicon/MLT liberations, coatings were prepared using glass-slides as a substrate. These were previously cleaned in an ultrasonic bath (Sonoplus HD 3200) for 20 min at 30 W with a nitric acid solution (25% volume), and then, with distilled water under the same conditions. In addition, free films of distinct materials were obtained by pouring the sol-gel solutions into non-stick Teflon molds in order to carry out their chemical characterization. Finally, all samples were cured for 2 h at 80°C.

2.2.2. Physicochemical characterization

To evaluate how surface topography was modified by MLT incorporation, scanning electron microscopy (SEM) with a Leica–Zeiss LEO equipment under vacuum (Leica, Wetzlar, Germany)

was used. Before observation, the materials were treated with platinum sputtering to increase their conductivity. To measure surface roughness, an optical profilometer (interferometric and confocal) PLm2300 (Sensofar, Barcelona, Spain) was used in three discs of each material. For each disc, three measurements were done to calculate the average values of the Ra parameter. The contact angle was measured using an automatic contact angle meter OCA 20 (DataPhysics Instruments, Filderstadt, Germany). An aliquot of 10 µL of Milli-Q water was deposited on the disc surface at a dosing rate of 27.5 µL s^{-1} at room temperature. Contact angles were determined using the SCA 20 software (DataPhysics Instruments, Filderstadt, Germany). Six discs of each material were studied after depositing two drops on each disc.

To chemically characterize all materials, Fourier Transform Infrared Spectroscopy (FTIR; Thermo Nicolet 6700) was carried out with an attenuated total reflection system (ATR). The spectra were measured in the 4000 and 400 cm^{-1} wavelength range. Solid-state silicon nuclear magnetic resonance spectroscopy (^{29}Si-NMR; Bruker 400 Avance III WB Plus) with a probe for solid samples of ICP-MS was used to evaluate the crosslinking degree of the obtained silicon networks. The pulse sequence for the analysis was the Bruker standard: 79.5 MHz frequency, the spectral width of 55 kHz, 2 ms contact time, and 5 s delay time. The spinning speed was 7.0 kHz. Hydrolytic degradation was evaluated by sample measuring weight loss before and after soaking them in 50 mL of distilled water (ddH_2O) at 37°C during 1, 2, 4, and 8 weeks. The degradation of the coatings was registered by percentage (%) of mass lost in reference to the initial weight. Each data point is the average of three measurements performed in three different samples identically prepared.

To determine Si release, samples were incubated in 50 mL of Milli-Q water at 37ºC during 1, 2, 4, and 8 weeks. At these measuring points, aliquots of 50 µL were taken and measured using inductively coupled plasma mass spectrometry (ICP-MS, Agilent 7700). To measure MLT release, coated glass slides were submerged in 50 mL of Milli-Q water at 37°C. At 0, 1, 3, 5, 8, 24, 48, 72, 96, 168, and 336 hours the absorbance was measured at 222 nm (wavelength characteristic of MLT [20]) with a Helios Omega UV-VIS (Thomas Scientific, New Jersey, USA). The measurements were carried out in triplicate.

2.2.3. *IN VITRO* ASSAYS

2.2.3.1. *Cell culture*

Mouse calvaria osteosarcoma MC3T3-E1 cells and mouse murine macrophage RAW 264.7 cells were cultured in at 37°C in a humidified (95%) CO_2 incubator in Dulbecco's Modified Eagle Medium (DMEM; Gibco, Life Technologies, Grand Island, NY, USA) supplemented with 1%

penicillin/streptomycin (Biowest Inc., USA) and 10% FBS (Gibco, Life Technologies). After 24h, the MC3T3-E1 cells medium was replaced by osteogenic medium composed of DMEM, 1% of penicillin/streptomycin, 10% FBS, 1% ascorbic acid (5 mg mL^{-1}) and 0.21% β-glycerol phosphate. The culture medium was changed every other day. In each plate, wells with only cells were used as a control of culture conditions.

2.2.3.2. *Cytotoxicity*

Biomaterial cytotoxicity was assessed following the ISO 10993-5:2009 (Annex C) norm. MC3T3-E1 cells ($1x10^5$ cells cm^{-2}) were seeded on 96-well NUNC plates (Thermo Fisher Scientific, Waltham, MA, USA) for 24 h. The materials were also incubated for 24 h in 48-well NUNC plates (Thermo Fisher Scientific) in DMEM with 1% of penicillin/streptomycin and 10% FBS. Then, the cell culture medium was replaced with the medium exposed to the materials followed by an incubation of 24 h. To measure cell viability, the CellTiter 96® Proliferation Assay (MTS) (Promega, Madison, WI) was used according to manufacturer's guidelines. As a negative control, wells with only cells were used. As a positive control, cells were incubated in latex, a compound well known for being cytotoxic. The material was considered cytotoxic when presented cell viability below 70%.

2.2.3.2. *Cell proliferation*

To measure the effects of the biomaterials in cell proliferation, the alamarBlue™ cell viability reagent (Invitrogen, Thermo Fisher Scientific) was used. MC3T3-E1 cells were cultured in 24-well NUNC plates (Thermo Fisher Scientific) at a density of $3.5x10^4$ cells cm^{-2}. After culturing for 1, 3, and 7 days, cell proliferation was evaluated following the manufacturer's protocol. Additionally, an essay without cells was carried out to verify that the tested materials did not affect the alamarBlue™ cell viability reagent.

2.2.3.4. *Alkaline phosphatase activity assay*

To evaluate the effects of the materials in the mineralization capability of osteoblastic cells, the conversion of *p*-nitrophenylphosphate (*p*-NPP) to *p*-nitrophenol was used to assess the alkaline phosphatase (ALP) activity. MC3T3 cells were seeded onto the distinct surfaces in 24-well NUNC plates (Thermo Fisher Scientific) at a density of $3.5x10^4$ cells cm^{-2}. After culturing for 14 and 21 days, cells were rinsed twice with Dulbecco's phosphate-buffered saline (DPBS; Thermo Fisher Scientific), immersed in lysis buffer (0.2% Triton X-100, 10 mM Tris-HCl, pH 7.2) and incubated at 4°C for 10 minutes. Following centrifugation (7 min, 14000 rpm, 4°C), 100 µL of *p*-NPP (1mg mL^{-1}) in substrate buffer (50 mM glycine, 1 mM $MgCl_2$, pH 10.5) was added to 100 µL of the

supernatant. After 2 h of incubation in the dark (37°C, 5% CO_2), the absorbance at 405 nm was measured using a microplate reader. Alkaline phosphatase activity was calculated using a *p*-nitrophenol in 0.02 mM sodium hydroxide standard curve. A Pierce BCA assay kit (Thermo Fisher Scientific) was used to calculate total protein content in the sample and to normalize ALP levels. The experiment was carried out in triplicate.

2.2.3.5. *RNA extraction and cDNA synthesis*

To evaluate the effects on the gene expression of osteogenic and inflammatory targets, MC3T3-E1 cells were seeded on the discs in 48-well NUNC plates (Thermo Fisher Scientific) at a density of $3.5x10^4$ cells cm^{-2} for 7 and 14 days. RAW264.7 were seeded at a density of $30x10^4$ cells cm^{-2} for 1 day and $1.5x10^4$ cells cm^{-2} for 3 days. In each plate, wells without any material were used as control of culture conditions. Total RNA was extracted using TRIzol (1M guanidine thiocyanate, 1M ammonium thiocyanate, 3M sodium acetate, 5% glycerol, 38% aquaphenol). Briefly, 300 µL of TRIzol were added to the samples, and then they were incubated at room temperature for 5 min. Following centrifugation (5 min, 13000 rpm, 4°C), the supernatant was transferred, 200 µL of chloroform were added, and the samples were centrifuged (5 min, 13000 rpm, 4°C). The aqueous layer was mixed with 550 µL of isopropanol and kept at room temperature for 10 min. Samples were centrifuged (15 min, 13000 rpm, 4°C) and washed twice with 0.5 mL of 70% ethanol. The resulting pellet was dissolved in 30 µL of RNAse free water. RNA concentration, integrity, and quality were measured using NanoVue® Plus Spectrophotometer (GE Healthcare Life Sciences, Little Chalfont, UK). For cDNA synthesis, approximately 1 µg of total RNA was converted into cDNA using PrimeScript RT Reagent Kit (Perfect Real Time; TAKARA Bio Inc., Shiga, Japan) in a reaction volume of 20 µL. The reaction was conducted with the following conditions: 37°C for 15 min, 85°C for 5 secs, and a final hold at 4°C. The resulting cDNA quality and concentration were measured using a NanoVue® Plus Spectrophotometer (GE Healthcare Life Sciences), then diluted in DNAse-free water to a concentration suitable for reliable qRT-PCR analysis and stored at -20°C until further analysis. The experiment was carried out in quadruplicate.

2.2.3.6. *Quantitative real-time PCR*

Quantitative real-time PCRs (qRT-PCR) were carried out on 96-well plates (Applied Biosystems®, Thermo Fisher Scientific) with each sample represented by the gene of interest and one housekeeping gene (*glyceraldehyde phosphate dehydrogenase* (GAPDH)). Primers for each gene were designed using PRIMER3plus software tool (http://www.bioinformatics.nl/cgi-bin/primer3plus/primer3plus.cgi) from specific DNA sequences obtained from NCBI

(https://www.ncbi.nlm.nih.gov/nucleotide/) and purchased to Thermo Fischer Scientific. Targets studied are shown in **Table 2.1**. Individual reactions contained 1 µL of cDNA, 0.2 µL of specific primers (forward and reverse at a concentration of 10 µM L^{-1}) and 5 µL of SYBR Premix Ex Taq (Tli RNase H Plus; TAKARA) in a final volume of 10 µL. Amplification efficiency was analyzed before qRT-PCR to optimize measurements. Reactions were carried out in a StepOne Plus™ Real-Time PCR System (Applied Biosystems®, Thermo Fisher Scientific) at 95°C for 30s, followed by 40 cycles of 95°C for 5s, 60°C for 34s, 95°C for 15s and 60°C for 60s. The data were obtained using the StepOne Plus™ Software 2.3 (Applied Biosystems®, Thermo Fisher Scientific). Fold changes were calculated using the $2^{-\Delta\Delta}$Ct method and the data was normalized in relation to the blank wells (without any material). Six technical replicates for each sample were measured.

Table 2.1. Quantitative real-time PCR primer sequence.

Gene symbol	Sequence	Accession number	Product length
	Housekeeping		
GAPDH	F: TGCCCCCATGTTTGTGATG R: TGGTGGTGCAGGATGCATT	XM_017321385	83
	MC3T3-E1		
BGLAP	F: AAGCAGGAGGGCAATAAGGT R: TGCCAGAGTTTGGCTTTAGG	NM_001032298	212
RUNX2	F: CCCAGCCACCTTTACCTACA R: TATGGAGTGCTGCTGGTCTG	NM_001271631	150
BMP2	F: CCCCAAGACACAGTTCCCTA R: GAGACCGCAGTCCGTCTAAG	NM_007553	169
	RAW264.7		
IL1BETA	F: GCCCATCCTCTGTGACTCAT R: AGGCCACAGGTATTTTGTCG	NM_008361	230
TNFALFA	F: AGCCCCCAGTCTGTATCCTT R: CTCCCTTTGCAGAACTCAGG	NM_001278601	212
EGR2	F: CAGGAGTGACGAAAGGAAGC R: ATCTCACGGTGTCCTGGTTC	NM_001373987	202

2.2.3.7. *Cytokine quantification by ELISA*

To evaluate the influence of the materials in tumor necrosis factor (TNF)-α and interleukin 4 (IL-4) production, RAW264.7 cells were seeded in 48-well NUNC plates (Thermo Fisher Scientific) a density of $30x10^4$ cells cm^{-2} for 1 day and $1.5x10^4$ cells cm^{-2} for 3 days. Then, the cell culture media was collected and frozen until further analysis. The concentration of these cytokines was determined using an ELISA (Invitrogen, Thermo Fisher Scientific) kit and according to the manufacturer's instructions.

2.2.4. ADSORBED PROTEIN LAYER

For obtaining the proteins adsorbed by the material surface, discs doped with MLT were incubated for 3 h (37 °C, 5% CO_2) in 24-well NUNC plates (Thermo Fisher Scientific) with 1 mL of human blood serum from male AB plasma (Sigma–Aldrich). After incubation, the serum was removed and the discs were washed five times with ddH_2O and once with 100 mM NaCl, 50 mM Tris–HCl, pH 7.0 to eliminate non-adsorbed proteins. The materials were washed once with an elution (0.5 M triethylammonium bicarbonate buffer (TEAB), 4% of sodium dodecyl sulfate (SDS), 100 mM of dithiothreitol (DTT)) to obtain the adsorbed protein layer. The analysis was made in four independent replicates and each replicate was a pool of four discs. A Pierce BCA assay kit (Thermo Fisher Scientific) was used to calculate total protein content in the serum.

2.2.5. PROTEOMIC ANALYSIS

Proteomic analysis was performed as described by Romero-Gavilán *et al.* [19] with slight modifications. Briefly, the eluted protein was digested in-solution, following the FASP protocol established by Wiśniewski *et al.* [21], and loaded onto a nanoACQUITY UPLC system (Waters, Milford, MA, USA) connected online to a mass spectrometer (Thermo Fisher ScientificEach material was analyzed in quadruplicate. Differential protein analysis was carried out using Progenesis software (Nonlinear Dynamics, Newcastle, UK), and the functional annotation of the proteins was performed using DAVID Go annotation program (https://david.ncifcrf.gov/) and PANTHER classification system (http://www.pantherdb.org/).

2.2.6. STATISTICAL ANALYSIS

Based on the normal distribution and equal variance assumption test, the data were analyzed via a one-way analysis of variance (ANOVA) with a Newman-Keuls post hoc test. Results were expressed as mean ± standard deviation (SD). Statistical analysis was performed using GraphPad Prism 5.04 software (GraphPad Software Inc., La Jolla, CA, USA). The differences between

70M30T (control group) and 70M30T with different concentrations of MLT (experimental group) were considered statistically significant at $p \leq 0.05$ (*), $p \leq 0.01$ (**), and $p \leq 0.001$ (***).

2.3. RESULTS

2.3.1. PHYSICOCHEMICAL CHARACTERIZATION

The sol-gel materials with MLT were successfully synthesized and well-adhering coatings were obtained as it can be observed in SEM micrographs (**Figure 2.2**). In these images, it can be observed that the sol-gel material has completely covered the Ti surface. Furthermore, the coatings seem to have smoothed the initial morphology of the SAE treatment, accumulating more sol-gel in the irregularities caused by the previous sandblasting. **Figure 2.2g** displays the contact angle measurements. With the addition of MLT to 70M30T, there was a significant increase in the contact angle in a dose-response manner. Regarding the roughness, with the incorporation of MLT, there was an increase of Ra when compared to 70M30T; however, there were no statistical differences between the coatings with a distinct amount of MLT (**Figure 2.2h**).

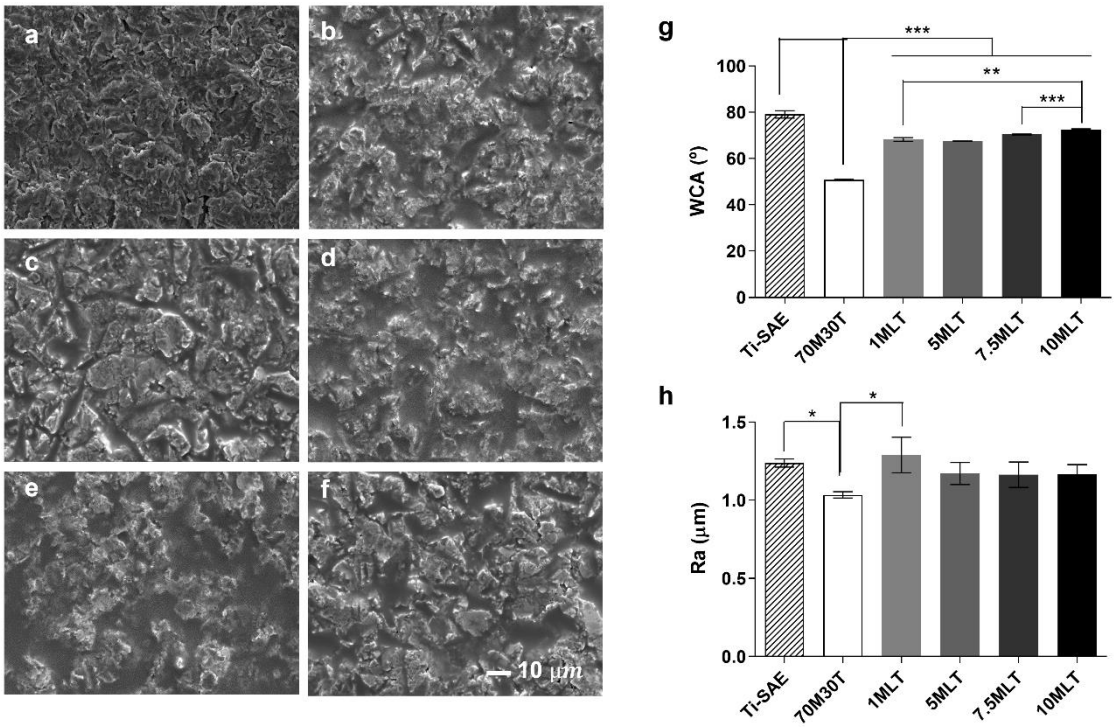

Figure 2.2. SEM microphotograph of Ti-SAE (a), 70M30T (b), 1MLT (c), 5MLT (d), 7.5MLT (e) and 10MLT (f) and contact angle (WCA; g) and average roughness (Ra; h). Results are shown as mean ± SD. The asterisks ($p \leq 0.05$ (*), $p \leq 0.01$ (**) and $p \leq 0.001$ (***)) indicate statistical differences in relation to 70M30T without melatonin (MLT).

2.3.2. FT-IR ANALYSIS

Sol-gel materials with different percentages of MLT were chemically characterized using FT-IR. The obtained spectra are shown in **Figure 2.3a**. All samples presented bands between 400 and 1200 cm^{-1}. The hydrolysis-condensation reaction was correctly carried out, as it was detected the presence of siloxane chain characteristic signals. The bands with the Si-O-Si appear proximally at 1090 cm^{-1} (asymmetric tension [22]), 770 cm^{-1} and 440cm^{-1} (symmetrical tension and vibration of deformation [23]). However, the condensation was not complete as bands at 970 cm^{-1} and 540 cm^{-1} related to the Si-OH bond of silanol groups were detected. The band related to the OH groups was observed around 3400 cm^{-1} and can be associated with the presence of water in the sol-gel structure [24]. The bands around 3000 cm^{-1} indicate the presence of C-H bonds [24], corresponding to the organic part of the MTMOS that has a methyl group (non-hydrolyzable). The band is composed of two peaks corresponding to vibrations of asymmetrical and symmetrical tension of the bond C-H. The bond associated with the Si-CH_3 group appears around 1275 cm^{-1} [25]. These methyl-associated signals show that the integrity of organic species has been maintained after processing. All identified signals are maintained and display similar intensity when the MLT is incorporated into the sol-gel. However, the materials with MLT show bands between 1500-1600 cm^{-1}, which corresponds to the CO group present in this molecule [26]. In addition, the spectra of these materials show bands at 1610 cm^{-1} and 1555 cm^{-1}, which correspond to N-H and C-N bounds present in MLT, correspondingly [23]. The intensity of these bands is slightly more intense as the amount of melatonin increases.

Figure 2.3b represents ^{29}Si solid NMR spectra of 70M30T and 70M30T supplemented with MLT. These spectra show T^n signals from MTMOS and Q^n signals from TEOS. The MTMOS spectra show T^2 and T^3 signals with higher intensity of T^3. Additionally, the spectra show Q^3 and Q^4 from TEOS, with a signal more intense in Q^3. It seems that the addition of MLT to the sol-gel network did not affect the final crosslinking degree of structure.

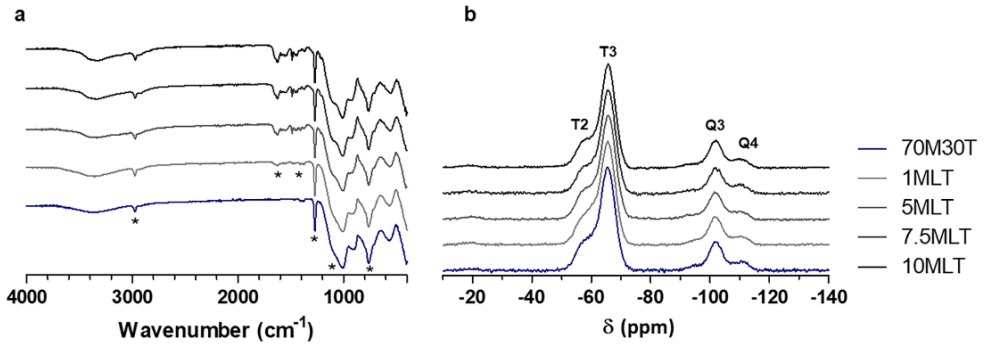

Figure 2.3. FT-IR spectra (a) and Si-NMR (b) of 70M30T with different concentrations of melatonin (MLT).

2.3.3. HYDROLYTIC DEGRADATION

Figure 2.4a shows the hydrolytic degradation (mass loss) of all materials for 56 days. All materials degraded and showed a significant mass loss during the first seven days. During the following days and until the end of the experiment, all materials lost weight in a more gradually. In the case of 70M30T, the mass loss was small (up to 16%), while the materials with MLT showed a higher weight loss. In these coatings, the degradation increased as the percentage of MLT in the network increased. Thus, the 10MLT showed the highest degradation in all materials studied.

2.3.4. SILICON AND MELATONIN LIBERATION

Figure 2.4b shows the liberation of silicon (Si released in mg L^{-1}) of all materials in the study. All materials showed a significant Si liberation during the first week. The base material 70M30T and 1MLT presented a similar liberation rate, reaching its maximum at 3 weeks. For the rest of the materials, the liberation was more gradual over the two months of the assay. Similarly, to the hydrolytic degradation, the material with a higher concentration of MLT released more Si (12.5 mg Si L^{-1} in 10MLT in two months of assay). **Figure 2.4c** shows MLT liberation for all materials. In similarity to the previously described parameters, MLT release showed a dose-response rate *i.e.,* the material with the highest percentage (10MLT) presented the highest liberation of MLT. Considering the liberation kinetics, MLT was released faster in the first 72 h and, for this time point onward, it had a liberation rate almost constant until the end of the assay (336 h) in all materials.

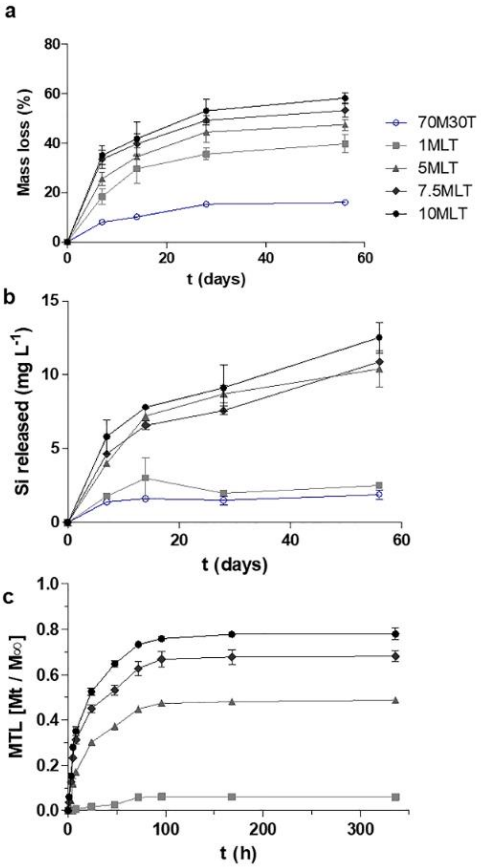

Figure 2.4. Hydrolytic degradation (a) of the sol-gel coating and kinetic liberation of silicon (b) and MLT (c) from the sol-gel coating through time.

2.3.5. *IN VITRO* ASSAYS

2.3.5.1. *Cytotoxicity, cell proliferation, and ALP activity*

Neither of the materials in the study was cytotoxic (data not shown). Cell proliferation and ALP activity assays did not show significant differences between the 70M30T with or without melatonin (**Figure 2.5**) in any measuring points.

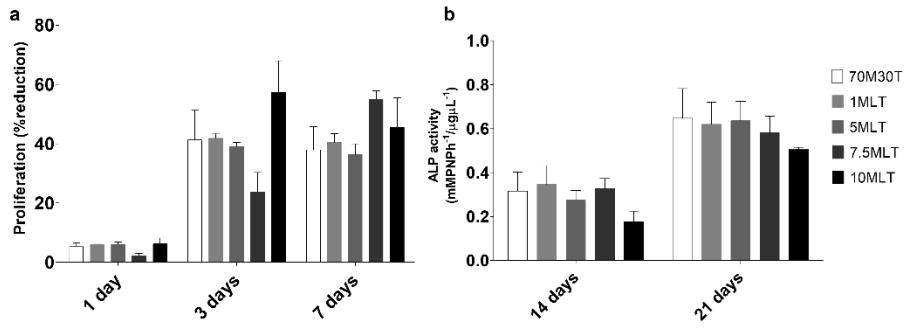

Figure 2.5. MC3T3-E1 *in vitro* assays: (a) cell proliferation at 1, 3, and 7 days and (b) ALP activity at 14 and 21 days. Results are shown as mean ± SD.

2.3.5.2. *Relative gene expression*

The expression of osteogenic and inflammation markers of the MC3T3-E1 and RAW264.7 cells cultured onto the distinct formulations is shown in **Figure 2.6**. After 14 days, all materials with MLT show a significant decrease in *BGLAP* expression (**Figure 2.6a**). On the other hand, *RUNX2* and *BMP2* expression showed an increase in 10MLT at 7 days. At 14 days, *RUNX2* expression increased in 10MLT, while *BMP2* expression decreased in all materials (**Figure 2.6b and c**). The expression of *IL-1β* and *TNF-α* showed no differences in any material at both time points (**Figure 2.6d and e**). In the *ERG2* expression, there was an increase in 7.5MLT at 1 day, while all materials showed a significant decrease at 3 days (**Figure 2.6f**).

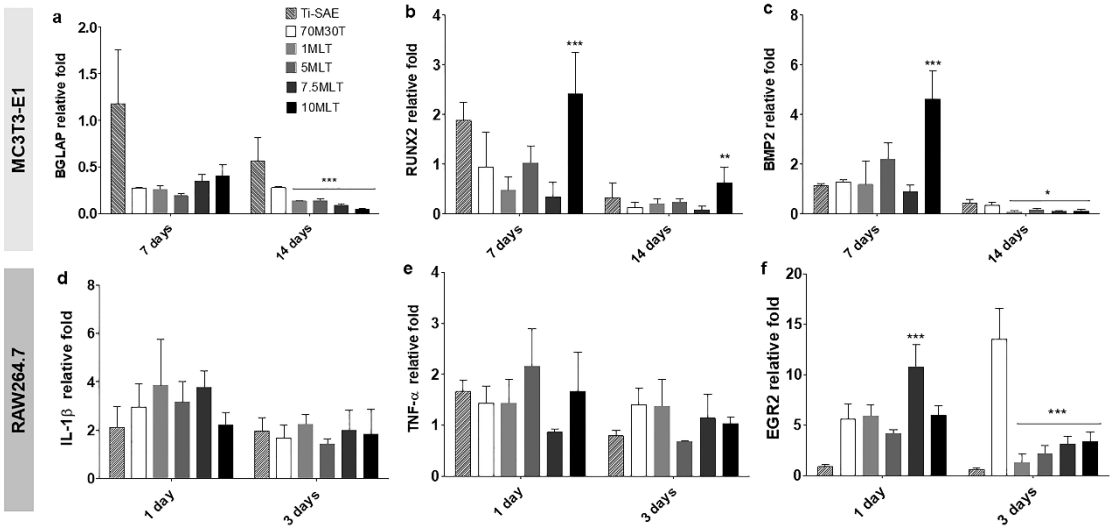

Figure 2.6. Relative gene expression of osteocalcin (*BGLAP*; a), runt-related transcription factor 2 (*RUNX2*; b), and bone morphogenetic protein (*BMP2*; c) in MC3T3-E1 at 7 and 14 days and interleukin- 1β (*IL-1β*; d), tumor necrosis α (*TNF-α*), and early growth response protein 2 (*EGR2*; f) in RAW264.7 at 1 and 3 days. Results are shown as mean ± SD and were normalized to the wells without materials (bottom of cultivation plate). The asterisks ($p \leq 0.05$ (*) and $p \leq 0.001$ (***)) indicate statistical differences in relation to 70M30T without melatonin (MLT).

2.3.5.3. *Cytokine quantification by ELISA*

To evaluate the effect of the materials with MLT on the inflammatory response, the secretion of anti (IL-4) and pro-inflammatory (TNF-α) cytokines by RAW264.7 macrophage was quantified at 1 day and 3 days. The secretion of IL-4 did not show differences at any of the times measured in any of the materials tested (**Figure 2.7a**). In the case of TNF-α, the profile was similar at 1 day for all materials (**Figure 2.7b**). After 3 days of culture, there is a general increase in the

production of this cytokine; however, is significantly lower in 1% MLT when compared to the 70M30T coating.

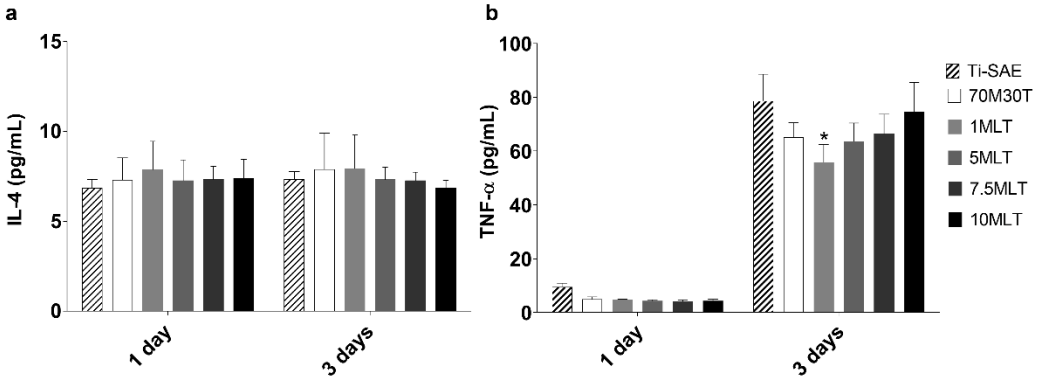

Figure 2.7. Cytokine quantification by ELISA in RAW264.7 at 1 and 3 days: (a) interleukin-4 (IL-4) and (b) tumor necrosis α (TNF-α). Results are shown as mean ± SD. The asterisk ($p \leq 0.05$ (*)) indicates statistical differences in relation to 70M30T without melatonin (MLT).

2.3.6. PROTEOMIC ANALYSIS

The eluted proteins were analyzed by LC-MS/MS, followed by identification with Progenesis QI software and DAVID system. Comparing MLT-enriched and the base sol-gel material, 26 proteins were differentially absorbed in the materials with MLT (**Supplementary Table 2.1**). The formulation with 10MLT shows the higher amount of differently absorbed proteins, with 16 proteins being less adsorbed onto its surface and five showing more affinity. Among the proteins with decreased adsorption, five are related to the complement system (CO7, IC1, CO5, CO8A, and CO9). On the other hand, these surfaces lead to higher adsorption with CXCL7, which plays a crucial role in neutrophil recruitment. Also related to immunological responses, the surface 1MLT and 5MLT showed a higher affinity with IGHA2, while 7.5MLT differentially absorbed CO5, IC1, CO8A, and CXCL7. The glycoproteins VTCN and SEPP1 were significantly less adsorbed in the material with 10MLT, while HEMO show higher affinity with the materials with 1MLT, 5MLT, and 10MLT. VTNC is known to inhibit/regulate the complement system activation. Depending on the concentration of MLT, the materials adsorbed fewer apolipoproteins (APOA-I, APOF, APOL1, and APOC4) and PON1. These proteins are related to the metabolism of high-density lipids. Regarding the coagulation process, HRG, HBB, PLMN, and KLKB1 were differentially adsorbed: HRG was more adsorbed in 1MLT, while KLKB1 was more adsorbed in 5MLT. In 7.5MLT and 10MLT proteins related to this process presented less affinity with these materials. Additionally, all materials except 7.5MLT showed a differential affinity with A2GL, a protein-related with the angiogenesis processes. The materials 1MLT and 5MLT adsorbed more of this protein, while

10MLT adsorbed less. ITIH2, ITIH4, and ITHI1, proteins from the inter-α-trypsin inhibitor family related to the hyaluronan metabolic process, were less adsorbed in the materials with 10MLT. ATPA, a mitochondrial membrane complex that produces ATP from ADP, was significantly more adsorbed in 1MLT. **Table 2.2** summarizes the most relevant proteins related to immune responses, coagulation, and angiogenesis processes found differentially absorbed onto each material surface.

PANTHER analysis was used to associate the differentially adsorbed proteins with their functions in distinct biological pathways. **Figure 2.8** shows pie-chart diagrams of the biological processes related to the proteins differentially adsorbed onto each surface when compared with 70M30T without MLT. ATP synthesis, blood coagulation, plasminogen activation, and B cell activation where the cascades identified and varied according to the concentration of MLT employed. In general, all materials showed less adsorbed proteins associated with blood coagulation, plasminogen activation; also, at higher concentrations of MLT (7.5 and 10), there was a general decrease of proteins associated with B cell activation pathways. Only the materials 1MLT and 5MLT showed significantly higher adsorption of proteins associated with the biological process: ATP synthesis (1MLT) and blood coagulation (5MLT).

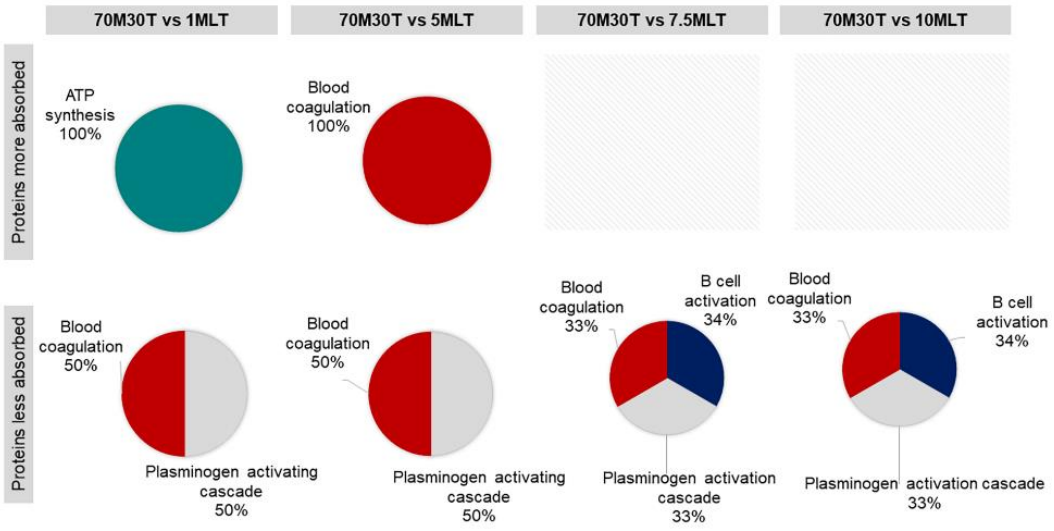

Figure 2.8. PANTHER diagram of the pathways associated with the proteins differentially adherent to MLT enriched coatings in comparison with 70M30T without MLT.

Table 2.2. Summary of the proteins of interest differentially adsorbed related to the immune, coagulation, and angiogenesis process differentially adsorbed onto each material surface when compared with 70M30T without MLT. MLT/70M30T ratios are shown between parentheses; red indicates more adsorbed, and green indicates less adsorbed.

70M30T *vs* 1MLT	**70M30T *vs* 5 MLT**	**70M30T *vs* 7.5 MLT**	**70M30T *vs* 10 MLT**
Immune			
IGHA2 (2.56)	IGHA2 (2.83) CXCL7 (1.65)	CO5 (0.66) CO8A (0.66) CXCL7 (2.67)	CO7 (0.46) IC1 (0.49) CO5 (0.57) VTNC (0.64) CO9 (0.66) CXCL7 (2.45)
Angiogenesis and coagulation			
HRG (1.60) A2GL (3.48)	A2GL (4.46) KLKB1 (2.91)	HBB (0.63)	HRG (0.36) A2GL (0.43) HBB (0.46) PLMN (0.51)

2.4. Discussion

In oral rehabilitation, dental implants have become a common procedure with many advantages. However, there is a need for bioactive surfaces that accelerate osseointegration because failure still occurs in patients somehow compromised. These surfaces can be obtained with a battery of techniques, such as sol-gel, and allow the usage of a diversity of biomolecules such as MLT. Melatonin has a wide variety of biological actions and its well-described properties have made it an attractive molecule for application in delivery systems in dentistry and regenerative medicine [27]. Considering this, the aim of the study was to develop a sol-gel coating (70M30T) supplemented with different percentages of MLT and characterize its effects in osteoblastic and immune cells, which are essential to determinate implant outcome.

The incorporation of MLT onto the 70M30T base introduced physicochemical changes in the surface properties, such as wettability. The contact angle significantly increased in relation to the base regardless of the concentration of MLT, surely by the organic character of this molecule. Regarding the material roughness, there is only a significant increase when comparing 70M30T with 1MLT. The ^{29}Si solid NMR shows that the incorporation of MLT did not affect the formation of the sol-gel network and FTIR analysis shows that it is present in the material. The hydrolytic degradation and the Si release increased in a dose-response manner with the amount of MLT incorporated in the network. This can be related to the liberation of MLT that also presented an increasing dose-response pattern depending on the amount of MLT initially added into the

coating. The measured release kinetics can help to understand how melatonin is going to be released *in vitro* from different materials, although the complexity of the medium employed for these essays may affect this liberation.

In cancer cells, the inhibitory effect of this MLT on cell proliferation is well documented [28]. In osteoblasts (hFOB 1.19), MLT showed an inhibitory effect on proliferation in a time-dependent manner, acting in genes related to the cell division cycle [29]. Zhang *et al.* [20] showed that MLT encapsulated in PLGA microspheres does not affect the proliferation of hMSCs at 1, 3, and 6 days, which is in accordance with our results. To understand how MLT affects the mineralization of osteoblasts, ALP activity assay was performed. Our results show that MLT did not significantly affect ALP activity at 14 and 21 days. Previous studies have shown MLT can increase ALP activity in MC3T3-E1 at 14 days [30] or with 50 nM of MLT for 3 days [8]; however, these findings are for when cultures are directly treated with the compound and at short times of incubation (< 14 days) with MLT. On the other hand, Zhang *et al.* [20] presented a significantly higher ALP activity in MLT encapsulated microspheres at 12 days. In what concerns gene expression, our results show an increase in *BMP2* and *RUNX2* expression in 10MTL. These markers have important roles in osteoblast differentiation, and previous works [4,8,31] showed that MLT can lead to their upregulation. However, further studies are needed to understand how MLT affects cells in long-term exposition (> 14 days) and how the incorporation in distinct release vehicles affects its action.

The LC-MS/MS characterization of the protein layers identified 26 proteins that were differentially absorbed in the materials with MLT. How and which proteins were adsorbed onto each surface depended on the amount of MLT incorporated on the sol-gel network. These proteins have functions associated with distinct biological pathways as shown in the PANTHER analysis. Apolipoproteins APOA-I, APOF, APOL1, and APOC4 were generally less adsorbed onto the surfaces with MLT. These proteins are known for their role in the metabolism of lipids, this protein family might also play a role in inhibiting complement system activation [32]. APOA-I is a major component of HDL that has been shown to inhibit LPS induced release of cytokines in monocytes [33], revealing an anti-inflammatory potential.

In addition, it was found differential adsorption of complement system proteins. In the materials with 7.5MLT and 10MLT, we could observe a decrease in the adsorption of complement C5 (CO5), complement component C8 alpha chain (CO8A), complement component (CO7) and component complement (CO9). The activation of C5 initiates an assembly with late-phase complement components, such as C6, C7, C8, and C9, leading to the formation of C5-C9 complex,

a multimolecular structure that leads to the formation of the lytic complex that will be responsible for the target cell lysis [34]. This is in agreement with the analysis PANTHER, which shows that the proteins less adsorbed by these materials have functions associated with B cell activation. The distinct complement pathways originate C3 and C4 fragments, which bind to complement receptors CD21 and CD35, whose co-expression is limited to B cells and leads to the enhancement of the activity of these cells [35,36]. On the other hand, vitronectin (VTNC) was less adsorbed in the materials with 10MLT. This protein has been described as an inhibitor of complement system action in bodily fluids [37]. Thus, the lower adsorption of complement proteins associated with the lower adsorption of VTNC can explain how the release of TNF-α and IL-4 cytokines by macrophage in contact with the 10MLT showed no statistical differences with respect to the base coating. Although, the anti-inflammatory potential of MLT is well described [11,38,39], its application in biomaterials can be dependent on the amount of hormone released by the material over time, and further studies are needed.

Coagulation and angiogenesis are key processes in bone regeneration. Proteomic analysis showed that MLT enriched materials differently adsorbed proteins related to both of these processes. In this sense, A2GL, a protein implicated in angiogenesis [40], was found to be more adsorbed onto the coatings 1MLT and 5MLT, but then, reduced its affinity with respect to the base material when 10% of MLT was incorporated. *In vitro*, MLT was reported to inhibit angiogenesis in cancer cells [41,42]. On the other hand, Ramírez-Fernandez *et al.* [14] reported that MLT promoted this process in rabbit tibiae following implantation of melatonin implants.

Regarding the coagulation process, HRG, which modulates various components in the coagulation cascade, such as heparin, increased its affinity for 1MLT. Similarly, KLKB1 was significantly more adsorbed onto the material 5MLT. This protein activates the coagulation cascade through the intrinsic pathway [43]. However, both KLKB1 and HRG reduced the affinity by the material when 10% of MLT was added.

Fibrinolysis is a highly regulated enzymatic process of clot removal tightly related to blood coagulation [44]. PLMN, a protein found less adsorbed onto 10MLT, has a role in tissue regeneration by dissolving preformed fibrin clots and extracellular matrix components allowing tissue remodeling [45]. These adsorption patterns are corroborated with PANTHER analysis, which showed a general decrease in proteins with functions related to blood coagulation and plasminogen activation.

MLT has a complex biological role and its potential effect on important pathways, such as inflammation, coagulation, and angiogenesis, in the early stages of tissue regeneration, can

determine how these processes will be carried out around an implant. However, its specific mechanism of action, timings, and doses needed to produce significant cellular effects still need further studies.

2.5. CONCLUSIONS

In this article, we developed new coatings with MLT to be applied in titanium dental implants using a hybrid sol-gel network as a release vehicle. The addition of MLT changed the superficial parameters of the coatings, with the coatings supplemented with the hormone showing a lower hydrophilia when compared to the base material. These materials revealed to be not cytotoxic and showed an increase *BMP2* and *RUNX2* gene expression in 10MLT. However, osteoblastic cells did not show an improvement in the capacity of proliferation and mineralization (ALP activity) *in vitro* when exposed to the coatings. The proteomic analysis of protein adsorption onto the materials showed differences in the adsorption patterns in proteins associated with the complement pathway when MLT added and in a dose-response manner. This behavior can explain the liberation of TNF-α, which was significantly lower in the 1MLT composition. In addition, it was found differences in adsorption of proteins related to coagulation and angiogenesis, which points out a possible effect of MLT in the activation and development of these pathways.

2.6. ACKNOWLEDGMENTS

This work was supported by MINECO [MAT MAT2017-86043-R; RTC-2017-6147-1], Universitat Jaume I under [UJI-B2017-37; POSDOC/2019/28], Generalitat Valenciana [GRISOLIAP/2018/091], University of the Basque Country under [UFI11/56] and Basque Government under [PRE_2017_2_0044]. CIC bioGUNE is supported by Basque Department of Industry, Tourism and Trade (Etortek and Elkartek programs), the Innovation Technology Department of the Bizkaia County; The ProteoRed-ISCIII (Grant PRB3 IPT17/0019); CIBERehd Network and Severo Ochoa Grant (SEV-2016-0644). Authors would like to thank Antonio Coso (GMI-Ilerimplant) for their inestimable contribution to this study, and Raquel Oliver, Jose Ortega (UJI) and Iraide Escobes (CIC bioGUNE) for their valuable technical assistance.

2.7. REFERENCES

1. Smeets, R. *et al.* Impact of Dental Implant Surface Modifications on Osseointegration. *Biomed Res. Int.* **2016**, 1–16 (2016).

2. Oshiro Junior, J. A. *et al.* Drug delivery systems obtained from silica based organic-inorganic hybrids. *Polymers (Basel).* **8**, 91 (2016).

3. Martínez-Ibáñez, M. *et al.* Biological characterization of a new silicon based coating developed for dental implants. *J. Mater. Sci. Mater. Med.* **27**, (2016).

4. Maria, S. & Witt-Enderby, P, A. Melatonin effects on bone: Potential use for the prevention and treatment for osteopenia, osteoporosis, and periodontal disease and for use in bone-grafting procedures. *J. Pineal Res.* **56**, 115–125 (2014).

5. Roth, J. A., Kim, B. G., Lin, W. L. & Cho, M. I. Melatonin promotes osteoblast differentiation and bone formation. *J. Biol. Chem.* **274**, 22041–22047 (1999).

6. Sethi, S. *et al.* Determination of the minimal melatonin exposure required to induce osteoblast differentiation from human mesenchymal stem cells and these effects on downstream signaling pathways. *J. Pineal Res.* **49**, 222–238 (2010).

7. Zhang, L. *et al.* Melatonin inhibits adipogenesis and enhances osteogenesis of human mesenchymal stem cells by suppressing PPARγ expression and enhancing Runx2 expression. *J. Pineal Res.* **49**, 364–372 (2010).

8. Park, K. H. *et al.* Melatonin promotes osteoblastic differentiation through the BMP/ERK/Wnt signaling pathways. *J. Pineal Res.* **51**, 187–194 (2011).

9. Ping, Z. *et al.* Inhibitory effects of melatonin on titanium particle-induced inflammatory bone resorption and osteoclastogenesis via suppression of NF-κB signaling. *Acta Biomater.* **62**, 362–371 (2017).

10. Kadena, M. *et al.* Microarray and gene co-expression analysis reveals that melatonin attenuates immune responses and modulates actin rearrangement in macrophages. *Biochem. Biophys. Res. Commun.* **485**, 414–420 (2017).

11. Xia, Y. *et al.* Melatonin in macrophage biology: Current understanding and future perspectives. *J. Pineal Res.* **66**, 1–21 (2019).

12. Hardeland, R. Melatonin and inflammation—Story of a double-edged blade. *J. Pineal Res.* **65**, 1–23 (2018).

13. Ma, Q., Reiter, R. J. & Chen, Y. Role of melatonin in controlling angiogenesis under physiological and pathological conditions. *Angiogenesis* **23**, 91–104 (2019).

14. Ramírez-Fernández, M. P. *et al.* Melatonin promotes angiogenesis during repair of bone defects: a radiological and histomorphometric study in rabbit tibiae. *Clin. Oral Investig.* **17**, 147–158 (2013).

15. Reiter, R. J. *et al.* Melatonin as an antioxidant: under promises but over delivers. *J. Pineal Res.* 253–278 (2016). doi:10.1111/jpi.12360

16. Araújo-Gomes, N. *et al.* Osseointegration mechanisms: a proteomic approach. *JBIC J. Biol. Inorg. Chem.* **23**, 459–470 (2018).

17. Sheikh, Z., Brooks, P. J., Barzilay, O., Fine, N. & Glogauer, M. Macrophages, foreign body giant cells and their response to implantable biomaterials. *Materials (Basel).* **8**, 5671–5701 (2015).

18. Romero-Gavilán, F. *et al.* Proteomic analysis of calcium - enriched sol – gel biomaterials. *JBIC J. Biol. Inorg. Chem.* **24**, 563–574 (2019).

19. Romero-Gavilan, F. *et al.* Proteomic analysis of silica hybrid sol-gel coatings: a potential tool for predicting the biocompatibility of implants *in vivo*. *Biofouling* **33**, 676–689 (2017).

20. Zhang, L. *et al.* Sustained release of melatonin from poly (lactic-co-glycolic acid) (PLGA) microspheres to induce osteogenesis of human mesenchymal stem cells in vitro. *J. Pineal Res.* **54**, 24–32 (2013).

21. Wiśniewski, J. R., Zougman, A., Nagaraj, N. & Mann, M. Universal sample preparation method for proteome analysis. *Nat. Methods* **6**, 359–362 (2009).

22. Romero-Gavilán, F. *et al.* Control of the degradation of silica sol-gel hybrid coatings for metal implants prepared by the triple combination of alkoxysilanes. *J. Non. Cryst. Solids* **453**, 66–73 (2016).

23. Li, Y. *et al.* Melatonin-loaded silica coated with hydroxypropyl methylcellulose phthalate for enhanced oral bioavailability: Preparation, and in vitro-in vivo evaluation. *Eur. J. Pharm. Biopharm.* **112**, 58–66 (2017).

24. Juan-Díaz, M. J. *et al.* Study of the degradation of hybrid sol-gel coatings in aqueous medium. *Prog. Org. Coatings* **77**, 1799–1806 (2014).

25. Vishnevskiy, A. S. *et al.* Effect of water content on the structural properties of porous

methyl-modified silicate films. *J. Sol-Gel Sci. Technol.* **92**, 273–281 (2019).

26. Sabzichi, M. *et al.* Sustained release of melatonin: A novel approach in elevating efficacy of tamoxifen in breast cancer treatment. *Colloids Surfaces B Biointerfaces* **145**, 64–71 (2016).

27. Maria, S. & Witt-Enderby, P. A. Melatonin effects on bone: Potential use for the prevention and treatment for osteopenia, osteoporosis, and periodontal disease and for use in bone-grafting procedures. *J. Pineal Res.* **56**, 115–125 (2014).

28. Cutando, A., López-Valverde, A., Arias-Santiago, S., De Vicente, J. & De Diego, R. G. Role of melatonin in cancer treatment. *Anticancer Res.* **32**, 2747–2754 (2012).

29. Liu, L., Zhu, Y., Xu, Y. & Reiter, R. J. Melatonin delays cell proliferation by inducing G 1 and G 2 / M phase arrest in a human osteoblastic cell line hFOB 1 . 19. *J. Pineal Res.* 222–231 (2011). doi:10.1111/j.1600-079X.2010.00832.x

30. Son, J. H. *et al.* Melatonin promotes osteoblast differentiation and mineralization of MC3T3-E1 cells under hypoxic conditions through activation of PKD/p38 pathways. *J. Pineal Res.* **57**, 385–392 (2014).

31. Ping, Z. *et al.* Melatonin attenuates titanium particle-induced osteolysis via activation of Wnt/β-catenin signaling pathway. *Acta Biomater.* **51**, 513–525 (2017).

32. Cho, N. H. & Seong, S. Y. Apolipoproteins inhibit the innate immunity activated by necrotic cells or bacterial endotoxin. *Immunology* **128**, 479–486 (2009).

33. Berbée, J. F. P., Havekes, L. M. & Rensen, P. C. N. Apolipoproteins modulate the inflammatory response to lipopolysaccharide. *J. Endotoxin Res.* **11**, 97–103 (2005).

34. Nesargikar, P., Spiller, B. & Chavez, R. The complement system: History, pathways, cascade and inhibitors. *Eur. J. Microbiol. Immunol.* **2**, 103–111 (2012).

35. Carroll, M. C. The complement system in regulation of adaptive immunity. *Nature Immunology* **5**, 981–986 (2004).

36. Carroll, M. C. The complement system in B cell regulation. in *Molecular Immunology* **41**, 141–146 (2004).

37. Mollnes, T. E. & Kirschfink, M. Strategies of therapeutic complement inhibition. *Mol. Immunol.* **43**, 107–121 (2006).

38. Mauriz, J. L., Collado, P. S., Veneroso, C., Reiter, R. J. & González-Gallego, J. A review of the molecular aspects of melatonin's anti-inflammatory actions: Recent insights and new perspectives. *J. Pineal Res.* **54**, 1–14 (2013).

39. Calvo, J. R., Gonzalez-Yanes, C. & Maldonado, M. D. The role of melatonin in the cells of the innate immunity: A review. *J. Pineal Res.* **55**, 103–120 (2013).

40. Druhan, L. J. *et al.* Leucine rich α-2 glycoprotein: A novel neutrophil granule protein and modulator of myelopoiesis. *PLoS One* **12**, 1–13 (2017).

41. Park, S. *et al.* Melatonin suppresses tumor angiogenesis by inhibiting HIF-1α stabilization under hypoxia. *J. Pineal Res.* **48**, 178–184 (2010).

42. Kim, K. *et al.* Melatonin suppresses tumor progression by reducing angiogenesis stimulated by HIF-1 in a mouse tumor model. *J. Pineal Res.* **54**, 264–270 (2013).

43. Wu, Y. Contact pathway of coagulation and inflammation. *Thromb. J.* **13**, 17 (2015).

44. Chapin, J. C. & Hajjar, K. A. Fibrinolysis and the control of blood coagulation. (2014). doi:10.1016/j.blre.2014.09.003

45. Sakharov, D. V., Nagelkerkel, J. F. & Rijken, D. C. Rearrangements of the fibrin network and spatial distribution of fibrinolytic components during plasma clot lysis: Study with confocal microscopy. *J. Biol. Chem.* **271**, 2133–2138 (1996).

2.8. SUPPLEMENTARY MATERIAL

Supplementary Table 2.1. Progenesis comparative analysis of proteins differentially adsorbed onto MLT enriched coatings (1MLT, 5MLT, 7.5MLT and 10MLT) in respect to 70M30T base material.

				70M30T *vs* 1MLT		70M30T *vs* 5MLT		70M30T *vs* 7.5MLT		70M30T *vs* 10MLT	
Accession	**Unique peptides**	**Confidence score**	**Description**	***p* value**	**Ratio**	***p* value**	**Ratio**	***p* value**	**Ratio**	***p* value**	**Ratio**
HRG_HUMAN	4	299.69	Histidine-rich glycoprotein	6.3E-01	1.60	9.9E-01	1.29	7.7E-01	1.28	3.5E-02	0.36
PON1_HUMAN	4	239.25	Serum paraoxonase/arylesterase 1	8.2E-01	0.99	6.6E-01	1.13	8.8E-02	0.66	9.1E-03	0.41
A2GL_HUMAN	2	54.68	Leucine-rich alpha-2-glycoprotein	4.9E-02	3.48	3.2E-02	4.46	8.7E-01	1.28	1.2E-01	0.43
CO7_HUMAN	5	230.9	Complement component C7	1.5E-02	0.72	1.3E-01	0.81	1.5E-01	0.75	4.8E-03	0.46
HBB_HUMAN	3	184.71	Hemoglobin subunit beta	9.6E-02	0.83	8.0E-01	1.00	7.3E-02	0.63	1.6E-02	0.46
IC1_HUMAN	3	234.02	Plasma protease C1 inhibitor	8.0E-01	0.99	7.4E-01	1.09	3.9E-01	0.87	3.0E-02	0.49
PLMN_HUMAN	12	640.22	Plasminogen	5.1E-03	0.74	1.0E-02	0.71	4.9E-02	0.73	1.3E-03	0.51
APOA1_HUMAN	13	962.33	Apolipoprotein A-I	1.8E-03	0.78	9.4E-02	0.85	6.7E-02	0.74	8.5E-03	0.55
CO5_HUMAN	8	451.8	Complement C5	3.7E-01	0.90	8.0E-01	0.97	2.8E-02	0.66	2.6E-02	0.57
ITIH2_HUMAN	2	155.95	Inter-alpha-trypsin inhibitor heavy chain H2	5.0E-01	1.27	2.0E-01	1.43	4.0E-01	0.87	1.3E-02	0.58
ITIH4_HUMAN	6	319.22	Inter-alpha-trypsin inhibitor heavy chain H4	3.8E-01	1.24	7.0E-02	1.53	5.0E-01	0.91	1.8E-02	0.60

GELS_HUMAN	11	810.28	Gelsolin	8.4E-02	0.73	2.6E-01	0.81	2.7E-01	1.18	1.6E-02	0.62
ITIH1_HUMAN	3	192.7	Inter-alpha-trypsin inhibitor heavy chain H1	5.0E-01	1.22	4.3E-01	1.55	3.8E-01	0.82	4.5E-02	0.64
VTNC_HUMAN	7	381.12	Vitronectin	1.9E-01	0.87	1.7E-01	1.20	3.0E-01	0.83	4.0E-02	0.64
SEPP1_HUMAN	3	253.34	Selenoprotein P	6.8E-02	0.71	9.9E-01	1.01	9.3E-01	1.17	3.2E-02	0.64
CO9_HUMAN	3	179.45	Complement component C9	2.0E-03	0.70	8.2E-02	0.73	3.4E-02	0.68	7.1E-03	0.66
CO8A_HUMAN	3	122.99	Complement component C8 alpha chain	3.5E-01	0.83	3.9E-01	0.87	2.5E-02	0.66	8.8E-02	0.70
APOF_HUMAN	2	129.98	Apolipoprotein F	4.9E-02	0.54	2.4E-02	0.53	8.1E-01	0.94	3.3E-01	0.80
KLKB1_HUMAN	2	92.23	Plasma kallikrein	9.0E-01	1.23	3.9E-02	2.91	7.7E-01	0.93	4.5E-01	0.81
APOL1_HUMAN	2	137.86	Apolipoprotein L1	1.0E-02	0.55	1.0E-01	0.73	4.6E-01	0.89	5.5E-01	0.91
APOC4_HUMAN	3	140.38	Apolipoprotein C-IV	4.2E-01	0.90	8.0E-03	0.56	3.1E-01	0.84	5.6E-01	0.92
IGHA2_HUMAN	1	163.51	Ig alpha-2 chain C region	1.7E-03	2.56	2.1E-01	2.83	6.7E-01	1.18	9.3E-01	1.44
HEMO_HUMAN	2	89.92	Hemopexin	8.7E-01	1.68	3.3E-02	4.60	7.8E-01	1.04	8.4E-01	1.75
CXCL7_HUMAN	3	188.44	Platelet basic protein	1.6E-01	1.43	7.0E-02	1.65	8.9E-03	2.67	2.7E-01	2.45
H90B2_HUMAN	2	75.74	Putative heat shock protein HSP 90-beta 2	2.5E-02	0.45	9.6E-02	0.50	5.7E-01	1.21	4.6E-01	9.03
ATPA_HUMAN	2	95.71	ATP synthase subunit alpha. mitochondrial	4.4E-02	49.50	2.0E-01	54.39	6.4E-01	3.02	6.3E-02	376.00

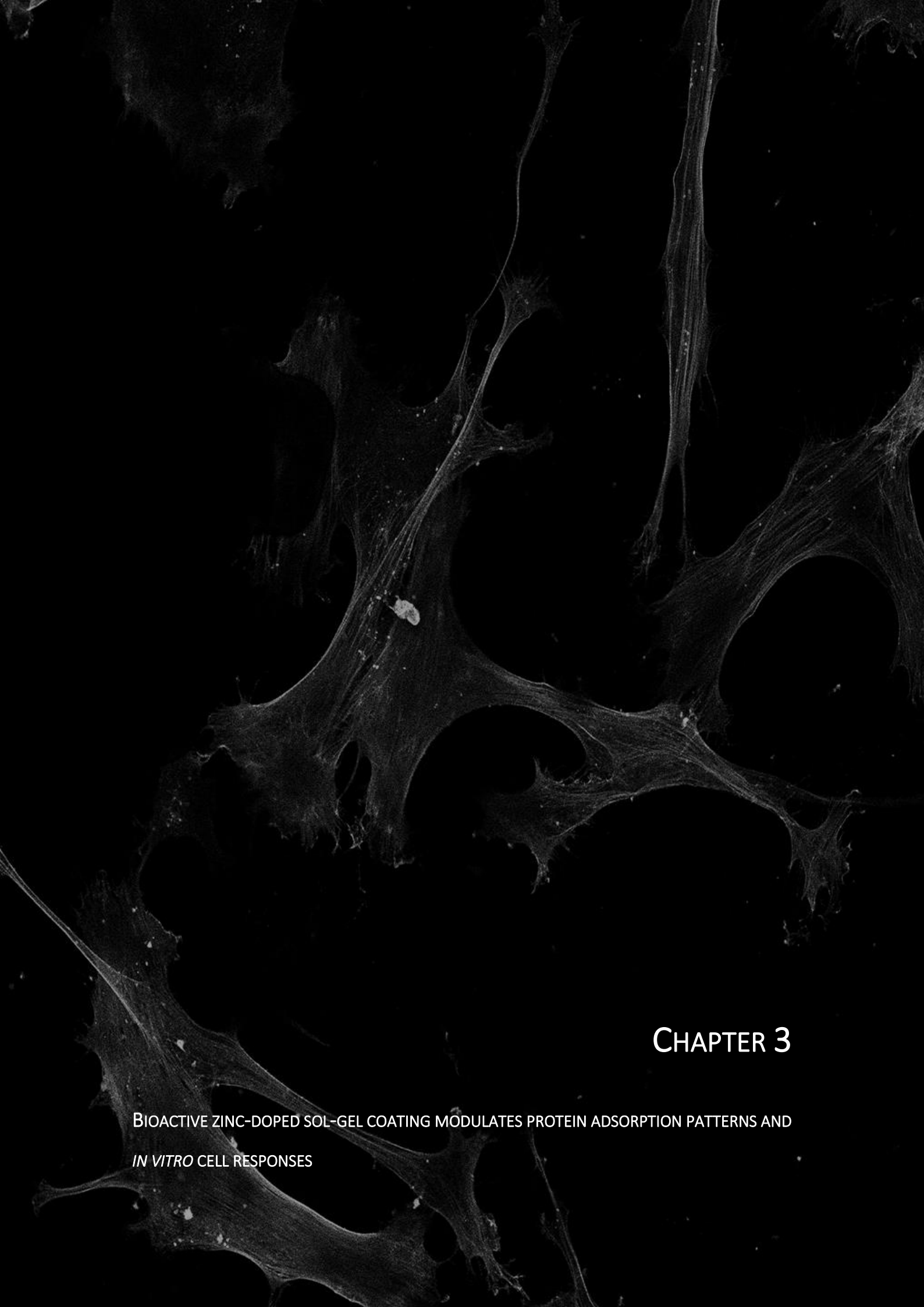

CHAPTER 3

BIOACTIVE ZINC-DOPED SOL-GEL COATING MODULATES PROTEIN ADSORPTION PATTERNS AND *IN VITRO* CELL RESPONSES

CHAPTER 3

BIOACTIVE ZINC-DOPED SOL-GEL COATING MODULATES PROTEIN ADSORPTION PATTERNS AND *IN VITRO* CELL RESPONSE

ARTICLE 2

Andreia Cerqueira[1], Francisco Romero-Gavilán[1], Iñaki García-Arnáez[2], Cristina Martinez-Ramos[3], Seda Ozturan[4], Ibon Iloro[5], Mikel Azkargorta[5], Felix Elortza[5], Raúl Izquierdo[1], Mariló Gurruchaga[2], Isabel Goñi[2], Julio Suay[1]

[1]Department of Industrial Systems Engineering and Design, Universitat Jaume I, Av. Vicent Sos Baynat s/n, 12071 Castellón de la Plana, Spain

[2]Departament of Science and Technology of Polymers, Universidad del País Vasco, P. M. de Lardizábal, 3, 20018 San Sebastián, Spain

[3]Center for Biomaterials and Tissue Engineering, Universitat Politècnica de Valencia, Camino de Vera, s/n 46022 Valencia, Spain

[4]Department of Periodontology, Faculty of Dentristy, Istanbul Medeniyet University, Istanbul, Turkey

[5]Proteomics Platform, CIC bioGUNE, Basque Research and Technology Alliance (BRTA), CIBERehd, ProteoRed-ISCIII, Bizkaia Science and Technology Park, 48160 Derio, Spain

Published at Materials Science and Engineering: C

Volume 121, February 2021, 111839

ABSTRACT

Zinc is an essential element with an important role in stimulating the osteogenesis and mineralization and suppressing osteoclast differentiation. In this study, new bioactive $ZnCl_2$-doped sol-gel materials were designed to be applied as coatings onto titanium. The biomaterials were physicochemically characterized and the cellular responses evaluated *in vitro* using MC3T3-E1 osteoblasts and RAW264.7 macrophages. The effect of Zn on the adsorption of human serum proteins onto the material surface was evaluated through nLC-MS/MS. The incorporation of Zn did not affect the crosslinking of the sol-gel network. A controlled Zn^{2+} release was obtained, reaching values below 10 ppm after 21 days. The materials were no cytotoxic and lead to increased gene expression of *ALP*, *TGF-β*, and *RUNX2* in the osteoblasts. In macrophages, an increase of *IL-1β*, *TGF-β*, and *IL-4* gene expression was accompanied by a reduced TNF-α liberation. Proteomic results showed changes in the adsorption patterns of proteins associated with immunological, coagulative, and regenerative functions, in a Zn dose-dependent manner. The variations in protein adsorption might lead to the downregulation of the NF-κB pathway, thus explain the observed biological effects of Zn incorporation into biomaterials. Overall, these coatings demonstrated their potential to promote bone tissue regeneration.

KEYWORDS

Proteomics, Bioinorganic Chemistry, Biomaterials, Bone Regeneration, Hybrids

GRAPHICAL ABSTRACT

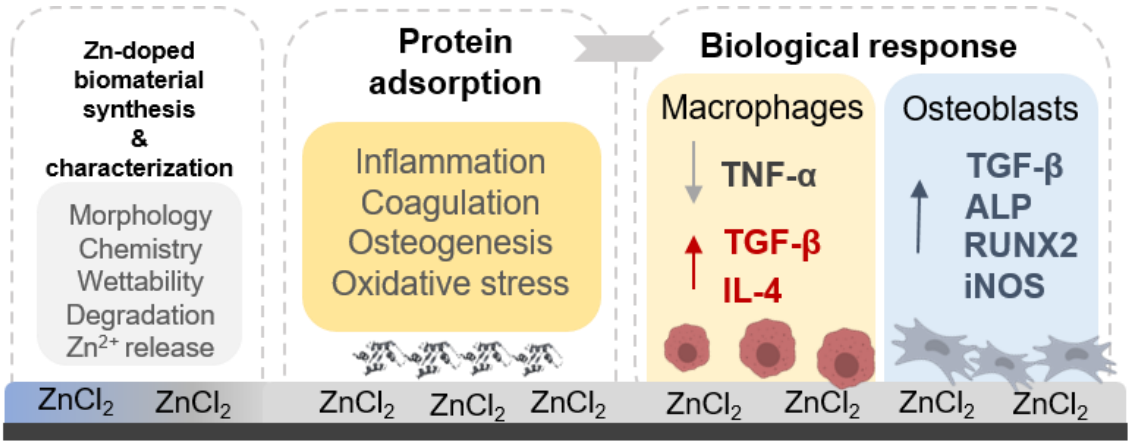

Figure 3.1. Graphical abstract of the paper "Bioactive zinc-doped sol-gel coating modulates protein adsorption patterns and *in vitro* cell responses"

3.1. INTRODUCTION

As an essential trace element, zinc (Zn) plays an important physiological role in the human body, performing various functions in growth, immunity, tissue maintenance, and wound healing [1]. Most of the Zn is stored in bone tissue, mainly as a component of the calcified matrix [2]. It plays a pivotal role in bone metabolism and remodeling [3], supporting osteoblastogenesis, and suppressing osteoclastogenesis [4]. Zinc can enhance osteogenesis and mineralization by activating the aminoacyl-RNA synthesis in osteoblastic cells [5], and stimulating the alkaline phosphatase (ALP) activity and collagen synthesis in a dose-dependent manner [6]. However, this divalent cation can also downregulate osteoclast differentiation due to its effect on the RANKL/RANK/OPG signaling pathway [7]. Zinc deficiency causes various diseases and skeletal abnormalities during fetal and postnatal development, such as bone growth retardation, abnormal mineralization, and osteoporosis [8]. Zinc is also known for its antioxidant and anti-inflammatory properties; it is used as a therapeutic agent in chronic diseases [9]. Moreover, Zn inhibits the induction of TNF-α and IL-1β in monocytes and prevents the TNF-α-induced NF-κB activation [10].

The intrinsic physiological relevance of this element has attracted the interest of researchers in the biomaterial field; its incorporation into bone-engineered materials could enhance the desired regenerative properties. Zinc-doped degradable materials such as hydroxyapatites, bioglasses, and metallic alloys have recently emerged demonstrating pro-regenerative capabilities [11,12]. However, delayed osseointegration induced by excessive release of Zn^{2+} ions has been observed in pure Zn-ion implants [5]. Thus, the control of the degradation product release is necessary to ensure the biosafety of these materials and optimize their therapeutic effects [13].

Immediately after implantation, a material interacts with surrounding tissues and fluids. A complex sequence of events is initiated in order to promote tissue repair and determine integration/rejection of the introduced foreign body [14,15]. The interaction between the biomaterial and body fluids, such as the blood, results in the adsorption of proteins onto the surface of the implant. These proteins compete against each other by a displacement mechanism known as the Vroman effect [16]. The regenerative processes, such as inflammation, coagulation, fibrinolysis, and angiogenesis, will depend on the type of proteins attached to the material [17,18]. Inflammation is one of the first reactions to implantation, playing a pivotal role in tissue regeneration, and can condition the subsequent responses to the implant [17,19]. Depending on the intensity of the inflammatory response, it can be initiated the regeneration process by

recruitment of the mesenchymal cells and boosting of the osteogenesis, or it can be triggered a foreign body reaction, causing the implant rejection [20,21].

This study aimed to synthesize and characterize a new organic-inorganic sol-gel release vehicle doped with Zn ions to be applied as coatings onto titanium. The materials were physiochemically characterized and the effects of Zn^{2+} on protein adsorption were studied using proteomic analysis. Also, *in vitro* assays of cell behavior were conducted using MC3T3-E1 osteoblast and RAW 264.7 macrophage cell lines. The correlation between the cellular responses and the Zn dose-dependent protein adsorption patterns will allow to better understand the role of this element in bone tissue regeneration.

3.2. Materials and methods

3.2.1. Substrate

Grade-4 Ti discs, 1-mm thick, 12 mm in diameter (Ilerimplant-GMI SL., Lleida, Spain), were employed as a substrate for the coatings. Disc surfaces were first modified using the sandblasting and acid-etching treatment (SAE) described in the previous study [22] and sterilized with UV radiation.

3.2.2. Sol-gel synthesis and coating preparation

The Zn-containing hybrid materials were developed using the sol-gel synthesis. Organically modified alkoxysilanes, methyltrimethoxysilane (MTMOS; M) and tetraethyl orthosilicate (TEOS; T), were employed as precursors. The proportion of these reagents was 70% of M to 30% of T (molar ratio), as described in previous studies [23]. The solvent used in the synthesis was 2-Propanol (volume ratio of alcohol to siloxane, 1:1). The precursor hydrolysis was conducted by adding the corresponding stoichiometric amount of H_2O at a rate of 1 drop s^{-1}. The water was acidified with HNO_3 (0.1 M) to catalyze the sol-gel reactions. An appropriate amount of $ZnCl_2$ was dissolved in this solution for its incorporation into the sol-gel mixture. The preparations were kept for 1h under stirring and then 1h at rest at room temperature. Four different compositions were synthesized: the sol-gel network without Zn (MT; control) and enriched with 0.5, 1, and 1.5 wt% $ZnCl_2$ (designated as MT0.5Zn, MT1Zn, and MT1.5Zn, respectively). The mass percentages were relative to the total amount of alkoxysilane. Also, SAE uncoated titanium samples (Ti) were used as controls. All the reagents employed for the synthesis were purchased from Sigma-Aldrich (Merck KGaA, Darmstadt, Germany). The samples were prepared immediately after finishing the sol-gel synthesis. The coatings were applied onto the SAE-Ti discs with a dip-coater (KSV DC; KSV NIMA, Espoo, Finland). The discs were immersed in the sol-gel

solutions at a speed of 60 cm min^{-1}, left immersed for one minute, and removed at a 100 cm min^{-1}. To evaluate the hydrolytic degradation and Zn^{2+} release, glass slides were used as a substrate for the coatings. The glass surfaces were first cleaned with HNO_3 solution (25% v/v) in an ultrasonic bath (Sonoplus HD 3200) for 20 min at 30 W. A second wash with distilled water was performed under the same conditions. Then, the samples were coated by casting, adding the same amount of sol-gel in all cases. To carry out the chemical analyses, free films of the materials were obtained by pouring the sol-gel solutions into non-stick Teflon molds. Finally, all the samples were cured for 2 h at 80°C.

3.2.3. PHYSICOCHEMICAL CHARACTERIZATION

The morphology of the obtained coatings was analyzed using SEM with a Leica-Zeiss LEO equipment, under vacuum (Leica, Wetzlar, Germany). Platinum sputtering was used to increase the coating conductivity for the SEM examination. Fourier-transform infrared spectroscopy (FTIR; Thermo Nicolet 6700 spectrometer, Thermo Fisher Scientific, Waltham, MA, USA) with an attenuated total reflection system (ATR) was employed for chemical characterization of the synthesized materials. The spectra were recorded in the 400 to 4000 cm^{-1} wavelength range. The level of structural crosslinking was studied using silicon solid-state nuclear magnetic resonance spectroscopy (^{29}Si-NMR). To achieve this, a Bruker 400 Avance III WB Plus spectrometer (Bruker, Billerica, MA, USA) with a cross-polarization magic-angle spinning (CP-MAS) probe for solid samples was employed. The pulse sequence for the analysis was the Bruker standard: 79.5 MHz frequency, 55 kHz spectral width, 2 ms contact time and 5 s delay time. The spinning speed was 7.0 kHz. The surface roughness of the developed coatings was measured using an optical profilometer (interferometric and confocal) PLm2300 (Sensofar, Barcelona, Spain). Three discs were tested for each condition. Three measurements were performed for each disc to obtain an average Ra (arithmetic average roughness parameter). The wettability was characterized using contact angle measurements, employing an automatic contact angle meter OCA 20 (Dataphysics Instruments, Filderstadt, Germany). Drops of 10 µL of ultrapure water were deposited on the material surfaces at a 27.5 µL s^{-1} dosing rate. Contact angles were determined using SCA 20 software (DataPhysics Instruments). Six discs of each material were studied, after depositing two drops on each disc. Hydrolytic degradation of the coatings was examined by measuring the sol-gel mass loss after incubation in 50 mL of distilled water at 37°C for 7, 14, 28, 49, and 63 days. The degradation of the coatings was registered as the percentage of the original mass lost. Three different samples were used for each condition. The Zn^{2+} release kinetics were measured using an inductively coupled plasma mass spectrometer (Agilent 7700 Series ICPMS; Agilent Technologies, Santa Clara, CA, USA). Samples were incubated in ddH_2O at

37°C for 21 days. Aliquots of 0.5 mL were removed after 2, 4, 8, 168, 336, and 504h of immersion. Each data point is the average of three individual measurements.

3.2.4. *IN VITRO* ASSAYS

3.2.4.1. *Cell culture*

Mouse calvaria osteosarcoma (MC3T3-E1) cell line was cultured on the discs at a concentration of 1.75×10^4 cells cm^{-2} for 7 and 14 days. For the first 24 h, the culture medium was composed of low-glucose DMEM (Gibco, Thermo Fisher Scientific) supplemented with 1% penicillin/streptomycin (Biowest Inc., Riverside, MO, USA) and 10% FBS (Gibco). The samples were kept in a cell incubator (90% humidity, 37°C, 5% CO_2). Then, the cell culture medium was replaced with osteogenic medium (DMEM, 1% of penicillin/streptomycin, 10% FBS, 1% ascorbic acid (50 µg mL^{-1}), and 100 mM β-glycerol phosphate), which was changed every two days.

Mouse murine macrophage (RAW264.7) cell line was cultured on the materials at a concentration of 30×10^4 cells cm^{-2} for 2 and 4 days in high-glucose DMEM supplemented with 1% penicillin/streptomycin and 10% FBS in a cell incubator (90% humidity, 37°C, 5% CO_2).

3.2.4.2. *Cytotoxicity, proliferation, and ALP activity*

To evaluate the cytotoxicity of biomaterials, the ISO 10993-5:2009 (Annex C) norm [24] was followed. Samples were prepared according to the ISO 10993-12:2012 norm [25]. MC3T3-E1 cells were seeded and incubated in 96-well NUNC plates (Thermo Fisher Scientific) for 24h. For serum extraction, the materials were incubated in cell culture medium for the same period. Then, the cells were exposed to the material extract for another 24h. Based on the formazan formation, the CellTiter 96® Proliferation Assay (MTS; Promega, Madison, WI) was used according to manufacturer's guidelines. The negative control was composed of wells with only cells and the cells incubated with latex (cytotoxic compound) constituted the positive control. A material would be considered cytotoxic if the cell viability fell below 70%.

To measure the effects of the tested biomaterials on proliferation, MC3T3-E1 cells were cultured on the discs for 1, 3, and 7 days and the alamarBlue™ cell viability reagent (Invitrogen, Thermo Fisher Scientific) was used following the manufacturer's protocol.

The ALP activity was measured, following the protocol of Araújo-Gomes *et al.* [20], to evaluate the effect of the Zn-enriched materials on cell mineralization. Briefly, the MC3T3-E1 cells were seeded onto different disc surfaces in 48-well NUNC plates (Thermo Fisher Scientific). After culturing for 7 and 14 days, lysis buffer (0.2% Triton X-100, 10 mM Tris-HCl, pH 7.2) was added.

Then, 100 µL of *p*-NPP (1mg mL^{-1}) in substrate buffer (50 mM glycine, 1 mM $MgCl_2$, pH 10.5) was added to the samples. After 2h of incubation, the absorbance at 405 nm was measured using a microplate reader. The ALP activity was obtained using the standard curve of *p*-nitrophenol in 0.02 mM sodium hydroxide. It was normalized to protein content obtained employing a Pierce BCA assay kit (Thermo Fisher Scientific).

3.2.4.3. *Cytokine quantification by ELISA*

The level of tumor necrosis factor (TNF-α) was measured in the culture medium of RAW264.7 cells incubated on the discs for 2 and 4 days. Its concentration was determined using an ELISA (Invitrogen, Thermo Fisher Scientific) kit following the manufacturer's instructions.

3.2.4.4. *Relative gene expression: RNA extraction, cDNA synthesis, and qRT-PCR*

For total RNA extraction, MC3T3-E1 cells were grown on the tested materials for 7 and 14 days, and RAW264.7 for 2 and 4 days. The assays were carried out in 48-well NUNC plates (Thermo Fisher Scientific). At each time point, RNA was extracted using TRIzol as described in Cerqueira *et al.* [26]. RNA concentration, integrity, and quality were measured employing NanoVue® Plus spectrophotometer (GE Healthcare Life Sciences, Little Chalfont, UK).

For cDNA synthesis, approximately 1 µg of total RNA was converted into cDNA using PrimeScript RT Reagent Kit (Perfect Real-Time; TAKARA Bio Inc., Shiga, Japan). The reaction was carried out under the following conditions: 37°C for 15 min, 85°C for 5 secs, and a final hold at 4°C. The resulting cDNA was diluted in DNase-free water to a concentration suitable for gene expression evaluation. Quantitative real-time PCR (qRT-PCR) was carried out in 96-well plates (Applied Biosystems®, Thermo Fisher Scientific) for the genes of interest and the housekeeping gene (*GAPDH*). Primers were designed using PRIMER3plus software tool from sequences obtained from NCBI Nucleotide and purchased from Thermo Fisher Scientific. Targets are shown in **Table 3.1**. Individual qRT-PCR reactions contained 1 µL of cDNA, 0.2 µL of specific primers (forward and reverse, at 10 µM concentration) and 5 µL of SYBR Premix Ex Taq (Tli RNase H Plus; TAKARA), in a final volume of 10 µL. Reactions were carried out in a StepOnePlus™ Real-Time PCR System (Applied Biosystems®, Thermo Fisher Scientific). Fold changes were calculated using the $2^{-\Delta\Delta Ct}$ method and data normalized to the wells without any material.

Table 3.1. Targets studied in MC3T3-E1 and RAW264.7.

Gene	Accession	Sequence	Product length
GADPH	XM_017321385	F: TGCCCCCATGTTTGTGATG R: TGGTGGTGCAGGATGCATT	83
ALP	XM_006538499	F: CGGGACTGGTACTCGGATAA R: ATTCCACGTCGGTTCTGTTC	157
TGFβ	NM_011577	F: TTGCTTCAGCTCCACAGAGA R: TGGTTGTAGAGGGCAAGGAC	183
iNOS	NM_001313922	F: CACCTTGGAGTTCACCCAGT R: ACCACTCGTACTTGGGATGC	170
RUNX2	NM_001271631	F: CCCAGCCACCTTTACCTACA R: TATGGAGTGCTGCTGGTCTG	150
RANKL	AF019048	F: AGCCGAGACTACGGCAAGTA R: GCGCTCGAAAGTACAGGAAC	208
RANK	AF019046	F: GCTGGCTACCACTGGAACTC R: GTGCAGTTGGTCCAAGGTTT	182
TNF-α	NM_001278601	F: AGCCCCCAGTCTGTATCCTT R: CTCCCTTTGCAGAACTCAGG	212
IL-1β	NM_008361	F: GCCCATCCTCTGTGACTCAT R: AGGCCACAGGTATTTTGTCG	230
IL-4	NM_021283	F: TCAACCCCCAGCTAGTTGTC R: TGTTCTTCGTTGCTGTGAGG	177

3.2.5. PROTEIN LAYER ELUTION AND PROTEOMIC ANALYSIS

The protein layers on the distinct sol-gel formulations were examined after their incubation in a humidified atmosphere (37°C, 5% CO_2) for 3 h with 1 mL of human blood serum from male AB plasma (Sigma-Aldrich). The serum was removed, and non-adsorbed proteins were eliminated by five consecutive washes with ddH_2O and another with 100 mM NaCl, 50 mM Tris-HCl, pH 7.0. The adsorbed proteins were eluted by washing the surfaces with 0.5 M triethylammonium bicarbonate buffer (TEAB), with 4% sodium dodecyl sulfate (SDS) and 100 mM-dithiothreitol (DTT). The experiment was performed in quadruplicate for each material, and each of these replicas was the result of pooling four different processed samples. The total protein content of the serum was measured before the assay, obtaining a value of 51 mg mL^{-1}.

The eluted proteins were characterized using electrospray tandem mass spectrometry, employing a nanoACQUITY UPLC (Waters, Milford, MA, USA) coupled to an Orbitrap XL (Thermo Electron, Bremen, Germany). The protocol described by Romero-Gavilán *et al.* [15] was followed. Each condition was analyzed in quadruplicate. Proteomic results were examined using PEAKS (Bioinformatics Solutions Inc., Waterloo, Canada). Functional classification of the identified proteins was performed using DAVID Go annotation (https://david.ncifcrf.gov/) and PANTHER programs (http://www.pantherdb.org/).

3.2.6. STATISTICAL ANALYSIS

Physicochemical characterization and *in vitro* assay data, after evaluation of the normal distribution and equal variances, were submitted to one-way analysis of variance (ANOVA) with Tukey *post-hoc* test. Statistical analysis was performed using SigmaPlot v. 12.5 software for Windows (Systat Software Inc., Chicago, IL, USA). The differences between the MT materials and MT enriched with Zn were considered statistically significant at $p \leq 0.05$ (*), $p \leq 0.01$ (**), and $p \leq 0.001$ (***). Data were expressed as mean ± standard error (SE). For proteomic analysis, Student's *t*-test was performed, and protein adsorption differences were considered statistically significant at $p \leq 0.05$ and a ratio higher than 1.5 in either direction.

3.3. RESULTS

3.3.1. PHYSICOCHEMICAL CHARACTERIZATION

The organic-inorganic sol-gel materials with increasing amounts of $ZnCl_2$ were successfully synthesized and applied as coatings onto the Ti discs. As can be seen in SEM micrographs (**Figure 3.2**), no cracks or holes resulting from the curing process were detected. Moreover, no salt precipitates were observed, so the $ZnCl_2$ was correctly incorporated into the sol-gel network.

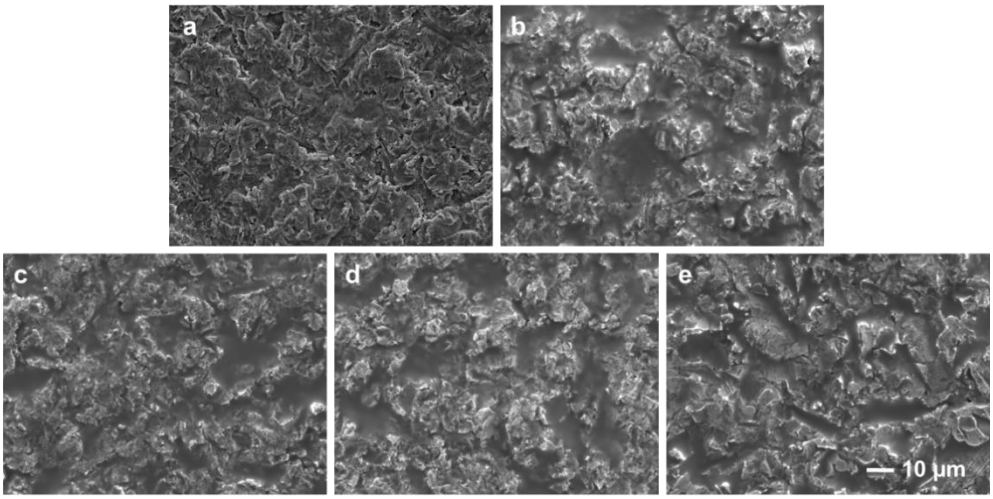

Figure 3.2. SEM microphotograph of SAE-Ti (a), MT (b), MT0.5Zn (c), MT1Zn (d) and MT1.5Zn (e). Scale bar, 10 µm.

The obtained sol-gel materials were chemically characterized using ^{29}Si-NMR and FT-IR (**Figure 3.3**). The ^{29}Si-NMR spectra showed no effects on the silica network condensation with the $ZnCl_2$ addition (**Figure 3.3a**). The signals detected in the range between -50 and -70 ppm can be assigned to the MTMOS trifunctional precursor (T units - $CH_3{\cdot}SiO_3$). The signals between -97.5 and -115 ppm represent the TEOS tetrafunctional alkoxysilane (Q units - SiO_4) [27]. Thus, the signals at -56 and -66 ppm indicate the presence of T^2 and T^3 species, while chemical shifts at -102 and -110 ppm can be associated with the formation of Q^3 and Q^4 structures, respectively [28]. In general, the networks reached a high degree of MTMOS crosslinking as T^3 signal was more intense than T^2, and no T^0 or T^1 shifts were observed. Similarly, no Q^0, Q^1 or Q^2 TEOS species were identified although, in this case, the level of condensation was probably lower as Q^3 peak was larger than Q^4. The FT-IR results are displayed in **Figure 3.3b**. Bands at 780, 1020 and 1125 cm^{-1} associated with the polysiloxane chain vibration reveal the formation of Si-O-Si bonds during the sol-gel synthesis [29]. The band at 950 cm^{-1} indicates the presence of non-condensed Si-OH species [30]. The methyl group integrity in the sol-gel structure is confirmed by its characteristics bands at 1265 and 2980 cm^{-1}, which are attributed to the Si-C and C-H bonds, respectively [29].

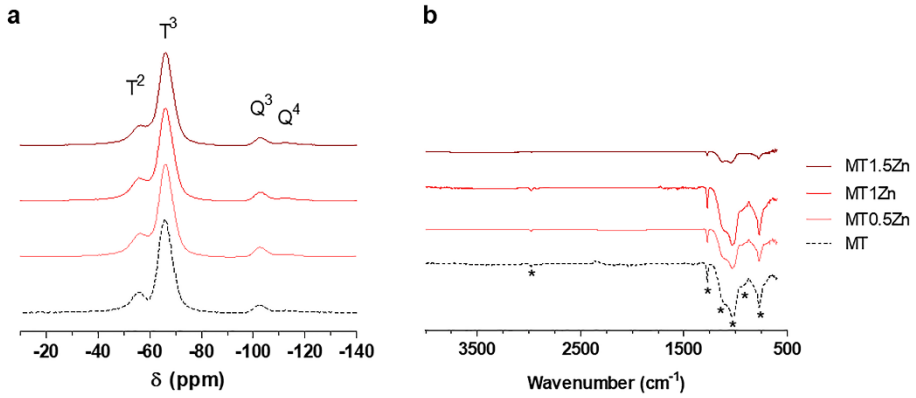

Figure 3.3. ^{29}Si MAS-NMR (a) and FTIR (b) spectra of sol-gel networks MT, 0.5MTZn, MT1Zn, and MT1.5Zn.

The surface roughness was evaluated using the Ra parameter. **Figure 3.4a** shows that the incorporation of $ZnCl_2$ into the coatings did not change their Ra values (in comparison with the material without Zn) significantly. **Figure 3.4b** displays the contact angle measurements. The addition of $ZnCl_2$ to the MT network, resulting in the reduction in surface hydrophilicity, caused a significant increase in the contact angle values.

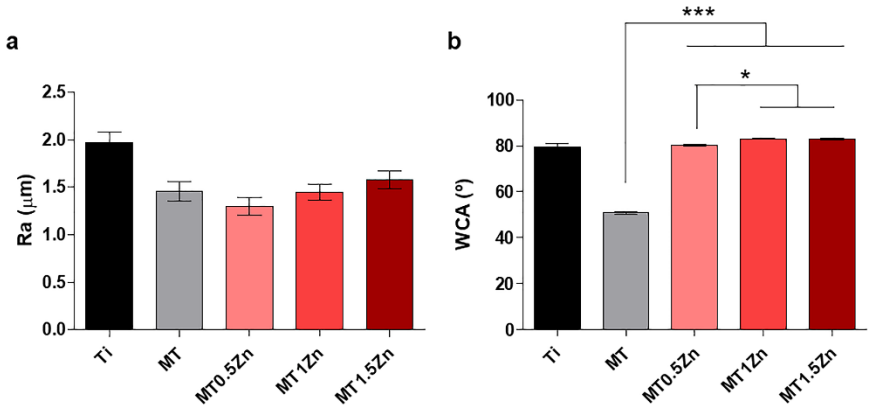

Figure 3.4. The arithmetic average of roughness (Ra; a) and contact angle (WCA; b). Results are shown as mean ± SE. The asterisks ($p \leq 0.05$ (*) and $p \leq 0.001$ (***)) indicate the statistical significance of differences between the materials with and without Zn (MT).

The hydrolytic degradation kinetics of the tested sol-gel materials are shown in **Figure 3.5a**. In general, all the formulations showed the highest mass-loss rates during the first week of incubation in water. Nevertheless, their degradation increased throughout the test period (63 days); reaching mass loss values of approximately 40% of the initial mass. The hydrolytic degradation of sol-gel coatings intensified with an increase in $ZnCl_2$ content. A continuous release of Zn^{2+} was observed until the end of the assay, at 21 days (**Figure 3.5b**). The largest

amounts of Zn^{2+} were released from the material with the highest proportion of $ZnCl_2$ in the MT network.

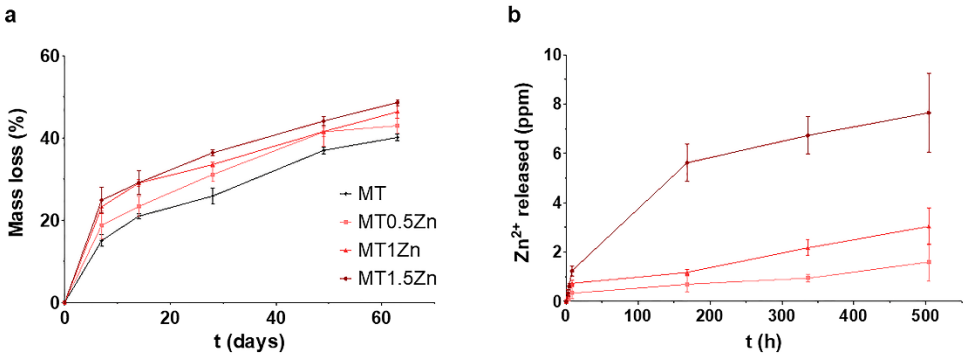

Figure 3.5. Hydrolytic degradation (a) and Zn^{2+} release kinetics (b) for the MT sol-gels doped with $ZnCl_2$. Bars indicate standard errors.

3.3.2. *IN VITRO* ASSAYS

3.3.2.1. *Osteogenic responses: effects on osteoblastic cells*

None of the materials tested were cytotoxic (**Supplementary Figure 3.1**). In tests of cell proliferation, a peak in cell growth was observed after 3 days in all cases, but no significant differences were found for any of the studied coatings (**Figure 3.6a**). The mineralization levels, evaluated by examining the ALP activity, showed a significant increase for MT0.5Zn after 7 days, in comparison with the MT. After 14 days, there was a general increase in the ALP activity; however, it was significantly lower for the MT1Zn and MT1.5Zn materials in comparison with the MT (**Figure 3.6b**).

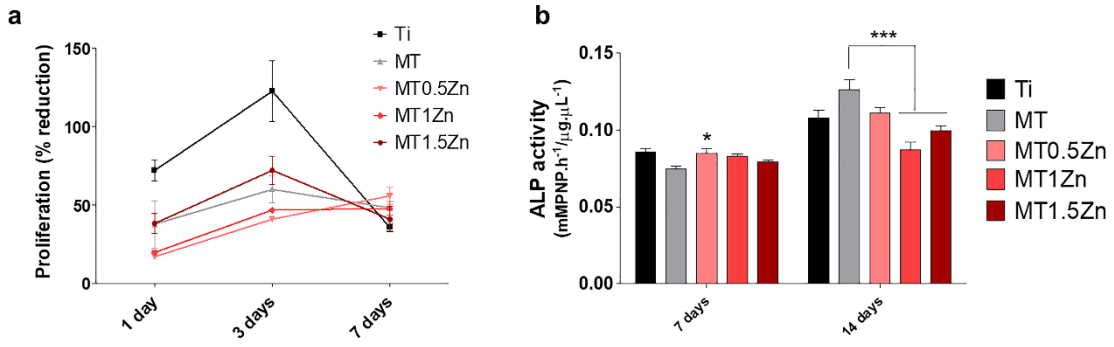

Figure 3.6. MC3T3-E1 (a) cell proliferation after 1, 3, and 7 days and (b) ALP activity after 7 and 14 days. Results are shown as mean ± SE. The asterisks ($p \leq 0.05$ (*) and $p \leq 0.001$ (***)) indicate statistically significant differences between the materials with Zn and the coating without Zn (MT).

To evaluate how Zn-enriched sol-gel coatings affect osteogenesis, gene expression was measured in MC3T3-E1 cells (**Figure 3.7**). An increase in *TGF-β* expression was observed on MT1.5Zn coating after 7 days (**Figure 3.7b**). After 14 days, there was an increase in *ALP* expression on MT1.5Zn and *TGF-β* expression levels on MT0.5Zn and MT1.5Zn coatings (**Figure 3.7a and b**). In what concerns *iNOS* (**Figure 3.7c**), an increase of these markers was detected at 7 days in MT0.5Zn and MT1.5Zn, while MT1Zn showed a significant decrease. After 14 days, this marker was increased in MT1Zn and MT1.5Zn. In the markers related to osteoclastogenesis, *RUNX2* showed an increase in MT1Zn and MT1.5Zn at 7 days (**Figure 3.7d**), while MT1.5Zn lead to an increase of *RANK* in the same time point (**Figure 3.7f**). At 14 days, *RUNX2* was significantly more expressed in MT1.5Zn. *RANKL* expression showed no differences between materials (**Figure 3.7e**).

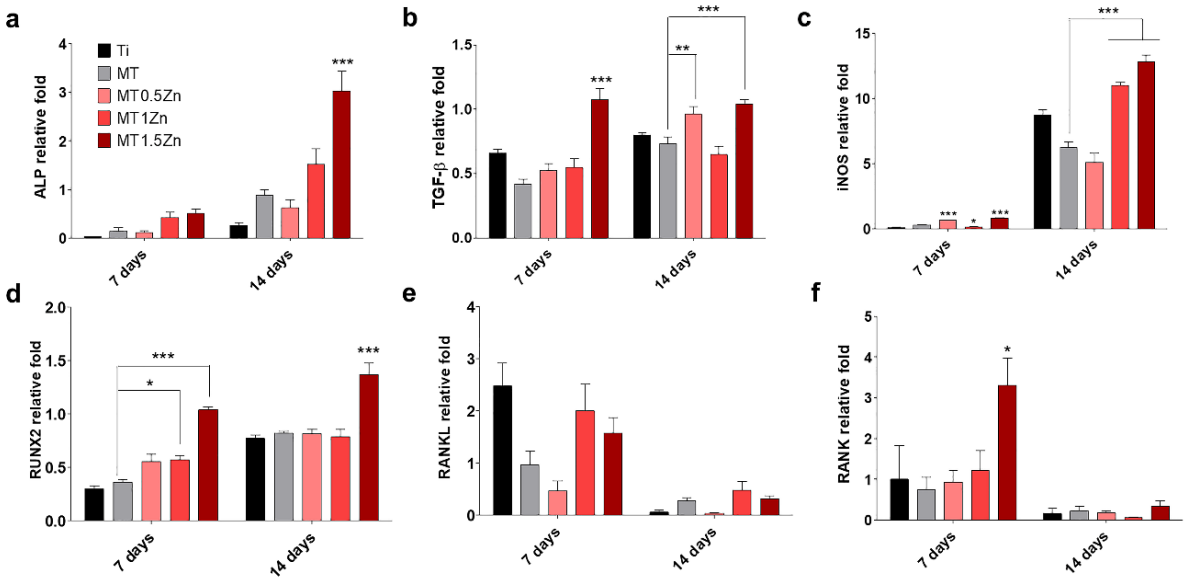

Figure 3.7. Gene expression of (a) ALP, (b) TGFβ, (c) iNOS, (d) RUNX2, (e) RANKL, and (f) RANK in MC3T3-E1 cells at 7 and 14 days of assay. Results are shown as mean ± SE. The asterisks ($p \leq 0.05$ (*), $p \leq 0.01$ (**), and $p \leq 0.001$ (***)) indicate statistically significant IL differences between the materials with Zn and the coating without Zn (MT). Data were normalized to blank wells (without any material) using the $2^{-\Delta\Delta Ct}$ method.

3.3.2.2. *Inflammatory responses: effects on macrophages*

Gene expression of RAW264.7 was examined to evaluate the effects of Zn-enriched sol-gel coatings on inflammatory-response markers (**Figure 3.8**). After 2 days of incubation, there were no changes in pro- or anti-inflammatory marker levels with Zn-coatings, except in *IL-1β*, which presented a significant increase in MT1.5Zn (**Figure 3.8b**). After 4 days, there was a significant increase in *TNF-α* and *IL-1β* gene expression on MT1.5Zn (**Figure 3.8a and b**). An increase in the

expression of *TGF-β* was seen on all the tested materials (**Figure 3.8c**), while *IL-4* showed an increase in MT0.5Zn and MT1.5Zn. The production of *TNF-α* by RAW264.7 cells was measured using ELISA (**Figure 3.8e**). For the first two days, there were no differences between the materials. After 4 days, there was a significant decrease in TNF-α production on Zn-coatings (MT0.5Zn and MT1Zn) in comparison with the MT.

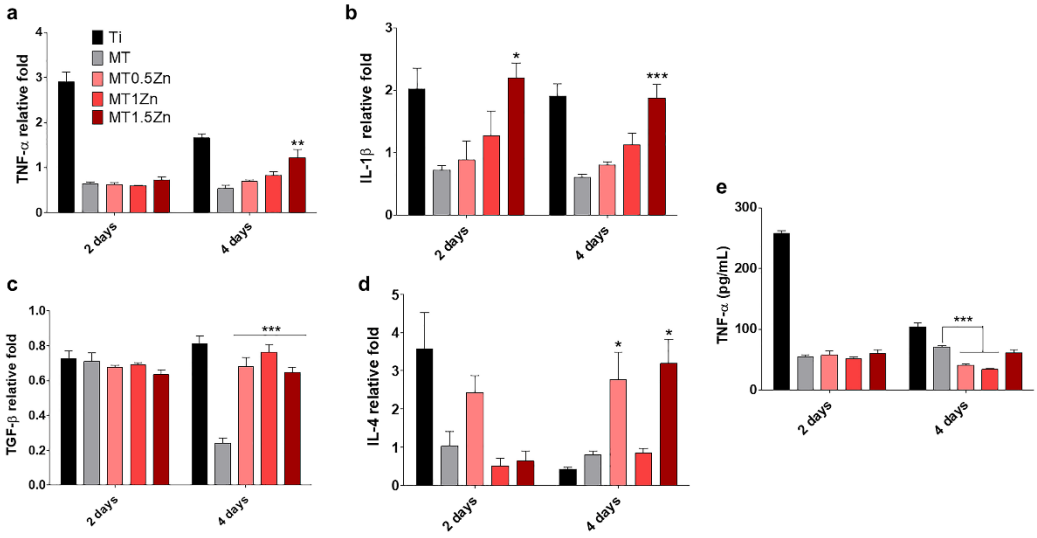

Figure 3.8. Gene expression of (a) TNF-α, (b) IL-1β, (c) TGF-β, and (d) IL-4, and (e) TNF-α cytokine liberation in RAW264.7 cells at 2 and 4 days of assay. Results are shown as mean ± SE. The asterisks ($p \leq 0.05$ (*), $p \leq 0.01$ (**), and $p \leq 0.001$ (***)) indicate statistically significant differences between the materials with Zn and the coating without Zn (MT). Gene expression data were normalized to blank wells (without any material) using the $2^{-\Delta\Delta Ct}$ method.

3.3.3. PROTEOMIC ANALYSIS

A total of 289 distinct proteins were identified in the elutions of the protein layers adsorbed onto the different materials. The comparative analysis using PEAKS detected 61 proteins differentially adsorbed onto the materials enriched with Zn (**Supplementary Table 3.1**). PANTHER and DAVID proteomic tools were employed to classify these proteins by their functions. The differentially adsorbed proteins and their functions associated with the regeneration process are listed in **Table 3.2**. Proteins associated with innate immunity and inflammation were detected in higher proportions on the surfaces with Zn. These were SAMP, CO4A, CO9, CXCL7, CO3, C1S, CO4B and immunoglobulins LAC3, IGJ, and IGKC, as well as FHR1, CLUS, IC1, and VTNC, which have regulatory/anti-inflammatory functions. A cluster of apolipoproteins, linked to lipid metabolism functions, also preferentially adsorbed onto Zn-containing coatings (APOF, APOL1, SAA4, APOC4, APOC3, APOC2, APOA2, and APOA1). HBB

showed increased adsorption to MT0.5Zn and MT1Zn, while reduced amounts of HRG adhered to MT0.5Zn. These two proteins are associated with metal-binding and blood-clotting functions. Similarly, PLF4, PROC, and IPSP proteins, which showed increased affinity to the Zn-containing coatings, were linked to blood coagulation processes. VTNC was found more adsorbed to all the Zn-coatings than to the control surface. This glycoprotein is associated with regenerative functions, but also to blood clotting and the inhibition of immune response. In contrast, TITIN, a metal-binding protein with tissue regeneration functions, showed weakened adsorption onto MT0.5Zn. However, TITIN showed an augmented affinity to the coating doped with 1 % $ZnCl_2$. CERU and KAIN glycoproteins were most abundant on the coating with the highest amount of Zn. CERU is associated with metal-binding, while KAIN is a protease inhibitor. PRDX1, which has a peroxidase activity, showed a weakened affinity to the MT1Zn material, whereas CATB, associated with proteolysis, was less abundant on MT1.5Zn.

Table 3.2. Proteins with important functions in the bone tissue regeneration process differentially adsorbed onto the Zn-containing coatings. Proteins with $p \leq 0.05$ and a ratio higher than 1.5 in either direction (UP: increased and DOWN: reduced) were considered differentially adsorbed.

		MT0.5Zn *vs* MT	**MT1Zn *vs* MT**	**MT1.5Zn *vs* MT**
Immune responses	**UP**	FHR1, IGJ, SAMP, CO4A, CLUS, LAC3, C1S, IGKC	IGJ, SAMP, CO4A, CLUS, CO3, CO4B	FHR1, IGJ, SAMP, CO4A, CO9, CXCL7, CLUS, CO3, IC1
	DOWN	-	-	-
Apolipoproteins	**UP**	APOF, APOL1, SAA4, APOC4, APOC3, APOC2	APOF, APOL1, SAA4, APOA2, APOA1	APOF, APOL1, SAA4, APOC4, APOC2, APOA2
	DOWN	-	-	-
Blood coagulation	**UP**	HBB	PLF4, PROC, HBB	PLF4, IPSP
	DOWN	HRG	-	-
Osteogenesis	**UP**	VTNC	VTNC, TITIN	CERU, VTNC, KAIN
	DOWN	TITIN	PRDX1	CATB

The proteomic tool PANTHER was used to classify the differentially adsorbed proteins according to their participation in biological processes (**Figure 3.9**). The proteins with increased adsorption to the Zn-containing coatings are associated with a wide range of different processes (such as biological regulation, response to a stimulus, developmental, locomotion, metabolic, cellular, multicellular, localization, biogenesis, signaling and immune system processes). In contrast, the proteins with reduced affinity to the Zn-coatings are mainly related to the response to stimulus, biological regulation, and metabolic, cellular, and multicellular functions in biological processes. The biological adhesion and immune system functions were also associated with some of the proteins with reduced affinity to the MT1Zn material.

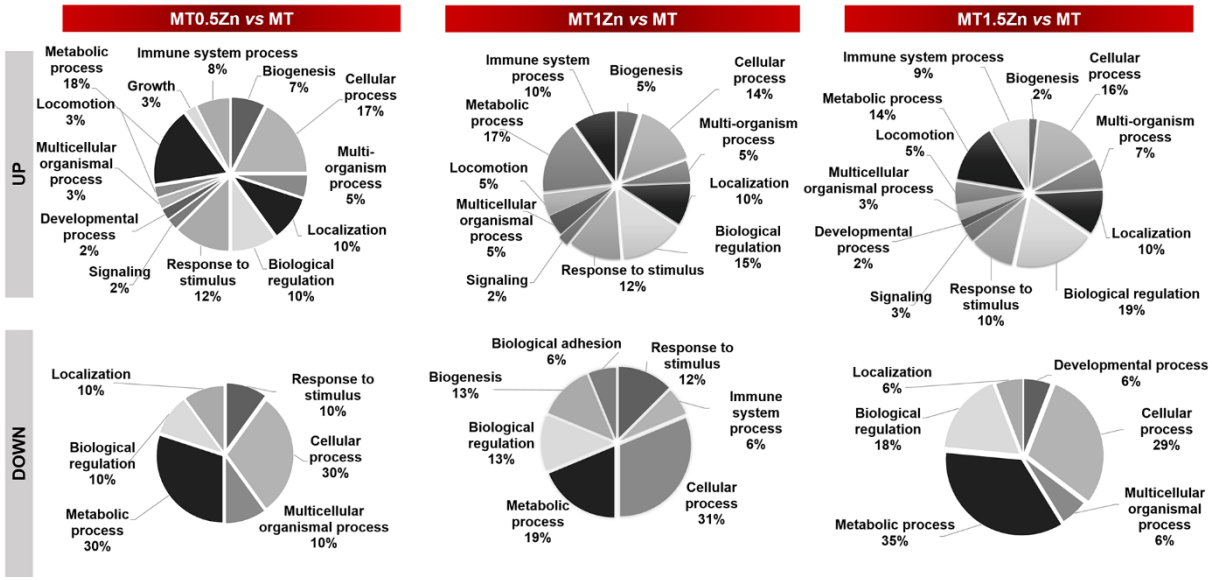

Figure 3.9. PANTHER functional classification of proteins differentially adsorbed onto the Zn-containing coatings in comparison with the control material MT. Proteins with $p \leq 0.05$ and a ratio higher than 1.5 in either direction (UP – increased and DOWN – reduced) were considered differentially adsorbed.

3.4. Discussion

The main aim of this study was to develop and characterize a new bioactive Zn-doped sol-gel coating for a Ti substrate. The effects of this element on protein adsorption and cellular responses in terms of osteogenesis and inflammation were evaluated. Zinc is an essential trace element with a stimulatory effect on bone growth and a pivotal role in bone maintenance. It has been described as the 'calcium of the twenty-first century' since Zn-containing biomaterials are showing great promise in applications for bone tissue regeneration [13].

The Zn-doped sol-gel coatings were obtained following the sol-gel route. The incorporation of this compound did not affect the degree of crosslinking in the new sol-gel network or caused

significant differences in surface roughness of the new coatings. However, increasing the amount of Zn in the sol-gel resulted in a significant reduction of the material hydrophilicity. The material without Zn lost approximately 40% of its mass after 63 days of incubation in water. The incorporation of $ZnCl_2$ increased the hydrolytic degradation rate; the MT1.5Zn composition lost around 50 % of its mass after the same period. A controlled Zn^{2+} release was achieved as more Zn salt was incorporated into the network; the more Zn was liberated. The release of this compound continued until the end of the essay (21 days), demonstrating consistent long-term release properties. The quantified Zn^{2+} concentrations were less than 10 ppm in all the cases, not reaching the limit of cellular toxicity of 26.2 ppm defined by Brauer *et al.* [31]. Moreover, *in vitro* results showed that these new Zn-containing coatings were not cytotoxic to MC3T3-E1 cells.

The analysis of MC3T3-E1 osteogenic markers showed that RUNX2 expression, a member of the runt domain family involved in bone development, was increased at 7 and 14 days. Yamaguchi *et al*. [32] showed zinc sulphate upregulates the RUNX2 expression. This was accompanied by the augmented ALP expression at 14 days in MT1.5Zn, whose activity is activated by RUNX2 [33] and stimulated by Zn in MC3T3-E1 cells [6]. Additionally, TGF-β gene expression was increased on MT0.5Zn and MT1.5Zn. This cytokine is critical in the promotion of bone formation, as it plays roles in the recruitment of osteoblast, and enhancement of osteoblast proliferation and differentiation [34], thus confirming the effects of these Zn-doped coatings in the osteoblastic differentiation.

Inflammation is required to protect the host from tissue damage, which leads to the restoration of homeostasis. The pro-inflammatory markers *TNF-α* and *IL-1β* [35] presented an increased gene expression in MT1.5Zn after 4 days of culture, while, at the same time point, MT0.5Zn and MT1Zn secreted significantly less TNF-α. Similarly, Giovanni *et al.* [36] developed zinc oxide nanoparticles that lead to an increased fold change in TNF-α and IL-1β in a dose-response manner. On the other hand, the overexpression of *TGF-β* and *IL-4* [35], two anti-inflammatory markers, in Zn-containing materials, confirming that the inflammatory responses might depend on the used Zn concentration.

The phenomenon of protein adsorption onto a material can affect the initial biological healing processes [37]. Therefore, studying how proteins are attached to a surface can help to predict a biomaterial outcome. The nLC-MS/MS analysis identified significant changes in the patterns of proteins adsorbed associated with increasing amounts of Zn incorporated onto the sol-gel coating. Among the proteins found, a set belonging to a cluster related to the innate immune

system was identified, containing immunoglobulins and complement system proteins such as C1S, CO3, CO4A, CO4B and CO9, which can activate the cascade of pro-inflammatory response [20]. In general, these proteins tended to increase their attachment affinity to the surfaces as more Zn was added to the sol-gel. However, a clear increase in the adsorption of proteins associated with inhibitory/regulatory functions of complement cascade was also observed. Proteins such as VTNC, IC1, FHR1, and CLUS, which showed augmented affinity to Zn-enriched coatings, can control the complement system activation. They act as anti-inflammatory factors [38]. The increased adsorption of this group of proteins is consistent with the anti-inflammatory potential observed *in vitro*. Likewise, the increased attachment of apolipoproteins onto the materials with Zn could affect the immune response regulation. This protein family can prevent the initiation of innate immune response by inhibition of NF-κB-dependent gene expression [39].

Moreover, the VTNC can promote the macrophage polarization into the M2 pro-regenerative phenotype [40]. This protein is associated with the coagulation system; it contributes to thrombus formation and participates in vascular homeostasis and tissue regeneration [41]. VTNC is also involved in bone metabolism as it can promote the osteogenic differentiation of mesenchymal stem cells [42]. It improves the bone healing capacity of Ti implants [43] and the biomaterial vascularization process [44]. The rise in VTCN adsorption with increasing Zn content in the coatings might be correlated with their increased osteogenic activity. Moreover, TITIN, more abundant on the MT1Zn, has been associated with signaling in bone remodeling. It has also been linked with an increase in cell proliferation of MG-63 osteoblasts via activation of the Wnt/β-catenin pathway [45]. Similarly, CXCL7, preferentially adsorbed onto MT1.5Zn, can significantly stimulate the recruitment of human mesenchymal stem cells (MSC) *in vitro* [46].

The studies of the role of Zn^{2+} in bone resorption have revealed that the osteoclasts are sensitive to this ion; a significant decrease in bone resorption occurs at the concentration as low as 10^{-14} M [47]. Binding of RANKL to its receptor RANK activates NF-kB, inducing osteoclast differentiation. Zn^{2+} may reduce osteoclastogenesis via suppression of RANK expression through prevention of oxidative stress species production [7]. In this study, no differences in the expression RANKL were found. Similarly, Yusa et *al.* [33] found that Zn did not affect RANKL or OPG mRNA expression in zinc-modified titanium surfaces, which is consistent with these results. However, *RANK* expression increased for MT1.5Zn; in parallel *iNOS* marker resulted overexpressed for MT1Zn and MT1.5Zn. Thus, the effect of Zn-enriched materials on osteoclastogenesis could depend on the added Zn concentration.

The proteomic results indicate that Zn could also affect the coagulation processes around the implant materials. The proteins with pro-coagulant (VTNC, PLF4, IPSP, and HBB) and anti-coagulant functions (PROC) showed increased adsorption to Zn-containing surfaces, in a Zn dose-dependent manner. It is difficult to predict the real-life effect of these proteins on the implant surface. Some studies have described a potential anticoagulation role of Zn-alloy biomaterials [48,49]. However, it has also been reported that high concentrations of Zn^{2+} might promote thrombosis [49].

Interestingly, CERU, an acute-phase protein with antioxidant properties, showed increased adsorption to the surfaces with Zn (a 21-fold increase on the MT1.5Zn material in comparison with the control surface). This protein is known as the main warehouse of plasma copper, but it can also bind to Zn via its copper-binding sites [50]. Its augmented adsorption in MT1.5Zn supports these findings. High levels of CERU in plasma have been associated with osteoporosis, independently of other inflammatory parameters [51]. However, its role in this bone disease is unknown. KAIN, which belongs to the serine proteinase inhibitor superfamily, was also significantly more abundant on the MT1.5Zn surface. This protein exerts its anti-inflammatory effect via the canonical Wnt pathway [52]. It can stimulate the M2 phenotype in cultured RAW 264.7 macrophages, causing overexpression of IL-10 [53]. However, KAIN plays a dual role in angiogenesis. It inhibits the process by blocking VEGF-induced effects and TNF-α-induced VEGF synthesis, but it can also stimulate neovascularization by increasing the levels of endothelial nitric oxide synthase (eNOS) and VEGF [54].

The adsorption of the proteins CATB and PRDX1 was reduced on the MT1.5Zn and MT1Zn surfaces (33-fold and 25-fold decrease), respectively. The peroxidase PRDX1 is associated with various biological processes such as the detoxification of oxidants and cell apoptosis. Du *et al.* have reported that the association between oestrogen and this protein might affect the osteoblast cell responses to oxidative stress [55]. CATB is an enzyme involved in promoting chronic inflammation, delaying tissue healing [56]. This protein is also responsible for NF-kB activation via autophagy degradation of IkBα in microglia/macrophages [57]. Moreover, elevated levels of CATB are typically observed in many chronic inflammatory diseases, including rheumatoid arthritis and periodontitis [58,59]. Thus, its diminished affinity to Zn-containing biomaterials might have a positive effect on tissue regeneration.

3.5. Conclusion

New sol-gel materials doped with increasing amounts of Zn were applied as coatings onto Ti discs, allowing the control of the release kinetics of this ion. The presence of Zn affected the *in*

vitro responses of osteoblasts and macrophages and protein adsorption onto the coated surfaces. The levels of *ALP*, *TGF-β*, and *RUNX2* gene expression in osteoblasts increased for the materials with Zn, showing the osteogenic potential of these materials. The fold-changes in *TNF-α*, *IL-1β*, *TGF-β* and *IL-4* show that the inflammatory responses these are dependent on the amount of Zn is incorporated into the material. The nLC-MS/MS proteomic analysis revealed that the addition of Zn significantly changed the attachment of proteins involved in the immune, coagulation, and regenerative processes. Zinc sharply increased the adsorption of proteins regulating the immune reaction, such as VTNC, IC1, FHR1, CLUS, and KAIN. In contrast, it decreased the adsorption of CATB protein, which is associated with chronic inflammation and delayed healing. Moreover, an increased proportion of proteins with osteogenic function, such as VTNC, attached to the Zn-containing coatings. Thus, the proteomic results were consistent with the biological responses observed *in vitro*. Our results show the future possibility of clinical application of these new coatings to bioactivate Ti prostheses.

3.6. Acknowledgments

This work was supported by MINECO [MAT2017-86043-R; RTC-2017-6147-1], Generalitat Valenciana [GRISOLIAP/2018/091], Universitat Jaume I under [UJI-B2017-37, Posdoc/2019/28], the University of the Basque Country under [GIU18/189] and Basque Government under [PRE_2017_2_0044]. The authors would like to thank Raquel Oliver, Jose Ortega and Iraide Escobés for their valuable technical assistance, and Antonio Coso (GMI-Ilerimplant) for producing the titanium discs.

3.7. References

1. Dalisson, B. & Barralet, J. Bioinorganics and Wound Healing. *Adv. Healthc. Mater.* **1900764**, 1–22 (2019).
2. Pemmer, B. *et al.* Spatial distribution of the trace elements zinc, strontium and lead in human bone tissue. *Bone* **57**, 184–193 (2013).
3. Huang, T., Yan, G. & Guan, M. Zinc homeostasis in bone: Zinc transporters and bone diseases. *Int. J. Mol. Sci.* **21**, (2020).
4. O'Neill, E., Awale, G., Daneshmandi, L., Umerah, O. & Lo, K. W. H. The roles of ions on bone regeneration. *Drug Discovery Today* **23**, 879–890 (2018).
5. Yang, H. *et al.* Enhanced Osseointegration of Zn-Mg Composites by Tuning the Release of Zn Ions with Sacrificial Mg-Rich Anode Design. *ACS Biomater. Sci. Eng.* **5**, 453–467 (2019).
6. Seo, H., Cho, Y., Kim, T., Shin, H. & Kwun, I. Zinc may increase bone formation through stimulating cell proliferation , alkaline phosphatase activity and collagen synthesis in

osteoblastic MC3T3-E1 cells. *Nutr. Res. Pract.* **4**, 356–361 (2010).

7. Amin, N., Clark, C. C. T., Taghizadeh, M. & Djafarnejad, S. Zinc supplements and bone health: The role of the RANKL-RANK axis as a therapeutic target. *J. Trace Elem. Med. Biol.* **57**, 126417 (2020).
8. Prasad, A. S. Discovery of Human Zinc De fi ciency : Its Impact on. *Adv. Nutr.* **4**, 176–190 (2013).
9. Prasad, A. S. Zinc is an antioxidant and anti-inflammatory agent : its role in human health. *Front. Nutr.* **1**, 1–10 (2014).
10. Prasad, A. S., Bao, B., Beck, F. W., Kucuk, O. & Sarkar, F. H. Antioxidant effect of zinc in humans. *Free Radic. Biol. Med.* **37**, 1182–1190 (2004).
11. Jiménez, M., Abradelo, C., San Román, J. & Rojo, L. Bibliographic review on the state of the art of strontium and zinc based regenerative therapies. Recent developments and clinical applications. *J. Mater. Chem. B* **7**, 1974–1985 (2019).
12. Osorio, R., Cabello, I. & Toledano, M. Bioactivity of zinc-doped dental adhesives. *Journal of dentistry* **42**, 403–412 (2014).
13. Su, Y. *et al.* Zinc-Based Biomaterials for Regeneration and Therapy. *Trends Biotechnol.* **37**, 428–441 (2019).
14. Vishwakarma, A. *et al.* Engineering Immunomodulatory Biomaterials To Tune the Inflammatory Response. *Trends Biotechnol.* **34**, 470–482 (2016).
15. Romero-Gavilán, F. *et al.* Proteomic analysis of silica hybrid sol-gel coatings: a potential tool for predicting the biocompatibility of implants in vivo. *Biofouling* **In press**, (2017).
16. Huang, J., Yue, Y. & Zheng, C. Vroman effect of plasma protein adsorption to biomaterials surfaces. *J. Biomed. Eng.* **16**, 371–6 (1999).
17. Nicolin, V., Iaco, D. De & Valentini, R. Osteoimmunology represents a link between skeletal and immune system. *Ital. J. Anat. Embrylogy* **121**, 37–42 (2016).
18. Romero Gavilán, F. *et al.* Proteomic analysis of calcium-enriched sol-gel biomaterials. *JBIC J. Biol. Inorg. Chem.* **24**, 563–574 (2019).
19. Markiewski, M. M., Nilsson, B., Ekdahl, K. N., Mollnes, T. E. & Lambris, J. D. Complement and coagulation : strangers or partners in crime ? *Trends Immunol.* **28**, 184–192 (2007).
20. Araújo Gomes, N. *et al.* Complement proteins regulating macrophage polarisation on biomaterials. *Colloids Surfaces B Biointerfaces* **181**, 125–133 (2019).
21. Romero-Gavilan, F. *et al.* Bioactive potential of silica coatings and its effect on the adhesion of proteins to titanium implants. *Colloids Surfaces B Biointerfaces* **162**, 316–325 (2018).
22. Romero-Gavilán, F. *et al.* Proteome analysis of human serum proteins adsorbed onto

different titanium surfaces used in dental implants. *Biofouling* **33**, 98–111 (2017).

23. Martinez-Ibañez, M. *et al.* Biological characterization of a new silicon based coating developed for dental implants. *J. Mater. Sci. Mater. Med.* **27**, (2016).
24. International Organization for Standardization. Biological evaluation of medical devices - Part 5: Tests for in vitro cytotoxicity. **3 ED**, 42 (2009).
25. International Organization for Standardization. Biological evaluation of medical devices - Part 12: Sample preparation and reference materials. 20 (2012). Available at: https://www.iso.org/standard/53468.html. (Accessed: 6th April 2020)
26. Cerqueira, A. *et al.* A possible use of melatonin in the dental fi eld : Protein adsorption and in vitro cell response on coated titanium. *Mater. Sci. Eng. C* **116**, 111262 (2020).
27. Kim, H. N. & Lee, S. K. Atomic structure and dehydration mechanism of amorphous silica: Insights from 29Si and 1H solid-state MAS NMR study of SiO2 nanoparticles. *Geochim. Cosmochim. Acta* **120**, 39–64 (2013).
28. Juan-Díaz, M. J. *et al.* Study of the degradation of hybrid sol–gel coatings in aqueous medium. *Prog. Org. Coatings* **77**, 1799–1806 (2014).
29. Romero-Gavilán, F. *et al.* Control of the degradation of silica sol-gel hybrid coatings for metal implants prepared by the triple combination of alkoxysilanes. *J. Non. Cryst. Solids* **453**, 66–73 (2016).
30. Almeida, J. C. *et al.* Structural characterization of PDMS–TEOS–CaO–TiO2 hybrid materials obtained by sol–gel. *Mater. Chem. Phys.* **143**, 557–563 (2014).
31. Brauer, D. S., Gentleman, E., Farrar, D. F., Stevens, M. M. & Hill, R. G. Benefits and drawbacks of zinc in glass ionomer bone cements. *Biomed. Mater.* **6**, 045007 (2011).
32. Yamaguchi, M., Goto, M., Uchiyama, S. & Nakagawa, T. Effect of zinc on gene expression in osteoblastic MC3T3-E1 cells: Enhancement of Runx2, OPG, and regucalcin mRNA expressions. *Mol. Cell. Biochem.* **312**, 157–166 (2008).
33. Yusa, K. *et al.* Eluted zinc ions stimulate osteoblast differentiation and mineralization in human dental pulp stem cells for bone tissue engineering. *Arch. Oral Biol.* **71**, 162–169 (2016).
34. Janssens, K., Ten Dijke, P., Janssens, S. & Van Hul, W. Transforming growth factor-β1 to the bone. *Endocrine Reviews* **26**, 743–774 (2005).
35. Gu, Q., Yang, H. & Shi, Q. Macrophages and bone inflammation. *J. Orthop. Transl.* **10**, 86–93 (2017).
36. Giovanni, M. *et al.* Pro-inflammatory responses of RAW264.7 macrophages when treated with ultralow concentrations of silver, titanium dioxide, and zinc oxide nanoparticles. *J. Hazard. Mater.* **297**, 146–152 (2015).

37. Romero-Gavilán, F. *et al.* The effect of strontium incorporation into sol-gel biomaterials on their protein adsorption and cell interactions. *Colloids Surfaces B Biointerfaces* **174**, 9–16 (2019).

38. Mollnes, T. E. & Kirschfink, M. Strategies of therapeutic complement inhibition. *Mol. Immunol.* **43**, 107–121 (2006).

39. Cho, N. H. & Seong, S. Y. Apolipoproteins inhibit the innate immunity activated by necrotic cells or bacterial endotoxin. *Immunology* **128**, 479–486 (2009).

40. Chen, Z. *et al.* Osteoimmunomodulation for the development of advanced bone biomaterials. *Mater. Today* **19**, 304–321 (2016).

41. Leavesley, D. I. *et al.* Vitronectin - Master controller or micromanager? *IUBMB Life* **65**, (2013).

42. Salasznyk, R. M., Williams, W. A., Boskey, A., Batorsky, A. & Plopper, G. E. Adhesion to Vitronectin and Collagen I Promotes Osteogenic Differentiation of Human Mesenchymal Stem Cells. *J. Biomed. Biotechnol.* **2004**, 24–34 (2004).

43. Cho, C. *et al.* A Vitronectin-Derived Bioactive Peptide Improves Bone Healing Capacity of SLA Titanium Surfaces. *Materials (Basel).* **12**, 1–11 (2019).

44. Hessenauer, M. E. T. *et al.* Acta Biomaterialia Vitronectin promotes the vascularization of porous polyethylene biomaterials. *Acta Biomater.* **82**, 24–33 (2018).

45. Qi, J., Chi, L., Labeit, S. & Banes, A. J. Nuclear localization of the titin Z1Z2Zr domain and role in regulating cell proliferation. *Am. J. Physiol. - Cell Physiol.* **295**, 975–985 (2008).

46. Kalwitz, G. *et al.* Gene expression profile of adult human bone marrow-derived mesenchymal stem cells stimulated by the chemokine CXCL7. *Int. J. Biochem. Cell Biol.* **41**, 649–658 (2009).

47. Moonga, B. S. & Dempster, D. W. Zinc is a potent inhibitor of osteoclastic bone resorption in vitro. *J Bone Min. Res* **10**, 453–457 (1995).

48. Yin, Y. X. *et al.* Hemocompatibility of biodegradable Zn-0.8 wt% (Cu, Mn, Li) alloys. *Mater. Sci. Eng. C* **104**, 109896 (2019).

49. Ma, J., Zhao, N. & Zhu, D. Endothelial Cellular Responses to Biodegradable Metal Zinc. *ACS Biomater. Sci. Eng.* **1**, 1174–1182 (2015).

50. Samygina, V. R. *et al.* Rat ceruloplasmin: A new labile copper binding site and zinc/copper mosaic. *Metallomics* **9**, 1828–1838 (2017).

51. Karakas, E. Y. *et al.* Usefulness of ceruloplasmin testing as a screening methodology for geriatric patients with osteoporosis. *J. Phys. Ther. Sci.* **28**, 235–239 (2016).

52. Liu, X. *et al.* Antiangiogenic and antineuroinflammatory effects of kallistatin through interactions with the canonical wnt pathway. *Diabetes* **62**, 4228–4238 (2013).

53. Bing, L. *et al.* Kallistatin Inhibits Atherosclerotic Inflammation by Regulating Macrophage Polarization. *Hum. Gene Ther.* **30**, 339–351 (2019).

54. Chao, J., Li, P. & Chao, L. Kallistatin: Double-edged role in angiogenesis, apoptosis and oxidative stress. *Biol. Chem.* **398**, 1309–1317 (2017).

55. Du, J. *et al.* Ovariectomy upregulated the expression of Peroxiredoxin 1 & 5 in osteoblasts of mice. *Sci. Rep.* **6**, 1–11 (2016).

56. Li, X. *et al.* Cathepsin B Regulates Collagen Expression by Fibroblasts via Prolonging TLR2/NF-κB Activation. *Oxid. Med. Cell. Longev.* **2016**, (2016).

57. Ni, J. *et al.* The critical role of proteolytic relay through cathepsins B and E in the phenotypic change of microglia/macrophage. *J. Neurosci.* **35**, 12488–12501 (2015).

58. Tong, B. *et al.* Role of cathepsin B in regulating migration and invasion of fibroblast-like synoviocytes into inflamed tissue from patients with rheumatoid arthritis. *Clin. Exp. Immunol.* **177**, 586–597 (2014).

59. Cox, S. W. *et al.* Collagen degradation by interleukin-1 β-stimulated gingival fibroblasts is accompanied by release and activation of multiple matrix metalloproteinases and cysteine proteinases. *Oral Dis.* **12**, 34–40 (2006).

3.8. SUPPLEMENTARY MATERIAL

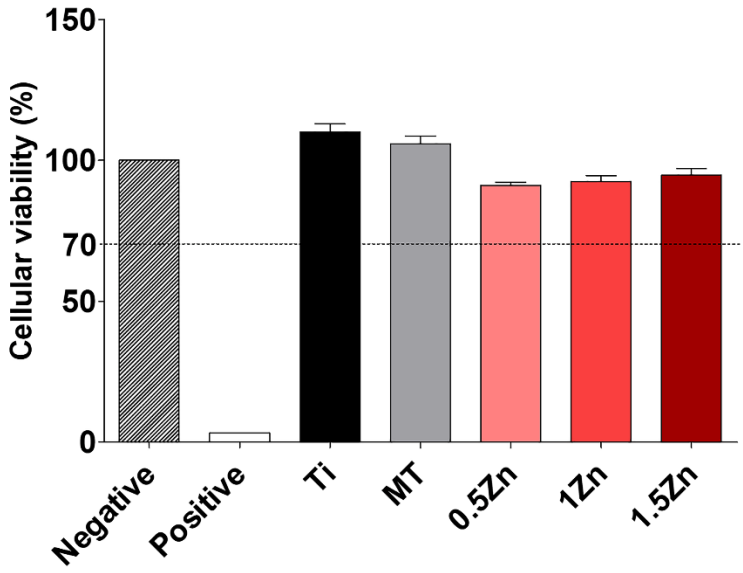

Supplementary figure 3.1. MC3T3-E1 cellular viability when exposed to the materials in study. A cellular viability below 70% indicates that the material is cytotoxic. Results are shown as mean ± SE.

Supplementary table 3.1. Progenesis comparative analysis between the proteins identified onto the Zn-containing materials with respect to the control treatment without Zn. Proteins with ANOVA $p < 0.05$ (yellow) and a ratio higher than 1.5 in either direction was considered as significantly different. Proteins with increased affinity to $ZnCl_2$ coatings in comparison to MT are marked in red, while those with reduced affinity appear in green.

		MT0.5Zn *vs* MT		**MT1Zn *vs* MT**		**MT1.5Zn *vs* MT**	
Accession	**Description**	***p* value**	**Ratio**	***p* value**	**Ratio**	***p* value**	**Ratio**
HORN_HUMAN	Hornerin	1.86E-01	3.31	2.02E-01	9.15	9.73E-05	334.94
ITIH2_HUMAN	Inter-alpha-trypsin inhibitor heavy chain H2	1.45E-01	5.19	1.01E-01	7.23	9.40E-03	35.42
APOF_HUMAN	Apolipoprotein F	5.46E-03	33.51	4.84E-03	37.14	1.87E-02	22.61
CERU_HUMAN	Ceruloplasmin	3.81E-01	2.84	1.51E-01	4.28	1.57E-02	21.28
PLF4_HUMAN	Platelet factor 4	3.55E-01	0.47	1.37E-02	1.95	8.23E-04	15.07
TRY1_HUMAN	Trypsin-1	1.07E-01	1.48	9.77E-02	2.17	4.76E-03	15.02
APOL1_HUMAN	Apolipoprotein L1	1.74E-04	7.47	5.49E-04	5.86	2.64E-05	14.18
SAA4_HUMAN	Serum amyloid A-4 protein	3.72E-02	5.91	4.87E-02	6.50	1.05E-02	12.27
CO1A1_HUMAN	Collagen alpha-1(I) chain	8.47E-01	0.88	6.43E-01	1.66	8.38E-03	11.74
VTNC_HUMAN	Vitronectin	3.25E-02	3.15	1.76E-02	4.36	1.86E-03	9.04
FHR1_HUMAN	Complement factor H-related protein 1	1.23E-02	5.15	2.62E-01	2.40	3.13E-02	7.89
IGJ_HUMAN	Immunoglobulin J chain	6.90E-03	3.78	4.18E-03	4.83	1.24E-03	7.33
APOC4_HUMAN	Apolipoprotein C-IV	3.42E-02	5.29	1.94E-01	2.84	4.49E-02	6.93
DEF3_HUMAN	Neutrophil defensin 3	7.91E-01	0.87	9.88E-01	1.00	3.42E-03	6.40
APOC3_HUMAN	Apolipoprotein C-III	4.49E-02	5.20	1.05E-01	3.45	5.33E-02	6.25

SAMP_HUMAN	Serum amyloid P-component	1.95E-02	3.03	7.22E-03	3.78	1.14E-02	5.94
CO4A_HUMAN	Complement C4-A	2.61E-02	3.10	1.95E-02	3.43	1.17E-02	4.94
CO9_HUMAN	Complement component C9	2.60E-01	1.93	1.73E-01	2.20	1.22E-02	4.68
CXCL7_HUMAN	Platelet basic protein	8.98E-01	0.92	5.02E-01	1.39	2.08E-02	4.63
APOC2_HUMAN	Apolipoprotein C-II	1.16E-02	3.25	6.06E-02	2.55	1.97E-02	4.56
ITIH1_HUMAN	Inter-alpha-trypsin inhibitor heavy chain H1	5.75E-01	1.55	2.67E-01	2.31	3.75E-02	4.50
CLUS_HUMAN	Clusterin	7.33E-03	5.04	2.12E-02	4.14	1.32E-02	4.32
KAIN_HUMAN	Kallistatin	5.31E-02	2.67	5.30E-01	1.58	1.50E-02	4.28
IPSP_HUMAN	Plasma serine protease inhibitor	4.46E-01	1.60	2.37E-01	2.10	2.26E-02	3.89
HBA_HUMAN	Hemoglobin subunit alpha	2.98E-02	5.53	2.54E-02	4.87	4.38E-02	3.65
TITIN_HUMAN	Titin	3.74E-02	0.23	1.68E-02	4.89	5.95E-02	3.18
CO3_HUMAN	Complement C3	1.14E-01	1.67	3.00E-02	1.91	7.14E-03	2.76
IC1_HUMAN	Plasma protease C1 inhibitor	1.51E-01	1.72	1.17E-01	1.77	1.11E-02	2.60
APOA2_HUMAN	Apolipoprotein A-II	3.56E-01	1.30	4.28E-04	2.74	4.91E-02	2.59
LAC3_HUMAN	Ig lambda-3 chain C regions	4.25E-02	2.75	9.10E-02	2.25	7.15E-02	2.48
C1S_HUMAN	Complement C1s subcomponent	3.11E-02	2.46	7.24E-02	2.14	1.41E-01	2.02
PROC_HUMAN	Vitamin K-dependent protein C	1.00E+00	1.00	4.49E-02	2.26	5.10E-02	2.02
CO4B_HUMAN	Complement C4-B	1.15E-01	2.33	3.48E-02	3.16	3.66E-01	2.00
CO7A1_HUMAN	Collagen alpha-1(VII) chain	4.31E-02	3.34	2.76E-01	1.86	2.99E-01	1.85
IGKC_HUMAN	Ig kappa chain C region	4.35E-02	2.38	3.09E-01	1.48	1.95E-01	1.71
HBB_HUMAN	Hemoglobin subunit beta	4.58E-02	2.38	3.69E-02	3.11	1.72E-01	1.54

APOA1_HUMAN	Apolipoprotein A-I	2.48E-01	1.38	2.40E-02	1.89	4.85E-01	1.27
HRG_HUMAN	Histidine-rich glycoprotein	4.37E-03	0.33	2.88E-01	0.68	9.81E-01	1.01
RS13_HUMAN	40S ribosomal protein S13	1.79E-02	4.46	3.62E-01	1.99	9.27E-01	0.96
DCD_HUMAN	Dermcidin	4.56E-02	2.02	9.72E-01	0.98	8.70E-01	0.92
HSP7C_HUMAN	Heat shock cognate 71 kDa protein	1.40E-02	9.56	3.74E-01	2.42	6.54E-01	0.64
EF1A3_HUMAN	Putative elongation factor 1-alpha-like 3	1.31E-02	4.74	8.75E-01	1.13	6.98E-02	0.34
TBA1B_HUMAN	Tubulin alpha-1B chain	9.80E-01	1.03	2.45E-02	0.09	1.70E-01	0.29
VIME_HUMAN	Vimentin	5.95E-01	0.50	7.35E-02	0.37	3.78E-02	0.28
PLEC_HUMAN	Plectin	4.03E-01	0.37	3.41E-02	0.08	1.39E-01	0.24
DSG1_HUMAN	Desmoglein-1	2.66E-01	0.43	3.67E-02	0.14	1.34E-01	0.23
K1109_HUMAN	Uncharacterized protein KIAA1109	2.43E-02	6.88	9.09E-01	0.83	1.85E-01	0.20
GSDMA_HUMAN	Gasdermin-A	4.69E-01	0.44	4.88E-02	0.06	1.79E-01	0.20
PGK1_HUMAN	Phosphoglycerate kinase 1	3.30E-01	2.90	1.08E-01	0.20	3.77E-02	0.19
PSA6_HUMAN	Proteasome subunit alpha type-6	4.00E-02	0.08	7.81E-02	0.13	1.03E-01	0.15
FILA2_HUMAN	Filaggrin-2	1.75E-01	0.36	1.15E-01	0.24	3.72E-02	0.14
DR9C7_HUMAN	Short-chain dehydrogenase/reductase family 9C member 7	3.79E-02	5.58	8.66E-01	0.82	6.49E-02	0.13
PRDX1_HUMAN	Peroxiredoxin-1	5.14E-01	0.43	3.79E-02	0.04	1.28E-01	0.12
PSA3_HUMAN	Proteasome subunit alpha type-3	1.66E-01	0.26	1.14E-01	0.22	3.96E-02	0.11
ALDOA_HUMAN	Fructose-bisphosphate aldolase A	2.17E-01	2.04	3.37E-01	0.63	1.94E-02	0.10
CAN1_HUMAN	Calpain-1 catalytic subunit	1.87E-01	0.27	5.30E-01	0.50	4.32E-02	0.10

PSA7_HUMAN	Proteasome subunit alpha type-7	4.03E-02	0.05	1.19E-01	0.10	7.37E-02	0.09
TGM1_HUMAN	Protein-glutamine gamma-glutamyltransferase K	2.82E-01	0.17	4.90E-02	0.08	8.24E-02	0.07
CASPE_HUMAN	Caspase-14	2.46E-01	0.21	2.99E-02	0.02	5.94E-02	0.04
SPB3_HUMAN	Serpin B3	3.86E-01	0.28	8.90E-02	0.08	4.50E-02	0.04
CATB_HUMAN	Cathepsin B	1.79E-01	0.08	1.17E-01	0.06	4.43E-02	0.03

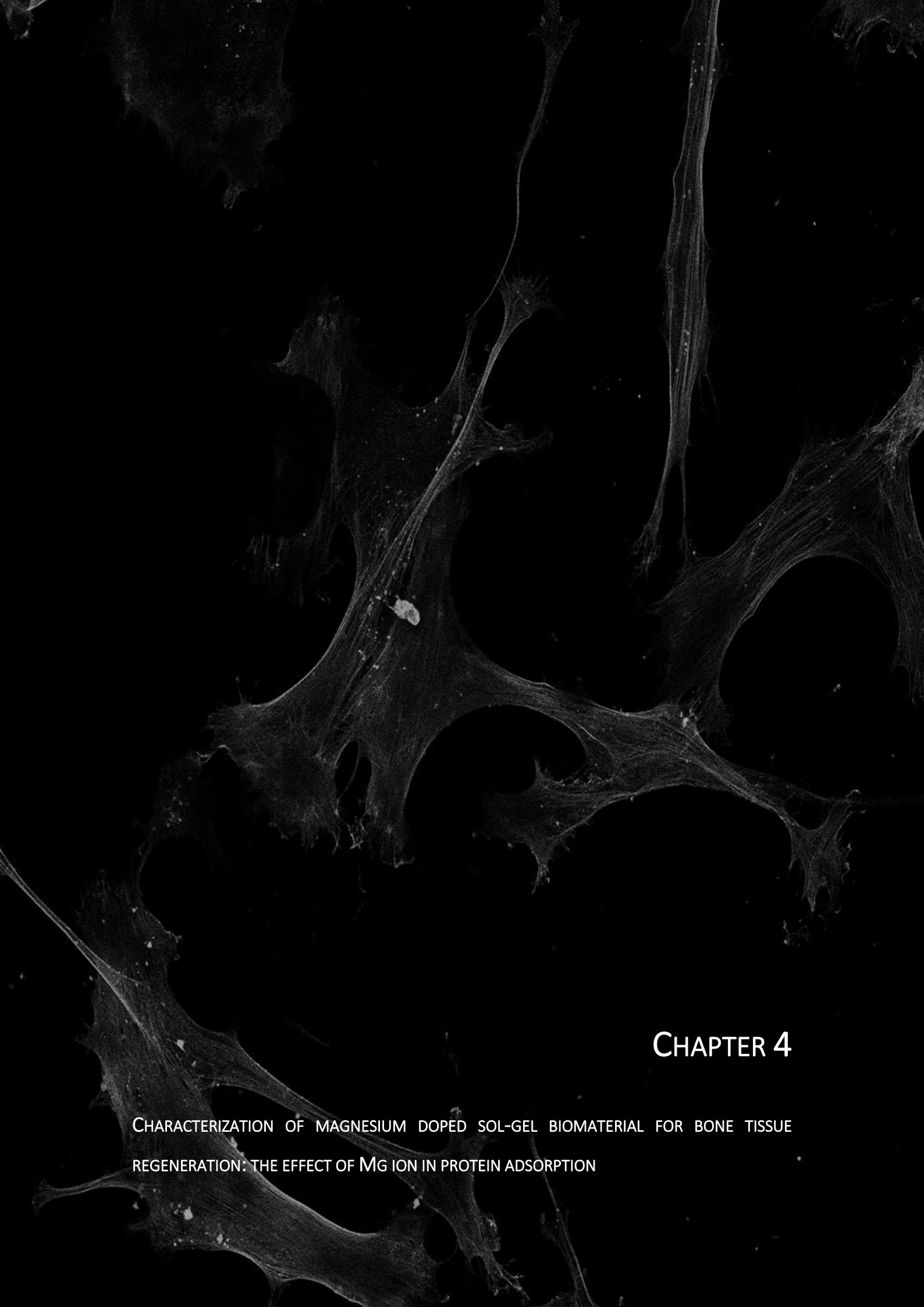

CHAPTER 4

CHARACTERIZATION OF MAGNESIUM DOPED SOL-GEL BIOMATERIAL FOR BONE TISSUE REGENERATION: THE EFFECT OF MG ION IN PROTEIN ADSORPTION

CHAPTER 4

CHARACTERIZATION OF MAGNESIUM DOPED SOL-GEL BIOMATERIAL FOR BONE TISSUE REGENERATION: THE EFFECT OF MG ION IN PROTEIN ADSORPTION

ARTICLE 3

Andreia Cerqueira[1], Francisco Romero-Gavilán[1], Iñaki García-Arnáez[2], Cristina Martinez-Ramos[3], Seda Ozturan[4], Raúl Izquierdo[1], Mikel Azkargorta[5], Félix Elortza[5], Mariló Gurruchaga[2], Julio Suay[1], Isabel Goñi[2]

[1]Department of Industrial Systems Engineering and Design, Universitat Jaume I, Av. Vicent Sos Baynat s/n, 12071 Castellón de la Plana, Spain

[2]Departament of Science and Technology of Polymers, Universidad del País Vasco, P. M. de Lardizábal, 3, 20018 San Sebastián, Spain

[3]Center for Biomaterials and Tissue Engineering, Universitat Politècnica de Valencia, Camino de Vera, s/n 46022 Valencia, Spain

[4]Department of Periodontology, Faculty of Dentistry, Istanbul Medeniyet University, Dumlupınar D100 Karayolu, 98, 34720 Istanbul, Turkey

[5]Proteomics Platform, CIC bioGUNE, Basque Research and Technology Alliance (BRTA), CIBERehd, ProteoRed-ISCIII, Bizkaia Science and Technology Park, 48160 Derio, Spain

Published at Materials Science and Engineering: C

Volume 125, June 2021, 112114

ABSTRACT

Magnesium is the fourth most abundant element in the human body with a wide battery of functions in the maintenance of normal cell homeostasis. In the bone, this element incorporates in the hydroxyapatite structure, and it takes part in mineral metabolism and regulates osteoclast functions. In this study, sol-gel materials with increasing concentrations of $MgCl_2$ (0.5, 1, and 1.5%) were synthesized and applied onto Ti surfaces as coatings. The materials were first physicochemically characterized. *In vitro* responses were examined using the MC3T3-E1 osteoblastic cells and RAW264.7 macrophages. Human serum protein adsorption was evaluated employing nLC-MS/MS. The incorporation of Mg did not affect the crosslinking of the sol-gel network, and a controlled release of Mg was observed; it was not cytotoxic at any of the tested concentrations. The cytoskeleton arrangement of MC3T3-E1 cells cultured on the Mg-doped materials changed in comparison with controls; the cells became more elongated, with protruded lamellipodia and increased cell surface. The expression of integrins (*ITGA5* and *ITGB1*) was boosted by Mg-coatings. The ALP activity and expression of *TGF-β*, *OSX* and *RUNX2* genes were also increased. In RAW264.7 cells, TNF-α secretion was reduced, while *TGF-β* and IL-4 expression rose. These changes correlated with the altered protein adsorption patterns. The Mg-doped coatings showed increased adsorption of anti-inflammatory (CLUS, IC1, CFAH, and VTNC), cell adhesion (DSG1, FILA2, and DESP) and DSG1, FILA2, and DESP tissue regeneration (VTNC and CYTA) proteins. This integrated approach to biomaterial characterization revealed the potential of Mg in bone tissue regeneration.

KEYWORDS

Mg^{2+}, biomedical applications, osseointegration, proteomics, hybrids, integrins

GRAPHICAL ABSTRACT

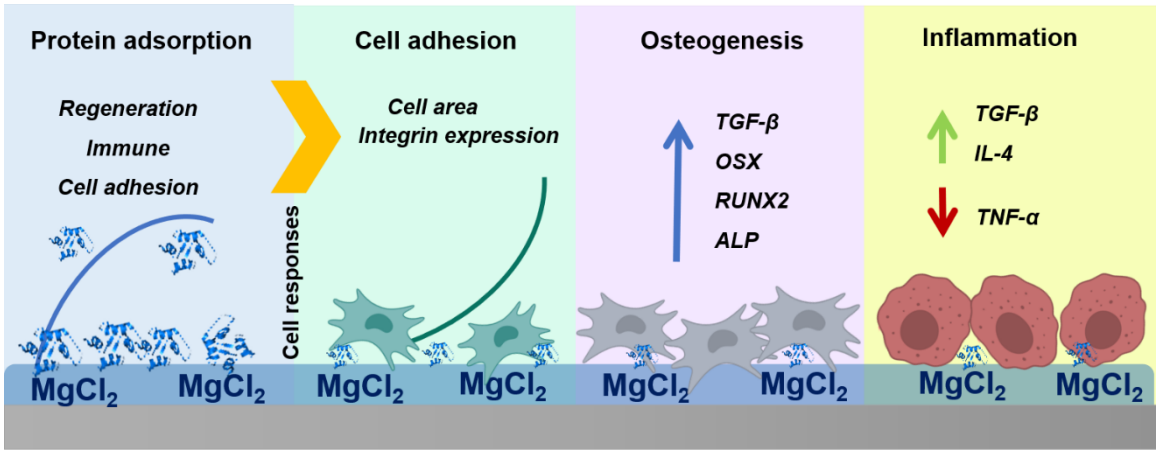

Figure 4.1. Graphical abstract of the paper "Characterization of magnesium doped sol-gel biomaterial for bone tissue regeneration: the effect of Mg ion in protein adsorption"

4.1. INTRODUCTION

Magnesium (Mg) is the fourth most abundant element in the human body [1]. Approximately 60% of this element is stored in the bone as a part of the hydroxyapatite structure and takes part in the mineral metabolism [2,3]. Magnesium is involved in many normal cell functions, such as metabolic reactions and maintenance of cell membrane, DNA, and protein structure. It is a key factor in the translation of genetic information and adenosine triphosphate (ATP) synthesis [3–5]. Magnesium deficiency has been associated with the promotion of osteoclastogenesis, which results in decreased bone formation and increased resorption [5]. Moreover, Mg modulates immune responses by regulating cytokine production [6] and the activation/suppression of the NF-κB signalling pathway [6,7]. The properties of Mg-based materials have been attracting increasing attention in the biomedical field. Bioactive glasses [8], biodegradable alloys (reviewed in [9]), bioglasses (reviewed in [10]) and Mg-enriched hydroxyapatites [11] have been studied, showing the potential of new Mg-based materials in bone repair and substitution [12,13].

Titanium (Ti) and its alloys are commonly employed in orthopedic implants used for bone and dental repair because of their attractive properties such as mechanical strength, excellent resistance to corrosion and biocompatibility [3]. The successful implementation of these materials depends on the capacity of host bone to establish intimate contact with the implant surface [14]. However, the relatively bioinert surface of Ti often causes implant failure and limits its clinical application [3]. Bioactive surface coatings, enhancing the osteoinductive properties of Ti materials, might present an interesting alternative.

The sol-gel technique can be employed to obtain metal surface coatings with a wide variety of advantages, such as improved control of the chemical composition of the coating and the film microstructure [15]. These coatings can also be used as controlled release vehicles [16]. Sol-gel precursors are easily available and mix at a molecular level, allowing the decrease of the sintering temperatures, making it a relatively inexpensive method [15]. Using 70% of methyltrimethoxysilane (MTMOS) and 30% of tetraethyl orthosilicate (TEOS) as precursors (MT), Martínez-Ibañez *et al.* [17] have obtained a sol-gel material with biomedical potential. It showed good osteointegration and osteogenic activity both *in vitro* and *in vivo* [18]. Thus, given the regenerative potential of magnesium, the development of a sol-gel coating capable of releasing Mg represents an interesting alternative to bioactivate titanium prostheses.

Biological response to an implanted device is determined by the conjugation factors. The initial processes are crucial. They determine a material outcome *in vivo*, and the provisional matrix formed by blood proteins adsorbed onto a surface upon implantation defines the consequent

cellular and tissular responses [19]. This protein adsorption depends on the material surface properties, such as wettability, roughness and charge [20].

New sol-gel coatings doped with increasing percentages of Mg (0.5%, 1% and 1.5%) were synthetized to be applied to a Ti surface. We synthesized the coatings and characterized its physicochemical properties and examined *in vitro* cell responses using the MC3T3-E1 osteoblasts and RAW264.7 macrophages. Human serum protein adsorption onto the material surface was analyzed employing the nLC-MS/MS. With these results, we aim to give a broad insight and improve the understanding of the potential of Mg ion in biomedical applications.

4.2. MATERIALS AND METHODS

4.2.1. SOL-GEL SYNTHESIS AND SAMPLE PREPARATION

To obtain the hybrid coatings with different percentages of $MgCl_2$ (**Table 4.1**), the sol-gel route was employed, using MTMOS and TEOS precursors in a molar ratio of 7:3. The alkoxysilanes were dissolved in 2-propanol (50% v/v). The corresponding stoichiometric amount of 0.1N HNO_3 (to hydrolyze the precursors completely), and the appropriate amounts of $MgCl_2$ were added to the mix at a rate of 1-drop s^{-1}. All the reagents were purchased from Merck (Darmstadt, Germany). The sol-gel mixtures were kept under stirring for 1h and then 1h at rest. Sandblasted, acid-etched (Romero-Gavilán *et al.* [21]) grade-4 Ti discs (12-mm diameter, 1-mm thick) were used as a substrate for the coatings. The sol-gels were applied with a dip-coater (KSV DC; KSV NIMA, Espoo, Finland). The discs were immersed in the sol-gel solutions at a speed of 60 cm min^{-1}, kept submerged for one minute, and removed at a 100 cm min^{-1}. Glass-slides were employed as a substrate to prepare samples for hydrolytic degradation and Mg^{2+} release assays. The slides were pre-treated with HNO_3 solution (25% v/v) in an ultrasonic bath (Sonoplus HD 3200; Bandelin Electronic, Berlin, Germany) for 20 min at 30 W. Next, they were washed in the ultrasonic bath with distilled water and dried at 100°C. This pre-treatment aimed to clean the glass surfaces and ensure the material-glass adhesion. At this point, the glass substrates were coated by casting. The coating adherence and thickness was measured applying the sol-gel formulations onto AISI 316-L stainless steel plates (5 cm x 5 cm; RNSinox S.L., Spain). The stainless-steel surfaces were pre-treated by polishing and cleaned with acetone to remove impurities. The coatings were applied onto the stainless steel by dip-coating in the same conditions as Ti discs. For thickness measurements, adhesive tape was applied to the substrate covering a part of it. After dip-coating, the tape was removed creating a border that allows the thickness measurement of the deposited sol-gel film. For chemical characterization, free films of the synthesized sol-gel

compositions were obtained by pouring the 5 mL of each solution into non-stick Teflon molds. Finally, to cure the sol-gel, all the samples were subjected to heat treatment, at 80°C for 2h.

Table 4.1. Nomenclature of the sol-gel networks with different amounts of $MgCl_2$. The mass percentages are relative to the total amount of alkoxysilane.

Nomenclature	Sol-gel network	$MgCl_2$ (wt%)
MT	70M30T	0
MT0.5Mg	70M30T	0.5
MT1Mg	70M30T	1
MT1.5Mg	70M30T	1.5

4.2.2. PHYSICOCHEMICAL CHARACTERIZATION

A Thermo Nicolet 6700 Fourier-transform infrared spectrometer (FT-IR; Thermo Fisher Scientific, NY, US) with an attenuated total reflection system (ATR) was employed to characterize the sol-gel networks. The spectra were measured in the 4000–400 cm^{-1} wavenumber range. In parallel, the solid-state ^{29}silicon nuclear magnetic resonance spectroscopy (^{29}Si-NMR) technique was used to study the reticulation level of the synthesized structures. To this purpose, we employed a Bruker 400 AVANCE III WB Plus spectrometer (Bruker, Billerica, MA, US) with a cross-polarization magic-angle spinning (CP-MAS) probe for solid samples. The pulse sequence was the Bruker standard: 79.5-MHz frequency, 5-kHz spectral width, 2-ms contact time and 5-s delay time. The spinning speed was 7.0 kHz. X-ray diffraction analysis (XRD) was carried out to study the crystalline or amorphous nature of the synthetized materials with a Bruker D4-Endeavor diffractometer (Bruker). Measurements in the range of 5–70° (2θ) with a step size of 0.02°(2θ) and a scanning rate 4 s $step^{-1}$ were collected with filtered CuKα radiation (λ = 1.54 A), an operating voltage of 40 kV and a filament current of 40 mA. In addition to analyzing the different formulations, with and without magnesium, an $MgCl_2$ sample was analyzed as a control.

The coating attachment was analyzed, evaluated, and classified by the cross-cut test following the UNE EN-ISO 2409 norm. A mechanical profilometer Dektack 6 (Veeco; Munich, Germany) was employed to measure the thickness of the coating applied onto the stainless steel plates. Profiles from the uncoated area to the coated area were taken, measuring the rise between coated and uncoated areas. Three individual samples were analyzed, performing three measurements in each of them.

A scanning electron microscope (SEM; Leica-Zeiss LEO, Leica, Wetzlar, Germany) was used to examine the coating morphologies onto Ti discs. Platinum sputtering was employed to increase the sample conductivity. An optical profilometer PLm2300 (Sensofar, Barcelona, Spain) was used to characterize the sample roughness. Three samples of each material were evaluated, and three measurements were carried out for each sample to obtain an average value of Ra (arithmetic average roughness parameter) for each surface. An automatic contact angle meter OCA 20 (DataPhysics Instruments, Filderstadt, Germany) was employed to characterize the surface wettability of the coated Ti surfaces. Ultrapure water drops of 10 µL were deposited on the material at a speed of 27.5 µL s^{-1}. The drop images were examined using SCA 20 software (DataPhysics Instruments). Six samples of each type were tested, depositing two drops on each disc.

The mass loss during sample incubation in 50 mL of distilled water at 37°C was recorded to examine the rate of hydrolytic degradation. Samples were removed after 7, 14, 28, 42, and 56 days of incubation. The results were calculated as a percentage (%) of the initial mass lost. Three independent samples were evaluated for each condition. The amount of Mg^{2+} released from the coatings was measured using an inductively coupled plasma mass spectrometer (Agilent 7700 Series ICPMS; Agilent Technologies, Santa Clara, CA, US). The materials were incubated in ddH_2O at 37°C for 28 days. Aliquots of 0.5 mL were removed after 2, 4, 6, 8, 24, 72, 168, 336, 504 and 672 h of incubation. Each data point is the average of the values obtained for three replicas.

4.2.3. *IN VITRO* ASSAYS

4.2.3.1. *Cell culture*

Mouse calvaria osteosarcoma (MC3T3-E1) cell line was seeded onto the materials in low-glucose DMEM (Gibco, Life Technologies, Thermo Fisher Scientific) with 1% penicillin/streptomycin (Gibco) and 10% foetal bovine serum (FBS; Gibco). After 24h, the cell culture medium was replaced with osteogenic medium (DMEM, 1% penicillin/streptomycin, 10% FBS, 1% ascorbic acid (5 µg mL^{-1}), and 100 mM β-glycerol phosphate), which was changed every two days. Mouse murine macrophage (RAW264.7) cell line was cultured in high-glucose DMEM supplemented with 1% penicillin/streptomycin and 10 % FBS. Cell culture was carried out in a humidified (95%) incubator at 37°C, with 5 % CO_2.

4.2.3.2. *Cytoskeleton arrangement*

For the evaluation of cytoskeleton arrangement, MC3T3-E1 cells were seeded on the materials at a density of 1 x 10^4 cells cm^{-2} for 1 day. Then, the samples were washed once with PBS, fixed

with 4 % paraformaldehyde (PFA) for 20 min at room temperature and permeabilized with 0.1% Triton X-100 for 5 min. Next, the samples were incubated with phalloidin (1:100; Abcam, Cambridge, UK) diluted in 0.1% w/v bovine serum albumin (BSA)-PBS for 1h at room temperature. For nuclei staining, after washing twice with PBS, the samples were incubated for 5 min in a mounting medium with DAPI (Abcam). A Leica TCS SP8 Confocal Laser Scanning Microscope with 20x (dry) lenses was employed for fluorescence detection. The images were obtained using LAS X software (Leica) and analyzed using Image J software (National Institutes of Health, Maryland, USA).

4.2.3.3. *Cytotoxicity and ALP activity*

Biomaterial cytotoxicity was assessed using the MC3T3-E1 cells, following the ISO 10993-5:2009 (Annex C) [22] standards, and samples were prepared according to the ISO 10993-12:2012 [23]. The CellTiter 96® Proliferation Assay (MTS; Promega, Madison, WI), based on the formazan formation, was used according to manufacturer's guidelines. For controls, cells incubated without (negative control) and with latex (positive control) were used. The material was considered cytotoxic when the cell viability fell below 70%.

To evaluate the effects on cell mineralization, the MC3T3-E1 cells were cultured on the materials at a density of 1.75 x 10^4 cells cm^{-2} for 7 and 14 days. At each time point, alkaline phosphatase activity (ALP) activity was measured following the protocol of Araújo-Gomes *et al*. [18] and normalized to protein content obtained using a Pierce BCA assay kit (Thermo Fisher Scientific).

4.2.3.4. *Cytokine quantification using ELISA*

For measuring the levels of secreted cytokines, the cell culture medium used to incubate the RAW264.7 cell-seeded discs was collected and frozen until further analysis. The concentrations of tumor necrosis factor (TNF)-α and transforming growth factor (TGF)-β were determined using an ELISA (Invitrogen, Thermo Fisher Scientific) kit, according to the manufacturer's instructions.

4.2.3.5. *Relative gene expression: RNA extraction, cDNA synthesis and qRT-PCR*

To examine the effects of the Mg-doped materials on gene expression, the MC3T3-E1 cell line was cultured at a density of 1.75 x 10^4 cells cm^{-2} for 7 and 14 days and RAW264.7 at a density of 30 x 10^4 cells cm^{-2} for 2 and 4 days. Total RNA was extracted with TRIzol as described in Cerqueira *et al.* [24]. RNA concentration, integrity, and quality were measured using NanoVue® Plus Spectrophotometer (GE Healthcare Life Sciences, Little Chalfont, UK). For cDNA synthesis, approximately 1 µg of total RNA was converted into cDNA using PrimeScript RT Reagent Kit (Perfect Real Time; TAKARA Bio Inc., Shiga, Japan). The reaction was carried out in a Prime

Thermal Cycler (Techne, Staffordshire, UK) as described in Cerqueira *et al.* [24]. The resulting cDNA was diluted in DNase-free water to a concentration suitable for gene expression evaluation.

Quantitative real-time PCRs (qRT-PCR) were carried out in 96-well plates (Applied Biosystems®, Thermo Fisher Scientific). Each sample represented the gene of interest and the housekeeping gene (*GAPDH*). Primers for each gene were designed (using *Primer3Plus* software tool) from specific DNA sequences obtained from NCBI and purchased from Thermo Fisher Scientific. The targets studied for each cell line are shown in **Supplementary Table 4.1**. Reactions were carried out as described in Cerqueira *et al.* [24] in a StepOne Plus™ Real-Time PCR System (Applied Biosystems®). Fold changes were calculated using the $2^{-\Delta\Delta Ct}$ method, and data were normalized to blank wells (without materials).

4.2.4. Adsorbed protein layer and proteomic analysis

To obtain the proteins adsorbed onto the material surface, samples were incubated for 3h (37°C, 5 % CO_2) in 24-well NUNC plates (Thermo Fisher Scientific) with 1 mL of human serum from male AB plasma (Merck). The materials were washed five times with ddH_2O and once with wash buffer (100 mM NaCl, 50 mM Tris–HCl, pH 7.0) to eliminate non-adsorbed proteins. Adsorbed proteins were obtained by elution (0.5 M triethylammonium bicarbonate buffer (TEAB), 4% sodium dodecyl sulfate (SDS), 100 mM dithiothreitol (DTT); Merck). For each surface, four independent replicates were analyzed, and each replicate was a pool of eluate from four discs. Total serum protein concentration was determined using a Pierce BCA assay kit (Thermo Fisher Scientific).

For proteomic analysis, the eluate was characterized employing electrospray tandem mass spectrometry, using a nanoACQUITY UPLC (Waters, Milford, MA) coupled to an Orbitrap XL (Thermo Electron, Bremen, Germany), following the protocol described in Romero-Gavilán *et al*. [25]. Each sample was analyzed in quadruplicate. Proteomic results were examined using PEAKS (Bioinformatics Solutions Inc., Waterloo, Canada), and the functional classification of the identified proteins was performed employing PANTHER software (http://www.pantherdb.org/).

4.2.5. Statistical analysis

Physicochemical and *in vitro* assay data were analyzed via one-way analysis of variance (ANOVA) with Tukey post hoc test, after confirming normal distribution and equal variance. Statistical analysis was performed using GraphPad Prism 5.04 software (GraphPad Software Inc., La Jolla, CA). The differences between MT and Mg-doped MT were considered statistically significant at $p \leq 0.05$ (*), $p \leq 0.01$ (**), and $p \leq 0.001$ (***). Data were expressed as means ± standard error (SE).

In the proteomic analysis, a student's *t*-test was conducted to evaluate differences between MT and MT with different Mg concentrations, using Progenesis software. Differences were considered statistically significant at $p \leq 0.05$ and the ratio difference bigger than 1.5 in either direction (higher or lower).

4.3. RESULTS

4.3.1. PHYSICOCHEMICAL CHARACTERIZATION

Hybrid sol-gel networks containing different amounts of $MgCl_2$ were synthesized using the sol-gel route. The effect of this compound on the sol-gel structure was studied using FT-IR, ^{29}Si-NMR and XRD (**Figure 4.2**). The FT-IR spectra demonstrated the presence of MTMOS-associated organic groups in the final networks; the bands corresponding to Si-C and C-H bonds were detected at 1270 and 2980 cm^{-1} [26], respectively. The signals seen at 760, 1020 and 1120 cm^{-1} were related to the formation of Si-O-Si bonds, and the band at 950 cm^{-1} indicated the presence of non-condensed Si-OH species [21]. These results are confirmed by the ^{29}Si-NMR spectra, which can verify the proper formation of the polysiloxane network (**Figure 4.2b**). Signals associated with the MTMOS trifunctional alkoxysilane (T units) are detected between -50 and -70 ppm. Within this range, the peaks at -57 and -66 ppm indicate the presence of T^2 and T^3 species [26], respectively. The TEOS tetrafunctional (Q units) chemical shifts are in the range between -97.5 and -115 ppm; the signals at -102 and -110 ppm reflect the presence of Q^3 and Q^4 species, respectively [27]. A good degree of crosslinking was achieved in the materials synthesized here; only the species with the highest degree of condensation were detected in the sol-gel structure. Moreover, it seems that the $MgCl_2$ incorporation into the sol-gel did not affect the final silica network crosslinking as all the spectrum shapes were similar. **Figure 4.2c** shows the XRD spectra obtained for the different sol-gel materials and for the $MgCl_2$. The obtained patterns for all the sol-gel formulations doped with $MgCl_2$ can be associated with an amorphous nature as no peaks related to $MgCl_2$ or other crystalline structures were detected. In addition, no significant differences were found between the distinct Mg-doped compositions and MT. The broad and undefined peak around 10° (2θ) in the sol-gel material spectra can be associated with the presence of not completely hydrolyzed precursors. Another peak with similar shaped but less intensity was detected around 21° (2θ), being this signal characteristic of the SiO_2 amorphous sol-gel structures [28].

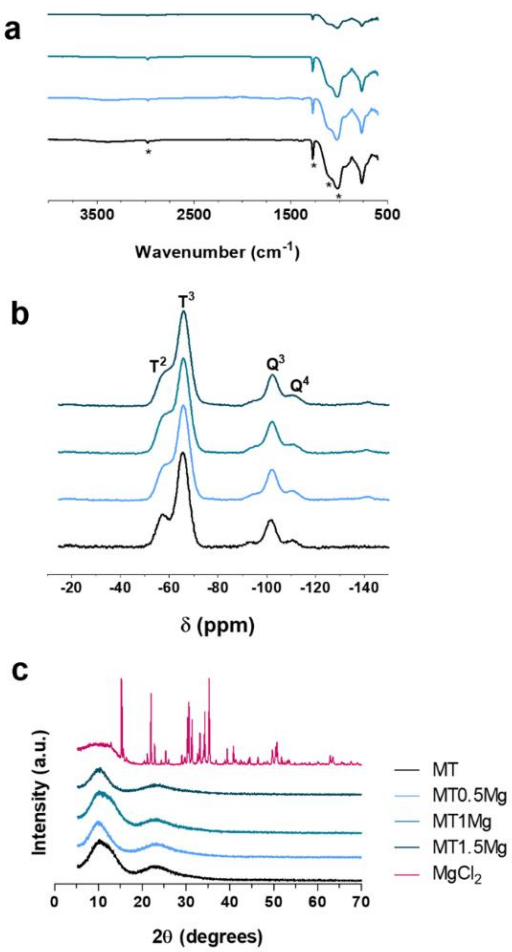

Figure 4.2. (a) FT-IR, (b) ^{29}Si-NMR and (c) XRD spectra of the studied sol-gel networks.

All sol-gel materials coatings showed a high degree of adherence (Class 0) based on the cross-cut test, as the edges of the cuts were smooth, and detachments were not observed (**Supplementary Figure 4.1a**). The coatings applied onto Ti were morphologically evaluated by SEM. The micrographs show that the different compositions covered the whole area of Ti substrates (**Figure 4.3a-e**). Nevertheless, the sol-gel seemed to accumulate in the cavities associated with the Ti roughness, smoothing the initial morphological irregularities of the Ti surface. No $MgCl_2$ precipitates were detected. However, small holes of around 0.2–0.3 µm in diameter can be seen in the film with the largest amount of $MgCl_2$ (MT1.5Mg); these are not observed in other compositions (**Figure 4.3f**). The materials with $MgCl_2$ have the Ra roughness values similar to the Ra of the coating without Mg salt (**Figure 4.3g**). Additionally, the thickness measurements for the different coatings showed that the obtained sol-gel films do not have differences in thickness regardless of the amount of $MgCl_2$ added (**Supplementary Figure 4.1b**). The wettability results showed higher contact angles for materials with Mg than for the MT base material (**Figure 4.3h**). The coatings with MgCl2 were more hydrophobic than MT, reaching the values of around 80° (close to those for uncoated Ti).

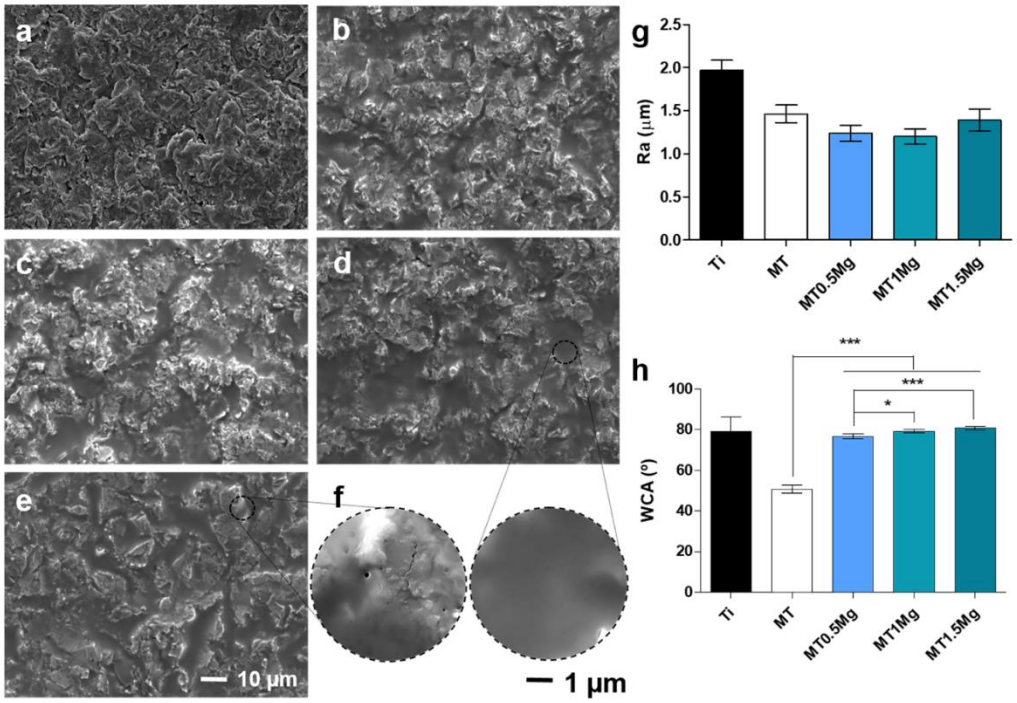

Figure 4.3. SEM microphotographs of (a) Ti, (b) MT, (c) MT0.5Mg, (d) MT1Mg, (e) MT1.5Mg and (f) enlarged areas of MT1Mg and MT1.5Mg coatings. Scale bars: (a-e) 10 and (f) 1 µm. Roughness Ra (g) and contact angle (WCA; h) are also displayed. Results are shown as means ± SE. The asterisks ($p \leq 0.05$ (*) and $p \leq 0.001$ (***)) indicate significant differences between MT and Mg-doped MT.

The Mg-containing coatings had a higher degradation rate than the base coating MT (**Figure 4.4a**). The base network showed a mass loss of around 18 % after 56 days of incubation. This mass loss increased as more $MgCl_2$ was incorporated into the sol-gel, reaching a value of around 28 % for the MT1.5Mg coating. The amount of Mg^{2+} ions released also rose with the increasing salt content in the sol-gel compositions (**Figure 4.4b**). Moreover, the Mg^{2+} liberation process continued throughout the studied period (28 days).

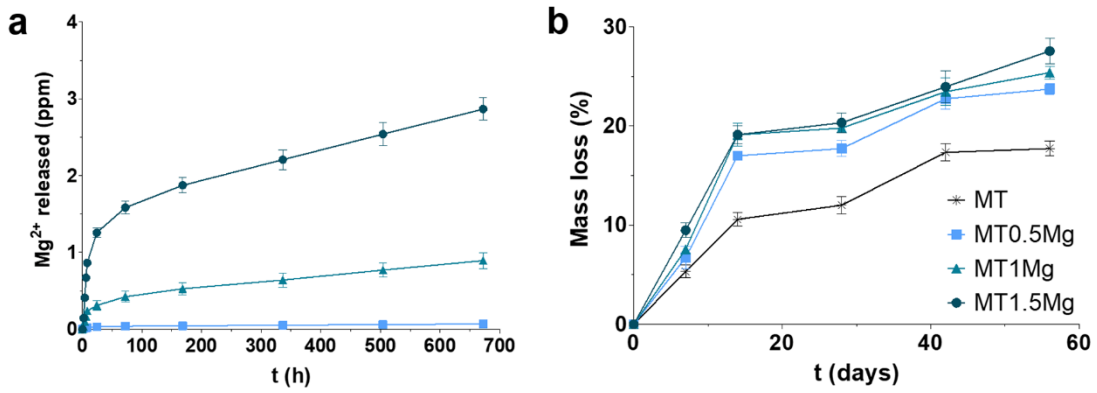

Figure 4.4. Release kinetics of Mg^{2+} ions (a) and hydrolytic degradation (b) of the sol-gel coatings enriched with $MgCl_2$. Bars indicate standard errors.

4.3.2. *IN VITRO* ASSAYS

4.3.2.1. *Cytoskeleton arrangement, cytotoxicity and ALP activity*

To examine the arrangement of cellular cytoskeleton, the cells were stained with phalloidin after 1 day of culture (**Figure 4.5 a-e**). The cells cultured on Ti and MT showed a triangular shape with few lamellipodia, while cells on the materials with Mg displayed a more elongated with protruding lamellipodia (white arrows). The MC3T3-E1 cells cultured on MT1Mg and MT1.5Mg also displayed protruding filopodia. Cells growing on MT1Mg and MT1.5Mg materials had significantly larger surface area than those cultured on the MT discs (**Figure 4.5f**).

None of the materials in the study was cytotoxic (data not shown). ALP activity showed a small decrease for MT0.5Mg and MT1Mg at 7 and 14 days, and a significant activity increase at 7 and 14 days for MT1.5Mg (**Figure 4.5g**).

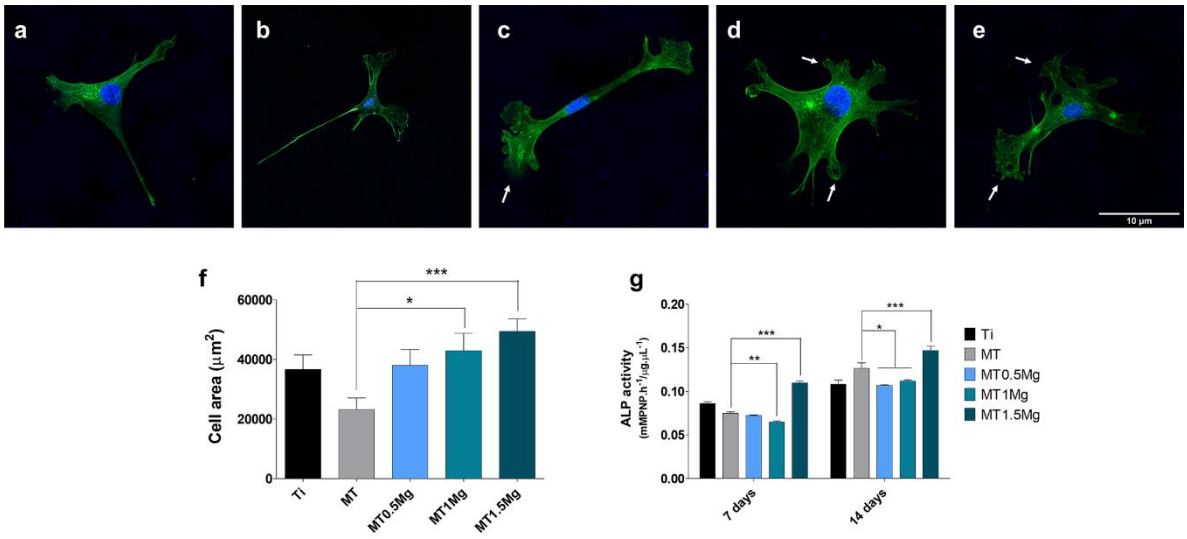

Figure 4.5. Fluorescent confocal images of cytoskeleton arrangement of MC3T3-E1 on (a) Ti, (b) MT, (c) MT0.5Mg, (d) MT1Mg and (e) MT1.5Mg and (f) area of the cells adhered to the materials. Actin filaments were stained with phalloidin (green), and nuclei were stained with DAPI (blue). Scale bar: 10 µm. ALP activity (g) of MC3T3-E1 cells at 7 and 14 days. Results are shown as means ± SE. The asterisks ($p \leq 0.05$ (*), $p \leq 0.01$ (**), and $p \leq 0.001$ (***)) indicate statistically significant differences between MT and Mg-doped MT.

4.3.2.2. *Cytokine secretion measurements by ELISA*

To evaluate the effect of Mg-doped materials on inflammation, cytokine secretion to the RAW264.7 cell culture medium was examined. The levels of anti-inflammatory cytokine TGF-β increased significantly only in cultures on MT1.5Mg, at 4 days (**Figure 4.6a**). In contrast, after 2 days, the amounts of secreted pro-inflammatory cytokine TNF-α significantly decreased for all materials (**Figure 4.6b**). After 4 days, the TNF-α excretion levels were similar for all the materials, with a significant decrease for MT1Mg in comparison with MT.

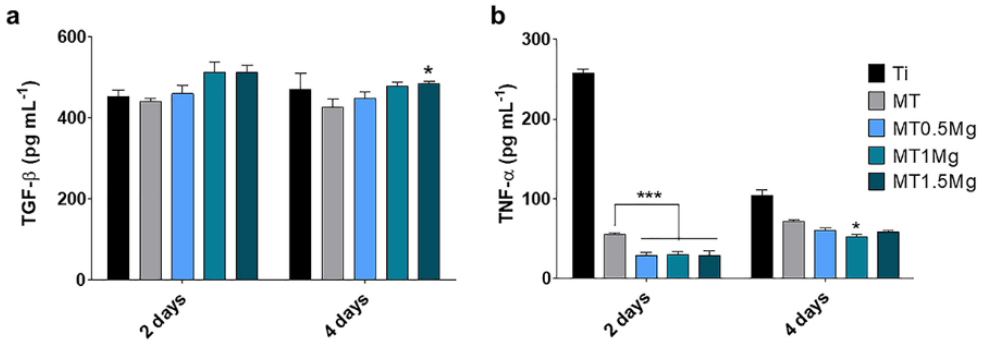

Figure 4.6. ELISA results for (a) TGF-β and (b) TNF-α for RAW264.7 cultures at 2 and 4 days. Data are shown as means ± SE. The asterisks ($p \leq 0.05$ (*) and $p \leq 0.001$ (***)) indicate statistically significant differences between MT and Mg-doped MT.

4.3.3.3. *Relative gene expression*

To further understand the effects of the Mg-doped materials on osteogenesis (*ALP*, *TGF-β*, *OSX*, and *RUNX2*), cell adhesion (*ITGA5* and *ITGB1*), and inflammatory responses (*IL-6*, *TNF-α*, *TGF-β*, and *IL-4*), gene expression of selected targets was measured. In the case of osteogenic markers, after 7 days of culture, the *ALP* expression was similar for all materials. However, there was a significant increase in its expression on MT0.5Mg at 14 days (**Figure 4.7a**). The *TGF-β* expression was increased in MT0.5Mg and MT1.5Mg after 7 days. After 14 days, it was significantly augmented in MT0.5Mg and MT1Mg cultures and decreased on MT1.5Mg materials (**Figure 4.7b**). The expression of *OSX* showed a significant increase for all Mg-doped materials at both time points (**Figure 4.7c**). The expression of *RUNX2* was only augmented for MT1.5Mg at 7 days. After 14 days, it increased significantly in the MT1Mg cultures and decreased for MT1.5Mg (**Figure 4.7d**). In the case of cell adhesion markers, *ITGA5* expression rose for MT0.5Mg at 7 days and for MT1Mg and MT1.5Mg at 14 days (**Figure 4.7e**). The expression of *ITGB1* increased for MT1.5Mg at 7 days and for MT1Mg at 14 days (**Figure 4.7f**).

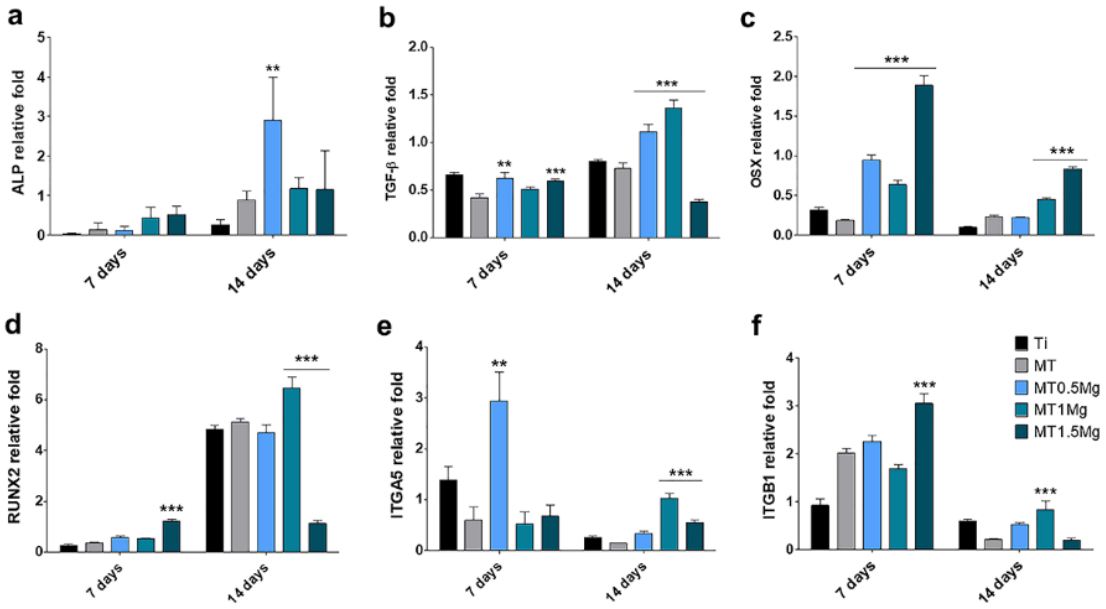

Figure 4.7. Gene expression of (a) alkaline phosphatase (*ALP*), (b) transforming growth factor (*TGF*)-β, (c) osterix (*OSX*), (d) runt-related transcription factor 2 (RUNX2), (e) α5-integrin (*ITGA5*), and (f) β1-integrin (*ITGB1*) in MC3T3-E1 cultures at 7 and 14 days. Gene expression was normalized to blank wells (without any material) using the $2^{-\Delta\Delta Ct}$ method. Results are shown as means ± SE. The asterisks ($p \leq 0.05$ (*), $p \leq 0.01$ (**), and $p \leq 0.001$ (***)) indicate statistically significant differences between MT and Mg-doped MT.

Among the genes related to macrophages responses, the expression of pro-inflammatory marker IL-6 was significantly altered only in MT1.5Mg cultures at 4 days (**Figure 4.8a**), while *TNF-α* expression increased for MT1Mg and MT1.5Mg at 2 days (**Figure 4.8b**). The expression of anti-inflammatory marker *TGF-β* (**Figure 4.8c**) increased on MT1Mg and MT1.5Mg at 2 days. All the materials showed an increase in its expression at 4 days. The expression of *IL-4* was rose for MT0.5Mg at 2 days and for MT1Mg, at 4 days (**Figure 4.8d**).

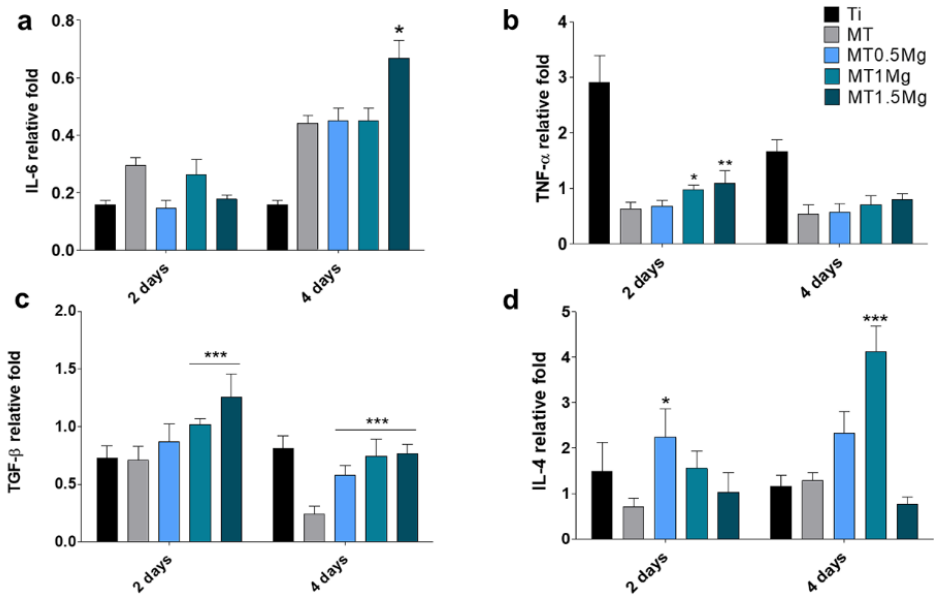

Figure 4.8. Gene expression of (a) interleukin (*IL*)-6, (b) tumor necrosis factor (*TNF*)-α, (c) transforming growth factor (*TGF*)-β, and (d) *IL*-4 in RAW264.7 macrophages after 2 and 4 days of culture. Gene expression was normalized to blank wells (without any material) using the $2^{-\Delta\Delta Ct}$ method. Results are shown as means ± SE. The asterisks ($p \leq 0.05$ (*), $p \leq 0.01$ (**), and $p \leq 0.001$ (***)) indicate statistically significant differences between MT and Mg-doped MT.

4.3.3. PROTEOMIC ANALYSIS

The nLC-MS/MS analysis of eluted proteins identified 22 proteins preferentially adsorbed on the materials with Mg in comparison with the MT base material (**Supplementary Table 4.2**; **Table 4.2**). Among these, six proteins are related to complement system activation (CO9, CO3 and C1QC) and its inhibition (IC1, CLUS, and CFAH). Some other proteins associated with immune responses were also more abundant on the Mg-doped coatings. A1AT, which regulates the activity of neutrophil granulocytes, two immunoglobulins (LAC3 and IGHM) and a pentraxin (SAMP) were more absorbed. Three cell adhesion proteins preferentially attached to the materials containing Mg (DSG1, FILA2 and DESP). Similarly, VTNC and CYTA, which present a battery of functions related to tissue regeneration, regulation/inhibition of immune responses

and cell attachment, preferentially adhered to Mg-doped MT. Moreover, several apolipoproteins related to lipid metabolism (APO2, APOA1, APOA4 and APOL1) were identified as well as two proteins associated with coagulation (SPB12 and A2MG) and one associated with DNA damage repair (UBB).

PANTHER analysis was used to associate the differentially adsorbed proteins with their biological functions and pathways. **Figure 4.9** shows pie-chart diagrams of the biological functions and pathways for the proteins differentially adsorbed onto the Mg-doped surfaces in comparison with MT. Among the various biological functions found, the immune system, cellular organization and process, multi-organism and multicellular organismal process, biological regulation, developmental and metabolic process, and biological adhesion were identified for all materials with Mg. For MT1Mg and MT1.5Mg, signaling and biological functions also appeared. The search for pathway associations revealed blood coagulation pathway for proteins from MT0.5Mg and MT1Mg materials. For the MT1Mg material, CCKR signaling map and B cell activation were also identified. For MT1.5Mg, only the CCKR signaling map pathway appeared.

Table 4.2. Ratios of different proteins differentially adsorbed onto the sol-gel materials doped with Mg, associated with relevant biological processes (immune response, cell adhesion, tissue regeneration and coagulation).

		Ratio		
Protein	**Biological process**	**MT0.5Mg/MT**	**MT1Mg/MT**	**MT1.5Mg/MT**
CO9	**Immune responses**	2.13	16.17	11.05
SAMP		6.97	12.77	9.63
CLUS		6.20	8.07	7.36
CFAH		3.63	5.51	5.34
A1AT		4.04	3.96	4.16
LAC3		1.00	6.54	3.69
IC1		2.91	3.47	3.56
C1QC		2.25	3.14	3.31
CO3		1.51	1.79	1.86
IGHM		1.37	2.17	1.84
APOA2		1.66	17.26	10.16
APOA1		1.18	2.73	3.52
APOA4		1.68	3.97	2.42
APOL1		1.18	4.50	2.32
CYTA	**Tissue regeneration**	2.24	10.68	10.89
VTNC		2.07	3.28	3.86
DSG1	**Cell adhesion**	11.36	19.75	10.57
FILA2		3.18	39.49	5.21
DESP		6.07	3.78	1.90
SPB12	**Coagulation**	1.50	6.05	4.00
A2MG		5.29	5.11	2.13

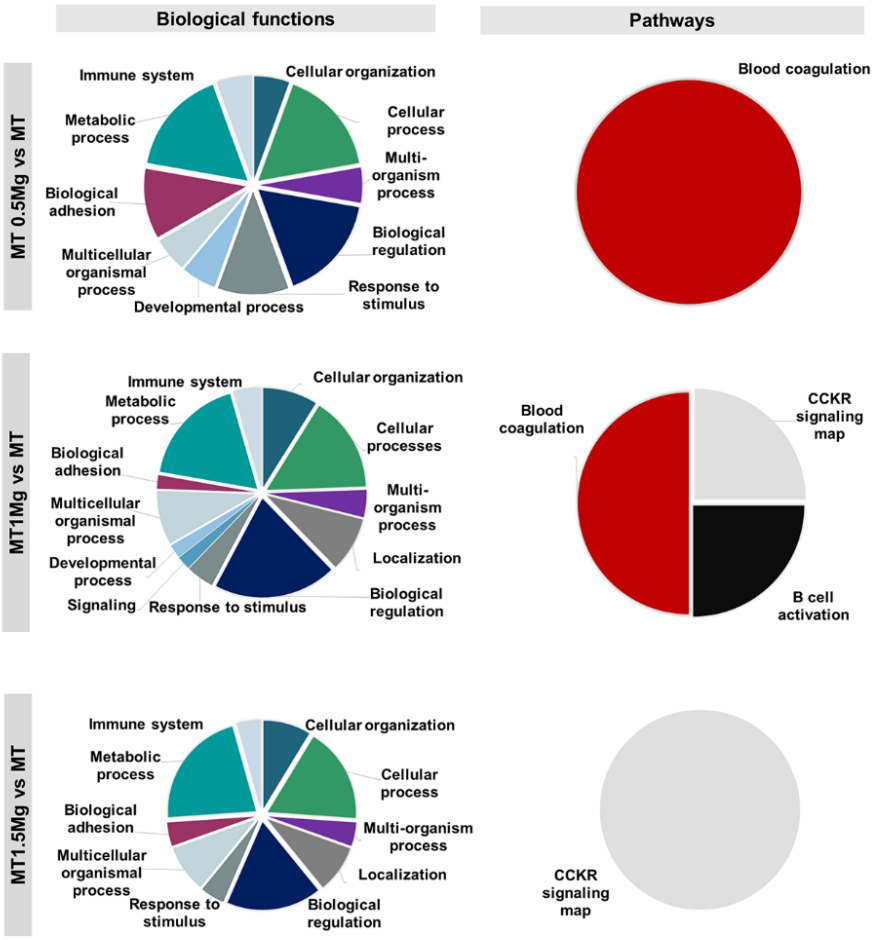

Figure 4.9. PANTHER diagram of biological functions and pathways associated with the proteins differentially adhering to Mg-enriched coatings in comparison with MT (without Mg).

4.4. Discussion

For a successful bone substitution, a material should have high mechanical strength and good biocompatibility and bioactivity [29]. Titanium and its alloys used to manufacture implants and have a wide application. However, from a biological standpoint, this type of material is relatively bioinert. A promising research line in the development materials is creating bioactive coatings capable of enhancing the tissue regeneration responses. Sol-gels have been already used as coatings for Ti surfaces as they can release ions and other molecules in a controlled manner [24,30,31]. Magnesium is an important ion involved in a wide range of biological functions; it has been attracting increasing interest because of its potential applications in the biomedical field. The aim of this study was to develop a new sol-gel coating acting as a release vehicle of Mg, to enhance bioactivity of Ti materials and analyze the potential of this cation in bone regeneration. The ^{29}Si-solid NMR showed that the incorporation of $MgCl_2$ into the sol-gel network did not affect the final silica network crosslinking. In addition, Mg ions did not form crystalline structures

(as $MgCl_2$ precipitates), being were likely trapped on the hybrid structure through hydrogen bonding, Van der Waals or electrostatic forces. Even though the Mg-doping did not change the material roughness, the contact angle significantly increased in comparison with the non-Mg coating regardless of the Mg concentration. Given that the roughness does not vary between compositions and that the degree of condensation of the synthetized networks is similar according to the chemical characterization, a possible explanation for the reduction observed in hydrophilicity could be associated with the presence of ions in the sol-gel structure and their effect in the Van der Waals and electrostatic forces [32]. As expected [20,24], the rate of hydrolytic degradation increased as more $MgCl_2$ was incorporated into the sol-gel network, and more Mg^{2+} was liberated. The release of this ion was stable until the end of the assay, reaching the values of 3 ppm in the material with the highest concentration of Mg (MT1.5Mg). None of the materials was cytotoxic to the MC3T3-E1 cells. Similarly, Romero-Gavilán *et al.* [33] and Martinez-Ibañez *et al*. [17] developed sol-gel coatings using MTMOS, TEOS and 3-glycidoxypropyltrimethoxysilane (GPTMS) that showed good bioactivity and biocompatibility. Yoshizawa *et al.* [34] have reported that the Mg ion is non-cytotoxic at concentrations as high as 10 mM, thus confirming that the levels of Mg in the sol-gel coatings studied here were within the safe range.

Osteoblast cell adhesion and growth are promoted by Mg as it interacts with integrins, well-known transmembrane receptors necessary for cell adhesion and stability [12]. Yan *et al*. [3] have shown that bone-marrow-derived stem cells (BMDSCs) seeded onto the titania nanotube arrays containing Mg develop extended filopodia and thicker cell walls, thus benefiting cell adhesion. Similarly, the MT1Mg and MT1.5Mg sol-gel coatings led to wide-spreading MC3T3-E1 osteoblastic cells, with protruding lamellipodia and a significantly higher surface area compared to the cells cultured in the MT. Zreiqat *et al*. [8] have shown that Mg ions added to a bioceramic substrate increase the cell adhesion and the expression of β1-, α5β1- and α3β1-integrins in human bone-derived cells (HBDC). Likewise, we showed that the Mg-doped coatings increase the expression of the β1- and α5-integrin genes, depending on the cation concentration and exposure time, thus confirming the effects of the coatings on cell adhesion.

Cell differentiation is critical for new bone formation [35], and Mg-based biomaterials have proven effects on osteogenesis. Yan *et al*. [3] and Yoshizawa *et al.* [34] have shown that Mg-treated materials promote osteogenic differentiation in BMSCs. Gao *et al.* [35] have demonstrated an increase in ALP activity and osteogenic gene expression in MC3T3-E1 cells exposed to Mg-coated Ti6Al4V. Li *et al.* [36] evaluated the osteogenic properties of a nanoporous titanium coating with different concentrations of magnesium acetate, which was able to promote the adhesion, proliferation, and differentiation of bone marrow mesenchymal stem cells (BMSCs). Similarly, our Mg-doped

sol-gel coatings increase the ALP activity on MT1.5Mg and *TGF-β*, *OSX*, and *RUNX2* gene expression, thus indicating an augmented osteoblastic cell differentiation and proliferation, which are indicators of bone formation [37,38].

Chronic inflammation caused by implanted materials is associated with macrophages, which are the key players in the immune system [39]. They can assume two phenotypes: M1 and M2. The M1 macrophages are involved in pro-inflammatory functions and the production of IL-1β, IL-12, and TNF-α. The M2 macrophages promote tissue healing and the production of IL-10 and TGF-β [40]. There are several reports of magnesium effect on inflammation [6,41] and the response to biomaterials [7,42–44] by the regulation of macrophage polarization [7]. In this study, culturing the cells on the Mg-doped sol-gel materials caused a significant decrease in TNF-α secretion. It also significantly promoted the expression of *IL-4* and *TGF-β* genes and the secretion of TGF-β in MT1.5Mg. These results suggest that the Mg-doped materials modulate the macrophage polarization towards the M2 phenotype. Li *et al.* [7] have reported similar results in RAW 264.7 cells exposed to Mg-doped titanium. They have verified that these materials cause a significant decrease in the levels of pro-inflammatory markers (CCR7, TNF-α, IL-1β) and increase the abundance of anti-inflammatory markers (CD206, IL-4, IL-10).

The proteins from biological fluids spontaneously adsorbing onto the biomaterial surfaces play a major role in determining the interactions between implants and tissues. Understanding this phenomenon is essential to comprehend the cell responses and improve the design of biocompatible materials [13]. Here, the nLC-MS/MS analysis of the protein layer identified 22 proteins preferentially adsorbed onto the sol-gel coatings with Mg. Three proteins related to the complement system (CO9, C1QC, and CO3) and one associated with innate/adaptive immunological responses (SAMP) [43] were detected on these coatings. The complement system uses many proteins that can induce an inflammatory response and opsonize pathogens [46]. However, this immunological response is controlled by numerous factors, which affect this cascade at its different stages. Among these are the plasma protease C1 inhibitor (IC1), vitronectin (VTNC), clusterin (CLUS) and complement factor H (CFAH) [45]. These four proteins were significantly more adsorbed onto the surfaces with Mg. The CLUS protein (8-fold increase in adsorption) prevents excessive inflammation through the regulation of complement activity and NF-κB pathway and reduces the apoptosis and oxidative stress [46,47]. IC1, a member of the serpin family of protease inhibitors, exerts an anti-inflammatory effect by regulating the complement system and interacting with extracellular matrices and cells [48]. Similarly, VTNC can moderate the intensity and duration of the inflammatory response to injury [49]. The CFAH protein is a critical regulator of the alternative complement pathway and has been directly associated

with the maintenance of bone architecture. The balance in the interactions between osteoblasts and osteoclasts can be altered in the absence of CFAH, leading to a reduction in tissue quality [50]. Moreover, four apolipoproteins (APO2, APOA1, APOA4, and APOL1), known for their role in the metabolism of lipids and the inhibition of the complement system [51], were also preferentially adsorbed onto Mg-containing surfaces. The increased affinity of Mg-doped coatings to these immune-response regulatory proteins can explain the anti-inflammatory potential observed *in vitro*.

The interaction of the host tissue cells with the implant surface is the key process in the integration of implanted material, modulating tissue regeneration. Several proteins related to cell adhesion and tissue regeneration preferentially adhered to the Mg-doped coatings. This is consistent with the *in vitro* results, which showed an increase in the osteogenic potential and cell adhesion on these materials. Desmoglein-1 (DSG1) and desmoplakin (DESP), mediators of cell–cell adhesion, are transmembrane glycoprotein components of desmosomes [52] and preferentially adhere to the Mg-enriched coatings. Moreover, VTCN, also found on the Mg-doped coatings, is one of the many proteins that regulate cell adhesion and tissue remodeling through the interaction with integrins [53,54]. Rivera-Chacon *et al.* [55] have shown that the nanoporous TiO_2 templates that absorbed more VTNC boosted the osteoblast attachment and proliferation and, consequently, improve osteoconduction. Li *et al.* [56] have reported that the VTNC adsorption onto a biomaterial surface affects the spreading of human mesenchymal stem cells (hMSCs) and integrin expression. The increase in cell adhesion observed on the Mg-doped coatings is likely to be a result of the augmented gene expression of the integrins regulated by Mg. However, the increased abundance of VTNC on such surfaces and its subsequent interactions with these transmembrane receptors might also contribute to the overall effect. The impact of Mg-based biomaterials on cell adhesion have been associated with the stimulation of integrins [8]. However, the role of proteins adsorbed onto the biomaterials, as far as we know, has never been considered. Further studies are needed to better understand the way the adsorbed proteins, such as VTNC, might affect the interaction between Mg and integrins, and thus promote the cell adhesion.

Among the proteins associated with tissue regeneration, cystatin-A (CYTA), also known as stefin A, belongs to a family of cysteine protease inhibitors and is coded by the *CSTA* gene. One of the functions of this protein is the inhibition of cathepsin B (CATB), H, and L. These lysosomal cysteine proteinases that can modulate the architecture of the extracellular matrix [57]. They are associated with several inflammatory diseases, including periodontitis [58–60]. Moreover, the VTCN regulates cascades related to other biological processes, such as coagulation and fibrinolysis.

This is achieved through its interaction with heparin and thrombin–antithrombin III complexes [53]. Another protein associated with coagulation, alpha-2-macroglobulin (A2MG), also preferentially adsorbs to the Mg-doped coatings. This protein is an antiprotease that functions as an inhibitor of plasmin, kallikrein, and thrombin [61] and has important functions in the clearance of active proteases. Such proteases are important agents in connective tissue diseases and well-known virulence factors [62]. The A2MG has been suggested as a marker for the blood compatibility with a biomaterial as it is a sensitive marker for plasma protease activation on artificial surfaces [63].

These results show the potential of Mg in the development of biomaterials, revealing not only its overall effect on *in vitro* cell responses but also its role in the modulation of the protein adsorption patterns. It is possible to hypothesize that the well-known effects of magnesium biomaterials on cell adhesion, osteogenesis, and inflammation not only come from the properties of the ion itself, but also from the identified Mg-related proteins that attach to the surface upon implantation. With this, the results presented in this study shows a novel perspective of Mg in biomaterials as well as its effects on tissue regeneration.

4.5. Conclusion

The aim of this study was to further understand the effect of Mg on tissue regenerative processes. For that, we developed and characterized new Mg-enriched sol-gel coatings with a control release of the ion. The materials were successfully synthesized, with $MgCl_2$ well incorporated onto the sol-gel network, leading to a significant increase in the surface wettability in comparison with the base material. Unsurprisingly, the degradation increased with increasing Mg content, resulting in a steady release of Mg^{2+} until the end of the assay. The Mg-doped coatings preferentially adsorbed proteins related to inflammatory responses, cell adhesion, tissue regeneration, and coagulation. Concerning the inflammatory response, the reduction in TNF-α secretion and the increase in *TGF-β* and *IL-4* gene expression indicate that the materials induced an anti-inflammatory phenotype. This was consistent with the increased adsorption of immune-system regulatory proteins (CLUS, CFAH, IC1 and VNTC). Moreover, the Mg-doped materials showed an increased affinity to the proteins related to cell adhesion (DESP, FILA2, and DSG1) and to the VTNC. This can explain the changes in the cell cytoskeleton arrangement with the consequent observed increase in the cell surface area. The Mg-doped materials also provoked an increase in the integrin gene expression (*ITGA5* and *ITGB1*). In MC3T3-E1 osteoblastic cells, ALP activity was augmented in MT1.5Mg; this was accompanied by increased expression of *TGF-β*, *OSX* and *RUNX2* genes. This preferential adsorption of proteins related to

tissue regeneration (CYTA and VTNC) indicated the regenerative potential of these materials. The anti-inflammatory properties of these materials in combination with improved cell adhesion and the observed osteogenic responses demonstrate their potential for enhanced bone healing, being this effect more prominent at the highest concentrations.

4.6. Acknowledgments

This work was supported by MINECO [MAT2017-86043-R; RTC-2017-6147-1], Generalitat Valenciana [GRISOLIAP/2018/091, APOSTD/2020/036, PROMETEO/2020/069], Universitat Jaume I under [UJI-B2017-37, Posdoc/2019/28], the University of the Basque Country under [GIU18/189] and Basque Government under [PRE_2017_2_0044]. The authors would like to thank Raquel Oliver, Jose Ortega, José Miguel Pedra and Iraide Escobés for their valuable technical assistance and Antonio Coso (GMI-Ilerimplant) for producing the titanium discs.

4.7. References

1. O'Neill, E., Awale, G., Daneshmandi, L., Umerah, O. & Lo, K. W. H. The roles of ions on bone regeneration. *Drug Discovery Today* vol. 23 879–890 (2018).

2. Castiglioni, S., Cazzaniga, A., Albisetti, W. & Maier, J. Magnesium and Osteoporosis: Current State of Knowledge and Future Research Directions. *Nutrients* **5**, 3022–3033 (2013).

3. Yan, Y. *et al.* Enhanced osteogenic differentiation of bone mesenchymal stem cells on magnesium-incorporated titania nanotube arrays. *Colloids Surfaces B Biointerfaces* **179**, 309–316 (2019).

4. Nassif, N. & Ghayad, I. Corrosion Protection and Surface Treatment of Magnesium Alloys Used for Orthopedic Applications. *Adv. Mater. Sci. Eng.* **2013**, (2013).

5. Belluci, M. M. *et al.* Magnesium deficiency results in an increased formation of osteoclasts. *J. Nutr. Biochem.* **24**, 1488–1498 (2013).

6. Sugimoto, J. *et al.* Magnesium Decreases Inflammatory Cytokine Production: A Novel Innate Immunomodulatory Mechanism. *J. Immunol.* **188**, 6338–6346 (2012).

7. Li, B. *et al.* In vitro and in vivo responses of macrophages to magnesium-doped titanium. *Sci. Rep.* **7**, 42707 (2017).

8. Zreiqat, H. *et al.* Mechanisms of magnesium-stimulated adhesion of osteoblastic cells to commonly used orthopaedic implants. *J. Biomed. Mater. Res.* **62**, 175–184 (2002).

9. Hornberger, H., Virtanen, S. & Boccaccini, A. R. Biomedical coatings on magnesium alloys - A review. *Acta Biomater.* **8**, 2442–2455 (2012).

10. Diba, M., Tapia, F., Boccaccini, A. R. & Strobel, L. A. Magnesium-Containing Bioactive Glasses for Biomedical Applications. *Int. J. Appl. Glas. Sci.* **3**, 221–253 (2012).

11. Zhao, S. fang, Jiang, Q. hong, Peel, S., Wang, X. xiang & He, F. ming. Effects of magnesium-substituted nanohydroxyapatite coating on implant osseointegration. *Clin. Oral Implants Res.* **24**, 34–41 (2013).

12. Wu, Z. *et al.* In vitro degradability, bioactivity and cell responses to mesoporous magnesium silicate for the induction of bone regeneration. *Colloids Surfaces B Biointerfaces* **120**, 38–46 (2014).

13. Höhn, S., Virtanen, S. & Boccaccini, A. R. Protein adsorption on magnesium and its alloys: A review. *Appl. Surf. Sci.* **464**, 212–219 (2019).

14. Galli, S. *et al.* Local release of magnesium from mesoporous TiO2 coatings stimulates the peri-implant expression of osteogenic markers and improves osteoconductivity in vivo. *Acta Biomater.* **10**, 5193–5201 (2014).

15. Wen, C. E., Xu, W., Hu, W. Y. & Hodgson, P. D. Hydroxyapatite/titania sol-gel coatings on titanium-zirconium alloy for biomedical applications. *Acta Biomater.* **3**, 403–410 (2007).

16. Oshiro Junior, J. A. *et al.* Drug delivery systems obtained from silica based organic-inorganic hybrids. *Polymers (Basel).* **8**, 91 (2016).

17. Martínez-Ibáñez, M. *et al.* Biological characterization of a new silicon based coating developed for dental implants. *J. Mater. Sci. Mater. Med.* **27**, (2016).

18. Araújo-Gomes, N. *et al.* Osseointegration mechanisms: a proteomic approach. *JBIC J. Biol. Inorg. Chem.* **23**, 459–470 (2018).

19. Oughlis, S. *et al.* Development of proteomic tools to study protein adsorption on a biomaterial, titanium grafted with poly(sodium styrene sulfonate). *J. Chromatogr. B Anal. Technol. Biomed. Life Sci.* **879**, 3681–3687 (2011).

20. Romero-Gavilán, F. *et al.* Proteomic analysis of calcium-enriched sol–gel biomaterials. *JBIC J. Biol. Inorg. Chem.* **24**, 563–574 (2019).

21. Romero-Gavilán, F. *et al.* Control of the degradation of silica sol-gel hybrid coatings for metal implants prepared by the triple combination of alkoxysilanes. *J. Non. Cryst. Solids*

453, 66–73 (2016).

22. International Organization for Standardization. Biological evaluation of medical devices - Part 5: Tests for in vitro cytotoxicity. vol. 3 ED 42 (2009).

23. International Organization for Standardization. Biological evaluation of medical devices - Part 12: Sample preparation and reference materials. 20 https://www.iso.org/standard/53468.html (2012).

24. Cerqueira, A. *et al.* A possible use of melatonin in the dental field: Protein adsorption and in vitro cell response on coated titanium. *Mater. Sci. Eng. C* **116**, 111262 (2020).

25. Romero-Gavilán, F. *et al.* Proteomic analysis of silica hybrid sol-gel coatings: a potential tool for predicting the biocompatibility of implants in vivo. *Biofouling* **In press**, (2017).

26. Romero-Gavilán, F. *et al.* Sol-gel coatings made using methyl-modified alkoxysilanes: The balance between protection and bioactivation. *Prog. Org. Coatings* **147**, 105770 (2020).

27. Kim, H. N. & Lee, S. K. Atomic structure and dehydration mechanism of amorphous silica: Insights from 29Si and 1H solid-state MAS NMR study of SiO2 nanoparticles. *Geochim. Cosmochim. Acta* **120**, 39–64 (2013).

28. Chernev, G. *et al.* Sol-gel silica hybrid biomaterials for application in biodegradation of toxic compounds. *J. Sol-Gel Sci. Technol.* **58**, 619–624 (2011).

29. Gao, C., Peng, S., Feng, P. & Shuai, C. Bone biomaterials and interactions with stem cells. *Bone Research* vol. 5 1–33 (2017).

30. Romero Gavilán, F. *et al.* Proteomic analysis of calcium-enriched sol-gel biomaterials. *JBIC J. Biol. Inorg. Chem.* **24**, 563–574 (2019).

31. Romero-Gavilán, F. *et al.* The effect of strontium incorporation into sol-gel biomaterials on their protein adsorption and cell interactions. *Colloids Surfaces B Biointerfaces* **174**, 9–16 (2019).

32. Novin, N., Shameli, A., Balali, E. & Zomorodbakhsh, S. How electrostatic and non-electrostatic interactions play a role in water wettability of possible nanostructure surfaces. *J. Nanostructure Chem.* **10**, 69–74 (2020).

33. Romero-Gavilan, F. *et al.* Bioactive potential of silica coatings and its effect on the adhesion of proteins to titanium implants. *Colloids Surfaces B Biointerfaces* **162**, 316–325 (2018).

34. Yoshizawa, S., Brown, A., Barchowsky, A. & Sfeir, C. Magnesium ion stimulation of bone marrow stromal cells enhances osteogenic activity, simulating the effect of magnesium alloy degradation. *Acta Biomater.* **10**, 2834–2842 (2014).

35. Gao, P. *et al.* Biofunctional magnesium coated Ti6Al4V scaffold enhances osteogenesis and angiogenesis in vitro and in vivo for orthopedic application. *Bioact. Mater.* **5**, 680–693 (2020).

36. Li, X. *et al.* A magnesium-incorporated nanoporous titanium coating for rapid osseointegration. *Int. J. Nanomedicine* **15**, 6593–6603 (2020).

37. Janssens, K., Ten Dijke, P., Janssens, S. & Van Hul, W. Transforming growth factor-β1 to the bone. *Endocr. Rev.* **26**, 743–774 (2005).

38. Wang, S. *et al.* Citric acid enhances the physical properties, cytocompatibility and osteogenesis of magnesium calcium phosphate cement. *J. Mech. Behav. Biomed. Mater.* **94**, 42–50 (2019).

39. Lozano, R. M. *et al.* Response of MC3T3-E1 osteoblasts, L929 fibroblasts, and J774 macrophages to fluoride surface-modified AZ31 magnesium alloy. *J. Biomed. Mater. Res. Part A* **101**, 2753–2762 (2013).

40. Gu, Q., Yang, H. & Shi, Q. Macrophages and bone inflammation. *J. Orthop. Transl.* **10**, 86–93 (2017).

41. Mazur, A. *et al.* Magnesium and the inflammatory response: Potential physiopathological implications. *Arch. Biochem. Biophys.* **458**, 48–56 (2007).

42. Cifuentes, S. C. *et al.* Incorporation of Mg particles into PDLLA regulates mesenchymal stem cell and macrophage responses. *J. Biomed. Mater. Res. Part A* **104**, 866–878 (2016).

43. Peng, Q. *et al.* Degradable magnesium-based implant materials with anti-inflammatory activity. *J. Biomed. Mater. Res. Part A* **101A**, 1898–1906 (2013).

44. Costantino, M. D. *et al.* Inflammatory response to magnesium-based biodegradable implant materials. *Acta Biomater.* **101**, 598–608 (2020).

45. Merle, N. S., Church, S. E., Fremeaux-Bacchi, V. & Roumenina, L. T. Complement system part I - molecular mechanisms of activation and regulation. *Front. Immunol.* **6**, 1–30 (2015).

46. Wu, Z. C., Yu, J. T., Li, Y. & Tan, L. Clusterin in Alzheimer's disease. in *Advances in Clinical*

Chemistry (ed. Elsevier) vol. 56 155–173 (Academic Press Inc., 2012).

47. Falgarone, G. & Chiocchia, G. Clusterin: A multifacet protein at the crossroad of inflammation and autoimmunity. *Advances in Cancer Research* vol. 104 139–170 (2009).

48. Davis, A. E., Mejia, P. & Lu, F. Biological activities of C1 inhibitor. *Molecular Immunology* vol. 45 4057–4063 (2008).

49. Leavesley, D. I. *et al.* Vitronectin - Master controller or micromanager? *IUBMB Life* **65**, (2013).

50. Alexander, J. J. *et al.* Absence of complement factor H alters bone architecture and dynamics. *Immunobiology* **223**, 761–771 (2018).

51. Cho, N. H. & Seong, S. Y. Apolipoproteins inhibit the innate immunity activated by necrotic cells or bacterial endotoxin. *Immunology* **128**, 479–486 (2009).

52. Johnson, J. L., Najor, N. A. & Green, K. J. Desmosomes: Regulators of cellular signaling and adhesion in epidermal health and disease. *Cold Spring Harb. Perspect. Med.* **4**, (2014).

53. Bierbaum, S., Hintze, V. & Scharnweber, D. Artificial Extracellular Matrices to Functionalize Biomaterial Surfaces. in *Comprehensive Biomaterials II* 147–178 (Elsevier, 2017). doi:10.1016/B978-0-12-803581-8.10206-1.

54. Rowland, T. J. *et al.* Roles of integrins in human induced pluripotent stem cell growth on matrigel and vitronectin. *Stem Cells Dev.* **19**, 1231–1240 (2010).

55. Rivera-Chacon, D. M. *et al.* Fibronectin and vitronectin promote human fetal osteoblast cell attachment and proliferation on nanoporous titanium surfaces. *J. Biomed. Nanotechnol.* **9**, 1092–1097 (2013).

56. Li, T., Hao, L., Li, J., Du, C. & Wang, Y. Insight into vitronectin structural evolution on material surface chemistries: The mediation for cell adhesion. *Bioact. Mater.* **5**, 1044–1052 (2020).

57. Soond, S. M., Kozhevnikova, M. V., Zamyatnin, A. A. & Townsend, P. A. Cysteine cathepsin protease inhibition: An update on its diagnostic, prognostic and therapeutic potential in cancer. *Pharmaceuticals* **12**, (2019).

58. Li, X. *et al.* Cathepsin B Regulates Collagen Expression by Fibroblasts via Prolonging TLR2/NF-κB Activation. *Oxid. Med. Cell. Longev.* (2016) doi:10.1155/2016/7894247.

59. Ichimaru, E. *et al.* Cathepsin B in gingival crevicular fluid of adult periodontitis patients: Identification by immunological and enzymological methods. *Inflamm. Res.* **45**, 277–282 (1996).

60. Kunimatsu, K., Yamamoto, K., Ichimaru, E., Kato, Y. & Kato, I. Cathepsins B, H and L activities in gingival crevicular fluid from chronic adult periodontitis patients and experimental gingivitis subjects. *J. Periodontal Res.* **25**, 69–73 (1990).

61. Cater, J. H., Wilson, M. R. & Wyatt, A. R. Alpha-2-Macroglobulin, a Hypochlorite-Regulated Chaperone and Immune System Modulator. *Oxid. Med. Cell. Longev.* **2019**, 9 (2019).

62. Armstrong, P. B. & Quigley, J. P. α2-macroglobulin: An evolutionarily conserved arm of the innate immune system. *Dev. Comp. Immunol.* **23**, 375–390 (1999).

63. Biltoft, D. *et al.* Fast form alpha-2-macroglobulin - A marker for protease activation in plasma exposed to artificial surfaces. *Clin. Biochem.* **50**, 1203–1208 (2017).

4.8. SUPPLEMENTARY MATERIAL

Supplementary Table 4.1. Targets studied in MC3T3-E1 osteoblasts and RAW264.7 macrophages.

Name	Accession	Sequence	Product length
GADPH (*Gadph)*	XM_017321385	F: TGCCCCCATGTTTGTGATG R: TGGTGGTGCAGGATGCATT	83
Osterix (*OSX/SP7*)	XM_006520519	F: ACTCATCCCTATGGCTCGTG R: GGTAGGGAGCTGGGTTAAGG	238
Alkaline Phosphatase (*ALP*)	XM_006538499	F: CGGGACTGGTACTCGGATAA R: ATTCCACGTCGGTTCTGTTC	157
β1-Integrin (*ITGB1*)	NM_010578	F: GCCAGGGCTGGTTATACAGA R: TCACAATGGCACACAGGTTT	226
α5-Integrin (*ITGA5*)	NM_001314041	F: AGCGACTGGAATCCTCAAGA R: TGCTGAGTCCTGTCACCTTG	184
Transforming Growth Factor-β (*TGFBETA*)	NM_011577	F: TTGCTTCAGCTCCACAGAGA R: TGGTTGTAGAGGGCAAGGAC	183
Tumor Necrosis Factor-α (*TNFALFA*)	NM_001278601	F: AGCCCCCAGTCTGTATCCTT R: CTCCCTTTGCAGAACTCAGG	212
Interleukin-4 (*IL4*)	NM_021283	F: TCAACCCCCAGCTAGTTGTC R: TGTTCTTCGTTGCTGTGAGG	177
Interleukin-6 (*IL6*)	NM_001314054	F: AGTTGCCTTCTTGGGACTGA R: TCCACGATTTCCCAGAGAAC	159

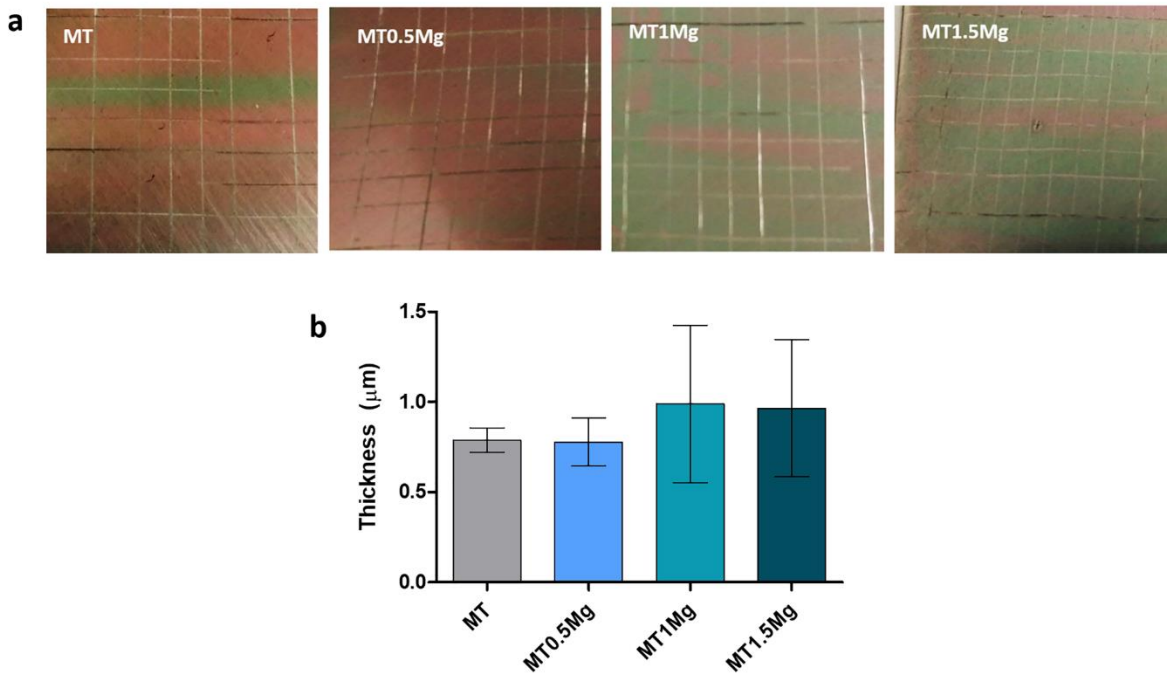

Supplementary Figure 4.1. Cross-cut test results (a) and thickness measurements (b). Results are shown as means ± SE.

Supplementary Table 4.2. Progenesis comparative analysis of proteins differentially adsorbed onto $MgCl_2$ enriched coatings (MT0.5Mg, MT1Mg, and MT1.5Mg) in respect to MT.

		MT0.5Mg *vs* MT		MT1Mg *vs* MT		MT1.5Mg *vs* MT	
Entry	**Description**	***p* value**	**Ratio**	***p* value**	**Ratio**	***p* value**	**Ratio**
CO9_HUMAN	Complement component C9	3.91E-01	2.13	9.35E-03	16.17	4.09E-02	11.05
CYTA_HUMAN	Cystatin-A	2.03E-01	2.24	4.87E-02	10.68	6.33E-02	10.89
DSG1_HUMAN	Desmoglein-1	3.27E-02	11.36	2.66E-02	19.75	4.36E-02	10.57
APOA2_HUMAN	Apolipoprotein A-II	6.87E-01	1.66	1.49E-02	17.26	1.06E-01	10.16
SAMP_HUMAN	Serum amyloid P-component	2.62E-02	6.97	8.16E-03	12.77	1.94E-02	9.63
CLUS_HUMAN	Clusterin	5.46E-02	6.20	2.49E-02	8.07	2.76E-02	7.36
CFAH_HUMAN	Complement factor H	6.36E-02	3.63	1.52E-02	5.51	1.76E-02	5.34
FILA2_HUMAN	Filaggrin-2	1.48E-01	3.18	3.70E-03	39.49	2.65E-01	5.21
A1AT_HUMAN	Alpha-1-antitrypsin	1.01E-02	4.04	1.16E-02	3.96	7.67E-02	4.16
SPB12_HUMAN	Serpin B12	5.92E-01	1.50	2.29E-02	6.05	1.32E-01	4.00
VTNC_HUMAN	Vitronectin	4.08E-02	2.07	3.09E-03	3.28	2.78E-03	3.86
LAC3_HUMAN	Ig lambda-3 chain C regions	9.97E-01	1.00	4.26E-02	6.54	1.16E-01	3.69
IC1_HUMAN	Plasma protease C1 inhibitor	4.61E-02	2.91	2.71E-04	3.47	2.38E-04	3.56
APOA1_HUMAN	Apolipoprotein A-I	6.80E-01	1.18	3.16E-02	2.73	2.12E-02	3.52
C1QC_HUMAN	Complement C1q subcomponent subunit C	4.07E-02	2.25	1.41E-02	3.14	7.59E-03	3.31
UBB_HUMAN	Polyubiquitin-B	8.19E-02	1.83	7.45E-02	2.21	2.09E-02	2.94
APOA4_HUMAN	Apolipoprotein A-IV	2.89E-01	1.68	4.55E-03	3.97	3.31E-02	2.42
APOL1_HUMAN	Apolipoprotein L1	7.55E-01	1.18	4.47E-03	4.50	4.47E-02	2.32
A2MG_HUMAN	Alpha-2-macroglobulin	4.03E-02	5.29	3.11E-02	5.11	5.97E-01	2.13
DESP_HUMAN	Desmoplakin	2.27E-02	6.07	1.16E-01	3.78	4.54E-01	1.90
CO3_HUMAN	Complement C3	3.75E-02	1.51	2.02E-02	1.79	1.70E-02	1.86
IGHM_HUMAN	Ig mu chain C region	3.57E-01	1.37	3.28E-02	2.17	8.49E-02	1.84

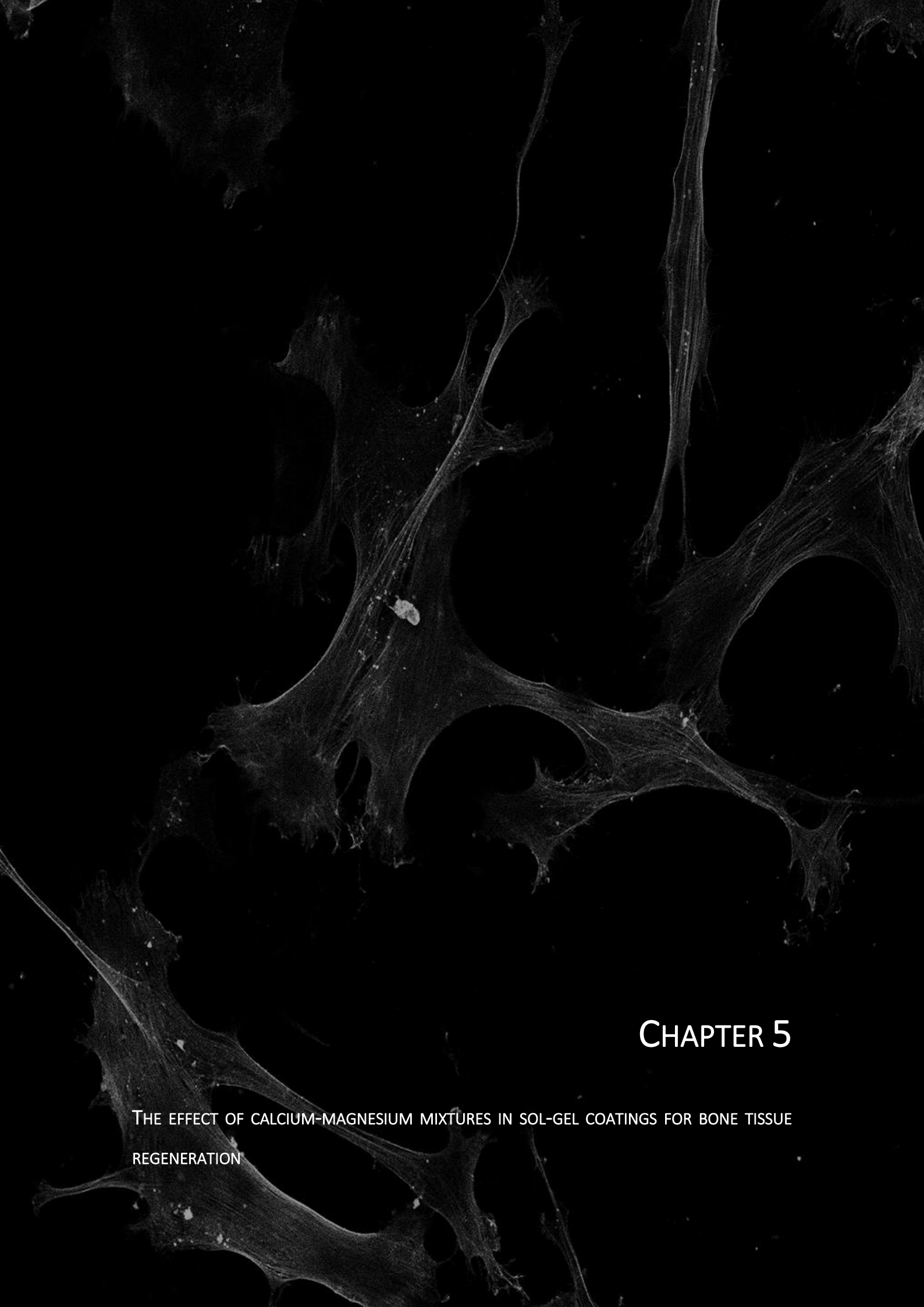

Chapter 5

The effect of calcium-magnesium mixtures in sol-gel coatings for bone tissue regeneration

\

CHAPTER 5

THE EFFECT OF CALCIUM-MAGNESIUM MIXTURES IN SOL-GEL COATINGS FOR BONE TISSUE REGENERATION

ARTICLE 4

In preparation for submission

ABSTRACT

Calcium (Ca) and magnesium (Mg) are two essential elements in bone structure and metabolism. However, their synergistic or competitive effects on bone regeneration are often neglected when developing a biomaterial. Here, we aimed to provide an insight into the interaction between Ca and Mg by developing a sol-gel coating doped with mixtures of $CaCl_2$ (0.5%) and $MgCl_2$ (0.5, 1, and 1.5%). After physicochemical characterization, the materials were studied *in vitro* with MC3T3-E1 osteoblastic cells and RAW264.7 macrophages, and the protein adsorption was analyzed through nLC-MS/MS. The incorporation of the ions did not lead to the formation of crystalline structures nor affected the sol-gel network crosslinking. A controlled release of the ions was obtained, which was revealed to be not cytotoxic at any tested concentration. Generally, the materials with Ca and Mg adsorbed more proteins associated with inflammatory response regulation (*e.g.*, ALBU, CLUS, HPT, HPTR, A1AG1, A1AG2) while decreasing adsorption immunoglobulins. CaMg coatings also presented less affinity for proteins associated with coagulation (*e.g.,* FA9, FA10, FA11, FA12) but adsorbed more proteins associated with cell adhesion (DSG1, DESP, FBLN1, ZA2G). *In vitro* assays revealed that cellular responsiveness was dependent on the concentration of Mg added to Ca. Our results show that the interaction in mixtures is dependent on the amount of each ion added to the mix and not a simple sum of properties.

KEYWORDS

Biomaterials, proteomics, coagulation, inflammation, cell adhesion

GRAPHICAL ABSTRACT

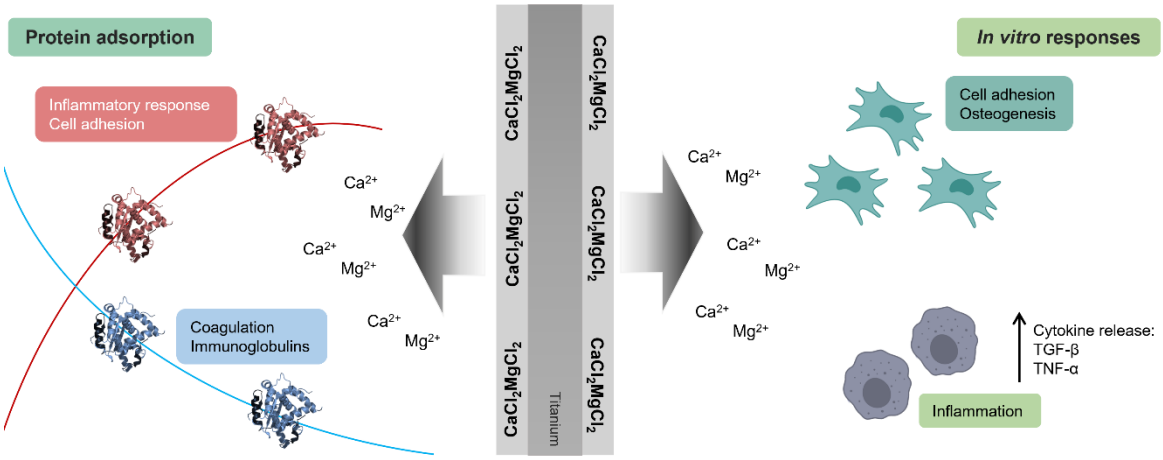

Figure 5.1. Graphical abstract of the paper "The effect of calcium-magnesium mixtures in sol-gel coatings for bone tissue regeneration".

5.1. INTRODUCTION

In the field of biomaterials, bone regeneration has been extensively investigated. It is a complex process characterized by the interactions between the material, cells/tissues, and environmental conditions [1]. The bone restorative process encompasses a wide battery of biological processes, such as inflammation, coagulation, or osteogenesis [2], and the way these carry out is essential to good implant integration.

Nowadays, biomaterials for bone tissue regeneration are no longer seen as biologically passive since their properties can orchestrate the process of tissue regeneration. Changing the surface texture, elasticity, or chemistry can give the materials instructive properties such as biocompatibility, mechanical strength, and controlled biodegradability [3]. Allied to changes in surface chemistry, the delivery of bioactive agents, such as inorganic ions, on the implant site can determine its outcome [4,5]. Numerous therapeutic systems have been developed with inorganic ions (*e.g.,* calcium, magnesium, strontium, zinc) to deliver these elements and ultimately improve the bone regenerative process [6]. However, most studies focus on a single element. The synergistic or competitive effects among the cations are neglected despite the fact they are simultaneously presented [7], which is unfavorable for optimizing bone regeneration processes.

Calcium ions (Ca^{2+}) have a multitude of roles and functions in biological systems. In bone, it is one of the most important elements of the mineralized matrix, and the inorganic phase of this tissue stores about 99% of the Ca in the body [6]. This inorganic ion has a prominent role in bone growth precursors cells by stimulating bone synthesis pathways in osteoblasts and bone homeostasis, serving as a signaling molecule between osteoblasts and osteoclasts [8]. Additionally, Ca plays a role in blood coagulation by mediating platelet activation by binding to factor IXa and factor Xa, which are required for the tenase and prothrombins complexes to operate [9]. Magnesium ions (Mg^{2+}) are the fourth most abundant in the human body participating in lipid, protein, nucleic acid, and adenosine triphosphate (ATP) synthesis [4,6]. Naturally found in bone, Mg^{2+} is essential in the metabolism of this tissue by stimulating bone formation and bone resorption [4]. Also, Mg ions enhance cell adhesion [10] via ligand binding of the integrin receptors [11] and present an anti-inflammatory potential [12,13]. Therefore, incorporating metal cations into biomaterial may modulate cell adhesion, differentiation, and protein adsorption, thus ensuring the bone regeneration process [14].

Studying the biomaterial-biological interface allows us to understand further how the tissue-material interaction carries out and will aid in designing and developing future biomaterials [15]. The adsorption of proteins onto the material surface is one of the first events upon biomaterial

implantation. The description of the phenomenon results as a potent tool to understand the interactions between cells/tissues and materials [15,16]. The quantity and properties of the adsorbed proteins are highly dependent on the surface properties. This process will modulate cell adhesion and the subsequent cellular events, such as proliferation and differentiation, coagulation, fibrinolysis, and osteogenesis [17,18].

This study aimed to develop and characterize coatings applied to Ti surfaces enriched with Ca (0.5% in weight) and different amounts of Mg (0.5, 1, and 1.5% in weight). The physicochemical properties were studied, as well as the protein adsorption patterns and *in vitro* cell responses. With this, we will further understand the effects of ion mixtures in bone regeneration processes and determine potential synergetic effects.

5.2. Materials and methods

5.2.1. Sol-gel synthesis and sample preparation

The sol-gel technique was used to develop hybrid coatings able to release both Ca and Mg ions. MTMOS and TEOS alkoxysilanes in a molar ratio of 7:3 were mixed with 2-propanol (50% v/v). This precursor selection and its ratio were optimized in a previous study [19]. Under stirring conditions, the precursors were hydrolyzed by adding their stoichiometric amount of 0.1N HNO_3 at a 1-drop s^{-1} rate. The corresponding amount of both $CaCl_2$ and $MgCl_2$ were previously dissolved in this aqueous solution. In order to evaluate the effects of combining both cations, concentrations of Ca and Mg were defined. The proportion of $CaCl_2$ was fixed at 0.5% wt, which was established based on previous work [18], whereas the $MgCl_2$ was incorporated in increasing amounts (0.5, 1, 1.5% wt) (**Table 5.1**). A composition without salts (MT) and another only doped with Ca (without Mg; Ca) were used as controls. The different sol-gel mixtures were kept under stirring for 1h and then 1h at rest. Then, grade-4 Ti discs of 10-mm and 12-mm diameter (1-mm thick) were sandblasted and acid-etched as described in Romero-Gavilán *et al.* [20]. The 10-mm diameter discs were employed for *in vitro* assays and the 12-mm diameter for proteomics and physicochemical evaluations and were used as a coating substrate. The synthesized sol-gel compositions were applied onto the discs using a dip-coater (KSV DC; KSV NIMA, Espoo, Finland). The immersion was performed at 60 cm min^{-1} and, after one minute, the samples were removed at 100 cm min^{-1}. For evaluation of hydrolytic degradation and the cation kinetic release, coatings were applied onto glass slides. The glass surface was conditioned before coating in an HNO_3 solution (25% v/v) using an ultrasonic bath (Sonoplus HD 3200; Bandelin Electronic, Berlin, Germany) for 20 min at 30 W. The slides were washed sonicating them with distilled water and then were dried at 100°C. At this point, the glass substrates were coated by casting. For the

chemical characterization, free films of the distinct sol-gel compositions were made by pouring 5 mL of each solution into non-stick Teflon molds. Finally, heat treatment of 2h at 80°C was conducted on all the samples to cure the sol-gel. All the reagents were purchased in Sigma-Aldrich (St. Louis, MO, USA).

Table 5.1. Nomenclature of the designed sol-gel materials with the respective amounts of $CaCl_2$ and $MgCl_2$. The mass percentages were calculated concerning the total amount of alkoxysilane.

Nomenclature	$CaCl_2$ (wt %)	$MgCl_2$ (wt %)
MT	0	0
Ca	0.5	0
Ca0.5Mg	0.5	0.5
Ca1Mg	0.5	1
Ca1.5Mg	0.5	1.5

5.2.2. PHYSICOCHEMICAL CHARACTERIZATION

A solid-state silicon nuclear magnetic resonance spectroscope (^{29}Si-NMR; Bruker 400 Avance III WB Plus spectrometer, Billerica, MA, US) with a Cross Polarization Magic Angle Spinning (CP-MAS) probe for solid samples were used to study the crosslinking of the obtained sol-gel structures. The measurements were performed under the Bruker standard pulse sequence: 79.5 MHz frequency, 55 kHz spectral width, 2 ms contact time, and 5 s delay time. The spinning speed was 7.0 kHz. A Fourier Transform Infrared Spectrometer (FTIR; Thermo Nicolet 6700, Thermo Fisher Scientific, NY, US) with an attenuated total reflection system (ATR) was used to study the sol-gel materials. The spectra were measured in the 4000 - 400 cm^{-1} wavelength spectrum. A Bruker D4-Endeavor diffractometer (Bruker) was employed to perform X-ray diffraction analysis (XRD). Measurements in the range of 5–70° (2θ) with a step size of 0.05°(2θ) and a scanning rate 4 s $step^{-1}$ were collected with filtered CuKα radiation (λ = 1.54 A), an operating voltage of 40 kV and a filament current of 40 mA. The coatings applied onto Ti discs were morphologically characterized through a scanning electron microscope (SEM; Leica-Zeiss LEO, Leica, Wetzlar, Germany). The samples were sputtered with platinum before the evaluation to increase their conductivity. The sample roughness was measured with an optical profilometer PLm2300 (Sensofar, Barcelona, Spain). Three independent samples of each material were studied, and three measurements were performed in each of them. The results were displayed using the average value of Ra (arithmetic average roughness parameter). The sample wettability was evaluated using an automatic contact angle meter OCA 20 (Dataphysics Instruments, Filderstadt,

Germany). Ultrapure water drops (about 10 µL) were deposited on the discs at 27.5 µL s^{-1} speed. The drop angles were analyzed using SCA 20 software (DataPhysics Instruments). Six samples were tested for each condition, and two drops were deposited on each of them. The hydrolytic degradation of the coatings was determined by measuring their mass loss during their incubation in 50 mL of distilled water at 37°C. The results are displayed as a percentage (%) of mass loss in relation to their initial mass. The time points were 7, 14, 28, 42, and 56 days of incubation. Three distinct samples were studied for each condition. The Mg^{2+} and Ca^{2+} release kinetics were characterized using an inductively coupled plasma mass spectrometer (Agilent 7700 Series ICPMS, Agilent Technologies, Santa Clara, CA, US). The coatings were incubated in ddH_2O at 37°C for 28 days. After 2, 4, 6, 8, 24, 72, 168, 336, 504 and 672h of incubation, extracted aliquots of 0.5 mL were analyzed. Three individual samples were evaluated for each condition.

5.2.3. EVALUATION OF *IN VITRO* CELL RESPONSES

5.2.3.1. *Cell culture*

Mouse calvaria osteosarcoma (MC3T3-E1) cell medium was composed of low-glucose DMEM (Gibco, Life Technologies, Thermo Fisher Scientific, NY, USA) supplemented with 1% penicillin/streptomycin (Gibco) and 10% FBS (Gibco). After 24h, to stimulate osteogenic differentiation, the culture medium was replaced with osteogenic medium (DMEM, 1% of pen/strep, 10% FBS, ascorbic acid (50 µg mL^{-1}), and 100 mM β-glycerol phosphate), which was changed every two days. Mouse murine macrophage (RAW 264.7) cell medium was composed of high-glucose DMEM (Gibco) supplemented with 1% pen/strep and 10% FBS. Both cell lines were maintained in a cell incubator with 90% humidity and 5% CO_2 at 37°C.

5.2.3.2. *Biomaterial cytotoxicity*

Cytotoxicity was assessed following the ISO 10993-5:2009 (Annex C) norm, and samples were prepared according to the ISO 10993-12:2012 norm. MC3T3-E1 cells were seeded into 96-well NUNC plates (Thermo Fisher Scientific) at a density of $1x10^5$ cells cm^{-2} and maintained in a humidified incubator. In parallel, the materials were incubated in a cell culture medium for serum extraction. After 24h, cells were exposed to the material extract for another day. According to the manufacturer's guidelines, the CellTiter 96® Proliferation Assay (MTS; Promega, Madison, WI) was used. For controls, wells with only cells (negative control) and cells incubated with latex (positive control) were used. The material was considered cytotoxic with cell viability below 70%.

5.2.3.3. *Cytoskeletal arrangement in osteoblasts*

The MC3T3-E1 cells were seeded on the materials at a density of 1 x 10^4 cells cm^{-2} to study the effects on cytoskeleton arrangement. After 24h, the samples were washed once with PBS and fixed with 4% paraformaldehyde (PFA) for 20 min at room temperature. Then, the samples were permeabilized with 0.1% Triton X-100 for 5 min and incubated with phalloidin (1:100; Abcam, Cambridge, UK) diluted in 0.1% w/v bovine serum albumin (BSA)-PBS for 1h at room temperature. Nuclei were stained with a mounting medium with DAPI (Abcam). Fluorescence detection was performed on a Leica TCS SP8 Confocal Laser Scanning Microscope with 20x (dry) lenses. The collected images were analyzed with LAS X software (Leica) and Image J software (National Institutes of Health).

5.2.3.4. *Alkaline phosphatase activity in osteoblasts*

The cell mineralization capability was evaluated by ALP activity following the protocol by Araújo-Gomes *et al*. [21]. MC3T3-E1 cells were seeded onto the distinct surfaces in 48-well NUNC plates (Thermo Fisher Scientific) at a density of 1.75x10^4 cells cm^{-2}. After culturing for 7 and 14 days, cells were immersed in lysis buffer (0.2% Triton X-100, 10 mM Tris-HCl, pH 7.2) for 10 min at 4°C. Then, 100 µL of *p*-NPP (1mg mL^{-1}) in substrate buffer (50 mM glycine, 1 mM $MgCl_2$, pH 10.5) was added to 100 µL of the sample. After 2h of incubation in the dark, the absorbance at 405 nm was measured using a microplate reader. Alkaline phosphatase activity was calculated using a *p*-nitrophenol in 0.02 mM sodium hydroxide standard curve, and activity was normalized to protein content calculated using a Pierce BCA assay kit (Thermo Fisher Scientific).

5.2.3.5. *Cytokine secretion in macrophages*

The effect of the materials on the secretion of pro and anti-inflammatory cytokines was measured on a cell culture medium of RAW264.7 cells. The cell culture medium was collected and frozen until further analysis. Tumor necrosis factor (TNF)-α and transforming growth factor (TGF)-β concentration was determined using an ELISA (Invitrogen, Thermo Fisher Scientific) kit and according to the manufacturer's instructions.

5.2.3.6. *Relative gene expression: RNA extraction, cDNA synthesis, and qRT-PCR*

For RNA extraction, MC3T3-E1 cells were grown for 7 and 14 days at a density of 1.75x10^4 cells cm^{-2} for 7 and 14 days. RAW264.7 cells were seeded at a density of 30x10^4 cm^{-2} for 2 and 4 days. The assays were carried out in 48-well NUNC plates. At each time point, RNA was extracted with TRIzol following the protocol by Cerqueira *et al*. [22]. RNA concentration, integrity, and quality

were measured using NanoVue® Plus Spectrophotometer (GE Healthcare Life Sciences, Little Chalfont, UK).

For cDNA synthesis, approximately 1 µg of total RNA was converted into cDNA using PrimeScript RT Reagent Kit (Perfect Real Time; (TAKARA Bio Inc., Shiga, Japan). The reaction was carried out with the following conditions: 37°C for 15 min, 85°C for 5 s, and a final hold at 4°C. The resulting cDNA was diluted in DNase-free water to a concentration suitable for gene expression evaluation.

Quantitative real-time PCRs (qRT-PCR) were carried out on 96-well plates (Applied Biosystems®, Thermo Fisher Scientific). Primers for each gene were designed using the PRIMER3plus software tool from NCBI-specific DNA sequences and purchased to Thermo Fischer Scientific. Targets studied for each cell line are shown in **Supplementary Table 5.1**. Individual reactions contained 1 µL of cDNA, 0.2 µL of specific primers (forward and reverse at a concentration of 10 µM L^{-1}) and 5 µL of SYBR Premix Ex Taq (Tli RNase H Plus; TAKARA) in a final volume of 10 µL. Reactions were carried out in a StepOne Plus™ Real-Time PCR System (Applied Biosystems®). Fold changes were calculated using the $2^{-\Delta\Delta Ct}$ method.

5.2.4. PROTEOMIC ANALYSIS OF THE ADSORBED PROTEIN LAYER

The protocol described by Romero-Gavilán *et al.* [20] was followed for the proteomic analysis of the adsorbed protein layer. The materials were incubated for 3h (37°C, 5% CO_2) in 24-well NUNC plates (Thermo Fisher Scientific) with 1 mL of human serum from male AB plasma (Sigma–Aldrich). Then, to eliminate non-adsorbed proteins, the materials were washed five times with ddH_2O and once with wash buffer (100 mM NaCl, 50 mM Tris–HCl, pH 7.0). The adsorbed protein layer was obtained with a buffer (Thiourea 2M, Urea 7M, 4% Chaps, DTT 200 mM). Four independent replicates of each surface were analyzed, and each replicate was a pull of the protein layer adsorbed onto four discs. Total protein concentration in the serum was calculated with a Pierce BCA assay kit (Thermo Fisher).

The analysis of the proteins was performed using electrospray tandem mass spectrometry, employing a nanoACQUITY UPLC (Waters, Milford, MA, USA) coupled to an Orbitrap XL (Thermo Electron, Bremen, Germany) as described by Romero-Gavilán *et al.* [20]. Each sample was analyzed in quadruplicate. Differential protein analysis was carried out using PEAKS (Bioinformatics Solutions Inc., Waterloo, Canada).

5.2.5. STATISTICAL ANALYSIS

For physicochemical characterization and *in vitro* assay data, considering normal distribution and equal variance was analyzed via one-way variance analysis (ANOVA) with Tukey post hoc test. A student's *t*-test was performed after the ANOVA analysis to confirm the results. Data are expressed as mean ± standard error (SE). Statistical analysis was performed using GraphPad Prism 5.04 software (GraphPad Software Inc., La Jolla, CA, USA) and considered significant at $p \leq 0.05$. The asterisk (*) indicates differences between MT and the ion doped-coatings, and the rhombus (◆) indicates differences between the Ca-doped and the CaMg-doped materials.

A student's t-test was made to evaluate differences between MT and MT with Ca and CaMg concentrations using Progenesis software for proteomic analysis data. Differences were considered statistically significant at $p \leq 0.05$ and ratio different than 1.5 in either direction (higher or lower).

5.3. RESULTS

5.3.1. PHYSICOCHEMICAL CHARACTERIZATION

The different materials were chemically analyzed through FT-IR, ^{29}Si-NMR, and XRD (**Figure 5.2**). **Figure 5.2a** shows the FT-IR spectra for each material, which did not show significant changes due to the addition of only $CaCl_2$ or the mixture $CaCl_2$ and $MgCl_2$ with respect to the base material MT. Bands related to the polysiloxane chain vibration (770, 1020, and 1125 cm^{-1}) indicate the correct formation of Si-O-Si bonds [23]. On the other hand, the band at 950 cm^{-1} is associated with Si-OH bonds, characteristics of non-condensed groups [23]. Bands at 1265 and 2980 cm^{-1}, assigned to Si-C and C-H bonds, respectively [24], suggest the methyl group integrity maintenance in the sol-gel structure after the synthesis process. Similarly, the incorporation of salts in MT did not show significant differences in the ^{29}Si-NMR spectra (**Figure 5.2b**). The characteristic signals of the MTMOS trifunctional precursor (T units - $CH_3{\cdot}SiO_3$) were detected in the -50 and -75 ppm range, while the signals of the TEOS tetrafunctional precursor (Q units - SiO_4) were placed between – 97.5 and -120 ppm [24]. Peaks at -62 and -70 ppm were associated with T^2 and T^3 species formation in the network, while peaks at -99, -106, and -116 ppm represent Q^2, Q^3, and Q^4 reticulated structures, respectively [23]. All compositions attained a proper crosslinking degree as T^3 was the highest chemical shift in MTMOS and Q^3 in TEOS. In addition, non-condensed species (T^0 and Q^0) and structures with only one condensed bond (T^1 and Q^1) were not detected. **Figure 5.2c** shows the XRD patterns obtained for the different formulations. These results prove the amorphous nature of the synthesized materials, as no peaks associated with the formation of Ca or Mg-related crystalline structures were identified in the spectra. In addition, no significant

differences were found between the distinct compositions. The diffraction peak at 90° (2θ) can be associated with the presence of not completely hydrolyzed precursors, and the broad peak at 21° (2θ) is characteristic of the SiO_2 amorphous sol-gel network [25].

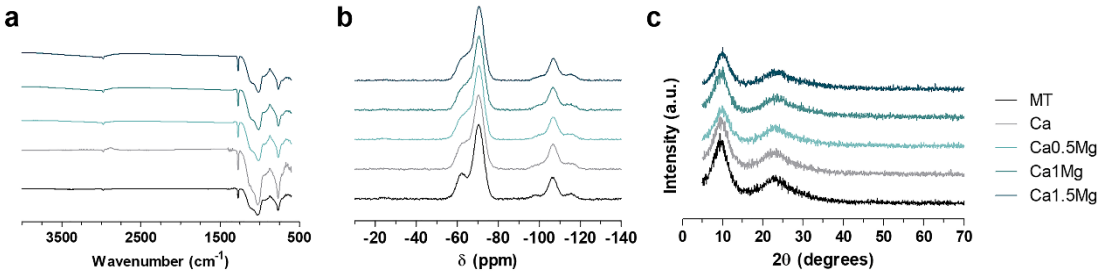

Figure 5.2. (a) ^{29}Si-NMR, (b) FT-IR spectra, and (c) XRD of the obtained sol-gel materials.

The synthesized sol-gel materials were applied as coatings onto Ti discs. The resulting coatings covered the Ti surface entirely, as can be observed in **Figure 5.3**. Contact angle measurements were carried out to evaluate changes in surface wettability because of the Ca^{2+} and Mg^{2+} addition (**Figure 5.3a**). Adding 0.5% $CaCl_2$ in the sol-gel network significantly increased the contact angle to values around 50° to 75°. The materials with both Ca and Mg ions showed greater contact angles than MT and Ca materials. However, the increasing addition of $MgCl_2$ did not imply significant changes in the wettability of the coatings.

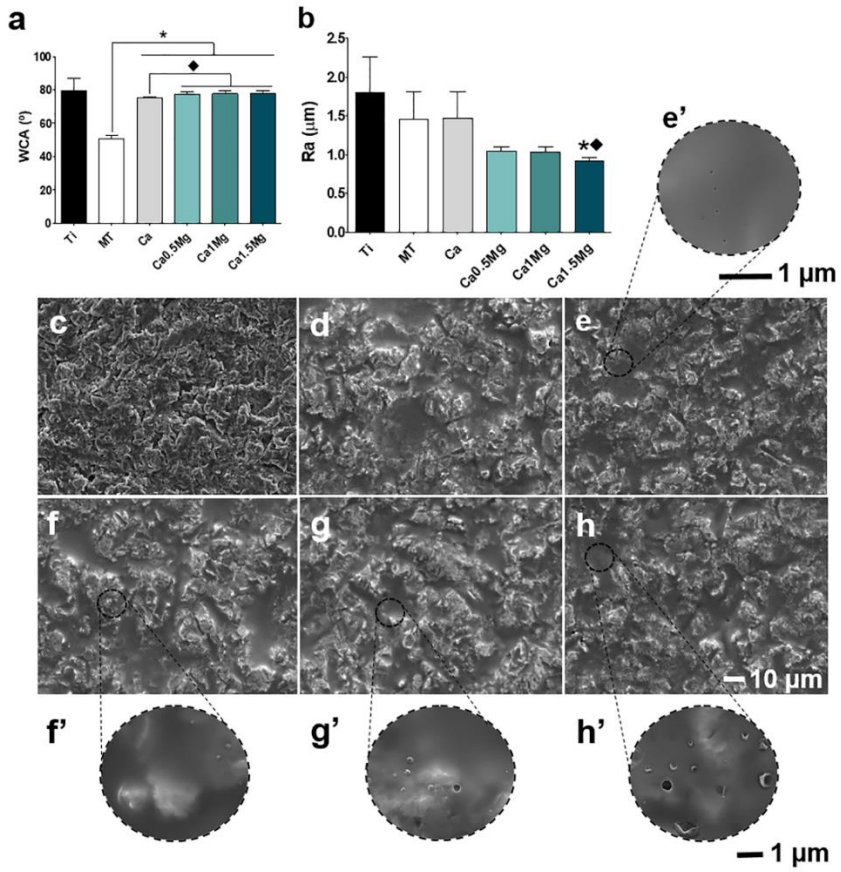

Figure 5.3. Contact angle (WCA; a) and roughness (Ra; b) results. Data are shown as mean ± SD. The asterisk (*) indicates differences between MT and the ion doped-coatings, and the rhombus (◆) indicates differences between the Ca-doped and the CaMg-doped materials. SEM microphotograph of (c) Ti, (d) MT, (e) Ca, (f) Ca0.5Mg, (g) Ca1Mg, (h) Ca1.5Mg, and (e'-h') extended images. Scale bars: (c-h) 10 and (e'-h') 1 µm.

Figure 5.3b shows the effects of Ca and Mg in the coating roughness. The values of Ra decreased when coated, and non-coated samples were compared. However, no changes in roughness were identified between the coatings MT and Ca. On the other hand, Ca0.5Mg, Ca1Mg, and Ca1.5Mg showed a significant reduction in Ra concerning both MT and Ca. The roughness results were consistent with the SEM analysis. The sol-gel tended to accumulate in the cavities of the initial Ti roughness, a fact that supposes a decrease in Ra (**Figure 5.3c-h**). The incorporation of 0.5% $CaCl_2$ in the coating supposes the appearance of small pores of about 45 nm in diameter that were not observed in the MT base material (**Figure 5.3e'**). The additional incorporation of Mg to Ca led to an increase in this type of irregularities, observing small bubbles and pores in the material (**Figure 5.3f'-h'**). Additionally, the defect size increased as more $MgCl_2$ was incorporated, reaching values up to around 0.5 µm-diameter for the Ca1.5Mg (**Figure 5.2h'**). However, no precipitates of the salts were observed.

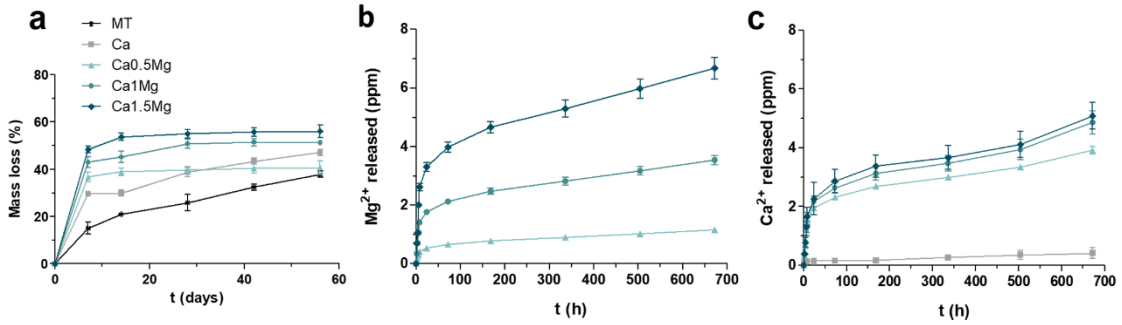

Figure 5.4. Hydrolytic degradation (a); Mg^{2+} (b) and Ca^{2+} (c) ion kinetic release for developed the sol-gel coatings. Data are shown as mean ± SE.

Figure 5.4a shows the mass loss of all coated samples versus time. In general, the degradation by hydrolysis was faster during the first week of incubation. After this period, the sol-gel coatings continue to degrade throughout the assay but slower. The addition of Ca into the MT network slightly the coating degradability, going from mass loss values of around 37.8% for MT to 47.0% for Ca after 56 days of testing. The kinetic of degradation showed by Ca0.5Mg was similar to the Ca degradation rates. However, the sol-gel network presented higher weight losses when more $MgCl_2$ was added to Ca. Thus, the mass lost after 56 days by Ca1Mg and Ca1.5Mg was 51.3 and 56.1%, respectively. **Figure 5.4b** and **c** show the kinetic liberation of Mg^{+2} and Ca^{2+} ions. Regarding the release of Mg, a continuous liberation of this ion was measured during the essay period, being faster than the release during the first 24h (**Figure 5.4b**). In addition, as expected, the more $MgCl_2$ was incorporated into the material composition, the more Mg^{2+} was released from it. The maximum release of this ion, 6.67 ppm of Mg^{2+}, was measured in the CaMT1.5Mg sample after 672h of incubation. The release of Ca^{2+} (**Figure 5.4c**) shows that similarly to Mg, Ca was liberated during all the test periods, and the release kinetic was higher during the first day of incubation. Although the Ca concentration is the same in all the developed materials, the release of this cation is significantly higher in coatings with both Ca and Mg than in Ca. Moreover, the release of Ca^{2+} increased as more $MgCl_2$ was added to the network, being 5.08 ppm of Ca^{2+}, the maximum concentration detected in the essay (CaMT1.5Mg; 672h).

5.3.2. *IN VITRO* CELL RESPONSES

5.3.2.1. *Cytotoxicity, cytoskeleton arrangement, and ALP activity*

In what concerns biomaterial cytotoxicity, none of the materials in the study was cytotoxic (data not shown). To evaluate the effects of the materials in cellular cytoskeleton arrangement, the cells were stained with phalloidin after culturing for 1 day (**Figure 5.5 a-f**). Cells cultured Ti and

MT showed a triangular shape with few lamellipodia (**Figure 5.5a and b**). The materials Ca, Ca0.5Mg and Ca1Mg showed a more elongated shape with protruded lamellipodia and filopodia (**Figure 5.5b-e**). Ca1.5Mg also present lamellipodia; however, the cell shape was generally less elongated (**Figure 5.5f**). Cell area measurements show that Ca, Ca0.5Mg, and Ca1Mg materials lead to a significant increase of this parameter when compared to MT (**Figure 5.5g**).

To understand the effects of the materials on mineralization capability, ALP activity was measured (**Figure 5.5h**). At 7 days, there was a significant increase in ALP activity in Ca and MT1.5Mg when compared to MT. On the other hand, Ca0.5Mg and Ca1Mg presented a significant decrease of this parameter when compared to Ca. After 14 days, all materials presented a significant decrease in ALP activity when compared to MT.

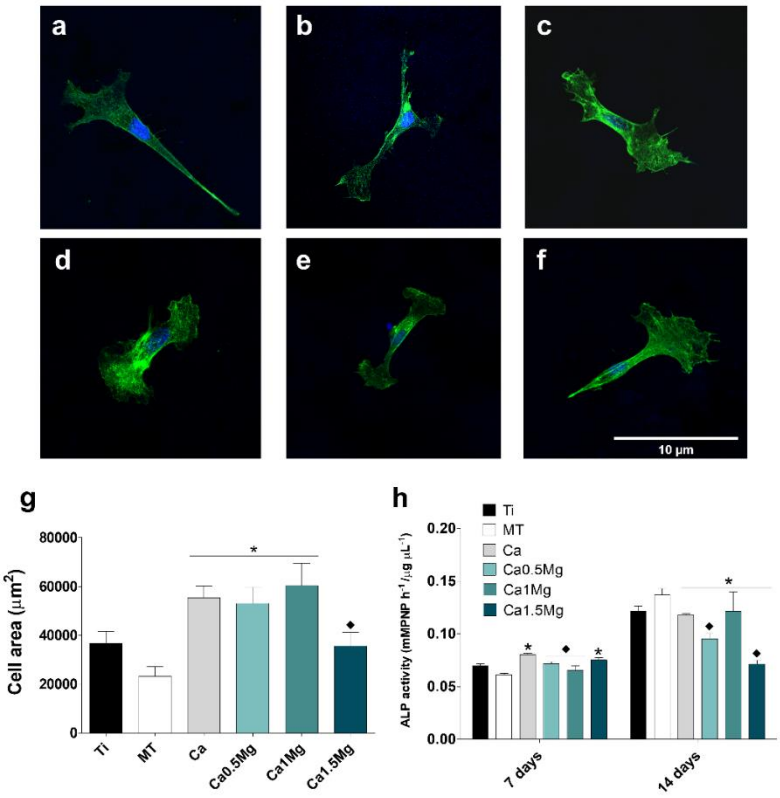

Figure 5.5. Fluorescent confocal images of cytoskeleton arrangement of MC3T3-E1 on (a) Ti, (b) MT, (c) Ca, (d) Ca0.5Mg, (e) Ca1Mg, (f) Ca1.5Mg, and (g) area of the cells adhered to the materials. Actin was stained with phalloidin (green), and nuclei were stained with DAPI (blue). Scale bar: 10 µm. ALP activity (h) in MC3T3-E1 at 7 and 14 days. Results are shown as mean ± SE. The asterisk (*) indicates differences between MT and the ion doped-coatings, and the rhombus (◆) indicates differences between the Ca-doped and the CaMg-doped materials.

5.3.2.2. *Cytokine secretion in macrophages*

To evaluate the effects of the ion-doped materials on inflammation, cytokine secretion in the RAW264.7 cell culture medium was measured. The anti-inflammatory cytokine TGF-β only showed a significant increase in relation to MT in Ca0.5Mg at 2 days and Ca1Mg at 4 days (**Figure 5.6a**). On the other hand, when comparing with Ca, all CaMg materials showed a significantly higher secretion of this cytokine at 4 days.

The pro-inflammatory cytokine TNF-α was significantly less secreted in Ca when compared to MT (**Figure 5.6b**) at 2 days. At the same time point, the addition of Mg leads to a higher production of this cytokine in Ca1.5Mg. After 4 days, all materials with CaMg showed a significantly higher production of TNF-α when compared to MT and Ca (**Figure 5.6b**).

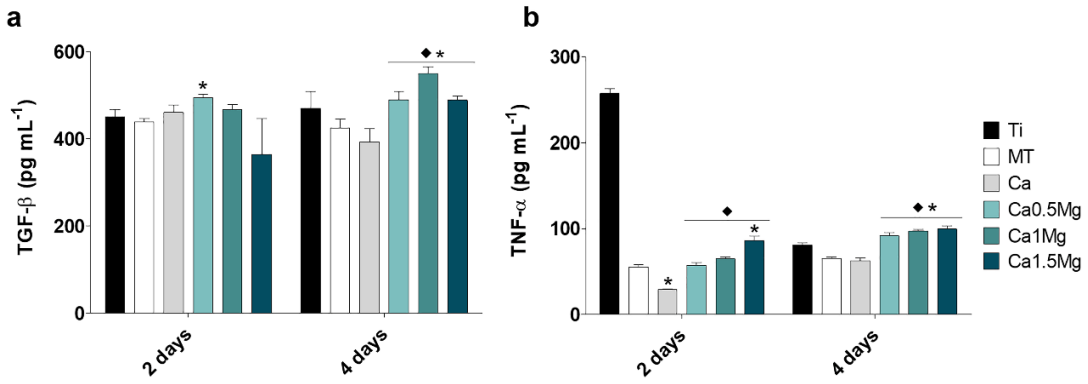

Figure 5.6. Cytokine secretion quantification through ELISA of (a) TGF-β and (b) TNF-α in RAW264.7 at 2 and 4 days. Results are shown as mean ± SE. The asterisk (*) indicates differences between MT and the ion doped-coatings, and the rhombus (◆) indicates differences between the Ca-doped and the CaMg-doped materials.

5.3.2.3. *Relative gene expression*

To better appreciate the effects of the materials on osteogenesis (ALP, TGF-β, SP7, and RUNX2), and inflammatory responses (TNF-α, IL-1β. TGF-β, and IL-10), gene expression was measured. At 7 and 14 days, Ca0.5Mg presented a significantly higher expression of ALP in relation to MT and Ca (**Figure 5.7a**). Similarly, Ca0.5Mg and Ca1.5Mg also increased the expression of SP7 at 7 days of assay; however, the fold-change was significantly lower in Ca0.5Mg at 14 days, while augmented in Ca, Ca1Mg, and Ca1.5Mg (**Figure 5.7b**). The TGF-β was higher at 7 days in Ca0.5Mg, but it was significantly decreased at 14 days in all materials except Ca (**Figure 5.7c**). No differences were found in the RUNX2 expression at 7 days. At 14 days, Ca led to a higher expression of RUNX2 in relation to MT and a significantly lower expression in all CaMg materials in relation to Ca (**Figure 5.7d**).

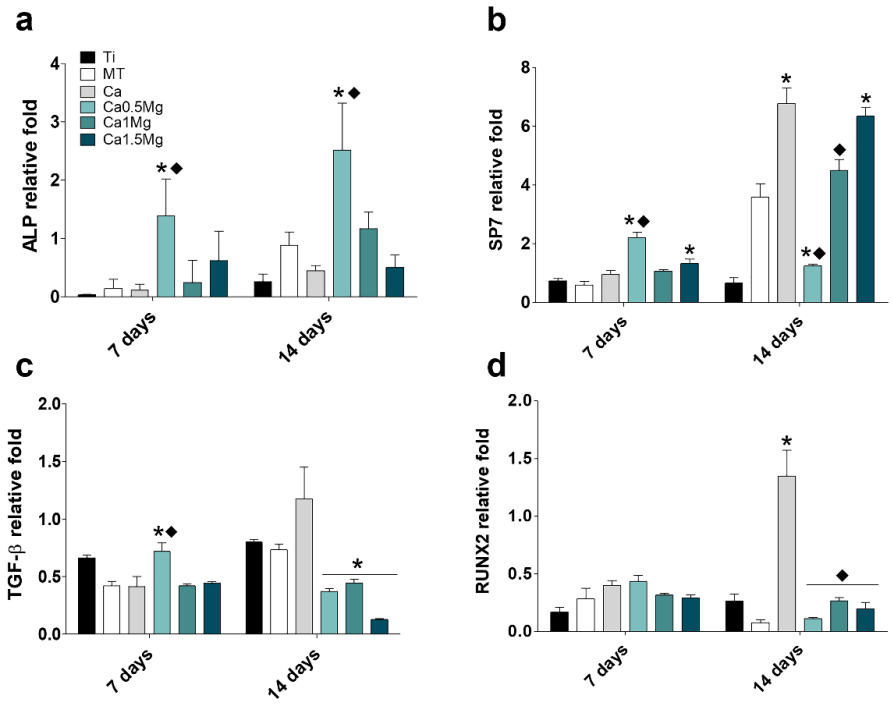

Figure 5.7. Relative gene expression of (a) alkaline phosphatase (*ALP*), (b) transcription factor SP7/osterix (*SP7*), (c) transforming growth factor (*TGF*)-β, and (d) runt-related transcription factor 2 (*RUNX2*) on MC3T3-E1 at 7 and 14 days. Data were normalized in relation to blank (wells without any material) with the $2^{-\Delta\Delta Ct}$ method. Results are shown as mean ± SE. The asterisk (*) indicates differences between MT and the ion doped-coatings, and the rhombus (◆) indicates differences between the Ca-doped and the CaMg-doped materials.

Regarding gene expression related to inflammatory responses, TNF-α gene expression was significantly reduced in Ca1Mg and Ca1.5Mg in relation to Ca (**Figure 5.8a**) after 2 days. At 4 days, all materials with Ca (both Ca and mixtures) presented a higher expression of this gene in comparison with MT. In parallel, Ca0.5Mg also presented an increased expression of TNF-α when compared to Ca. When evaluating the expression of IL-1β (**Figure 5.8b**) at 2 days, Ca, Ca1Mg and Ca1.5Mg presented an increment when compared to MT, while Ca0.5Mg showed a significantly higher expression in comparison to Ca. After 2 days, the anti-inflammatory marker TGF-β increased in Ca1Mg in comparison to MT, and Ca0.5Mg was significantly less expressed when compared to Ca (**Figure 5.8c**). Lastly, IL-10 (**Figure 5.8d**) presented a higher expression in Ca0.5Mg when compared with MT at 2 days; on the other hand, Ca1Mg and Ca1.5Mg were significantly less expressed in Ca1Mg and Ca1.5Mg at the same time point. On the fourth day of assay, IL-10 was significantly less expressed in all materials with Ca, regardless of the presence of Mg, in relation to MT. Ca1Mg and Ca1.5Mg also presented a lower expression of this marker when compared with Ca.

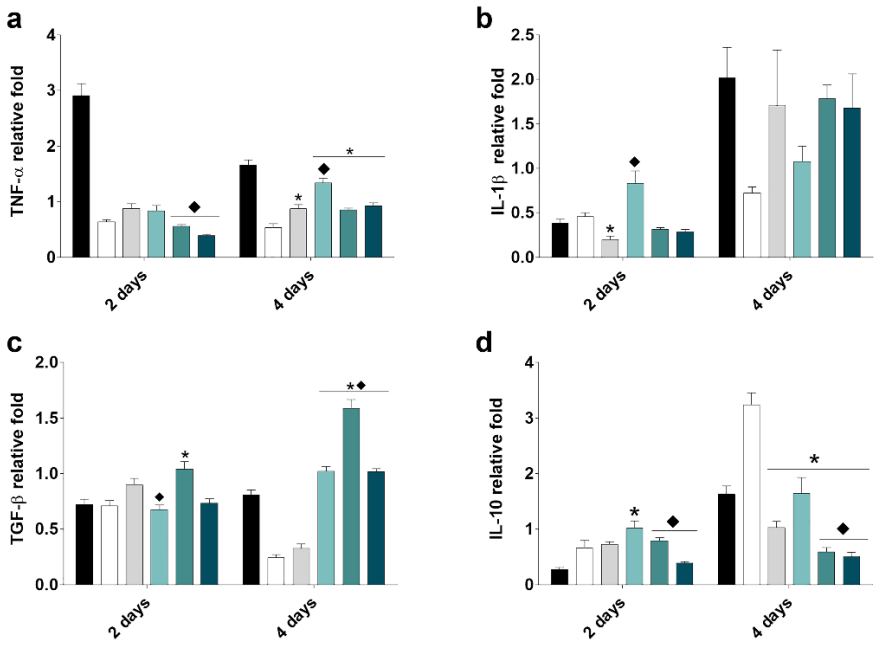

Figure 5.8. Relative gene expression of (a) tumor necrosis factor (*TNF*)-α, (b) interleukin (*IL*) 1-β**,** (c) transforming growth factor (*TGF*)-β, and (d) *IL-10* on RAW264.7 at 2 and 4 days. Data were normalized in relation to blank (wells without any material) with the $2^{-\Delta\Delta Ct}$ method. Results are shown as mean ± SE. The asterisk (*) indicates differences between MT and the ion doped-coatings, and the rhombus (◆) indicates differences between the Ca-doped and the CaMg-doped materials.

5.3.3. PROTEOMIC ANALYSIS

The nLC-MS/MS analysis of eluted proteins identified 84 proteins differentially adsorbed on the materials with CaMg in comparison with the MT base material (**Supplementary Table 5.2**). **Table 5.2** summarizes the adsorbed proteins found on the Ca and CaMg materials with associated biological functions. Among these, 16 proteins related to inflammatory responses, particularly the complement system activation (CO6, CO5, CO4B, CO4B, and CO9) and its regulation (CFAH and VTDB), presented a higher affinity with CaMg surfaces. Proteins with roles in the acute inflammatory responses (A1AG1, A1AG2, and AACT), immune system regulation (PIGR, PIP), and innate immune mediation (HPTR, HPT) were more detected in CaMg surfaces as well as ITIH2, which is associated with the localization, synthesis, and degradation of hyaluronan. CRP, a positive acute-phase protein, was more detected on Ca and Ca1Mg. Additionally, seven proteins associated with coagulation (HRG, HBA, ZPI, HEP2, and A2MG) and with roles in cell adhesion, (FBLN1 and HABP2) presented a higher ratio in CaMg materials. Moreover, proteins with functions in cell adhesion (ZA2G, LG3BP, DSG1, and DESP), several apolipoproteins (APOF, APOL1, APOA4, APOH, APOM, and APOA1), and tissue regeneration processes (CLUS and TSK)

were found more adsorbed onto CaMg surfaces. On the other hand, 14 proteins (PROS, THRB, KNG1, IPSP, FA11, PFAV, CXCL7, ANT3, FA10, PLF4, FA9, FA12, PROC, and CBPB2) associated with coagulation were found less adsorbed onto the CaMg materials. Seven immunoglobulins (KV320, KVD40, IGKC, IGHG2, KV127, HV118, and KV106) and FHR5 are associated with complement system regulation and were also less found on CaMg. Furthermore, two proteins associated with inflammatory responses (MASP2 and FCN2), one protein associated with cell adhesion (PKP1), and two apolipoproteins (APOC4 and APOE) were less adsorbed. Finally, three proteins associated with the cartilage structure (COMP, PCOC1, and PRG4) and tissue regeneration process (VTNC and IBP4) were also found less adhered to the CaMg materials with respect to MT.

Table 5.2. Summary of the proteins differentially adsorbed onto the sol-gel materials doped with Ca and CaMg associated with relevant biological processes (immune response, cell adhesion, tissue regeneration, and coagulation).

Biological process		Ca	Ca0.5Mg/MT	Ca1Mg/MT	Ca1.5Mg/MT
Immune responses	More adsorbed	PIGR CO6 CO5 CO4B A1AG1 ITIH2 CO9 VTDB ALBU AACT HPT CFAH A1AG2 IGHM ITIH1 HEMO IGHG4 CRP	PIGR CO6 PIP CO5 CO4B CO4A A1AG2	PIGR CO6 PIP CO5 CO4B CO4A ITIH2 CO9 VTDB HPTR AACT HPT A1AG2 ALBU ITIH1 HEMO	PIGR CO6 PIP CO5 CO4B CO4A ITIH2 CO9 HPTR AACT HPT CFAH ALBU

	Less adsorbed	KVD40 IGKC MASP2 KV127 KV106 FHR5 PRG4	KV320 KVD40 IGKC MASP2 IGHG2 KV127 HV118 KV106 FHR5 FCN2 BLMH	KVD40 MASP2 IGHG2 KV106 FHR5 FCN2 BLMH	MASP2 IGHG2 KV127 HV118 KV106 FHR5 FCN2 BLMH
Tissue regeneration	More adsorbed	CLUS	CLUS	CLUS	TSK CLUS
	Less adsorbed	COMP PCOC1 VTNC IBP4 PRG4	COMP PCOC1 VTNC IBP4 PRG4	COMP PCOC1 VTNC IBP4 PRG4	COMP PCOC1 VTNC IBP4 PRG4
Cell adhesion	More adsorbed	LG3BP DSG1 FBLN1 DESP HABP2	ZA2G LG3BP DSG1 DESP	ZA2G LG3BP DSG1 FBLN1 DESP HABP2	ZA2G LG3BP DSG1 FBLN1 DESP HABP2
	Less adsorbed	PKP1	PKP1	PKP1	
Coagulation	More adsorbed	HBA ZPI HABP2 A2MG	HRG HBA ZPI F13B	HRG HBA ZPI HABP2 HEP2 A2MG F13B	HRG HBA ZPI HABP2 HEP2 A2MG
	Less adsorbed	HRG PLMN THRB KNG1 IPSP FA11 ANT3 FA10 PLF4 FA9 FA12 PROC CBPB2	PROS THRB KNG1 IPSP FA11 PF4V CXCL7 ANT3 FA10 PLF4 FA9 FA12 PROC CBPB2	PROS THRB KNG1 IPSP FA11 PF4V CXCL7 ANT3 FA10 PLF4 FA9 FA12 PROC CBPB2	PROS THRB KNG1 IPSP FA11 PF4V CXCL7 ANT3 FA10 PLF4 FA9 FA12 PROC CBPB2

To further understand the mixture effect, a comparison between Ca and CaMg materials was made. A total of 17 proteins were found differentially adsorbed (**Supplementary Table 5.3**). Of those, five were associated with coagulation (HRG, SPB12, PLMN, HBA, and FA12), one related with inflammatory responses (PIP), one apolipoprotein (APOA4), and PLAK, associated with cell adhesion, were found more adsorbed on the surfaces with CaMg. On the other hand, HV551, CO8B, BLMH, and CRP, all associated with immune responses, and TSK were significantly less adsorbed onto CaMg when compared with Ca surfaces. **Figure 5.9** shows the mixture effect on the protein adsorption of the most relevant proteins. As the concentration of Mg in the mixture increases, the abundance of HRP, SPB12, PLMN, and HBA also increases (**Figure 5.9a, b, c, and d**). On the other hand, no differences in FA12 were found between Ca, Ca0.5Mg and Ca1.5Mg were found (**Figure 5.9e**). In what concerns proteins related to inflammatory responses, CRP significantly decreased in Ca1.5Mg (**Figure 5.9f**), while Ca0.5Mg adsorbed less CO8B (**Figure 5.9g**) and BLMH in Ca1Mg (**Figure 5.9h**).

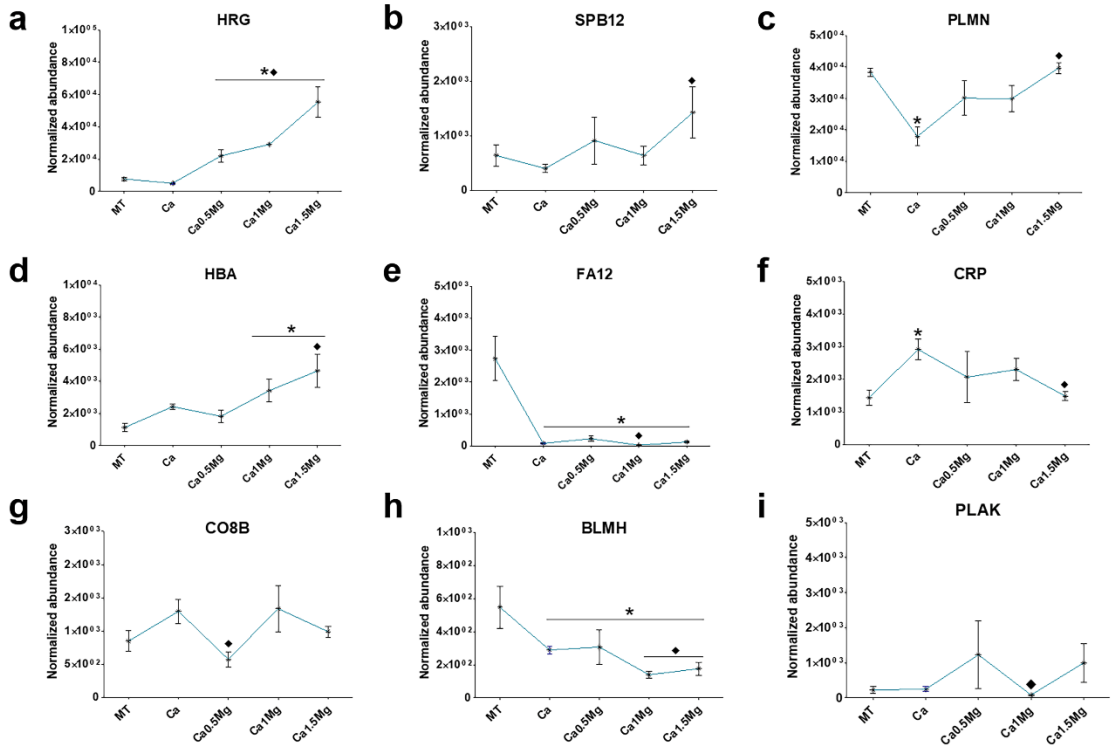

Figure 5.9. Normalized protein abundance of proteins associated with coagulation - (a) histidine-rich glycoprotein (HRG), (b) serpin B12 (SBP12), (c) plasminogen (PLMN), (d) hemoglobin subunit alpha, (e) coagulation factor XII (FA12) –, immune responses - (f) C-reactive protein (CRP), (g) complement component C8 beta chain (CO8B), bleomycin hydrolase (BLMH) -, and cell adhesion – (i) junction plakoglobin (PLAK). Results are shown as mean ± SE. The asterisk (*) indicates

differences between MT and the ion doped-coatings, and the rhombus (◆) indicates differences between the Ca-doped and the CaMg-doped materials.

5.4. Discussion

Calcium and magnesium are important elements in the biological systems, particularly in bone tissue and other associated processes, such as inflammation or coagulation. The individual effects of both ions of protein adsorption have previously been studied [10,18]. Ca presented a high affinity with proteins associated with coagulation and inflammatory responses, while Mg presented a higher affinity to cell adhesion. With this, a biomaterial that reconciles the regulatory properties of both ions presents an interesting path to be further investigated. Thus, the main aim of this study was to develop and characterize a new coating enriched with mixtures of Ca and Mg and understand how these elements affect protein adsorption patterns and *in vitro* cell responses.

The incorporation of $CaCl_2$ and $MgCl_2$ onto the sol-gel network did not affect the final silica network crosslinking as the ^{29}Si-solid NMR shows. No crystalline structures were found in the networks, and Ca^{2+} and Mg^{2+} are likely trapped on the hybrid cross-linked structure by hydrogen bonding, Van der Waals, or electrostatic forces [26]. The $CaCl_2$ incorporation onto the sol-gel network led to a significant increase of the contact angle, and changes were observed in the roughness. Romero-Gavilán *et al.* [18] reported that incorporating 0.5% (in weight) of $CaCl_2$ in a sol-gel network did not significantly change the material roughness and increased the contact angle. The incorporation of the CaMg mixture also did not affect the final network. However, it led to a significant decrease in roughness, probably due to increased sol-gel viscosity. The release measurements revealed that more $MgCl_2$ was added to the network, more Mg^{2+} and Ca^{2+} were released. As expected [18,22], the hydrolytic degradation corroborates these results. As more $MgCl_2$ was added to the network, more mass was lost by the coating, explaining why significantly more Ca2+ was released in the CaMg coating than Ca. Also, the incorporation of Ca and CaMg led to small pores formation on the coatings, as observed on the SEM microphotographs. These pores allow water entrance onto the network, which leads to an increasing degradation and Mg^{2+} and Ca^{2+} release and a decrease in the coating barrier effect. The release kinetics assays were stable until 30 days (end of the assay), reaching 6 ppm of Mg^{2+} and about 5 ppm of Ca^{2+} in the material with the highest concentration of both ions (Ca1.5Mg). Mg is non-cytotoxic at concentrations as high as 10 mM [27] and Ca at concentrations up to 150 ppm [28], explaining the cytotoxicity results.

Upon biomaterial implantation, nonspecific protein adsorption onto the material surface occurs nearly instantaneously [16]. This phenomenon plays a major role in determining the following

interactions between implants and tissues. Its comprehension is essential to understand the cell responses and improve the design of biomaterials [15]. In this work, the nLC-MS/MS analysis of the protein layer formed upon incubation with human serum allowed the identification of 84 proteins differentially adsorbed onto CaMg surfaces compared to MT. Five proteins found more adsorbed onto the CaMg materials are associated with activating the complement system (CO6, CO5, CO4B, CO4B, and CO9). The complement system is an important effector of innate immunity participating in the opsonization of foreign bodies [29]. However, once activated, the complement system needs to be tightly controlled, as the exacerbated reaction can lead to severe inflammation and cell damage [30]. Three proteins associated with its regulation (CFAH, VTDB, and CLUS) presented a higher affinity to CaMg surfaces in a dose-response manner. Complement factor H (CFAH) is a critical regulator of the alternative complement pathway and is associated with the balance between osteoblasts and osteoclasts and consequent determination of bone tissue quality [30,31]. Vitamin D binding protein (VTDB) plays a major role in the transport of vitamin D metabolites. It has been implicated in the enhancement of the complement C5 system in association with annexin A2 [32]. Additionally, VTDB stimulates reactive oxygen intermediates (ROIs) and cellular debris ingestion, leading to macrophage activation [33]. The apolipoprotein clusterin (CLUS) regulates the complement proteins C6, C7, C8, and C9 and the membrane attack complex (MAC) formation. Also, CLUS regulates the NF-κB pathway and reduces apoptosis and oxidative stress in immune cells [34].

Moreover, seven other apolipoproteins (APOF, APOL1, APOA4, APOH, APOM, and APOA1) were also presented a higher affinity onto CaMg-containing surfaces. These proteins are also involved in the regulation of the complement system [35] and lipid metabolism. In contrast, ficolin-2 (FCN2), known to activate the lectin pathway of complement activation [36], was found less adsorbed onto the CaMg materials. The normal immune responses also involve the formation of immune complexes by specific immunoglobulins with target antigens to facilitate the clearance or neutralization of foreign bodies [37]. The CaMg coatings lead to a significant decrease in this type of protein (IGH2, KV127, HV118, KV106, KV320, KVD40, and IGKC) adsorption. In contrast, several regulators of the immune responses were found more adsorbed onto CaMg surfaces, such as alpha-1-acid glycoproteins (A1AG1 and A1AG2), that inhibit immune cells and regulate the induction of IL-1 and IL-1β [38], and haptoglobin (HPT) and haptoglobin-related protein (HPTR), associated with the regulation of acute inflammation and tissue repair [39]. Albumin (ALBU), a well-known negative acute-phase regulator [40], was also found more adhered to CaMg surfaces. When comparing Ca and CaMg materials, we found that one immunoglobulin (HV551), one complement protein (CO8B), and two proteins associated with the regulation of immune responses (BLMH and CRP) were differentially adsorbed. C-reactive protein (CRP), a positive

acute-phase protein produced in response to inflammatory conditions [40,41], such as infection, or trauma in a Ca-dependent manner, was found significantly less in Ca1.5Mg. Likewise, BLMH, known for regulating inflammatory chemokines (CXCL8 and GROα) and wound healing [42] presented a lower affinity to Ca1Mg and Ca1.5Mg when compared to Ca.

Ca's *in vitro* inflammatory response depends on the ion concentration incorporated in a material [18], while Mg generally presents an anti-inflammatory activity [10]. In this study, the CaMg sol-gel coatings led to an increment in TNF-α and TGF-β secretion and gene expression, while decreased IL-10 expression in a dose-response manner to the amount of Mg incorporated. Similarly, Wang *et al*. [43] developed Mg-Ca phosphate cement that leads to an increase of *TGF-β* gene expression, while the expression of *IL-6*, *IL-1β*, and *IL-10* is reduced. These results indicate that the inflammatory potential of these materials probably comes from a balance between pro and anti-inflammatory proteins adsorbed into the surface and cytokine expression/release, as well as an equilibrium between the amount of Ca and Mg incorporated onto the material.

Another key process in bone regeneration is coagulation. Even though the CaMg coatings adsorbed seven proteins associated with coagulatory processes (HRG, HBA, ZPI, FBLN1, HABP2, HEP2, and A2MG), others (*e.g.,* FA11, FA10, FA9, FA12) showed less affinity with these materials, depending on the concentration of Mg incorporated onto the network. With this, the comparison between Ca and CaMg coatings allowed us to comprehend better the effect of mixtures on the adsorption of these proteins. The addition of Mg led to an increase in the adsorption of 4 proteins (HRG, SPB12, PLMN, and HBA) in a dose-response manner. In particular, histidine-rich glycoprotein (HRG) presents anticoagulant activity by binding to heparin and neutralizing it, thus preventing the formation of heparin-antithrombin III complexes that inhibit activated coagulation factors (*e.g.,* thrombin) [37]. Moreover, plasminogen (PLMN) is the zymogen of plasmin, a vital enzyme of the coagulation system that dissolves preformed fibrin clots and regulates wound healing, tissue remodeling, tumor metastasis, and angiogenesis [44].

For optimal tissue regeneration around a biomaterial, good cell adhesion is essential. Mg ion is well-known for promoting cell adhesion [11]. Therefore, it was not surprising to find that CaMg materials presented a higher affinity to proteins associated with cell adhesion processes (ZA2G, LG3BP, DSG1, FBLN1, DESP, and HABP2). The area measurements of MC3T3-E1 cells cultured onto the materials are in accordance with these results, except for Ca1.5Mg. Increasing amounts (0 to 20%) of Mg-phosphate cement in Ca-phosphate cement led to a higher cell spreading up to 10%, while decreased at higher concentrations. These results indicate that incorporating certain amounts of Mg with Ca in a material cannot enhance the cell adhesion and spreading [14]. Furthermore, the CaMg materials showed a significantly lower affinity to proteins associated with this process (COMP, PCOC1, VTNC, and IBP4).

Interestingly, differences in ALP activity and osteogenic gene expression (*ALP*, *SP7*, *TGF-β*, and *RUNX2*) are dependent on the concentration of Mg added to the coating; however, the effect was more evident for materials with a lower concentration of Mg. Similarly, Mg-Ca phosphate cements have been shown to promote osteogenesis both *in vitro* and *in vivo*, especially for materials with lower Mg content [43]. Similar to what was observed for inflammatory responses, the amount of Mg added to a Ca can determine the effects observed on cell response, either antagonistic or synergetic.

5.5. Conclusion

The main goal of this study was to understand how mixtures of Ca and Mg affect *in vitro* cell responses and protein adsorption patterns in materials for bone regeneration. For that, we developed and characterized new sol-gel coatings with a controlled release of both elements. Both ions were successfully incorporated onto the sol-gel network without affecting the final network crosslinking or forming crystalline structures. A controlled release of both ions was obtained and, as the amount of Mg added to the network increased, more Mg and Ca were liberated, and more the materials degraded. The CaMg materials generally adsorbed more proteins related to the regulation of inflammatory responses (A1AG1, A1AG2, HPTR, HPT, and ALBU). They presented a lower affinity for proteins associated with induction of inflammation (*e.g.*, immunoglobulins). However, adding Mg to Ca led to a decrease in the adsorption of significant inflammatory proteins (CRP and BLMH), showing the potential of Mg in controlling Ca-induced inflammation. *In vitro* cell responses of RAW264.7 macrophages showed that the CaMg coatings led to an increase of TNF-α and TGF-β while decreasing *IL-10* expression. Moreover, CaMg coatings generally showed higher adsorption of proteins related to cell adhesion (ZA2G, LG3BP, DSG1, FBLN1, and DESP), and MC3T3-E1 cell area increment was dependent on the amount of Mg incorporated onto the material. Even though all the material presented less affinity to proteins related to tissue regeneration processes (COMP, PCOC1, VTNC, IBP4), the *in vitro* assays showed that the amount of proportion of Ca to Mg modulated the ALP activity and osteogenic gene expression (*ALP*, *SP7*, and *TGF-β*). With this, we can conclude that the desired equilibrium effect in ion mixtures depends on the amount of each ion added to the mix, rather than a simple sum of properties.

5.6. Acknowledgments

The work was supported by MINECO [MAT2017-86043-R; RTC-2017-6147-1], Generalitat Valenciana [GRISOLIAP/2018/091, APOSTD/2020/036, PROMETEO/2020/069], Universitat Jaume I under [UJI-B2017-37, GACUJI/2021/14], the University of the Basque Country under [GIU18/189] and Basque Government under [PRE_2017_2_0044]. The authors would like to thank Raquel Oliver, Jose Ortega, José Miguel Pedra, and Iraide Escobés for their valuable technical assistance, and Antonio Coso (GMI-Ilerimplant) for producing the titanium discs.

5.7. References

1. Jeong, J., Kim, J. H., Shim, J. H., Hwang, N. S. & Yeong Heo, C. Bioactive calcium phosphate materials and applications in bone regeneration. *Biomater. Res.* **23**, 1–11 (2019).
2. Ansari, M. Bone tissue regeneration: biology, strategies and interface studies. *Prog. Biomater.* **8**, 223–237 (2019).
3. Dai, C. *et al.* Osteogenic evaluation of calcium/magnesium-doped mesoporous silica scaffold with incorporation of rhBMP-2 by synchrotron radiation-based μCT. *Biomaterials* **32**, 8506–8517 (2011).
4. O'Neill, E., Awale, G., Daneshmandi, L., Umerah, O. & Lo, K. W. H. The roles of ions on bone regeneration. *Drug Discovery Today* vol. 23 879–890 (2018).
5. Yan, Y. *et al.* Enhanced osteogenic differentiation of bone mesenchymal stem cells on magnesium-incorporated titania nanotube arrays. *Colloids Surfaces B Biointerfaces* **179**, 309–316 (2019).
6. Lakhkar, N. J. *et al.* Bone formation controlled by biologically relevant inorganic ions: Role and controlled delivery from phosphate-based glasses. *Adv. Drug Deliv. Rev.* **65**, 405–420 (2013).
7. Yuan, X. *et al.* Immunomodulatory effects of calcium and strontium co-doped titanium oxides on osteogenesis. *Front. Immunol.* **8**, 1196 (2017).
8. Liu, D. *et al.* Activation of extracellular-signal regulated kinase (ERK1/2) by fluid shear is Ca2+- and ATP-dependent in MC3T3-E1 osteoblasts. *Bone* **42**, 644–652 (2008).
9. Anitua, E., Prado, R., Orive, G. & Tejero, R. Effects of calcium-modified titanium implant surfaces on platelet activation, clot formation, and osseointegration. *J. Biomed. Mater. Res. - Part A* **103**, 969–980 (2015).
10. Cerqueira, A. *et al.* Characterization of magnesium doped sol-gel biomaterial for bone tissue regeneration: the effect of Mg ion in protein adsorption. *Mater. Sci. Eng. C* **125**, 112114 (2021).

11. Zreiqat, H. *et al.* Mechanisms of magnesium-stimulated adhesion of osteoblastic cells to commonly used orthopaedic implants. *J. Biomed. Mater. Res.* **62**, 175–184 (2002).
12. Li, B. *et al.* In vitro and in vivo responses of macrophages to magnesium-doped titanium. *Sci. Rep.* **7**, 42707 (2017).
13. Sugimoto, J. *et al.* Magnesium Decreases Inflammatory Cytokine Production: A Novel Innate Immunomodulatory Mechanism. *J. Immunol.* **188**, 6338–6346 (2012).
14. Zhang, J. *et al.* Magnesium modification of a calcium phosphate cement alters bone marrow stromal cell behavior via an integrin-mediated mechanism. *Biomaterials* **53**, 251–264 (2015).
15. Othman, Z., Cillero Pastor, B., van Rijt, S. & Habibovic, P. Understanding interactions between biomaterials and biological systems using proteomics. *Biomaterials* **167**, 191–204 (2018).
16. Swartzlander, M. D. *et al.* Linking the foreign body response and protein adsorption to PEG-based hydrogels using proteomics. *Biomaterials* **41**, 26–36 (2015).
17. Romero-Gavilán, F. *et al.* Proteomic analysis of silica hybrid sol-gel coatings: a potential tool for predicting the biocompatibility of implants in vivo. *Biofouling* **In press**, (2017).
18. Romero Gavilán, F. *et al.* Proteomic analysis of calcium-enriched sol-gel biomaterials. *JBIC J. Biol. Inorg. Chem.* **24**, 563–574 (2019).
19. Martinez-Ibañez, M. *et al.* Biological characterization of a new silicon based coating developed for dental implants. *J. Mater. Sci. Mater. Med.* **27**, (2016).
20. Romero-Gavilan, F. *et al.* Proteomic analysis of silica hybrid sol-gel coatings: a potential tool for predicting the biocompatibility of implants *in vivo*. *Biofouling* **33**, 676–689 (2017).
21. Araújo-Gomes, N. *et al.* Osseointegration mechanisms: a proteomic approach. *JBIC J. Biol. Inorg. Chem.* **23**, 459–470 (2018).
22. Cerqueira, A. *et al.* A possible use of melatonin in the dental field: Protein adsorption and in vitro cell response on coated titanium. *Mater. Sci. Eng. C* **116**, 111262 (2020).
23. Romero-Gavilan, F. *et al.* Bioactive potential of silica coatings and its effect on the adhesion of proteins to titanium implants. *Colloids Surfaces B Biointerfaces* **162**, 316–325 (2018).
24. Romero-Gavilán, F. *et al.* Sol-gel coatings made using methyl-modified alkoxysilanes: The balance between protection and bioactivation. *Prog. Org. Coatings* **147**, 105770 (2020).
25. Chernev, G. *et al.* Sol-gel silica hybrid biomaterials for application in biodegradation of toxic compounds. *J. Sol-Gel Sci. Technol.* **58**, 619–624 (2011).
26. Romero-Gavilán, F. *et al.* The effect of strontium incorporation into sol-gel biomaterials on their protein adsorption and cell interactions. *Colloids Surfaces B Biointerfaces* **174**,

9–16 (2019).

27. Yoshizawa, S., Brown, A., Barchowsky, A. & Sfeir, C. Magnesium ion stimulation of bone marrow stromal cells enhances osteogenic activity, simulating the effect of magnesium alloy degradation. *Acta Biomater.* **10**, 2834–2842 (2014).
28. Saravanapavan, P., Selvakumaran, J. & Hench, L. L. Indirect Cytotoxlcity Evaluation of Soluble Silica, Calcium, Phosphate and Silver Ions. in *Key Engineering Materials* vols 254–256 785–788 (Trans Tech Publications Ltd, 2004).
29. Carroll, M. C. The complement system in regulation of adaptive immunity. *Nature Immunology* vol. 5 981–986 (2004).
30. Skerka, C., Chen, Q., Fremeaux-Bacchi, V. & Roumenina, L. T. Complement factor H related proteins (CFHRs). *Mol. Immunol.* **56**, 170–180 (2013).
31. Alexander, J. J. *et al.* Absence of complement factor H alters bone architecture and dynamics. *Immunobiology* **223**, 761–771 (2018).
32. Bouillon, R., Schuit, F., Antonio, L. & Rastinejad, F. Vitamin D Binding Protein: A Historic Overview. *Front. Endocrinol. (Lausanne).* **10**, 910 (2020).
33. White, P. & Cooke, N. The multifunctional properties and characteristics of vitamin D-binding protein. *Trends Endocrinol. Metab.* **11**, 320–327 (2000).
34. Falgarone, G. & Chiocchia, G. Clusterin: A multifacet protein at the crossroad of inflammation and autoimmunity. *Advances in Cancer Research* vol. 104 139–170 (2009).
35. Cho, N. H. & Seong, S. Y. Apolipoproteins inhibit the innate immunity activated by necrotic cells or bacterial endotoxin. *Immunology* **128**, 479–486 (2009).
36. Kilpatrick, D. C. & Chalmers, J. D. Human L-ficolin (ficolin-2) and its clinical significance. *J. Biomed. Biotechnol.* **2012**, (2012).
37. Poon, I. K. H., Patel, K. K., Davis, D. S., Parish, C. R. & Hulett, M. D. Histidine-rich glycoprotein: The Swiss Army knife of mammalian plasma. *Blood* **117**, 2093–2101 (2011).
38. Bteich, M. An overview of albumin and alpha-1-acid glycoprotein main characteristics: highlighting the roles of amino acids in binding kinetics and molecular interactions. *Heliyon* **5**, e02879 (2019).
39. Schaer, D. J., Vinchi, F., Ingoglia, G., Tolosano, E. & Buehler, P. W. Haptoglobin, hemopexin and related defense pathways-basic science, clinical perspectives and drug development. *Front. Physiol.* **5**, 415 (2014).
40. Jain, S., Gautam, V. & Naseem, S. Acute-phase proteins: As diagnostic tool. *J. Pharm. Bioallied Sci.* **3**, 118–127 (2011).
41. Sproston, N. R. & Ashworth, J. J. Role of C-reactive protein at sites of inflammation and infection. *Front. Immunol.* **9**, 754 (2018).

42. Riise, R. *et al.* Bleomycin hydrolase regulates the release of chemokines important for inflammation and wound healing by keratinocytes. *Sci. Rep.* **9**, 1–10 (2019).

43. Wang, M. *et al.* Improved osteogenesis and angiogenesis of magnesium-doped calcium phosphate cement: Via macrophage immunomodulation. *Biomater. Sci.* **4**, 1574–1583 (2016).

44. Barthel, D., Schindler, S. & Zipfel, P. F. Plasminogen is a complement inhibitor. *J. Biol. Chem.* **287**, 18831–18842 (2012).

5.8. SUPPLEMENTARY MATERIAL

Supplementary Table 5.1. Targets studied in MC3T3-E1 osteoblasts and RAW264.7 macrophages.

Name	Accession	Sequence	Product length
GADPH (*GADPH)*	XM_017321385	F: TGCCCCCATGTTTGTGATG R: TGGTGGTGCAGGATGCATT	83
Osterix (*OSX/SP7*)	XM_006520519	F: ACTCATCCCTATGGCTCGTG R: GGTAGGGAGCTGGGTTAAGG	238
Alkaline Phosphatase (*ALP*)	XM_006538499	F: CGGGACTGGTACTCGGATAA R: ATTCCACGTCGGTTCTGTTC	157
Transforming Growth Factor-β (*TGFBETA*)	NM_011577	F: TTGCTTCAGCTCCACAGAGA R: TGGTTGTAGAGGGCAAGGAC	183
Runt-related transcription factor 2 (*RUNX2*)	NM_001271631	F: CCCAGCCACCTTTACCTACA R: TATGGAGTGCTGCTGGTCTG	150
Interleukin-1β (*IL-1β*)	NM_008361	F: GCCCATCCTCTGTGACTCAT R: AGGCCACAGGTATTTTGTCG	230
Tumor Necrosis Factor-α (*TNFALFA*)	NM_001278601	F: AGCCCCCAGTCTGTATCCTT R: CTCCCTTTGCAGAACTCAGG	212
Interleukin-10 (*IL10*)	XM_036162094	F: CCAAGCCTTATCGGAAATGA R: TTTCACAGGGGAGAAATCG	161

Supplementary Table 5.2. Progenesis comparative analysis between the proteins identified onto the CaMg materials with respect to the control treatment without ions. Proteins with ANOVA $p < 0.05$ (yellow) and a ratio higher than 1.5 in either direction was considered as significantly different. Proteins with increased affinity to coatings doped with the ion mixtures in comparison to MT are marked in red, while those with reduced affinity appear in green.

Accession	Description	Peptides	*p* value	Ca *vs* MT	*p* value	Ca0.5Mg *vs* MT	*p* value	Ca1Mg *vs* MT	*p* value	Ca1.5Mg *vs* MT
PIGR_HUMAN	Polymeric immunoglobulin receptor	4	0.08826327	8.21038572	0.10398244	2.110492935	0.050879168	21.2844809	0.01913551	53.39896966
CO6_HUMAN	Complement component C6	4	0.02416573	5.40835555	0.09847591	3.734693893	2.52197E-05	13.56916463	9.5234E-05	9.344775468
HRG_HUMAN	Histidine-rich glycoprotein	5	0.0375673	0.66162516	0.00301627	2.807138021	0.000137496	4.173795744	0.00011276	7.037290164
APOF_HUMAN	Apolipoprotein F	3	8.0828E-06	8.33602729	2.3546E-05	6.377981885	9.92202E-05	6.768705744	1.55E-05	5.695727005
CLUS_HUMAN	Clusterin	9	1.4678E-06	4.95113745	1.9753E-05	3.844404123	3.96251E-05	4.83769562	3.174E-06	5.573022585
APOL1_HUMAN	Apolipoprotein L1	6	0.00321596	3.11117598	0.00325282	2.425866234	9.48681E-05	3.828608121	1.5747E-05	5.09689983
APOA4_HUMAN	Apolipoprotein A-IV	7	0.00014115	2.68391689	0.00034181	2.413321295	0.000226966	3.253065791	2.6419E-06	4.170123181
HBA_HUMAN	Hemoglobin subunit alpha	4	0.00885666	2.29586848	0.16567348	1.620827998	0.013696828	3.006823116	0.00275588	4.145195083

PIP_HUMAN	Prolactin-inducible protein	2	0.9909 0078	1.0048 8821	0.7024 283	1.501848 201	0.59730 0667	1.31830 5742	0.0234 7686	3.356947 559
ZA2G_HUMAN	Zinc-alpha-2-glycoprotein	4	0.2129 9333	2.1562 5828	0.1940 5016	2.274327 476	0.04324 6404	3.94523 1615	0.0588 0849	2.802860 612
ZPI_HUMAN	Protein Z-dependent protease inhibitor	2	0.0029 506	4.1282 7764	0.4207 9251	1.895639 988	0.00359 0377	3.83817 3691	0.0273 0235	2.438408 775
CO5_HUMAN	Complement C5	13	0.0791 389	3.0683 435	0.1442 8461	2.656193 042	0.04066 8673	4.43904 705	0.1329 3459	2.432668 943
CO4B_HUMAN	Complement C4-B	22	0.0112 7639	2.3624 2741	0.0083 029	2.566834 003	0.00246 621	2.36503 2485	0.0046 6659	2.335708 12
CO4A_HUMAN	Complement C4-A	22	0.5724 1895	1.3587 867	0.0153 904	3.693247 636	0.02685 0353	2.80659 3261	0.0312 2914	2.317404 682
LG3BP_HUMAN	Galectin-3-binding protein	2	0.0051 4695	3.8012 6604	0.0285 4303	2.499518 145	0.00775 7111	3.05014 9592	0.0321 3735	2.273744 267
A1AG1_HUMAN	Alpha-1-acid glycoprotein 1	4	0.0771 9159	2.0226 6865	0.2242 3324	1.625266 161	0.01209 0103	3.10256 1912	0.1086 7634	2.136130 816
DSG1_HUMAN	Desmoglein-1	9	0.0444 8361	1.7034 8471	0.0075 2749	2.617011 021	0.01969 2008	1.88201 8748	0.0182 6585	2.127058 925
FBLN1_HUMAN	Fibulin-1	4	0.0250 8707	2.1530 4728	0.6405 6912	0.738493 946	0.03348 4206	1.71580 0717	0.0602 9065	2.112527 321
TSK_HUMAN	Tsukushin	2	0.0330 5217	3.4893 2989	0.9752 7255	0.982383 476	0.47319 5929	1.43854 7641	0.2907 6625	2.087650 202

A1BG_HUMAN	Alpha-1B-glycoprotein	4	0.30243427	1.58531881	0.26606699	1.65680177	0.02799102	2.96138 0766	0.12404949	2.057838838
DESP_HUMAN	Desmoplakin	18	0.04458205	1.77846182	0.16430924	1.724168771	0.76355267	1.09496 8221	0.10522671	2.02763785
HABP2_HUMAN	Hyaluronan-binding protein 2	2	0.00678531	1.71867052	0.09779575	1.442411696	0.02347 4697	1.70053 1818	0.00531704	2.000360469
ITIH2_HUMAN	Inter-alpha-trypsin inhibitor heavy chain H2	9	0.09362029	1.94649144	0.38069573	1.38392523	0.02184 8921	2.69271 2123	0.12960925	1.969051712
CO9_HUMAN	Complement component C9	7	0.0015704	1.87317281	0.05261142	1.349900433	0.00417 5515	1.82137 7541	0.00333818	1.916337943
P02787|TRFE_HUMAN	Serotransferrin	31	0.01265494	2.07397715	0.10752216	1.454053145	0.00495 7241	2.41695 3974	0.05353404	1.717070173
HEP2_HUMAN	Heparin cofactor 2	3	0.33753592	1.30892642	0.25451302	1.311291107	0.01054 6297	2.12361 1707	0.01912009	1.705170498
VTDB_HUMAN	Vitamin D-binding protein	9	0.03379637	1.68614897	0.2102592	1.391934187	0.00374 2398	2.36065 956	0.14394381	1.658864444
HPTR_HUMAN	Haptoglobin-related protein	9	0.02107318	1.47429579	0.29437641	1.268433601	0.00447 6824	1.69014 9659	0.00731964	1.643014258
A2MG_HUMAN	Alpha-2-macroglobulin	28	0.02276355	1.55826543	0.30541334	1.311045722	0.01210 9884	1.84857 6823	0.01882348	1.637494431
ALBU_HUMAN	Serum albumin	43	0.04208429	1.73418162	0.19712695	1.468226961	0.01301 7273	2.07121 885	0.1121507	1.636540153

AACT_HUMAN	Alpha-1-antichymotrypsin	6	0.02029878	1.72269823	0.02396238	1.562788994	0.019634055	1.876766283	0.06191559	1.58782619
HPT_HUMAN	Haptoglobin	10	0.0948899	1.651951 12	0.10858604	1.519850057	0.02157645	2.148887566	0.15597967	1.55856465
APOH_HUMAN	Beta-2-glycoprotein 1	10	0.19287369	1.18889063	0.01135978	1.288445934	0.144532661	1.195804048	0.0013633	1.55558691
CFAH_HUMAN	Complement factor H	25	0.0045753	1.71286209	0.23019347	1.282320597	0.087861781	1.269434538	0.00112857	1.55474071 4
APOM_HUMAN	Apolipoprotein M	3	0.05483148	1.50621738	0.74526547	1.066398237	0.296658639	1.239358873	0.00136345	1.54742984
APOA1_HUMAN	Apolipoprotein A-I	16	0.05263808	1.36214851	0.00077732	1.596700804	0.000201141	1.740891149	0.00018596	1.52074577 9
A1AG2_HUMAN	Alpha-1-acid glycoprotein 2	4	0.01016015	2.09758606	0.23763751	1.581190289	0.005524844	2.989926459	0.2708869	1.44725385 6
IGHM_HUMAN	Immunoglobulin heavy constant mu	11	0.00037726	1.52150598	0.34718584	1.163109561	0.019254844	1.229063112	0.01424558	1.41018457
ITIH1_HUMAN	Inter-alpha-trypsin inhibitor heavy chain H1	10	0.02676825	1.82654083	0.29789005	1.350198948	0.009729712	2.667614137	0.36065088	1.39369995 3
HEMO_HUMAN	Hemopexin	9	0.00955983	1.76308619	0.6067517	1.141025473	0.037304395	1.648439 57	0.17253174	1.38172259 6
F13B_HUMAN	Coagulation factor XIII B chain	7	0.04999424	1.47741794	0.01888557	1.790405037	0.011449064	1.723719471	0.10763983	1.31781970 1

IC1_HUMAN	Plasma protease C1 inhibitor	7	0.02127257	1.70110595	0.24780953	1.247464707	0.124112065	1.342840542	0.21323378	1.254190937
ENOA_HUMAN	Alpha-enolase	3	0.03674599	0.39036348	0.34278041	0.629810188	0.215091377	0.649370162	0.71322573	1.251189231
IGHG4_HUMAN	Immunoglobulin heavy constant gamma 4	10	0.01198312	1.57811791	0.37269022	1.131145095	0.022783477	1.383496506	0.44249361	1.130734328
CRP_HUMAN	C-reactive protein	2	0.01078897	2.07851045	0.56948855	1.25150582	0.069414468	1.619822802	0.76810749	1.062170525
PLMN_HUMAN	Plasminogen	12	0.00389691	0.44858087	0.18238495	0.74589683	0.101866879	0.758385875	0.58361037	1.033262058
SAA1_HUMAN	Serum amyloid A-1 protein	2	0.994866	1.00296815	0.00342949	0.362760681	0.093654791	0.569868518	0.72002736	0.940299138
FA5_HUMAN	Coagulation factor V	7	0.01286353	0.67192541	0.01888513	0.601380503	0.24522458	0.855003363	0.21590962	0.904617619
C4BPA_HUMAN	C4b-binding protein alpha chain	10	0.21828656	0.80328676	0.13529819	0.713766452	0.046690659	0.665699966	0.38625668	0.860660403
PROS_HUMAN	Vitamin K-dependent protein S	5	0.23535856	0.80903835	0.04451537	0.618247755	0.0276777	0.682445622	0.23047828	0.811614756
KV320_HUMAN	Immunoglobulin kappa variable 3-20	3	0.04356623	0.75962221	0.00022457	0.596910278	0.006962577	0.729976032	0.12960239	0.788436242
KVD40_HUMAN	Immunoglobulin kappa variable 2D-40	2	0.00146869	0.62312219	0.00409619	0.54523308	0.017069076	0.640128745	0.00072934	0.674676586

PKP1_HUMAN	Plakophilin-1	5	0.00461148	0.58013035	0.00233367	0.455451709	0.033985213	0.56633241	0.27752046	0.671163889
IGKC_HUMAN	Immunoglobulin kappa constant	6	0.00447548	0.68296663	0.00057265	0.634223834	0.008089655	0.73054852	0.00087975	0.649136597
COMP_HUMAN	Cartilage oligomeric matrix protein	2	0.00985099	0.3622958	0.00239613	0.426019095	0.028662892	0.30687 4357	0.12041262	0.605453891
THRB_HUMAN	Prothrombin	16	0.00128979	0.47359639	2.7546E-05	0.436390016	0.000335398	0.51071 8775	0.00209108	0.604171066
MASP2_HUMAN	Mannan-binding lectin serine protease 2	2	0.00315333	0.36569429	0.07424377	0.336498038	0.27863 3288	0.54253 2324	0.20394215	0.594187022
IGHG2_HUMAN	Immunoglobulin heavy constant gamma 2	11	0.07106569	0.70450947	0.00320442	0.51299654	0.09045 4463	0.69737 1833	0.01439097	0.564601161
APOC4_HUMAN	Apolipoprotein C-IV	2	0.01262641	0.40795163	0.00369012	0.231831739	0.018856887	0.35901 1012	0.03628273	0.546144266
KNG1_HUMAN	Kininogen-1	7	0.00056849	0.43447648	0.0010493	0.46513777	1.02797E-06	0.51631 5567	0.0027325	0.541188842
KV127_HUMAN	Immunoglobulin kappa variable 1-27	2	0.02094884	0.4599344	0.00288888	0.381699711	0.08446368	0.54982 7511	0.00447136	0.510570115
HV118_HUMAN	Immunoglobulin heavy variable 1-18	2	0.00310485	0.70087351	0.00833969	0.507199068	0.24835 2765	0.88019 19	0.00338003	0.510477401
IPSP_HUMAN	Plasma serine protease inhibitor	3	0.00190436	0.44773903	0.06514034	0.314556265	0.06474 1089	0.60270 795	0.09452572	0.493584844

G3P_HUMAN	Glyceraldehyde-3-phosphate dehydrogenase	4	5.9913 E-05	0.1550 4404	0.0315 3988	0.247559 977	0.00047 0219	0.22538 603	0.0075 87	0.486792 889
APOE_HUMAN	Apolipoprotein E	10	7.0304 E-06	0.3336 876	8.6878 E-05	0.314076 956	1.33647 E-05	0.36248 6708	0.0007 8784	0.451641 512
PCOC1_HUMAN	Procollagen C-endopeptidase enhancer 1	4	0.0126 1915	0.4941 7023	0.0049 6135	0.317502 532	0.03628 6911	0.56776 2709	0.0017 6457	0.386347 241
KV106_HUMAN	Immunoglobulin kappa variable 1-6 O	2	0.0001 5378	0.5039 2188	0.0027 381	0.410342 361	2.18963 E-05	0.40465 3786	0.0002 9485	0.381736 753
FHR5_HUMAN	Complement factor H-related protein 5	3	0.0015 0259	0.1879 6944	6.5313 E-05	0.171429 821	5.63729 E-05	0.20441 5996	0.0015 7496	0.332166 849
BLMH_HUMAN	Bleomycin hydrolase	4	0.0889 5288	0.5758 4323	0.1796 2716	0.509626 075	0.00513 8188	0.27000 3497	0.0290 5026	0.312805 98
FA11_HUMAN	Coagulation factor XI	6	0.0439 9365	0.3955 7688	0.0118 5605	0.248462 495	0.02554 9947	0.34486 4134	0.0058 7016	0.304684 919
PF4V_HUMAN	Platelet factor 4 variant	2	0.8142 3319	0.8527 6256	0.1766 7699	0.590204 162	0.04232 4321	0.35941 6862	0.0387 1596	0.284843 226
CXCL7_HUMAN	Platelet basic protein	3	0.9895 9691	1.0099 9986	0.9304 7927	1.081047 564	0.92145 4086	1.12603 7599	0.0110 4435	0.259013 644
VTNC_HUMAN	Vitronectin	7	2.6918 E-07	0.1743 8889	3.2613 E-05	0.182635 611	3.81505 E-06	0.20373 9837	9.1113 E-06	0.248886 52
KCRM_HUMAN	Creatine kinase M-type	3	0.0094 9008	0.2696 7992	0.0002 342	0.120130 135	0.00057 0125	0.06314 096	0.0269 6932	0.238413 858

ANT3_HUMAN	Antithrombin-III	10	8.7368E-05	0.21752754	5.6204E-05	0.17778925	0.00017 0381	0.22082 4171	0.0004 7094	0.204923 877
FCN2_HUMAN	Ficolin-2	2	0.1417 2093	0.3282 7801	3.7158E-05	0.108112 107	0.00121 7727	0.18615 6771	4.1054E-06	0.171206 573
FA10_HUMAN	Coagulation factor X	3	0.0001 3868	0.0898 2308	0.0001 1459	0.071489 244	0.00053 4564	0.04944 2997	1.7319E-05	0.146593 191
PLF4_HUMAN	Platelet factor 4	2	0.0045 5166	0.1082 2382	0.0016 3426	0.084840 092	0.00276 3631	0.14717 5558	0.0019 8701	0.100748 482
IBP4_HUMAN	Insulin-like growth factor-binding protein 4	2	2.1185E-05	0.0721 2134	2.0333E-05	0.127672 525	0.00063 5726	0.07068 5593	0.0114 1616	0.084996 662
FA9_HUMAN	Coagulation factor IX	3	0.0002 8426	0.0871 1712	0.0221 3502	0.173100 284	0.00070 4628	0.09993 7504	3.6727E-06	0.066378 968
PRG4_HUMAN	Proteoglycan 4	2	0.0001 1352	0.0258 28	0.0005 973	0.038883 179	0.00026 4423	0.04225 9807	0.0010 8483	0.049228 923
FA12_HUMAN	Coagulation factor XII	2	0.0002 1144	0.0316 2633	0.0039 5959	0.075342 097	0.00011 3826	0.00932 8753	0.0007 5675	0.046949 708
PROC_HUMAN	Vitamin K-dependent protein C	5	1.1482E-06	0.0442 3187	1.1698E-05	0.026978 8	9.34846E-05	0.03768 6458	0.0001 333	0.024263 98
CBPB2_HUMAN	Carboxypeptidase B2	3	2.5944E-05	0.0234 8804	2.5152E-05	0.023869 795	4.8156E-06	0.03235 3823	0.0001 1242	0.022713 597

Supplementary Table 5.3. Progenesis comparative analysis between the proteins identified onto the CaMg materials with respect to the Ca coatings. Proteins with ANOVA $p < 0.05$ (yellow) and a ratio higher than 1.5 in either direction was considered as significantly different. Proteins with increased affinity to coatings doped with CaMg in comparison to Ca are marked in red, while those with reduced affinity appear in green.

Accession	Description	Peptides	*p* value	Ca0.5Mg *vs* Ca	*p* value	Ca1Mg *vs* Ca	*p* value	Ca1.5Mg *vs* Ca
HRG_HUMAN	Histidine-rich glycoprotein	5	2,65E-04	4,24	8,25E-06	6,31	1,87E-05	10,64
PIP_HUMAN	Prolactin-inducible protein	2	7,04E-01	1,49	5,94E-01	1,31	2,02E-02	3,34
PLAK_HUMAN	Junction plakoglobin	5	2,85E-01	2,46	3,52E-02	0,38	8,77E-02	3,18
SPB12_HUMAN	Serpin B12	4	5,59E-01	1,49	5,58E-01	1,35	2,47E-02	3,14
G3P_HUMAN	Glyceraldehyde-3-phosphate dehydrogenase	4	4,13E-01	1,60	2,35E-01	1,45	4,39E-03	3,14
PLMN_HUMAN	Plasminogen	12	9,60E-02	1,66	5,57E-02	1,69	3,41E-03	2,30
HBA_HUMAN	Hemoglobin subunit alpha	4	1,88E-01	0,71	3,25E-01	1,31	3,33E-02	1,81
APMAP_HUMAN	Adipocyte plasma membrane-associated protein	2	3,48E-02	0,53	1,83E-01	1,41	3,55E-01	1,67
APOA4_HUMAN	Apolipoprotein A-IV	7	5,47E-01	0,90	3,48E-01	1,21	2,09E-02	1,55
FA12_HUMAN	Coagulation factor XII	2	1,27E-01	2,38	3,21E-02	0,29	3,51E-01	1,48
HV551_HUMAN	Immunoglobulin heavy variable 5-51	2	5,37E-03	0,66	1,44E-01	1,37	9,91E-01	1,00
TGM3_HUMAN	Protein-glutamine gamma-glutamyltransferase E	4	1,19E-02	0,56	1,04E-02	0,60	9,81E-01	0,99
KCRM_HUMAN	Creatine kinase M-type	3	1,12E-01	0,45	3,55E-02	0,23	8,44E-01	0,88
CO8B_HUMAN	Complement component C8 beta chain	3	1,03E-02	0,43	8,84E-01	0,96	1,74E-01	0,78

TSK_HUMAN	Tsukushin	2	7,59E-03	0,28	1,60E-03	0,41	2,99E-01	0,60
BLMH_HUMAN	Bleomycin hydrolase	4	7,53E-01	0,89	6,09E-03	0,47	1,10E-01	0,54
CRP_HUMAN	C-reactive protein	2	1,96E-01	0,60	2,01E-01	0,78	3,38E-03	0,51

CHAPTER 6

PROTEOME CHARACTERIZATION REVEALS THE COMPLEXITY OF THE MG-BIOMATERIALS ON THE ENTIRE OSTEOBLASTIC MACHINERY: FROM CELL ADHESION TO OSTEOGENESIS

CHAPTER 6

PROTEOME CHARACTERIZATION REVEALS THE COMPLEXITY OF THE MG-BIOMATERIALS ON THE ENTIRE OSTEOBLASTIC MACHINERY: FROM CELL ADHESION TO OSTEOGENESIS

ARTICLE 5

In preparation for submission

ABSTRACT

Magnesium is essential in bone, being well-known for promoting cell adhesion and osteogenesis. The growing demand for improved biomaterials increased the need to comprehend better cell-material interactions, and *omics* are a viable alternative to the traditional *in vitro* methods. We applied proteomics to describe the unique cellular protein expression profiles upon exposure to a sol-gel coating doped with Mg (MT1.5Mg). For that, human osteoblasts (HOb) were seeded on the materials for 1, 3, and 7 days, and proteins were identified by LC-MS/MS. PANTHER, DAVID, and IPA databases were applied for analysis. MT1.5Mg mainly regulated pathways of early osteoblast differentiation (PI3/AKT, mTOR, ERK/MAPK), insulin metabolism (IGF-1, insulin secretion, and receptor signaling, JAK/STAT), cell adhesion (integrin and FAK signaling, actin cytoskeleton regulation), and oxidative stress (oxidative phosphorylation, superoxide radicals degradation). Collagens (CO3A1, CO5A2, CO2A1, CO4A2), insulin (IGFBP3), MAPK1 (MK01), myosins (MYO5A, MYO9B, MYL3, MYLK), integrins (ITA5, ITB5, ITA6) were identified as significantly modified by MT1.5Mg. Additionally, several other proteins with roles in cell adhesion (Cdc42, MXRA8, PAXI, LPXN) and anti-oxidant system (PRDX2, SOD, CATA, GTSO1) were identified. These results prove the proteomics potential for biomaterial characterization and the Mg role in the cellular machinery, showing that its effects on osteogenesis and adhesion come from an overall impact on the cell rather than an effect on individual processes.

KEYWORDS

Biomaterials, cell-material interactions, proteomics, cell adhesion, osteogenesis

GRAPHICAL ABSTRACT

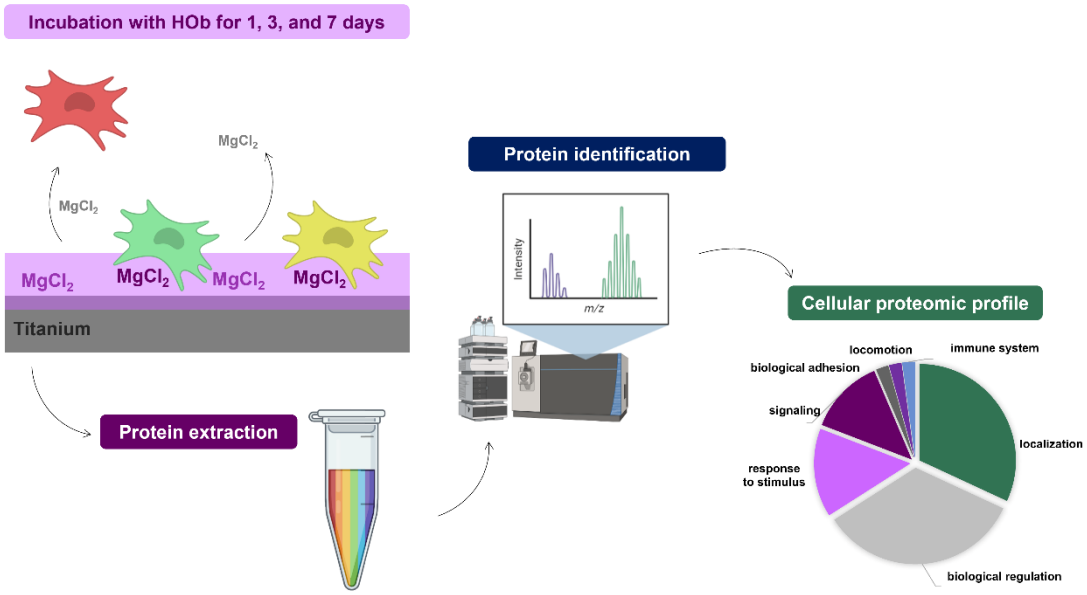

Figure 6.1. Graphical abstract of the paper "The complexity of the Mg-biomaterials effects on the entire osteoblastic machinery: a proteomic study"

6.1. INTRODUCTION

Magnesium (Mg) is essential in cellular processes and important in bone constitution and metabolism [1]. Mg is known to enhance matrix mineralization and collagen type X expression in mesenchymal stem cells (MSCs) [2] and stimulate osteoblastic differentiation, ALP activity, and mineral deposition in osteoblastic cells [3]. Additionally, Mg enhances cell adhesion by mediating membrane-associated adhesion receptors, such as integrin receptors α5β1, β1, and α3β1 [4]. The potential of Mg on biomaterials has been proven in bioactive glasses [4], biodegradable alloys [5], and sol-gel coatings for titanium (Ti) surfaces as described by our group [6]. We demonstrated that Mg-doped materials improved cellular adhesion, reduced inflammation, and increased osteogenic markers expression in a dose-response manner.

The growing demand for the improvement of biomaterials for medical applications has increased the need to understand cell-material interactions better. In addition, the difficulty in translating current *in vitro* methods into patient outcomes has increased the interest in developing alternative early-stage assays predictive of *in vivo* response and optimizing biomaterial testing [7]. The application of *omics* in biomaterials can tackle the complexity of materials-biological systems interactions [8]. Proteomics helps comprehend said interaction by describing unique cellular protein expression profiles exposed to biomaterials [9]. In recent years, this technique was employed to understand how different biomaterials modulate the expression of proteins associated with cell adhesion, proliferation, and differentiation in osteosarcoma cells [10] and mesenchymal stem cells (MSCs) [11,12]. Even though the number of studies is still quite limited, they demonstrate the potential of proteomics to predict a biomaterial outcome and how it still needs to be further explored.

The present work aimed to characterize the proteomic profile of human osteoblasts exposed to a biomaterial with Mg. We selected the Mg-doped sol-gel coating with good *in vitro* behavior based on Cerqueira *et al*. [6]. Liquid chromatographic tandem mass spectrometry (LC-MS/MS) was employed to identify the proteins, and computational methods were used to evaluate protein interactions. With this, we hope to show how proteomics can be helpful for a biomaterial *in vitro* characterization and further existing knowledge of Mg affects cellular behavior.

6.2. Materials and methods

6.2.1. Material synthesis

Methyltrimethoxysilane (MTMOS; Merck, Darmstadt, Germany) and tetraethyl orthosilicate (TEOS; Merck) were used as precursors (molar ratio of 7:3) to obtain hybrids by the sol-gel route. The percentage of 1.5% (wt) $MgCl_2$ was selected based on results previously described in Cerqueira *et al*. [6], and the materials were synthesized as described in the same work. Grade-4 Ti discs (10-mm diameter, 1-mm thick) were sandblasted, acid-etched, and used as a substrate for the coatings. The discs were immersed in the sol-gel solutions at 60 cm min^{-1} for one minute and removed at 100 cm^{-1} with a dip-coater (KSV DC; KSV NIMA, Espoo, Finland).

6.2.2. Cell culture

Human osteoblasts (HOb) derived from healthy bone were purchased from Cell Applications Inc. (San Diego, CA) and expanded in a proliferation medium consisting of low-glucose Dulbecco's Modified Eagle's Medium enriched with L-glutamine (DMEM; Merck), 100 U/mL penicillin/streptomycin (Gibco, Life Technologies, Carlsbad, CA, USA), and 10% fetal bovine serum (FBS; Merck).

The cells were seeded on the discs at a density of $2.5x10^4$ per cm^{-2} for 1, 3, and 7 days in an osteogenic medium consisting of a low-glucose DMEM supplemented with 1% pen/strep, 10% FBS, 1% ascorbic acid (5 µg mL^{-1}; Merck), and 100 mM β-glycerol phosphate (Merck). The osteogenic medium was chosen to enable comparison with previous works. FBS was employed instead of human serum, which may be more clinically relevant because it is the standard for HOb culturing and easily allows distinguishing between the human proteins produced by the cells and the bovine proteins adsorbed onto the surface. Cell culture was maintained at 37°C in a humidified atmosphere (95%) with 5% CO_2. The cell culture medium was refreshed every three days.

6.2.3. Protein extraction

At each time point (n = 4 consisting of a pool of 3 discs), cells were washed four times with phosphate-buffered saline (PBS; Merck) and lysed with cell lysis buffer (CLB). The CLB consisted of 2M thiourea, 7M urea, 4% CHAPS, 200 mM dithiothreitol (DTT). All reagents were purchased from Merck. Then, the samples were incubated in CLB under agitation (280 rpm) for 30 min at room temperature. The lysate was collected and centrifuged (13 000 rpm, 4°C, 30 min). The supernatant was recovered and frozen at -80°C until further analysis.

6.2.4. Protein identification and statistical analysis

For protein identification, approximately 200 ng of the sample were directly loaded onto an Evosep ONE (Evosep, Odense C, Denmark) chromatograph and acquired in a hybrid trapped ion mobility spectrometry – quadrupole time of flight mass spectrometer (timsTOF Pro with PASEF, Bruker Daltonics, Billerica, MA, USA). Each sample was analyzed in quadruplicate and the obtained results were processed with MaxQuant (http://maxquant.org/) and Perseus software platform (https://www.maxquant.org/perseus/) software. A student's t-test was conducted to determine which proteins were differentially expressed on MT1.5Mg in relation to MT. Protein expression was considered statistically significant when $p \leq 0.05$, and the ratio difference was higher than 1.5 in either direction (under or overexpressed).

6.2.5. Protein functional classification and pathway analysis

The functional classification of the statistically significant proteins was performed employing PANTHER (http://www.pantherdb.org/), DAVID (https://david.ncifcrf.gov/), and UniProt (https://www.uniprot.org/).

The canonical pathways analysis, Upstream Regulator Analysis, and Molecule Activity Prediction (MAP) were made with QIAGEN Ingenuity® Pathway Analysis (QIAGEN IPA®, Hilden, Germany) software. In IPA®, the right-tailed Fisher's exact test was employed to calculate statistical differences. Differences in the expression of molecules, proteins, and pathways were significant when $p < 0.05$ (-log(p-value) > 1.3).

Data analysis focused on proteins and pathways associated with osteoblast metabolism and maturation.

6.3. Results

6.3.1. Functional classification with PANTHER

A total of 2545 proteins were identified on both MT and MT1.5Mg. The comparison between MT and MT1.5Mg determined that HOb seeded on MT1.5Mg differentially expressed 144 proteins after 1 day and 180 and 44 proteins after 3 and 7 days, respectively (**Supplementary Tables 6.1-6.3**). The PANTHER analysis of the biological functions revealed that MT1.5Mg regulated the expression of proteins associated with the cellular, metabolic, reproductive, and developmental processes, biological adhesion, signaling, response to stimulus, biological regulation, and localization (**Figure 6.2**).

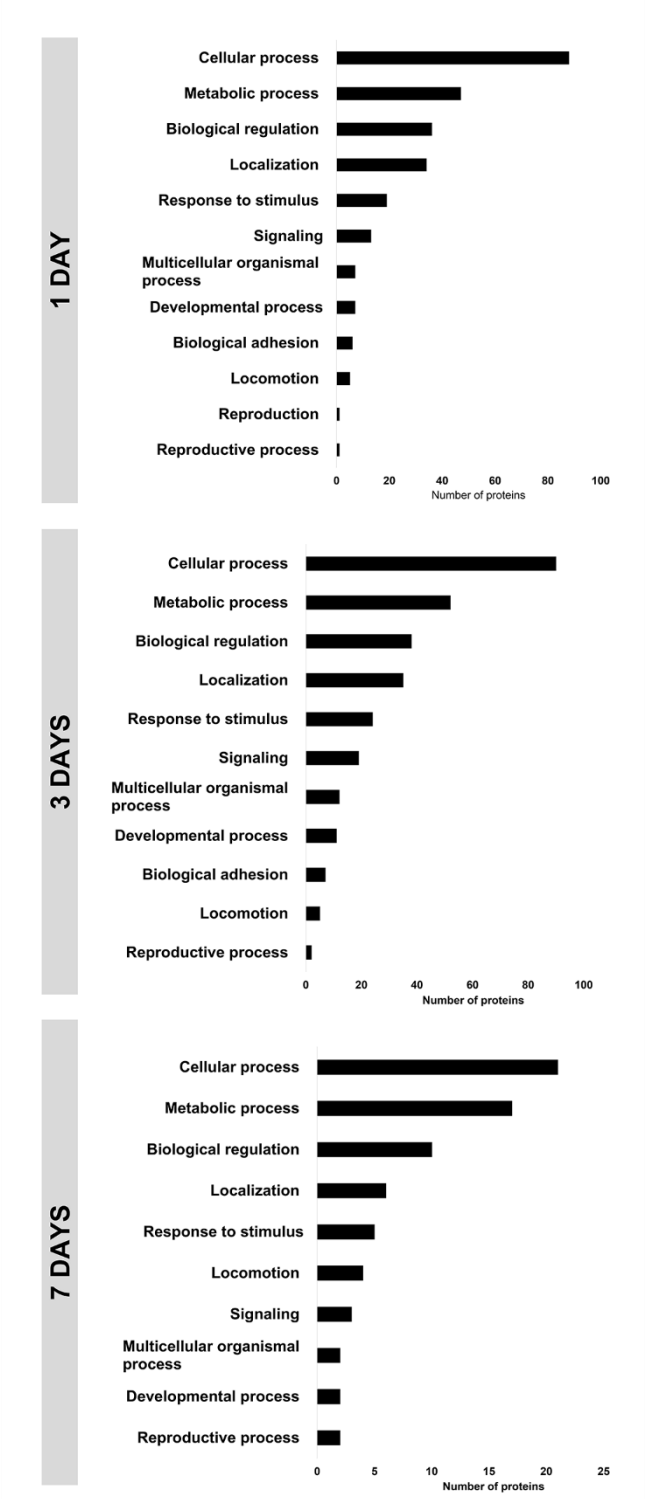

Figure 6.2. Biological processes of HOb cells regulated by MT1.5Mg at 1, 3, and 7 days.

Regarding protein class analysis, the proteins could be classified into 19 groups (**Figure 6.3**). The most dominant protein class was the metabolite interconversion enzyme for all time points. Other classes such as membrane traffic protein, nucleic acid metabolism, protein-binding activity modulator, cytoskeletal protein, cell adhesion protein, and extracellular matrix protein were also detected.

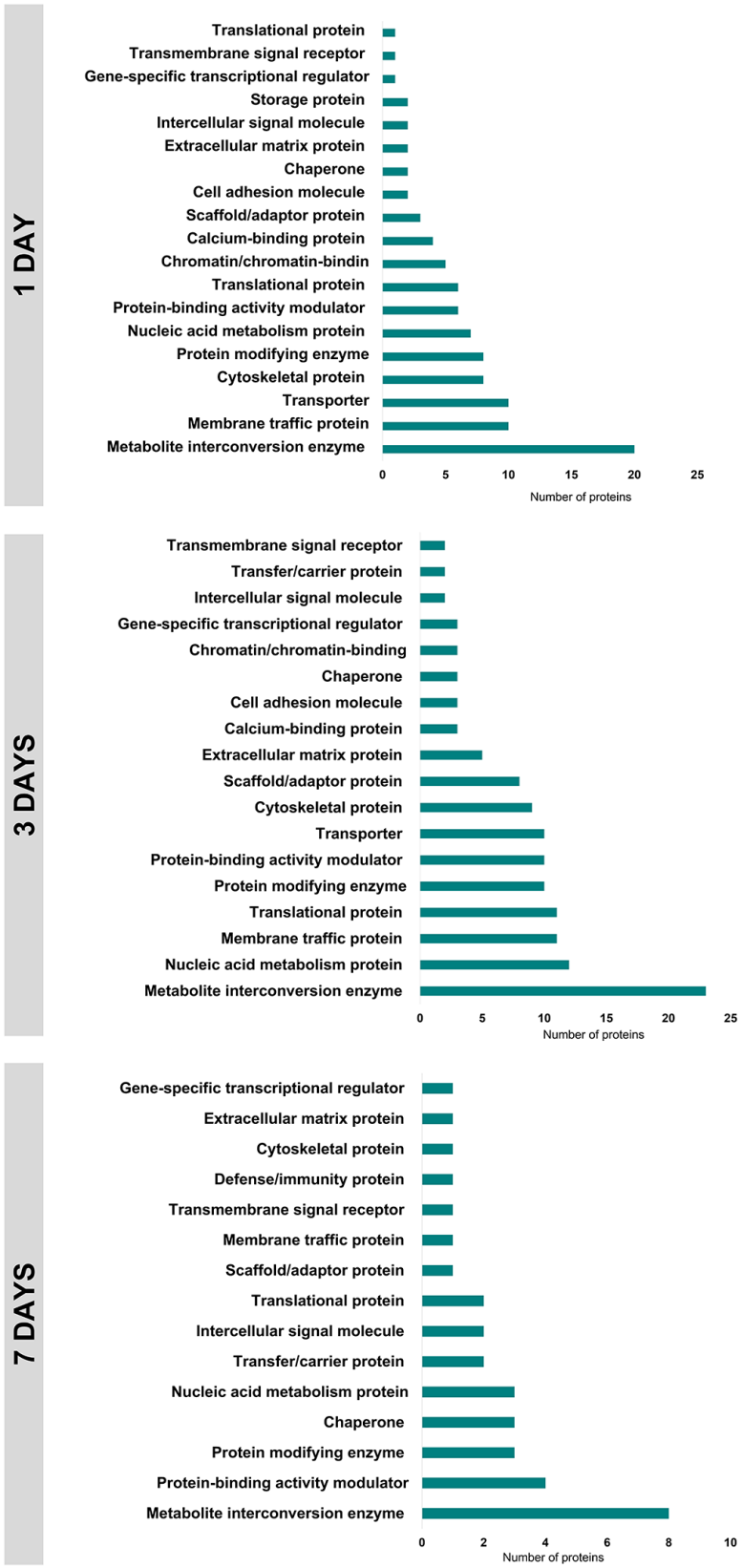

Figure 6.3. Protein classes associated with the proteins differentially expressed by Hob cells seeded onto MT1.5Mg at 1, 3, and 7 days.

6.3.2. IPA ANALYSIS

6.3.2.1. *Canonical pathway analysis*

The IPA analysis determined that MT1.5Mg mainly regulated the expression of pathways associated with osteogenesis, cell adhesion, and oxidative stress.

In what concerns osteogenesis, 21 pathways were significantly regulated by MT1.5Mg (**Figure 6.4A**). At 1 day, MT1.5Mg had effects on all detected pathways, except ascorbate recycling, fibroblast growth factor (FGF) signaling, platelet-derived growth factor (PDGF) signaling, growth hormone signaling, and JAK/STAT. Regulation of eukaryotic initiation factor 4F (eIF4) and p70S6K (-log(*p*-value) = 5.87), paxillin signaling (3.31), mechanistic target of rapamycin (mTOR) (3.53), insulin receptor signaling (2.93), and insulin growth factor (IGF)-1 signaling (2.45) were the most affected by MT1.5Mg in this time point. After 3 days, all the pathways, except for insulin secretion, macropinocytosis signaling, phospholipase C signaling, and phosphoinositide 3-kinase/protein kinase B (PI3K/AKT), were significantly regulated by MT1.5Mg. The effects of the material were more evident on eukaryotic initiation factor 2 (EIF2) (5.08), mTOR (2.93), platelet glycoprotein VI (GP6), and 14-3-3 signaling (1.80), and IGF-1 signaling (1.78). At 7 days, only EIF2 signaling (3.09), mTOR (2.14), regulation of eIF4 and p70S6K signaling (2.34), and IGF-1 signaling (1.55) presented statistically significant differences in their expression.

When considering cell adhesion, MT1.5Mg regulated 16 pathways (**Figure 6.4B**). After 1 day, all pathways associated with cell adhesion were found to be significantly regulated by MT1.5Mg, except for Gαq and sphingosine-1-phosphate signaling. At this time point, the effect of the material was more evident on pathways associated with actin arrangement (regulation of actin, actin cytoskeleton signaling, actin nucleation) with values of -log(*p*-value) of 2.44 to 3.17. p21-activated kinase (PAK) signaling (4.10) and tight junction signaling (3.14) were also two of the most affected pathways. After 3 days, the material did not affect five pathways (CXCR4 signaling, Gα12/13, integrin-linked kinase (ILK), RAC, and tight junction signaling). Pathways associated with integrin signaling (3.63), paxillin signaling (3.31), regulation of actin (2.72), and actin cytoskeleton signaling (2.72) were the most regulated by MT1.5Mg at this time point. After 7 days, the effects on adhesion subside, and only ephrin receptor signaling (2.20) showed regulation by MT1.5Mg.

Four pathways associated with oxidative stress were regulated by MT1.5Mg (**Figure 6.4C**). At 1 day, the material significantly held oxidative phosphorylation (2.36). At the same time, pathways associated with anti-oxidant action of vitamin C (1.99) and vitamin C transport (1.88) and

superoxide radicals degradation (1.82) presented significant differences at 3 and 7 days, respectively.

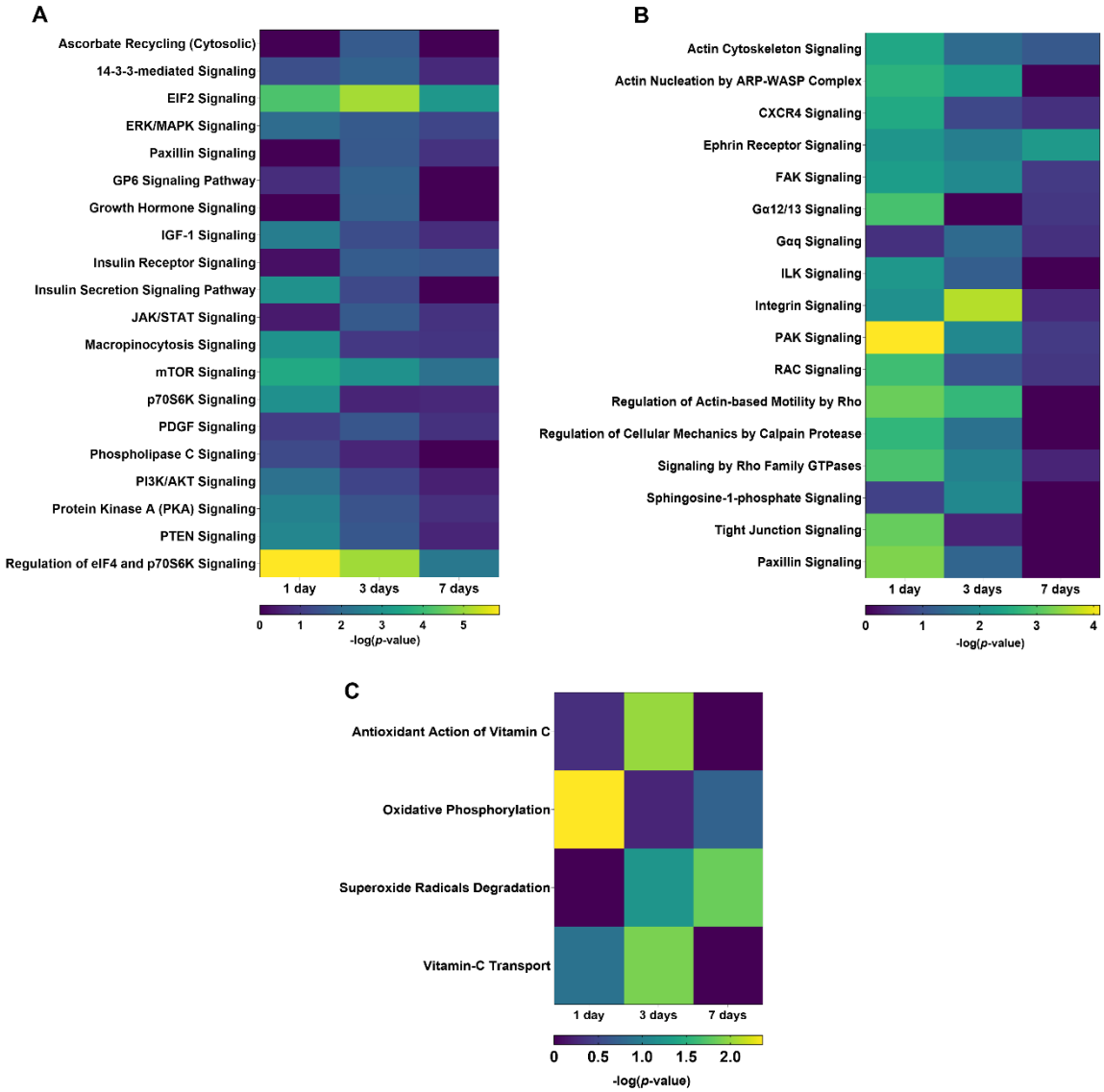

Figure 6.4. Heat map of enriched canonical pathways (A) osteogenesis, (B) cell-matrix and focal adhesion, and (C) oxidative stress expressed by HOb seeded onto MT1.5Mg at 1, 3, and 7 days. Pathways were considered significantly regulated when -log(*p*-value) > 1.3.

6.3.2.2. *Upstream regulator analysis and MAP*

The upstream regulator analysis was used to calculate the upstream molecules that may cause the observed effects on protein expression. IPA® predicted 1202 molecules might explain the differences observed in protein expression (**Supplementary Table 6.4**). **Table 6.1** shows the top 30 regulators with functions in osteogenesis and cell adhesion.

Table 6.1. Upstream regulators determined by IPA® on MT1.5Mg. The molecules were considered significantly regulated when -log(*p*-value) > 1.3.

Upstream regulators	1 day	3 days	7 days
TGFB1	5.62	3.26	2.47
Sirolimus	5.17	0.96	2.19
Torin1	2.22	3.11	4.59
OSM	4.22	1.82	1.61
RICTOR	4.05	2.08	0.00
Collagen(s)	3.74	2.26	0.00
IGF1	3.38	1.66	0.00
CTNNB1	1.61	3.39	0.00
Cdc42	1.93	3.04	0.00
MAPK1	2.48	0.00	0.00
COL5A1	2.83	2.54	0.00
Cadherin	2.20	0.00	0.00
MAP4K4	2.18	0.00	0.00
TGFB2	2.19	0.00	0.00
WNT1	2.00	0.00	0.00
IGF1R	1.95	0.00	0.00
MAP4K3	1.90	0.00	0.00
PTEN	1.83	2.76	0.00
CTNNB1	1.61	3.39	0.00
Collagen type V	1.51	0.00	0.00
TGFB3	1.40	0.00	0.00
FGF2	1.39	0.00	0.00
Alpha catenin	1.39	0.00	0.00
Collagen type III	1.36	0.00	0.00
FGF10	1.33	0.00	0.00
IGF2	0.00	1.93	1.36
MAPK	0.00	0.00	1.72
ERK1/2	0.00	1.43	1.64
Akt	0.00	1.91	1.40
CREB1	0.00	2.64	0.00

The MAP hypothesized the up or down-regulation of canonical pathways and sub-networks by selecting a molecule of interest, simulating directional consequences of downstream molecules, and inferring the upstream activity in the pathway. Two molecules obtained from the upstream regulator analysis (TGFB1 and IGF1) were selected as main regulators of with molecules obtained from that analysis and the proteins found regulated by MT1.5Mg that allowed their prediction. This selection was based on their prominent roles in osteogenesis and cell adhesion. **Figure 6.5** shows the network analysis obtained with the interactions between the molecules, and the communal activity predicted was the binding of osteoblasts.

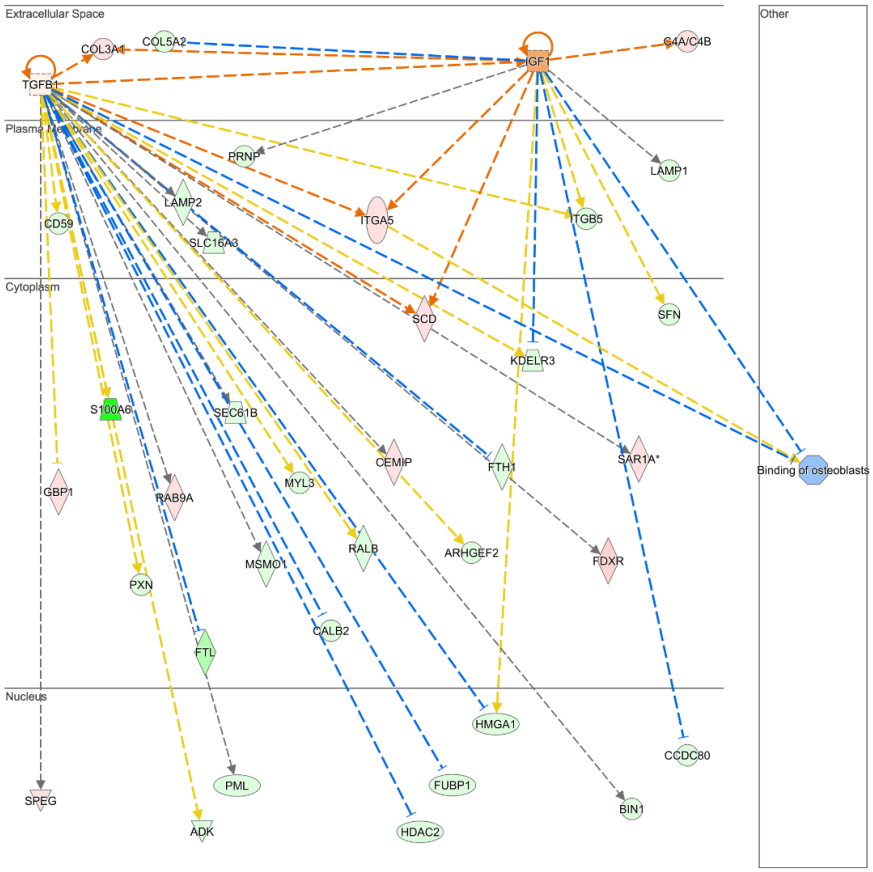

Figure 6.5. Network analysis from IPA® for associations among upstream regulators associated with TFGB1, IGF1, binding of osteoblasts activity and the relationships with proteins obtained from HOb seeded on MT1.5Mg after 1 day of assay that justify the predictions. Upregulated proteins are found in red, while downregulated are found in green. Orange lines indicate *predicted activation*; blue lines indicate *predicted inhibition*; yellow lines indicate *findings inconsistent with state of downstream molecule*; grey lines indicate *effect not predicted*.

The MAP was also be employed to predict the activity of specific molecules in the protein expression observed. RICTOR was selected based on the previously-mentioned upstream regulator analysis and for being an mTOR complex subunit responsible for cell proliferation and survival [13]. MAP predicted that ten proteins (ATP6P1, COX6B1, NDUFA9, PSME2, PXN, RPS10, RPS29, UQCRB, ATP5PF) detected on MT1.5Mg at 1 day upregulated the activity of RICTOR (**Figure 6.6**).

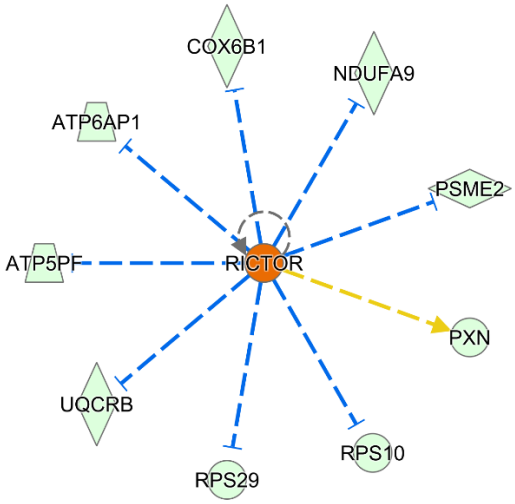

Figure 6.6. RICTOR predicted activity from IPA® on HOb seeded on MT1.5Mg at 1 day. Molecules with *predicted activation* are found in orange, while downregulated proteins are found in green. Blue lines indicate *predicted inhibition*; yellow lines indicate *findings inconsistent with state of downstream molecule*; grey lines indicate *effect not predicted*.

6.3.2.3. *Protein and function association: IPA and DAVID analysis*

Proteins regulated by MT1.5Mg were associated with osteogenesis, cell adhesion, and oxidative stress functions (**Table 6.2**). Each function corresponded to a group of pathways identified by the databases previously mentioned. The pathways considered were the following: Wnt, ERK/MAPK, Ras, PI3K/AKT, collagen, insulin and growth hormone signaling, mTOR for osteogenesis; cell-matrix adhesion, cytoskeletal regulation, integrin and cadherin signaling for cell-matrix and focal adhesion; and antioxidant action, oxidative phosphorylation, and superoxide radicals degradation for oxidative stress.

In what concerns osteogenesis, after 1 day, MT1.5Mg induced the expression of six proteins (PLCB4, RAB9A, RAB35, EIF3M, CO3A1, and CEMIP), while seven (PSME2, CSK22, CUL1, PAIP1, 2A5D, RALB, and CO5A2) were downregulated. After 3 days, MT1.5Mg upregulated MK01, IBP3, ST38L, STK24, and PP1B, and downregulated GBB1, PLCG1, CO2A1, and CO4A2. At 7 days of

assay, no proteins were upregulated in MT1.5Mg concerning MT, but MP2K2 was significantly less expressed.

For cell-matrix and focal adhesion, after 1 day of culture, the cells seeded on MT1.5Mg overexpressed seven proteins (PI4KA, ITA5, LPXN, ADSV, VNN2, MYO5A, and CDC42) and under-expressed 1433S, ARHG2, CAD13, ITB5, PAXI, MYL3, RALB, and YKT6. At 3 days *in vitro*, MT1.5Mg induced the expression of MXRA8, PCDGL, MYLK, PTN1, ST38L, STK24, MA7D1, and MYO9B. On the other hand, seven proteins (LEG3, TES, FBLI1, LTBP2, VASP, RHOG, and ITA6) were downregulated. After 7 days, no proteins were found upregulated, while LTBP2 and RAB10 were found downregulated.

In oxidative stress responses, no proteins were found upregulated at any time point. However, MT1.5Mg led to the downregulation of two proteins (PRDX2 and GPX1) after 1 day, three proteins (GSTO1, SODM, and UCRI) at 3 days, and one protein (CATA) after 7 days of assay.

Table 6.2. Proteins differentially expressed on MT1.5Mg with functions in osteogenesis, cell-matrix and focal adhesion, and oxidative stress. Proteins with $p \leq 0.05$ and a ratio higher than 1.5 in either direction (UP: increased and DOWN: reduced) were considered significant.

Function		1 day	3 days	7 days
Osteogenesis	**UP**	PLCB4, RAB9A, RAB35, EIF3M, CO3A1, CEMIP	MK01, IBP3, ST38L, STK24, PP1B	-
	DOWN	PSME2, CSK22, CUL1, PAIP1, 2A5D, RALB, CO5A2	PLCG1, CO2A1, CO4A2	MP2K2
Cell-matrix and focal adhesion	**UP**	PI4KA, ITA5, CDC42, LPXN, ADSV, VNN2	MXRA8, PCDGL, MYLK, PTN1, ST38L, STK24, MA7D1, MYO9B	-
	DOWN	1433S, ARHG2, CAD13, ITB5, PAXI, MYL3, RALB, YKT6	LEG3, TES, FBLI1, LTBP2, VASP, ITA6, RHOG	RAB10, LTBP2
Oxidative stress	**UP**	-	-	-
	DOWN	PRDX2, GPX1	GSTO1, SODM, UCRI	CATA

6.4. DISCUSSION

The description of proteomic profiles of cells presents an alternative to overcome the difficulties of traditional methods of biological characterization. In this work, we characterized the proteome of HOb exposed to sol-gel coatings doped with Mg. Mg is involved in many physiological processes, from metabolic reactions to the cell membrane, DNA, and protein structure maintenance. Martínez-Sánchez *et al.* [14] demonstrated that Mg extracts affected the expression of proteins associated with cell attachment, growth, differentiation, and survival on human umbilical cord perivascular (HUCPV) cells undergoing chondrogenesis. Thus, it was unsurprising to find that MT1.5Mg mainly regulated metabolic reactions, nucleic acid metabolism, cytoskeleton, binding, and transport functions.

Bone regeneration is a well-orchestrated process that involves numerous cell types and intracellular and extracellular molecular signaling pathways [15]. PI3K/AKT has been described as the central nexus between the signaling pathways responsible for osteoblast differentiation and homeostasis [16]. Mg is known for activating PI3K/AKT on rat calvarial osteoblasts [17]. MT1.5Mg affected PI3K/AKT expression and other associated paths such as PTEN signaling, regulation of eIF4 and p70S6K, and p70S6K signaling. PI3K/AKT is a known controller of many osteogenic markers, such as collagen [18]. The expression of collagen alpha-1 (III) (CO3A1), collagen alpha-2(V) (CO5A2), collagen alpha-1 (II) (CO2A1), and collagen alpha-2 (IV) (CO4A2) was significantly regulated by MT1.5Mg. In bone, the major collagenous components are collagen type I, III, V, and X. CO3A1 is essential for early osteoblastic growth and the commitment of these cells to differentiation [19], and was upregulated at 1 day *in vitro*.

The IPA analysis also showed that MT1.5Mg regulated that mTOR at all time points, and MAP predicted RICTOR upregulation, which is a unique regulator of mTOR. This pathway is associated with PI3K/AKT, and its activation via the p70S6K phosphorylation and eIF4 translation is a key step in initiating protein synthesis and cell growth [20]. In bone, the mediation of Wnt and IGF-1 signaling by mTOR is essential in osteoblast maturation and differentiation during bone formation [21,22], and RICTOR/mTOR loss in primary osteoblasts significantly decreases bone mass [23]. Liu *et al.* [24] described mTOR enhancement the by Mg, while Cappadone *et al.* [25] showed that Mg depletion inhibits this pathway and cell proliferation. Curiously, the eukaryotic initiation factor 3 (eIF3; EIF3M) was found upregulated at 1 day. Holz *et al.* [26] described this protein as the mediator between mTOR/Raptor, eIF4, and S6K phosphorylation and acts as a scaffold in response to stimuli that promote efficient protein synthesis.

Moreover, the pathway analysis revealed that MT1.5Mg had a significant effect on IGF-1 signaling, insulin receptor, and insulin secretion signaling. Insulin and IGF-1 are two important hormones that regulate metabolism and growth. These ligands activate insulin and IGF-1 receptors, respectively, which will activate AKT and MAPK and regulate proliferation, differentiation, apoptosis, and metabolism [27]. IGF-1 is the most abundant growth factor in the bone matrix and regulates new bone formation by acting as a differentiation factor for osteoblasts [22]. At 3 days *in vitro*, insulin-like growth factor binding protein-3 (IGFBP3) was found significantly upregulated in MT1.5Mg. IGFBP3 is the third most abundant IGFBP found in osteoblasts and binds with IGF-1. In bone, the binding of IGFBP3 to IGF-1 leads to an increment of bone formation [22]. It has been shown that the local delivery of IGFBP3 by chitosan gold nanoparticles improves bone healing *in vivo* and enhances bone morphogenic protein (BMP) 2/7 and osteopontin (OPN) expression [28]. In addition, IGFBP3 is associated with transforming growth factor (TGF)-β, which was predicted as upregulated by MAP. TGF-β is a superfamily of ligands vital for cell growth, differentiation, apoptosis, cell motility and cell adhesion and IGFBP3 has been associated with its latency and amplification cascade [29]. TGF-β regulates several cell types directly involved in bone remodeling and fracture healing, and MT1.5Mg has been shown to upregulate its gene expression after 7 days *in vitro* [6]. Interestingly, JAK/STAT was regulated by MT1.5Mg. STAT is a transcriptional promoter of IGF-1 and is vital for osteoblast proliferation and differentiation through the growth hormone signaling [30], which MT1.5Mg also regulated. On the other hand, the growth hormone stimulates the production and secretion of IGF-1 and has well-described roles in incrementing bone density and length [31].

Mitogen-activated protein kinases (MAPKs) are a set of signal transducers of external stimuli that regulate cell proliferation and differentiation, and apoptosis [15]. Osteoblasts essentially express two isoforms of canonical extracellular signal-regulated kinases (ERK) MAPKs (MAPK1 and MAPK3), and the ERK/MAPK pathway is known for positively regulating osteoblast differentiation and bone formation [31]. Wang *et al.* [32] reported that Mg enhanced MC3T3-E1 cell proliferation by incrementing ERK phosphorylation. Additionally, stem cell differentiation can be boosted by Mg via the selective activation of ERK/MAPK and consequent upregulation of cAMP-responsive element-binding protein 1 (CREB1) and osterix (SP7) [33]. MT1.5Mg regulated ERK/MAPK after 1 and 3 days. MAPK1 (MK01) was enhanced after 3 days. Upon ERK/MAPK activation, MAPK1 phosphorylates RUNX2 to increase its transcriptional activity during early osteoblast differentiation [34]. Cerqueira *et al.* [6] demonstrated that MT1.5Mg induces the expression of RUNX2 and SP7 in osteoblasts, which can be explained by the regulation of ERK/MAPK here verified. With these results, we can observe that MT1.5Mg regulates

osteogenesis through multiple cellular processes essential for osteoblast differentiation and maturation.

Biomaterials for bone tissue regeneration need to act as a substrate for cell adhesion since it prompts signals that regulate differentiation, migration, and survival. Responsible for primary cell adhesion, integrins link the intracellular actin and extracellular matrix (ECM) and regulate cellular responses and cytoskeleton arrangement [35]. Mg is well known for its effects on cytoskeleton arrangement, and MT1.5Mg induces protruding lamellipodia and filopodia on MC3T3-E1 osteoblasts [6]. Here, MT1.5Mg regulated several pathways associated with the cytoskeleton, such as the regulation of actin-based motility by Rho. Belonging to the Rho GTPase family, the cell division control protein 42 homolog (Cdc42) was upregulated by MT1.5Mg. This protein is active in the lamellipodial region of cells and is the main contributor to filopodium formation [36]. In addition, PAK signaling presented effects by MT1.5Mg at 1 and 3 days. PAKs are effectors of Cdc42, and the action of these proteins promotes polymerized actin structures formation (*i.e.*, lamellipodia and filopodia), integrin-based adhesion turnover, the bond to the ECM, and cell motility and adhesion [37]. PAKs also control myosins, actin-based motor proteins that allow the cytoskeletal regulation and contraction and cellular force maintenance [38]. MT1.5Mg upregulated the expression of myosin-Va (MYO5A), myosin-IXb (MYO9B), and myosin light chain kinase (MYLK) and myosin light chain 3 (MYL3) was less expressed. These motor proteins need ATP to fuel their movement during the conformational changes. Studies demonstrated that Mg is an essential cofactor for ATP binding and hydrolysis in myosins. Recently, it was proven that Mg^{2+} modulates the motor activity of five myosins, including MYO5A and MYO9B [39], while Omidi *et al.* [40] showed that pure Mg materials affect myosins expression.

Regarding integrins, IPA software identified variations on integrin and ILK signaling expression. Integrins are membrane-associated adhesion receptors thought to be responsible for mediating cell-biomaterial interactions, and the effects of Mg on them are thoroughly described [4]. Previously, we demonstrated that MT1.5Mg induced the integrin gene expression on MC3T3-E1 osteoblasts [6]. In this work, MT1.5Mg not only modulated integrin-β5 (ITB5), integrin-α5 (ITA5), and integrin-α6 (ITA6) but also altered vascular non-inflammatory molecule 2 (VNN2), galectin-3 (LEG3), and matrix remodeling-associated protein 8 (MXRA8). Found 47.5 times more expressed on MT.5Mg, MXRA8, also known as DICAM, suppresses osteoclastogenesis via integrin-αVβ3 pathway attenuation and p38 MAPK inhibition [41] and promotes cell adhesion through specific binding to integrin-αvβ3 [42]. Integrin signaling is also one of the most potent inducers of focal adhesion (FA) formation. FAs are protein assemblies essential for extracellular signals transduction into intracellular responses, acting as a bridge between integrins and actin

[43,44]. MT1.5Mg affected focal adhesion kinase (FAK) signaling by downregulating paxillin (PAXI) and leupaxin (LPXN) upregulation. These major components of FA are homologous and responsible for FAK binding to integrins [45]. While PAXI and LPXN similarly target FA, they present distinct roles in cell adhesion and spreading [45]. These proteins' expression seems to depend on the cell lineage, and it has been proven that LPXN is responsible for cytoplasmic projections at sites of adhesion of osteoclasts [46]. So far, these proteins' action on HOb has not been described, and how Mg modulates their expression neither. With this, it was possible to learn that Mg effects on cell adhesion go beyond integrin expression and allow hypothesizing that this ion affects the whole machinery behind it.

Oxidative stress is a normal response to biomaterial implantation, and the production of reactive oxygen species (ROS) occurs naturally during normal cellular [47,48]. ROS act as a signal in many intracellular signaling pathways, and results show that MT1.5Mg regulated oxidative phosphorylation and superoxide radicals degradation. Proteins associated with the antioxidant system (PRDX2, GPX1, SODM, GTSO1, and CATA) were downregulated in the presence of MT1.5Mg. However, redox reactions are essential for cell adhesion. For example, Chiarugi *et al.* [49] demonstrated that redox signaling was crucial for FAK and MAPK phosphorylation, focal adhesion formation, and cell spreading, while Fernandes *et al.* [47] showed that ROS production increment and FAK phosphorylation accompanied the early stages of cell adhesion (30 min to 2h). On the other hand, Fiaschi *et al.* [50] proved that ROS produced by integrins are essential for actin fibers formation during cell spreading. Thus, the downregulation of the antioxidant system can be a consequence of cell adhesion, especially considering that the expression of oxidant proteins remained unaltered.

These results show the potential of proteomics for biomaterial characterization and how Mg in a release vehicle affects cellular responses. The effects of Mg on osteoblasts are complex, regulating several pathways associated with osteogenesis, cell-matrix and focal adhesion, and oxidative stress, showing that its effects on these processes come from an overall effect on the cell rather than an effect on individual processes.

6.5. Conclusion

This work aimed at studying Mg-enriched coating effects on the proteome of HOb at 1, 3, and 7 days *in vitro* by applying mass spectrometry. The results showed that MT1.5Mg mainly regulated pathways of early osteoblast differentiation (PI3/AKT, mTOR, ERK/MAPK), insulin metabolism (IGF-1, insulin secretion and receptor signaling, JAK/STAT), cell adhesion (integrin and FAK signaling, actin cytoskeleton regulation), and oxidative stress (oxidative phosphorylation,

superoxide radicals degradation). With this, it is possible to conclude that proteomics presents an excellent potential for biomaterial characterization, and Mg effects on the cell are rather complex, affecting the whole cellular machinery. Osteogenesis and cell adhesion modulation by Mg seem to come from an overall effect rather than on single processes. More studies applying proteomics in the biomaterials field are needed to better comprehend the *in vitro* responses induced by the materials and improve their design.

6.6. Acknowledgments

The work was supported by MINECO [MAT2017-86043-R; RTC-2017-6147-1], Generalitat Valenciana [GRISOLIAP/2018/091, APOSTD/2020/036, PROMETEO/2020/069], Universitat Jaume I under [UJI-B2017-37, GACUJI/2021/14], and the University of the Basque Country under [GIU18/189]. The authors would like to thank Raquel Oliver, Jose Ortega, and Iraide Escobés for their valuable technical assistance, and Antonio Coso (GMI-Ilerimplant) for producing the titanium discs.

6.7. References

. O'Neill, E., Awale, G., Daneshmandi, L., Umerah, O. & Lo, K. W. H. The roles of ions on bone regeneration. *Drug Discovery Today* vol. 23 879–890 (2018).

2. Yoshizawa, S., Brown, A., Barchowsky, A. & Sfeir, C. Magnesium ion stimulation of bone marrow stromal cells enhances osteogenic activity, simulating the effect of magnesium alloy degradation. *Acta Biomater.* **10**, 2834–2842 (2014).

3. Kim, H.-K. *et al.* Comprehensive study on the roles of released ions from biodegradable Mg-5 wt% Ca-1 wt% Zn alloy in bone regeneration. *J. Tissue Eng. Regen. Med.* **11**, 2710–2724 (2017).

4. Zreiqat, H. *et al.* Mechanisms of magnesium-stimulated adhesion of osteoblastic cells to commonly used orthopaedic implants. *J. Biomed. Mater. Res.* **62**, 175–184 (2002).

5. Hornberger, H., Virtanen, S. & Boccaccini, A. R. Biomedical coatings on magnesium alloys - A review. *Acta Biomater.* **8**, 2442–2455 (2012).

6. Cerqueira, A. *et al.* Characterization of magnesium doped sol-gel biomaterial for bone tissue regeneration: the effect of Mg ion in protein adsorption. *Mater. Sci. Eng. C* **125**, 112114 (2021).

7. Hulsart-Billström, G. *et al.* A surprisingly poor correlation between in vitro and in vivo

testing of biomaterials for bone regeneration: Results of a multicentre analysis. *Eur. Cells Mater.* **31**, 312–322 (2016).

8. Groen, N. *et al.* Stepping into the omics era: Opportunities and challenges for biomaterials science and engineering. *Acta Biomater.* **34**, 133–142 (2016).

9. Othman, Z., Cillero Pastor, B., van Rijt, S. & Habibovic, P. Understanding interactions between biomaterials and biological systems using proteomics. *Biomaterials* **167**, 191–204 (2018).

10. Kim, C. S. *et al.* Proteomic analysis of the biological response of MG63 osteoblast-like cells to titanium implants. *Odontology* **102**, 241–248 (2014).

11. Othman, Z. *et al.* Comparative proteomic analysis of human mesenchymal stromal cell behavior on calcium phosphate ceramics with different osteoinductive potential. *Mater. Today Bio* **7**, 100066 (2020).

12. Zhang, Z., Wang, J. & Lü, X. An integrated study of natural hydroxyapatite-induced osteogenic differentiation of mesenchymal stem cells using transcriptomics, proteomics and microRNA analyses. *Biomed. Mater.* **9**, (2014).

13. Treins, C., Warne, P. H., Magnuson, M. A., Pende, M. & Downward, J. Rictor is a novel target of p70 S6 kinase-1. *Oncogene* **29**, 1003–1016 (2010).

14. Martínez Sánchez, A. H. *et al.* Proteome analysis of human mesenchymal stem cells undergoing chondrogenesis when exposed to the products of various magnesium-based materials degradation. *Bioact. Mater.* **4**, 168–188 (2019).

15. Majidinia, M., Sadeghpour, A. & Yousefi, B. The roles of signaling pathways in bone repair and regeneration. *J. Cell. Physiol.* **233**, 2937–2948 (2018).

16. Grigoriadis, I. M. M. A. E., Lam, E. W. F., Price, J. S. & Sunters, A. A specific role for phosphoinositide 3-kinase and AKT in osteoblasts? *Front. Endocrinol. (Lausanne).* **3**, 1–8 (2012).

17. Wang, J. *et al.* Magnesium Ions Promote the Biological Behaviour of Rat Calvarial Osteoblasts by Activating the PI3K/Akt Signalling Pathway. *Biol. Trace Elem. Res.* **179**, 284–293 (2017).

18. Zhang, J. *et al.* Exosomes/tricalcium phosphate combination scaffolds can enhance bone regeneration by activating the PI3K/Akt signaling pathway. *Stem Cell Res. Ther.* **7**,

1–14 (2016).

19. Maehata, Y., Lee, M.-C. & Hata, R.-I. Roles of Collagen Molecules in Growth and Differentiation of Human Osteoblasts. *J. Oral Biosci.* **51**, 72–80 (2009).

20. Chen, J. & Long, F. mTOR signaling in skeletal development and disease. *Bone Res.* **6**, 1–6 (2018).

21. Karner, C. M., Lee, S.-Y. & Long, F. BMP Induces Osteoblast Differentiation through both Smad4 and mTORC1 Signaling. *Mol. Cell. Biol.* **37**, e00253-16 (2017).

22. Xian, L. *et al.* Matrix IGF-1 regulates bone mass by activation of mTOR in mesenchymal stem cells. *Nat. Med.* **18**, 1095 (2012).

23. Liu, D. mei *et al.* Rictor/mTORC2 loss in osteoblasts impairs bone mass and strength. *Bone* **90**, 50–58 (2016).

24. Liu, Y. *et al.* Magnesium supplementation enhances mTOR signalling to facilitate myogenic differentiation and improve aged muscle performance. *Bone* **146**, 115886 (2021).

25. Cappadone, C. *et al.* Assessment and Imaging of Intracellular Magnesium in SaOS-2 Osteosarcoma Cells and Its Role in Proliferation. *Nutrients* **13**, (2021).

26. Holz, M. K., Ballif, B. A., Gygi, S. P. & Blenis, J. mTOR and S6K1 Mediate Assembly of the Translation Preinitiation Complex through Dynamic Protein Interchange and Ordered Phosphorylation Events. *Cell* **123**, 569–580 (2005).

27. Zhang, W. *et al.* Effects of insulin and insulin-like growth factor 1 on osteoblast proliferation and differentiation: differential signalling via Akt and ERK. *Cell Biochem. Funct.* **30**, 297–302 (2012).

28. Bhattarai, G., Lee, Y. H., Lee, M. H., Park, I. S. & Yi, H. K. Insulin-like growth factor binding protein-3 affects osteogenic efficacy on dental implants in rat mandible. *Mater. Sci. Eng. C* **55**, 490–496 (2015).

29. Danielpour, D. & Song, K. Cross-talk between IGF-I and TGF-β signaling pathways. *Cytokine Growth Factor Rev.* **17**, 59–74 (2006).

30. Sanpaolo, E. R., Rotondo, C., Cici, D., Corrado, A. & Cantatore, F. P. JAK/STAT pathway and molecular mechanism in bone remodeling. *Mol. Biol. Rep.* **47**, 9087 (2020).

31. Dehkhoda, F., Lee, C. M. M., Medina, J. & Brooks, A. J. The Growth Hormone Receptor: Mechanism of Receptor Activation, Cell Signaling, and Physiological Aspects. *Front. Endocrinol. (Lausanne).* **0**, 35 (2018).

32. Kim, J. *et al.* The ERK MAPK Pathway Is Essential for Skeletal Development and Homeostasis. *Int. J. Mol. Sci.* **20**, 1803 (2019).

33. Wang, Y. *et al.* Unraveling the osteogenesis of magnesium by the activity of osteoblasts in vitro. *J. Mater. Chem. B* **6**, 6615–6621 (2018).

34. Zhou, H., Liang, B., Jiang, H., Deng, Z. & Yu, K. Magnesium-based biomaterials as emerging agents for bone repair and regeneration: from mechanism to application. *J. Magnes. Alloy.* **9**, 779–804 (2021).

35. Greenblatt, M. B., Shim, J.-H. & Glimcher, L. H. Mitogen-Activated Protein Kinase Pathways in Osteoblasts. *Annu. Rev. Cell Dev. Biol.* **29**, 63–79 (2013).

36. Khalili, A. A. & Ahmad, M. R. A review of cell adhesion studies for biomedical and biological applications. *Int. J. Mol. Sci.* **16**, 18149–18184 (2015).

37. Ridley, A. J. Rho GTPase signalling in cell migration. *Curr. Opin. Cell Biol.* **36**, 103–112 (2015).

38. Rane, C. K. & Minden, A. P21 activated kinases. *Small GTPases* **5**, e28003 (2014).

39. Anselme, K., Ploux, L. & Ponche, A. Cell/Material Interfaces: Influence of Surface Chemistry and Surface Topography on Cell Adhesion. *J. Adhes. Sci. Technol.* **24**, 831–852 (2012).

40. Swenson, A. M. *et al.* Magnesium Modulates Actin Binding and ADP Release in Myosin Motors. *J. Biol. Chem.* **289**, 23977–23991 (2014).

41. Omidi, M. *et al.* Investigation of the impact of magnesium: Versus titanium implants on protein composition in osteoblast by label free quantification. *Metallomics* **12**, 916–934 (2020).

42. Jung, Y.-K. *et al.* DICAM inhibits osteoclast differentiation through attenuation of the integrin αVβ3 pathway. *J. Bone Miner. Res.* **27**, 2024–2034 (2012).

43. Jung, Y.-K. *et al.* DICAM, a novel dual immunoglobulin domain containing cell adhesion molecule interacts with αvβ3 integrin. *J. Cell. Physiol.* **216**, 603–614 (2008).

44. López-Colomé, A. M., Lee-Rivera, I., Benavides-Hidalgo, R. & López, E. Paxillin: A crossroad in pathological cell migration. *J. Hematol. Oncol.* **10**, 1–15 (2017).

45. Bauer, M. S. *et al.* Structural and mechanistic insights into mechanoactivation of focal adhesion kinase. *Proc. Natl. Acad. Sci. U. S. A.* **116**, 6766–6774 (2019).

46. Chen, P. W. & Kroog, G. S. Leupaxin is similar to paxillin in focal adhesion targeting and tyrosine phosphorylation but has distinct roles in cell adhesion and spreading. *Cell Adhes. Migr.* **4**, 527–540 (2010).

47. Gupta, A. *et al.* Leupaxin Is a Critical Adaptor Protein in the Adhesion Zone of the Osteoclast. *J. Bone Miner. Res.* **18**, 669–685 (2003).

48. Fernandes, G. V. O. *et al.* Osteoblast adhesion dynamics: A possible role for ROS and LMW-PTP. *J. Cell. Biochem.* **115**, 1063–1069 (2014).

49. Cerqueira, A. *et al.* Evaluation of the inflammatory responses to sol–gel coatings with distinct biocompatibility levels. *J. Biomed. Mater. Res. Part A* **109**, 1539–1548 (2021).

50. Chiarugi, P. *et al.* Reactive oxygen species as essential mediators of cell adhesion: The oxidative inhibition of a FAK tyrosine phosphatase is required for cell adhesion. *J. Cell Biol.* **161**, 933–944 (2003).

51. Fiaschi, T. *et al.* Redox regulation of β-actin during integrin-mediated cell adhesion. *J. Biol. Chem.* **281**, 22983–22991 (2006).

6.8. SUPPLEMENTARY MATERIAL

Supplementary table 6.1. Progenesis comparative analysis between the proteins identified onto MT1.5Mg with respect to MT at 1 day *in vitro*. Proteins were considered differentially expressed when the ratio was higher than 1.5 in either direction and *p* value < 0.05. Proteins overexpressed in MT1.5Mg are marked in red, while those under expressed are marked in green.

Accession		Description	*p* value	MT1.5Mg *vs* MT
P06703	S10A6_HUMAN	Protein S100-A6	0.000	0.016
Q71DI3	H32_HUMAN	Histone H3.2	0.006	0.031
P02792	FRIL_HUMAN	Ferritin light chain	0.006	0.046
Q71UI9	H2AV_HUMAN	Histone H2A.V	0.036	0.086
O43583	DENR_HUMAN	Density-regulated protein	0.000	0.110
Q9H074	PAIP1_HUMAN	Polyadenylate-binding protein-interacting protein 1	0.018	0.111
Q13616	CUL1_HUMAN	Cullin-1	0.040	0.117
P11279	LAMP1_HUMAN	Lysosome-associated membrane glycoprotein 1	0.036	0.128
P46459	NSF_HUMAN	Vesicle-fusing ATPase	0.002	0.130
P60033	CD81_HUMAN	CD81 antigen	0.003	0.130
O60831	PRAF2_HUMAN	PRA1 family protein 2	0.002	0.131
P49207	RL34_HUMAN	60S ribosomal protein L34	0.002	0.138
Q9NZ01	TECR_HUMAN	Very-long-chain enoyl-CoA reductase	0.000	0.154
P04156	PRIO_HUMAN	Major prion protein	0.000	0.209
Q9Y512	SAM50_HUMAN	Sorting and assembly machinery component 50 homolog	0.020	0.210
P31947	1433S_HUMAN	14-3-3 protein sigma	0.017	0.226
P18859	ATP5J_HUMAN	ATP synthase-coupling factor 6. mitochondrial	0.014	0.244
P51572	BAP31_HUMAN	B-cell receptor-associated protein 31	0.007	0.251
P62273	RS29_HUMAN	40S ribosomal protein S29	0.008	0.262
P30520	PURA2_HUMAN	Adenylosuccinate synthetase isozyme 2	0.039	0.267
Q7L311	ARMX2_HUMAN	Armadillo repeat-containing X-linked protein 2	0.040	0.282
O15382	BCAT2_HUMAN	Branched-chain-amino-acid aminotransferase. mitochondrial	0.002	0.298

Q15006	EMC2_HUMAN	ER membrane protein complex subunit 2	0.023	0.317
P14209	CD99_HUMAN	CD99 antigen	0.045	0.317
O00499	BIN1_HUMAN	Myc box-dependent-interacting protein 1	0.039	0.330
Q9HD45	TM9S3_HUMAN	Transmembrane 9 superfamily member 3	0.001	0.335
P41208	CETN2_HUMAN	Centrin-2	0.002	0.338
Q63ZY3	KANK2_HUMAN	KN motif and ankyrin repeat domain-containing protein 2	0.017	0.344
P13987	CD59_HUMAN	CD59 glycoprotein	0.038	0.350
P49023	PAXI_HUMAN	Paxillin	0.024	0.350
O43598	DNPH1_HUMAN	2-deoxynucleoside 5-phosphate N-hydrolase 1	0.044	0.353
P35610	SOAT1_HUMAN	Sterol O-acyltransferase 1	0.042	0.353
Q9Y6A9	SPCS1_HUMAN	Signal peptidase complex subunit 1	0.050	0.360
Q9NUY8	TBC23_HUMAN	TBC1 domain family member 23	0.043	0.362
Q76M96	CCD80_HUMAN	Coiled-coil domain-containing protein 80	0.038	0.365
O00442	RTCA_HUMAN	RNA 3-terminal phosphate cyclase	0.041	0.368
Q14738	2A5D_HUMAN	Serine/threonine-protein phosphatase 2A 56 kDa regulatory subunit delta isoform	0.022	0.373
Q15904	VAS1_HUMAN	V-type proton ATPase subunit S1	0.000	0.376
Q96FZ7	CHMP6_HUMAN	Charged multivesicular body protein 6	0.038	0.384
P22676	CALB2_HUMAN	Calretinin	0.047	0.386
P42166	LAP2A_HUMAN	Lamina-associated polypeptide 2. isoform alpha	0.012	0.387
O15498	YKT6_HUMAN	Synaptobrevin homolog YKT6	0.013	0.390
P55263	ADK_HUMAN	Adenosine kinase	0.003	0.391
Q8NFW8	NEUA_HUMAN	N-acylneuraminate cytidylyltransferase	0.013	0.392
Q7L523	RRAGA_HUMAN	Ras-related GTP-binding protein A	0.030	0.407
P14854	CX6B1_HUMAN	Cytochrome c oxidase subunit 6B1	0.037	0.413
Q9UKM9	RALY_HUMAN	RNA-binding protein Raly	0.012	0.413
Q86VY9	T200A_HUMAN	Transmembrane protein 200A	0.044	0.415
P18084	ITB5_HUMAN	Integrin beta-5	0.000	0.415
P57105	SYJ2B_HUMAN	Synaptojanin-2-binding protein	0.001	0.416
Q13363	CTBP1_HUMAN	C-terminal-binding protein 1	0.003	0.430
O43252	PAPS1_HUMAN	Bifunctional 3-phosphoadenosine 5-phosphosulfate synthase 1	0.029	0.442

Q8TAT6	NPL4_HUMAN	Nuclear protein localization protein 4 homolog	0.023	0.445
Q96T51	RUFY1_HUMAN	RUN and FYVE domain-containing protein 1	0.018	0.460
P16401	H15_HUMAN	Histone H1.5	0.005	0.463
P60983	GMFB_HUMAN	Glia maturation factor beta	0.021	0.463
Q15020	SART3_HUMAN	Squamous cell carcinoma antigen recognized by T-cells 3	0.014	0.475
O00462	MANBA_HUMAN	Beta-mannosidase	0.033	0.477
P02794	FRIH_HUMAN	Ferritin heavy chain	0.027	0.477
O95865	DDAH2_HUMAN	N(G).N(G)-dimethylarginine dimethylaminohydrolase 2	0.031	0.482
Q8TF66	LRC15_HUMAN	Leucine-rich repeat-containing protein 15	0.005	0.489
Q99700	ATX2_HUMAN	Ataxin-2	0.048	0.495
Q9H444	CHM4B_HUMAN	Charged multivesicular body protein 4b	0.009	0.497
O43731	ERD23_HUMAN	ER lumen protein-retaining receptor 3	0.011	0.500
P19784	CSK22_HUMAN	Casein kinase II subunit alpha	0.019	0.502
P11234	RALB_HUMAN	Ras-related protein Ral-B	0.033	0.503
P12270	TPR_HUMAN	Nucleoprotein TPR	0.014	0.504
Q92688	AN32B_HUMAN	Acidic leucine-rich nuclear phosphoprotein 32 family member B	0.023	0.507
Q9UL46	PSME2_HUMAN	Proteasome activator complex subunit 2	0.010	0.510
Q96HY6	DDRGK_HUMAN	DDRGK domain-containing protein 1	0.016	0.513
P05997	CO5A2_HUMAN	Collagen alpha-2(V) chain	0.002	0.518
O75934	SPF27_HUMAN	Pre-mRNA-splicing faOSctor SPF27	0.015	0.522
P07203	GPX1_HUMAN	Glutathione peroxidase 1	0.029	0.522
Q5BJH7	YIF1B_HUMAN	Protein YIF1B	0.005	0.523
Q92974	ARHG2_HUMAN	Rho guanine nucleotide exchange factor 2	0.007	0.524
O43847	NRDC_HUMAN	Nardilysin	0.042	0.529
P13473	LAMP2_HUMAN	Lysosome-associated membrane glycoprotein 2	0.007	0.529
P29590	PML_HUMAN	Protein PML	0.012	0.531
P61604	CH10_HUMAN	10 kDa heat shock protein. mitochondrial	0.019	0.537
Q02952	AKA12_HUMAN	A-kinase anchor protein 12	0.018	0.537
P27105	STOM_HUMAN	Erythrocyte band 7 integral membrane protein	0.032	0.540
P62244	RS15A_HUMAN	40S ribosomal protein S15a	0.014	0.552

P32119	PRDX2_HUMAN	Peroxiredoxin-2	0.007	0.567
P61619	S61A1_HUMAN	Protein transport protein Sec61 subunit alpha isoform 1	0.006	0.575
O15427	MOT4_HUMAN	Monocarboxylate transporter 4	0.002	0.588
Q92769	HDAC2_HUMAN	Histone deacetylase 2	0.005	0.591
P08590	MYL3_HUMAN	Myosin light chain 3	0.043	0.591
Q9Y5U9	IR3IP_HUMAN	Immediate early response 3-interacting protein 1	0.022	0.591
Q08378	GOGA3_HUMAN	Golgin subfamily A member 3	0.027	0.591
O75400	PR40A_HUMAN	Pre-mRNA-processing factor 40 homolog A	0.038	0.594
P60468	SC61B_HUMAN	Protein transport protein Sec61 subunit beta	0.008	0.596
P62805	H4_HUMAN	Histone H4	0.028	0.605
Q15800	MSMO1_HUMAN	Methylsterol monooxygenase 1	0.007	0.609
Q9NUM4	T106B_HUMAN	Transmembrane protein 106B	0.044	0.610
P17096	HMGA1_HUMAN	High mobility group protein HMG-I/HMG-Y	0.019	0.611
Q96AE4	FUBP1_HUMAN	Far upstream element-binding protein 1	0.016	0.621
P55290	CAD13_HUMAN	Cadherin-13	0.012	0.627
P46783	RS10_HUMAN	40S ribosomal protein S10	0.021	0.631
Q16795	NDUA9_HUMAN	NADH dehydrogenase [ubiquinone] 1 alpha subcomplex subunit 9. mitochondrial	0.017	0.633
P61313	RL15_HUMAN	60S ribosomal protein L15	0.010	0.638
Q9NRY5	F1142_HUMAN	Protein FAM114A2	0.006	0.645
Q9Y5Z4	HEBP2_HUMAN	Heme-binding protein 2	0.016	0.648
P51452	DUS3_HUMAN	Dual specificity protein phosphatase 3	0.039	0.651
P14927	QCR7_HUMAN	Cytochrome b-c1 complex subunit 7	0.039	0.662
Q13867	BLMH_HUMAN	Bleomycin hydrolase	0.016	1.540
O60711	LPXN_HUMAN	Leupaxin	0.001	1.579
P08648	ITA5_HUMAN	Integrin alpha-5	0.025	1.642
O00391	QSOX1_HUMAN	Sulfhydryl oxidase 1	0.001	1.691
Q7L2H7	EIF3M_HUMAN	Eukaryotic translation initiation factor 3 subunit M	0.008	1.695
P02461	CO3A1_HUMAN	Collagen alpha-1(III) chain	0.031	1.704
P62166	NCS1_HUMAN	Neuronal calcium sensor 1	0.021	1.744
Q15772	SPEG_HUMAN	Striated muscle preferentially expressed protein kinase	0.004	1.811

P40616	ARL1_HUMAN	ADP-ribosylation factor-like protein 1	0.004	1.844
Q9NR31	SAR1A_HUMAN	GTP-binding protein SAR1a	0.040	1.853
Q15147	PLCB4_HUMAN	1-phosphatidylinositol 4.5-bisphosphate phosphodiesterase beta-4	0.006	1.880
Q9Y2S7	PDIP2_HUMAN	Polymerase delta-interacting protein 2	0.024	2.040
Q9Y4I1	MYO5A_HUMAN	Unconventional myosin-Va	0.042	2.156
Q8WUJ3	CEMIP_HUMAN	ell migration-inducing and hyaluronan-binding protein	0.023	2.231
P60953	CDC42_HUMAN	Cell division control protein 42 homolog	0.042	2.235
Q86VM9	ZCH18_HUMAN	Zinc finger CCCH domain-containing protein 18	0.029	2.293
P83111	LACTB_HUMAN	Serine beta-lactamase-like protein LACTB. mitochondrial	0.028	2.329
P52888	THOP1_HUMAN	Thimet oligopeptidase	0.024	2.334
P0C0L5	CO4B_HUMAN	Complement C4-B	0.048	2.414
Q15286	RAB35_HUMAN	Ras-related protein Rab-35	0.001	2.589
Q96DB5	RMD1_HUMAN	Regulator of microtubule dynamics protein 1	0.037	2.623
Q9NWV4	CZIB_HUMAN	CXXC motif containing zinc binding protein	0.046	2.637
P51151	RAB9A_HUMAN	Ras-related protein Rab-9A	0.047	2.862
O60488	ACSL4_HUMAN	Long-chain-fatty-acid--CoA ligase 4	0.007	2.911
Q8N5C1	CAHM5_HUMAN	Calcium homeostasis modulator protein 5	0.028	3.077
Q02252	MMSA_HUMAN	Methylmalonate-semialdehyde dehydrogenase [acylating]. mitochondrial	0.027	3.325
P42356	PI4KA_HUMAN	Phosphatidylinositol 4-kinase alpha	0.023	3.344
O00400	ACATN_HUMAN	Acetyl-coenzyme A transporter 1	0.013	3.509
Q9ULC4	MCTS1_HUMAN	Malignant T-cell-amplified sequence 1	0.004	3.686
Q9Y6U3	ADSV_HUMAN	Adseverin	0.016	3.757
P69905	HBA_HUMAN	Hemoglobin subunit alpha	0.021	3.814
O00767	ACOD_HUMAN	Acyl-CoA desaturase	0.032	3.867
O95498	VNN2_HUMAN	Vascular non-inflammatory molecule 2	0.000	4.063
Q9UBF2	COPG2_HUMAN	Coatomer subunit gamma-2	0.014	5.567
O75746	CMC1_HUMAN	Calcium-binding mitochondrial carrier protein Aralar1 O	0.024	5.810
P32455	GBP1_HUMAN	Guanylate-binding protein 1	0.025	6.872
P22570	ADRO_HUMAN	NADPH:adrenodoxin oxidoreductase. mitochondrial	0.008	9.988
O95202	LETM1_HUMAN	Mitochondrial proton/calcium exchanger protein	0.004	13.943

Q9UPU5	UBP24_HUMAN	Ubiquitin carboxyl-terminal hydrolase 24	0.000	16.201
Q02383	SEMG2_HUMAN	Semenogelin-2	0.017	47.346

Supplementary table 6.2. Progenesis comparative analysis between the proteins identified onto MT1.5Mg with respect to MT at 3 days *in vitro*. Proteins were considered differentially expressed when the ratio was higher than 1.5 in either direction and *p* value < 0.05. Proteins overexpressed in MT1.5Mg are marked in red, while those under expressed are marked in green.

Accession		Description	*p* value	MT1.5Mg *vs* MT
Q71DI3	H32_HUMAN	Histone H3.2	0.000	0.023
O15056	SYNJ2_HUMAN	Synaptojanin-2	0.000	0.027
P47985	UCRI_HUMAN	Cytochrome b-c1 complex subunit Rieske	0.000	0.042
P19174	PLCG1_HUMAN	1-phosphatidylinositol 4.5-bisphosphate phosphodiesterase gamma-1 O	0.020	0.047
Q9BSD7	NTPCR_HUMAN	Cancer-related nucleoside-triphosphatase	0.026	0.057
P23229	ITA6_HUMAN	Integrin alpha-6	0.000	0.058
Q8WWZ4	ABCAA_HUMAN	ATP-binding cassette sub-family A member 10	0.034	0.059
Q14956	GPNMB_HUMAN	Transmembrane glycoprotein NMB	0.001	0.063
P84095	RHOG_HUMAN	Rho-related GTP-binding protein RhoG	0.000	0.068
P32455	GBP1_HUMAN	Guanylate-binding protein 1	0.002	0.073
P09496	CLCA_HUMAN	Clathrin light chain A	0.000	0.080
P25686	DNJB2_HUMAN	DnaJ homolog subfamily B member 2	0.000	0.084
O15305	PMM2_HUMAN	Phosphomannomutase 2	0.000	0.089
P51809	VAMP7_HUMAN	Vesicle-associated membrane protein 7	0.001	0.089
P20962	PTMS_HUMAN	Parathymosin	0.022	0.090
Q96DB5	RMD1_HUMAN	Regulator of microtubule dynamics protein 1	0.014	0.094
Q92783	STAM1_HUMAN	Signal transducing adapter molecule 1	0.003	0.095
P11279	LAMP1_HUMAN	Lysosome-associated membrane glycoprotein 1	0.010	0.096
P02753	RET4_HUMAN	Retinol-binding protein 4	0.008	0.112
Q9BQA9	CYBC1_HUMAN	Cytochrome b-245 chaperone 1	0.049	0.116
Q9Y512	SAM50_HUMAN	Sorting and assembly machinery component 50 homolog	0.000	0.118
P78347	GTF2I_HUMAN	General transcription factor II-I	0.017	0.132
P18077	RL35A_HUMAN	60S ribosomal protein L35a	0.002	0.133
Q8WUP2	FBLI1_HUMAN	Filamin-binding LIM protein 1	0.002	0.136

Q15125	EBP_HUMAN	3-beta-hydroxysteroid-Delta(8).Delta(7)-isomerase	0.000	0.139
O75131	CPNE3_HUMAN	Copine-3	0.000	0.148
Q9NYL4	FKB11_HUMAN	Peptidyl-prolyl cis-trans isomerase FKBP11	0.001	0.154
Q96NW7	LRRC7_HUMAN	Leucine-rich repeat-containing protein 7	0.022	0.155
Q9NTK5	OLA1_HUMAN	Obg-like ATPase 1	0.007	0.185
Q13247	SRSF6_HUMAN	Serine/arginine-rich splicing factor 6	0.011	0.199
Q53S08	RAB6D_HUMAN	Ras-related protein Rab-6D	0.033	0.201
Q8WXF1	PSPC1_HUMAN	Paraspeckle component 1	0.025	0.204
Q15643	TRIPB_HUMAN	Thyroid receptor-interacting protein 11	0.030	0.211
O43747	AP1G1_HUMAN	AP-1 complex subunit gamma-1	0.040	0.214
Q14498	RBM39_HUMAN	RNA-binding protein 39	0.019	0.215
Q9NXG2	THUM1_HUMAN	THUMP domain-containing protein 1	0.003	0.218
Q9HA77	SYCM_HUMAN	Probable cysteine--tRNA ligase. mitochondrial	0.044	0.219
Q9BRJ2	RM45_HUMAN	39S ribosomal protein L45. mitochondrial	0.039	0.222
Q68EM7	RHG17_HUMAN	Rho GTPase-activating protein 17	0.005	0.224
P08572	CO4A2_HUMAN	Collagen alpha-2(IV) chain	0.023	0.224
P28072	PSB6_HUMAN	Proteasome subunit beta type-6	0.001	0.229
O75352	MPU1_HUMAN	Mannose-P-dolichol utilization defect 1 protein	0.000	0.229
O14558	HSPB6_HUMAN	Heat shock protein beta-6	0.002	0.240
P54105	ICLN_HUMAN	Methylosome subunit pICln	0.041	0.246
Q9UPQ0	LIMC1_HUMAN	LIM and calponin homology domains-containing protein 1	0.038	0.247
Q12841	FSTL1_HUMAN	Follistatin-related protein 1	0.011	0.251
P30626	SORCN_HUMAN	Sorcin	0.000	0.253
P62244	RS15A_HUMAN	40S ribosomal protein S15a	0.030	0.259
Q7L1Q6	BZW1_HUMAN	Basic leucine zipper and W2 domain-containing protein 1	0.044	0.270
P81605	DCD_HUMAN	Dermcidin	0.015	0.272
P35244	RFA3_HUMAN	Replication protein A 14 kDa subunit	0.007	0.276
P42226	STAT6_HUMAN	Signal transducer and activator of transcription 6	0.000	0.279
Q13336	UT1_HUMAN	Urea transporter 1	0.005	0.280
O43290	SNUT1_HUMAN	U4/U6.U5 tri-snRNP-associated protein 1	0.023	0.284

P11166	GTR1_HUMAN	Solute carrier family 2. facilitated glucose transporter member 1	0.033	0.288
P50552	VASP_HUMAN	Vasodilator-stimulated phosphoprotein	0.004	0.294
Q9Y6M7	S4A7_HUMAN	Sodium bicarbonate cotransporter 3	0.010	0.295
P07602	SAP_HUMAN	Prosaposin	0.039	0.296
P13473	LAMP2_HUMAN	Lysosome-associated membrane glycoprotein 2	0.000	0.297
Q9UGV2	NDRG3_HUMAN	Protein NDRG3	0.026	0.307
Q13488	VPP3_HUMAN	V-type proton ATPase 116 kDa subunit a isoform 3	0.019	0.312
P02458	CO2A1_HUMAN	Collagen alpha-1(II) chain	0.024	0.324
P27694	RFA1_HUMAN	Replication protein A 70 kDa DNA-binding subunit	0.018	0.335
P07099	HYEP_HUMAN	Epoxide hydrolase 1	0.012	0.340
Q9BXK5	B2L13_HUMAN	Bcl-2-like protein 13	0.010	0.349
P62269	RS18_HUMAN	40S ribosomal protein S18	0.013	0.352
Q99798	ACON_HUMAN	Aconitate hydratase. mitochondrial	0.009	0.363
Q9Y2X3	NOP58_HUMAN	Nucleolar protein 58	0.049	0.374
Q6NVY1	HIBCH_HUMAN	3-hydroxyisobutyryl-CoA hydrolase. mitochondrial	0.030	0.377
Q14699	RFTN1_HUMAN	Raftlin	0.042	0.383
Q9UGI8	TES_HUMAN	Testin	0.003	0.384
Q63ZY3	KANK2_HUMAN	KN motif and ankyrin repeat domain-containing protein 2	0.013	0.389
Q01581	HMCS1_HUMAN	Hydroxymethylglutaryl-CoA synthase. cytoplasmic	0.033	0.390
Q9NUM4	T106B_HUMAN	Transmembrane protein 106B	0.042	0.391
O95833	CLIC3_HUMAN	Chloride intracellular channel protein 3	0.008	0.392
P04179	SODM_HUMAN	Superoxide dismutase [Mn]. mitochondrial	0.001	0.392
P78417	GSTO1_HUMAN	Glutathione S-transferase omega-1	0.000	0.399
Q9HAV7	GRPE1_HUMAN	GrpE protein homolog 1. mitochondrial	0.041	0.400
P04156	PRIO_HUMAN	Major prion protein	0.037	0.414
Q07666	KHDR1_HUMAN	KH domain-containing. RNA-binding. signal transduction-associated protein 1	0.006	0.417
Q8WTS6	SETD7_HUMAN	Histone-lysine N-methyltransferase SETD7	0.018	0.421
Q92542	NICA_HUMAN	Nicastrin	0.033	0.426
P61619	S61A1_HUMAN	Protein transport protein Sec61 subunit alpha isoform 1	0.007	0.429
Q14767	LTBP2_HUMAN	Latent-transforming growth factor beta-binding protein 2	0.028	0.457

Q9UMX5	NENF_HUMAN	Neudesin	0.045	0.462
P49585	PCY1A_HUMAN	Choline-phosphate cytidylyltransferase A	0.032	0.469
P51116	FXR2_HUMAN	Fragile X mental retardation syndrome-related protein 2	0.042	0.472
P46937	YAP1_HUMAN	Transcriptional coactivator YAP1	0.035	0.476
Q9Y639	NPTN_HUMAN	Neuroplastin	0.039	0.484
Q96KP1	EXOC2_HUMAN	Exocyst complex component 2	0.026	0.508
Q96JC1	VPS39_HUMAN	Vam6/Vps39-like protein	0.019	0.508
O15270	SPTC2_HUMAN	Serine palmitoyltransferase 2	0.033	0.509
Q8IWB7	WDFY1_HUMAN	WD repeat and FYVE domain-containing protein 1	0.034	0.509
P26368	U2AF2_HUMAN	Splicing factor U2AF 65 kDa subunit	0.025	0.511
Q4G0N4	NAKD2_HUMAN	NAD kinase 2. mitochondrial	0.032	0.521
Q8IWU6	SULF1_HUMAN	Extracellular sulfatase Sulf-1	0.046	0.528
Q9HDC9	APMAP_HUMAN	Adipocyte plasma membrane-associated protein	0.007	0.541
Q9P0V3	SH3B4_HUMAN	SH3 domain-binding protein 4	0.046	0.556
Q08379	GOGA2_HUMAN	Golgin subfamily A member 2	0.033	0.557
P62851	RS25_HUMAN	40S ribosomal protein S25	0.007	0.568
P22307	NLTP_HUMAN	Non-specific lipid-transfer protein	0.048	0.570
P62873	GBB1_HUMAN	Guanine nucleotide-binding protein G(I)/G(S)/G(T) subunit beta-1	0.008	0.571
P18084	ITB5_HUMAN	Integrin beta-5	0.025	0.580
Q08431	MFGM_HUMAN	Lactadherin	0.036	0.588
Q96CV9	OPTN_HUMAN	Optineurin	0.010	0.594
P37235	HPCL1_HUMAN	Hippocalcin-like protein 1	0.016	0.598
P31949	S10AB_HUMAN	Protein S100-A11	0.000	0.616
P35637	FUS_HUMAN	RNA-binding protein FUS	0.042	0.622
O15260	SURF4_HUMAN	Surfeit locus protein 4	0.040	0.626
P17931	LEG3_HUMAN	Galectin-3	0.036	0.637
P68366	TBA4A_HUMAN	Tubulin alpha-4A chain O	0.002	0.639
Q99729	ROAA_HUMAN	Heterogeneous nuclear ribonucleoprotein A/B	0.007	0.639
O00303	EIF3F_HUMAN	Eukaryotic translation initiation factor 3 subunit F	0.047	0.655
Q15746	MYLK_HUMAN	Myosin light chain kinase. smooth muscle	0.008	1.501

Q96JB5	CK5P3_HUMAN	CDK5 regulatory subunit-associated protein 3	0.032	1.505
P62140	PP1B_HUMAN	Serine/threonine-protein phosphatase PP1-beta catalytic subunit	0.001	1.515
P61086	UBE2K_HUMAN	Ubiquitin-conjugating enzyme E2 K	0.030	1.633
Q99985	VPS4B_HUMAN	Semaphorin-3C	0.027	1.663
Q9UNF0	PACN2_HUMAN	Protein kinase C and casein kinase substrate in neurons protein 2	0.015	1.717
P52888	THOP1_HUMAN	Thimet oligopeptidase	0.047	1.765
P28482	MK01_HUMAN	Mitogen-activated protein kinase 1	0.015	1.909
Q8WU76	SCFD2_HUMAN	Sec1 family domain-containing protein 2	0.015	1.925
Q13228	SBP1_HUMAN	Methanethiol oxidase	0.022	1.927
Q15800	MSMO1_HUMAN	Methylsterol monooxygenase 1	0.006	2.022
Q96PK6	RBM14_HUMAN	RNA-binding protein 14	0.032	2.065
P47813	IF1AX_HUMAN	Eukaryotic translation initiation factor 1A. X-chromosomal	0.031	2.143
Q9UNS2	CSN3_HUMAN	COP9 signalosome complex subunit 3	0.033	2.153
Q92901	RL3L_HUMAN	60S ribosomal protein L3-like	0.001	2.195
P01024	CO3_HUMAN	Complement C3	0.043	2.197
Q9NVJ2	ARL8B_HUMAN	ADP-ribosylation factor-like protein 8B	0.033	2.489
Q96CM8	ACSF2_HUMAN	Medium-chain acyl-CoA ligase ACSF2. mitochondrial	0.006	2.589
P22059	OSBP1_HUMAN	Oxysterol-binding protein 1	0.036	2.595
Q9Y6E0	STK24_HUMAN	Serine/threonine-protein kinase 24	0.018	2.737
P61764	STXB1_HUMAN	Syntaxin-binding protein 1	0.004	2.810
P37198	NUP62_HUMAN	Nuclear pore glycoprotein p62	0.000	2.900
Q9Y3B4	SF3B6_HUMAN	Splicing factor 3B subunit 6	0.010	2.968
P48449	ERG7_HUMAN	Lanosterol synthase	0.014	3.187
P17405	ASM_HUMAN	Sphingomyelin phosphodiesterase	0.001	3.216
Q96JB6	LOXL4_HUMAN	Lysyl oxidase homolog 4	0.000	3.254
P30740	ILEU_HUMAN	Leukocyte elastase inhibitor	0.000	3.334
P40222	TXLNA_HUMAN	Alpha-taxilin	0.012	3.660
Q9Y2H1	ST38L_HUMAN	Serine/threonine-protein kinase 38-like	0.009	3.748
Q16832	DDR2_HUMAN	Discoidin domain-containing receptor 2	0.039	3.854
Q13610	PWP1_HUMAN	Periodic tryptophan protein 1 homolog	0.011	3.854

Q99666	RGPD5_HUMAN	RANBP2-like and GRIP domain-containing protein 5/6	0.022	3.948
Q13459	MYO9B_HUMAN	Unconventional myosin-IXb	0.003	4.022
P49419	AL7A1_HUMAN	Alpha-aminoadipic semialdehyde dehydrogenase	0.013	4.059
P46939	UTRO_HUMAN	Utrophin	0.039	4.110
Q53EL6	PDCD4_HUMAN	Programmed cell death protein 4	0.008	4.110
P17936	IBP3_HUMAN	Insulin-like growth factor-binding protein 3	0.044	4.392
Q9H307	PININ_HUMAN	Pinin	0.012	4.410
P42025	ACTY_HUMAN	Beta-centractin	0.033	4.542
Q01433	AMPD2_HUMAN	AMP deaminase 2	0.024	5.073
O95486	SC24A_HUMAN	Protein transport protein Sec24A	0.007	5.230
Q8N5C1	CAHM5_HUMAN	Calcium homeostasis modulator protein 5	0.009	5.666
Q8IZ81	ELMD2_HUMAN	ELMO domain-containing protein 2	0.019	5.860
Q14677	EPN4_HUMAN	Clathrin interactor 1	0.009	6.184
Q96I24	FUBP3_HUMAN	Far upstream element-binding protein 3	0.022	6.520
O75351	VPS4B_HUMAN	Vacuolar protein sorting-associated protein 4B	0.020	6.741
Q86V48	LUZP1_HUMAN	Leucine zipper protein 1	0.009	7.810
P48163	MAOX_HUMAN	NADP-dependent malic enzyme	0.000	7.942
Q9BVP2	GNL3_HUMAN	Guanine nucleotide-binding protein-like 3	0.000	8.247
Q9Y5F7	PCDGL_HUMAN	Protocadherin gamma-C4	0.032	8.293
P61916	NPC2_HUMAN	NPC intracellular cholesterol transporter 2	0.001	8.376
Q9NX40	OCAD1_HUMAN	OCIA domain-containing protein 1	0.002	8.410
Q9NZJ9	NUDT4_HUMAN	Diphosphoinositol polyphosphate phosphohydrolase 2	0.036	9.396
P62861	RS30_HUMAN	40S ribosomal protein S30	0.000	9.487
Q10472	GALT1_HUMAN	Polypeptide N-acetylgalactosaminyltransferase 1	0.023	9.929
Q99459	CDC5L_HUMAN	Cell division cycle 5-like protein	0.000	10.131
P63162	RSMN_HUMAN	Small nuclear ribonucleoprotein-associated protein N	0.018	10.276
Q3KQU3	MA7D1_HUMAN	MAP7 domain-containing protein 1	0.046	10.853
Q66K74	MAP1S_HUMAN	Microtubule-associated protein 1S	0.019	14.406
Q9Y2W1	TR150_HUMAN	Thyroid hormone receptor-associated protein 3	0.000	16.246
Q10713	MPPA_HUMAN	Mitochondrial-processing peptidase subunit alpha	0.030	17.296

Q9NUQ6	SPS2L_HUMAN	SPATS2-like protein	0.028	18.110
Q9UL25	RAB21_HUMAN	Ras-related protein Rab-21	0.006	26.897
Q96S66	CLCC1_HUMAN	Chloride channel CLIC-like protein 1	0.001	29.727
Q06124	PTN11_HUMAN	Tyrosine-protein phosphatase non-receptor type 11	0.013	31.764
Q96N67	DOCK7_HUMAN	Dedicator of cytokinesis protein 7	0.000	32.237
Q9BRK3	MXRA8_HUMAN	Matrix remodeling-associated protein 8	0.012	47.555

Supplementary table 6.3. Progenesis comparative analysis between the proteins identified onto MT1.5Mg with respect to MT at 7 days *in vitro*. Proteins were considered differentially expressed when the ratio was higher than 1.5 in either direction and *p* value < 0.05. Proteins overexpressed in MT1.5Mg are marked in red, while those under expressed are marked in green.

Accession		Description	*p* value	MT1.5Mg *vs* MT
P32455	GBP1_HUMAN	Guanylate-binding protein 1	0.00	0.0575
O43719	HTSF1_HUMAN	Tat-specific factor 1	0.04	0.0649
P02753	RET4_HUMAN	Retinol-binding protein 4	0.01	0.0845
Q9NTJ5	SAC1_HUMAN	Phosphatidylinositide phosphatase SAC1	0.05	0.0855
O14964	HGS_HUMAN	Hepatocyte growth factor-regulated tyrosine kinase substrate	0.04	0.0897
P25686	DNJB2_HUMAN	DnaJ homolog subfamily B member 2	0.02	0.1115
A0FGR8	ESYT2_HUMAN	Extended synaptotagmin-2	0.01	0.1216
P21912	SDHB_HUMAN	Succinate dehydrogenase [ubiquinone] iron-sulfur subunit. mitochondrial	0.04	0.1228
P22570	ADRO_HUMAN	NADPH:adrenodoxin oxidoreductase. mitochondrial OS=Homo sapiens	0.02	0.1398
P54819	KAD2_HUMAN	Adenylate kinase 2. mitochondrial	0.03	0.1629
P20337	RAB3B_HUMAN	Ras-related protein Rab-3B	0.04	0.1718
Q8WXF1	PSPC1_HUMAN	Paraspeckle component 1	0.04	0.1888
P61769	B2MG_HUMAN	Beta-2-microglobulin	0.04	0.1929
P05067	A4_HUMAN	Amyloid-beta precursor protein	0.03	0.2101
O15372	EIF3H_HUMAN	Eukaryotic translation initiation factor 3 subunit H O	0.05	0.2118
Q99798	ACON_HUMAN	Aconitate hydratase. mitochondrial	0.02	0.2623
Q9UNF1	MAGD2_HUMAN	Melanoma-associated antigen D2	0.01	0.2659
Q92878	RAD50_HUMAN	DNA repair protein RAD50	0.03	0.2864
Q9P2R3	ANFY1_HUMAN	Rabankyrin-5	0.01	0.2904
Q13642	FHL1_HUMAN	Four and a half LIM domains protein 1 OS=Homo sapiens	0.03	0.2973
P63220	RS21_HUMAN	40S ribosomal protein S21	0.03	0.3086
Q6P996	PDXD1_HUMAN	Pyridoxal-dependent decarboxylase domain-containing protein 1	0.00	0.3117
Q9HB40	RISC_HUMAN	Retinoid-inducible serine carboxypeptidase	0.03	0.3156

P29317	EPHA2_HUMAN	Ephrin type-A receptor 2	0.01	0.3288
Q9Y5C1	ANGL3_HUMAN	Angiopoietin-related protein 3	0.00	0.3405
Q15006	EMC2_HUMAN	ER membrane protein complex subunit 2	0.04	0.3574
P04040	CATA_HUMAN	Catalase	0.03	0.3607
P49773	HINT1_HUMAN	Histidine triad nucleotide-binding protein 1	0.05	0.3616
P36507	MP2K2_HUMAN	Dual specificity mitogen-activated protein kinase kinase 2	0.05	0.3785
Q9HCJ1	ANKH_HUMAN	Progressive ankylosis protein homolog	0.01	0.3985
P05230	FGF1_HUMAN F	Fibroblast growth factor 1	0.02	0.3993
Q96K17	BT3L4_HUMAN	Transcription factor BTF3 homolog 4	0.04	0.4133
Q7Z4F1	LRP10_HUMAN	Low-density lipoprotein receptor-related protein 10	0.00	0.4450
Q14767	LTBP2_HUMAN	Latent-transforming growth factor beta-binding protein	0.04	0.4811
Q9BR76	COR1B_HUMAN	Coronin-1B	0.05	0.4823
P0DN76	U2AF5_HUMAN	Splicing factor U2AF 35 kDa subunit-like protein	0.02	0.4873
Q14435	GALT3_HUMAN	Polypeptide N-acetylgalactosaminyltransferase 3	0.01	0.5528
P48307	TFPI2_HUMAN	Tissue factor pathway inhibitor 2	0.02	0.5780
P62942	FKB1A_HUMAN	Peptidyl-prolyl cis-trans isomerase FKBP1A	0.01	0.5871
P62136	PP1A_HUMAN	Serine/threonine-protein phosphatase PP1-alpha catalytic subunit	0.04	0.5970
P61026	RAB10_HUMAN	Ras-related protein Rab-10	0.05	0.6193
Q9Y6M5	ZNT1_HUMAN	Zinc transporter 1	0.03	0.6361
P0C0L5	CO4B_HUMAN	Complement C4-B	0.04	0.6575
Q8IVF2	AHNK2_HUMAN	Protein AHNAK2	0.02	1.5081

Supplementary table 6.4. Upstream regulators determined by IPA® on MT1.5Mg. The molecules were considered significantly regulated when -log(*p*-value) > 1.3.

Upstream Regulators	1 day	3 days	7 days
TP53	5.91	5.39	6.38
TGFB1	5.62	3.26	2.47
HRAS	5.22	3.97	0.00
sirolimus	5.17	0.96	2.19
ERBB2	5.12	2.44	0.00
MASTL	4.99	0.00	0.00
5-fluorouracil	4.88	1.67	1.51
torin1	4.59	3.11	2.22
BACH1	4.25	0.00	0.00
OSM	4.22	1.82	1.61
vancomycin	4.15	5.01	0.00
Lh	4.12	5.32	2.31
RICTOR	4.05	2.08	0.00
glycerophosphoric acid	3.93	3.73	0.00
FTMT	3.93	0.00	0.00
metronidazole	3.91	0.00	0.00
ZNF106	3.78	3.39	0.00
Collagen(s)	3.74	2.26	0.00
topotecan	3.70	0.00	0.00
CYP4V2	3.63	3.43	0.00
CHRM4	3.63	1.50	0.00
arsenic trioxide	3.56	2.26	0.00
YAP1	3.52	0.00	0.00
TRIM2	3.46	0.00	0.00

ASPSCR1-TFE3	3.39	2.93	0.00
IGF1	3.38	1.66	0.00
ABCB7	3.24	0.00	0.00
colistin	3.20	0.00	0.00
ATP5IF1	3.17	0.00	2.17
kanamycin A	3.16	0.00	0.00
butyric acid	3.15	2.92	0.00
CDKN2A	3.15	1.45	0.00
XBP1	3.06	3.85	1.93
VTN	3.02	0.00	0.00
dexamethasone	2.98	2.64	2.40
SIRT6	2.98	1.72	0.00
CDK19	2.98	1.79	1.62
NPPB	2.94	3.88	0.00
ATM	2.93	0.00	0.00
RAB1B	2.90	1.53	0.00
imatinib	2.87	1.74	0.00
AP3B1	2.86	2.66	0.00
Presenilin	2.86	0.00	1.76
COL5A1	2.83	2.54	0.00
beta-estradiol	2.81	3.61	0.00
crizotinib	2.79	0.00	0.00
FTH1	2.77	0.00	0.00
KRAS	2.77	1.57	1.70
SUMO3	2.76	0.00	0.00
8-bromo-cAMP	2.74	0.00	0.00
filgrastim	2.71	0.00	0.00
VHL	2.71	0.00	0.00
hydrogen peroxide	2.71	0.00	3.25

LARP1	2.71	3.26	1.93
CA074-methyl ester	2.68	2.48	1.67
Irp	2.68	0.00	3.69
MGAT1	2.68	0.00	0.00
HNF4A	2.66	3.69	3.13
NFYA	2.65	0.00	0.00
FN1	2.64	0.00	0.00
MLXIPL	2.61	2.18	0.00
ferric chloride	2.60	0.00	0.00
erastin	2.60	0.00	0.00
ferric ammonium citrate	2.60	0.00	0.00
MM-589	2.57	0.00	0.00
forskolin	2.55	2.56	0.00
mir-29	2.55	0.00	0.00
RV 538	2.53	2.34	0.00
MAX	2.53	0.00	0.00
PTC-209	2.52	0.00	0.00
MAPK1	2.48	0.00	0.00
ACO1	2.47	2.27	3.47
LPCAT3	2.47	0.00	0.00
DNAJC3	2.47	0.00	0.00
ETV5	2.45	0.00	0.00
OMA1	2.41	0.00	0.00
COPS5	2.38	0.00	0.00
FSH	2.37	3.38	1.34
NREP	2.35	0.00	0.00
acyline	2.33	2.78	0.00
CD3 group	2.32	0.00	0.00
uranyl nitrate	2.30	1.95	0.00

FANCD2	2.30	2.10	1.48
TOR1A	2.30	0.00	0.00
BIRC5	2.28	0.00	0.00
homocysteine	2.26	0.00	0.00
glucagon	2.25	0.00	0.00
MYCBP2	2.25	0.00	0.00
TAF1	2.25	0.00	0.00
CYB561A3	2.25	0.00	0.00
trichloroethylene	2.23	1.96	0.00
benzene	2.23	0.00	0.00
ELL2	2.23	0.00	0.00
SLC29A1	2.20	0.00	1.44
FKBP10	2.20	2.10	0.00
glucosamine-2-O-methyl inositol octadecyl phosphate	2.20	2.10	0.00
D-glucosaminylphosphatidylinositol	2.20	2.10	0.00
ECSCR	2.20	0.00	0.00
ferric citrate	2.20	0.00	0.00
CAND1	2.20	0.00	0.00
Cadherin	2.20	0.00	0.00
FARP2	2.20	0.00	0.00
ELSPBP1	2.20	0.00	0.00
ISCU	2.20	0.00	0.00
TRNAU1AP	2.20	0.00	0.00
AMPH	2.20	0.00	0.00
RHOU	2.20	0.00	0.00
TGFB2	2.19	0.00	0.00
MAP4K4	2.18	0.00	0.00
gentamicin	2.17	2.15	0.00
SUCNR1	2.16	0.00	0.00

PTP4A3	2.16	0.00	0.00
QKI	2.15	1.88	0.00
CD3	2.14	1.87	2.09
CD28	2.13	0.00	2.29
idarubicin	2.12	0.00	3.11
HNF1B	2.12	1.77	0.00
KAT2A	2.12	0.00	0.00
NRG1	2.11	2.20	1.79
MAPT	2.11	1.51	3.18
NRG2	2.10	0.00	0.00
methylmercury	2.08	0.00	0.00
MFSD2A	2.08	0.00	0.00
INSR	2.06	3.28	2.35
HAND2	2.06	0.00	0.00
geldanamycin	2.01	2.09	2.62
ELOVL3	2.01	1.74	0.00
NFE2L2	2.00	2.86	0.00
IREB2	2.00	3.05	4.86
MMP11	2.00	0.00	0.00
WNT1	2.00	0.00	0.00
FOXO1	1.97	2.81	0.00
SOX6	1.97	0.00	0.00
IGF1R	1.95	0.00	0.00
CPT1B	1.94	0.00	2.07
CDC73	1.94	1.75	2.93
CD9	1.94	1.75	0.00
medroxyprogesterone acetate	1.93	1.39	0.00
PD98059	1.93	3.60	0.00
molybdenum disulfide	1.92	3.88	1.51

ADAM10	1.92	0.00	1.51
SPI1	1.92	0.00	0.00
ERG	1.92	2.11	0.00
rifaximin	1.91	0.00	0.00
ruxolitinib	1.91	0.00	0.00
AGT	1.90	3.45	1.49
RILP	1.90	1.80	0.00
BB 3103	1.90	1.80	0.00
ginkgolide A	1.90	1.80	0.00
MYOF	1.90	1.80	0.00
SURF4	1.90	0.00	0.00
AGXT	1.90	0.00	0.00
PIGA	1.90	0.00	0.00
SLIT3	1.90	0.00	0.00
IPO9	1.90	0.00	0.00
ZRL5P4	1.90	0.00	0.00
MAP4K3	1.90	0.00	0.00
NUBP1	1.90	0.00	0.00
TMPRSS4	1.90	0.00	0.00
NDUFS1	1.90	0.00	0.00
STX6	1.90	0.00	0.00
COPS6	1.90	0.00	0.00
CYRIA	1.90	0.00	0.00
Gk	1.90	0.00	0.00
SLC9A9	1.90	0.00	0.00
DMD	1.90	1.51	0.00
EWSR1-FLI1	1.85	2.42	0.00
EGFR	1.85	2.63	1.78
S100A6	1.85	0.00	0.00

BCAP31	1.85	0.00	0.00
arsenic	1.85	0.00	0.00
PTEN	1.83	2.76	0.00
dihydrotestosterone	1.82	2.45	3.77
TRIM37	1.82	0.00	0.00
NFATC4	1.82	0.00	0.00
FLT1	1.81	0.00	0.00
NUPR1	1.80	0.00	0.00
SLC22A5	1.79	1.60	0.00
RB1	1.79	1.27	0.00
IFNG	1.78	2.28	2.03
mycophenolic acid	1.78	1.52	1.92
TLE3	1.77	0.00	0.00
HSF1	1.77	0.00	0.00
NCOA4	1.76	0.00	0.00
LIN28A	1.76	0.00	0.00
OGA	1.76	2.68	1.30
enalapril	1.75	3.19	1.90
EML4-ALK	1.75	2.29	0.00
PRDM5	1.75	0.00	0.00
APP	1.75	2.78	2.61
SCAP	1.74	2.27	0.00
cinnamaldehyde	1.74	0.00	1.89
pentosan polysulfate	1.73	1.63	0.00
EMP2	1.73	1.63	0.00
SMCR8	1.73	1.63	0.00
IVNS1ABP	1.73	1.63	0.00
NHLRC1	1.73	1.63	0.00
EPM2A	1.73	1.63	0.00

TAPI	1.73	1.63	0.00
mycosporine-like amino acid	1.73	0.00	0.00
(S)-duloxetine	1.73	0.00	0.00
G3BP2	1.73	0.00	0.00
tolylfluanid	1.73	0.00	0.00
ELOVL2	1.73	0.00	0.00
MLF1	1.73	0.00	0.00
IPPK	1.73	0.00	0.00
FTL	1.73	0.00	0.00
arjunolic acid	1.73	0.00	0.00
mir-122	1.70	1.44	0.00
APOB	1.69	0.00	0.00
PML	1.69	0.00	0.00
elaidic acid	1.68	2.19	0.00
Hbb-b1	1.68	0.00	0.00
VCAN	1.67	1.97	0.00
NVP-TAE684	1.67	0.00	0.00
MDK	1.67	0.00	0.00
desmopressin	1.67	0.00	0.00
tert-butyl-hydroquinone	1.65	0.00	0.00
isoproterenol	1.65	0.00	0.00
thioacetamide	1.65	2.37	0.00
metribolone	1.65	2.03	1.96
Ifn gamma	1.63	0.00	0.00
PAK2	1.62	0.00	0.00
CLOCK	1.62	0.00	1.85
CTNNB1	1.61	3.39	0.00
APLP2	1.60	1.50	0.00
PDIA3	1.60	1.50	0.00

DEETGE-CAL-Tat	1.60	1.50	0.00
Vacuolar H+ ATPase	1.60	1.50	0.00
CV 6209	1.60	1.50	0.00
cilazapril	1.60	0.00	0.00
RGL2	1.60	0.00	0.00
4beta-hydroxycholesterol	1.60	0.00	0.00
ARID5B	1.60	0.00	0.00
FDXR	1.60	0.00	0.00
FDX2	1.60	0.00	0.00
MCU	1.60	0.00	0.00
glucuronyl glucosamine glycan sulfate	1.60	0.00	0.00
NSC719239	1.60	0.00	0.00
bumetanide	1.60	0.00	0.00
GNPTAB	1.60	0.00	0.00
ACSL3	1.60	0.00	0.00
lamotrigine	1.60	0.00	0.00
VSNL1	1.60	0.00	0.00
DIO1	1.60	0.00	0.00
CYRIB	1.60	0.00	0.00
NUP133	1.60	0.00	0.00
AHCTF1	1.60	0.00	0.00
ABI1	1.60	0.00	0.00
CARM1	1.60	0.00	0.00
sucrose	1.60	0.00	0.00
CSF1	1.59	2.90	0.00
fluvastatin	1.58	0.00	0.00
CALCA	1.57	0.00	0.00
nonylphenol	1.56	0.00	0.00
ShK-223	1.55	0.00	0.00

arachidonic acid	1.54	0.00	0.00
chloropromazine	1.54	2.35	0.00
SUMO2	1.54	0.00	0.00
HES3	1.52	1.34	2.49
Cdc42	1.52	3.43	0.00
MHC II	1.52	0.00	0.00
SP1	1.51	2.16	1.57
CST5	1.51	0.00	0.00
halofuginol	1.51	3.21	0.00
CREB3L4	1.51	0.00	2.01
globotriaosylceramide	1.51	1.41	0.00
FDPS	1.51	1.41	0.00
LAMP1	1.51	1.41	0.00
sodium chlorate	1.51	1.41	0.00
chondroitin sulfate	1.51	1.41	0.00
CLDN2	1.51	0.00	0.00
CMA1	1.51	0.00	0.00
RMST	1.51	0.00	0.00
NCK2	1.51	0.00	0.00
TXLNG	1.51	0.00	0.00
SIRT	1.51	0.00	0.00
tofogliflozin	1.51	0.00	0.00
inositol	1.51	0.00	0.00
Collagen type V	1.51	0.00	0.00
darusentan	1.51	0.00	0.00
RACGAP1	1.51	0.00	0.00
MARCHF8	1.51	0.00	0.00
GIT1	1.51	0.00	0.00
NCGC00186528	1.51	0.00	0.00

ARHGEF25	1.51	0.00	0.00
PRKN	1.50	0.00	0.00
verapamil	1.50	0.00	0.00
LGALS3	1.50	0.00	0.00
caffeic acid phenethyl ester	1.50	0.00	0.00
SPP1	1.50	0.00	0.00
let-7a-2-3p (and other miRNAs w/seed UGUACAG)	1.49	0.00	0.00
2-amino-1-methyl-6-phenylimidazo-4-5-b-pyridine	1.49	0.00	0.00
Hbb-b2	1.47	0.00	0.00
ZFTA-RELA	1.45	0.00	0.00
NR4A1	1.45	0.00	0.00
TNF	1.44	2.82	1.92
resiquimod	1.44	0.00	1.72
decitabine	1.44	3.96	0.00
dimethylnitrosamine	1.44	0.00	0.00
D-fructose	1.44	0.00	0.00
ADRA1B	1.44	0.00	0.00
n-3 fatty acids	1.44	0.00	0.00
ADRA1D	1.44	0.00	0.00
ZFA-fmk	1.43	3.04	0.00
octyl gallate	1.43	0.00	1.93
(S)-mevalonic acid	1.43	0.00	1.93
COX6A2	1.43	0.00	1.93
taselisib	1.43	1.33	0.00
PDZ1i	1.43	1.33	0.00
UFL1	1.43	1.33	0.00
ZYX	1.43	1.33	0.00
obinutuzumab	1.43	1.33	0.00
Z-VRPR-FMK	1.43	1.33	0.00

Pik3r	1.43	1.33	0.00
GRIA2	1.43	1.33	0.00
GMFG	1.43	0.00	0.00
Cbp/p300-Maf-Nfe2l2	1.43	0.00	0.00
TUT1	1.43	0.00	0.00
PMCH	1.43	0.00	0.00
BB-Cl-amidine	1.43	0.00	0.00
2,2'-dipyridyl	1.43	0.00	0.00
NEFL	1.43	0.00	0.00
salvianolic acid A	1.43	0.00	0.00
EN2	1.43	0.00	0.00
adenosine dialdehyde	1.43	0.00	0.00
HOXB1	1.43	0.00	0.00
DOHH	1.43	0.00	0.00
OBP2B	1.43	0.00	0.00
SAG	1.43	0.00	0.00
eprosartan	1.43	0.00	0.00
POM121/POM121C	1.43	0.00	0.00
tirbanibulin	1.43	0.00	0.00
HSD17B12	1.43	0.00	0.00
Fructus xanthii aqueous extract	1.43	0.00	0.00
ECT2	1.43	0.00	0.00
ANLN	1.42	0.00	0.00
AURK	1.42	0.00	0.00
AVP	1.40	0.00	0.00
TGFB3	1.40	0.00	0.00
FGF2	1.39	0.00	0.00
EDN1	1.39	0.00	0.00
CD 437	1.39	0.00	0.00

STK11	1.39	0.00	1.68
TEAD2	1.39	2.11	0.00
Alpha catenin	1.39	0.00	0.00
NR3C1	1.38	0.00	1.86
TEAD3	1.37	2.09	0.00
inosine	1.37	2.09	0.00
ADRA1A	1.37	0.00	0.00
1,2-dithiol-3-thione	1.37	2.85	0.00
IRF3	1.37	0.00	2.10
temsirolimus	1.36	2.89	0.00
PDE6B	1.36	0.00	1.86
benzoquinone	1.36	0.00	1.86
TMPO	1.36	0.00	0.00
catumaxomab	1.36	0.00	0.00
geranylgeraniol	1.36	0.00	0.00
DGAT2	1.36	0.00	0.00
GLP-1 (7-36) amide	1.36	0.00	0.00
SLC39A14	1.36	0.00	0.00
Collagen type III	1.36	0.00	0.00
NUP107	1.36	0.00	0.00
urotensin II	1.36	0.00	0.00
N-methyl mesoporphyrin IX	1.36	0.00	0.00
penfluridol	1.36	0.00	0.00
HMGCR	1.36	0.00	0.00
PHIP	1.36	0.00	0.00
acetic acid	1.36	2.18	0.00
CKAP2L	1.36	0.00	0.00
ROCK	1.34	0.00	0.00
3-nitropropionic acid	1.34	0.00	0.00

FGF10	1.33	0.00	0.00
iron	1.33	0.00	0.00
SRC	1.33	2.44	1.58
SMARCA4	1.32	0.00	0.00
LMNB1	1.31	2.00	0.00
STEAP3	1.31	0.00	0.00
ACSL4	1.31	0.00	0.00
simvastatin	1.31	0.00	0.00
C4BP	1.31	2.77	0.00
MDL 28170	1.31	0.00	1.81
HELZ2	1.31	0.00	0.00
PLA2G5	1.31	0.00	0.00
ANGPTL8	1.31	0.00	0.00
BLACAT1	1.31	0.00	0.00
DKC1	1.31	0.00	0.00
JNJ-39933673	1.31	0.00	0.00
PPM1A	1.31	0.00	0.00
levetiracetam	1.31	0.00	0.00
retinaldehyde	1.31	0.00	0.00
cholestyramine	1.31	0.00	0.00
PLP2	1.31	0.00	0.00
GAL3ST1	1.31	0.00	0.00
3,5-L-diiodothyronine	1.31	0.00	0.00
EMX2	1.31	0.00	0.00
PBX2	1.31	0.00	0.00
ADGRG3	1.31	0.00	0.00
LATS	1.31	0.00	0.00
ibudilast	1.31	0.00	0.00
FBXL5	1.31	0.00	0.00

SMARCA1	1.31	0.00	0.00
ARX	1.31	0.00	0.00
NUAK1	1.31	0.00	0.00
Cyclin A	1.31	0.00	0.00
TP73	0.93	0.00	1.33
nitrofurantoin	0.00	6.05	1.38
puromycin aminonucleoside	0.00	5.56	1.70
allopurinol	0.00	4.88	1.80
SYVN1	0.00	2.24	3.75
PSEN1	0.00	1.85	3.93
Fus	0.00	5.77	0.00
GABARAPL2	0.00	2.81	2.83
mibolerone	0.00	3.05	2.58
GABARAPL1	0.00	2.77	2.80
GABARAP	0.00	2.73	2.77
cisplatin	0.00	1.58	3.84
rosiglitazone	0.00	0.00	5.36
indomethacin	0.00	2.44	2.87
(-)-norephedrine	0.00	5.31	0.00
ciprofloxacin	0.00	3.58	1.70
hexachlorobenzene	0.00	5.22	0.00
SREBF2	0.00	5.12	0.00
MITF	0.00	5.11	0.00
GABA	0.00	5.08	0.00
trichostatin A	0.00	4.97	0.00
WDFY2	0.00	3.04	1.93
gentamicin C	0.00	4.93	0.00
lomustine	0.00	4.89	0.00
triamterene	0.00	4.85	0.00

fenamic acid	0.00	4.74	0.00
phenacetin	0.00	4.70	0.00
captopril	0.00	2.44	1.98
pitavastatin	0.00	2.95	1.30
tamoxifen	0.00	4.23	0.00
SYNJ1	0.00	1.80	2.41
HTT	0.00	0.00	4.17
SREBF1	0.00	4.10	0.00
RPTOR	0.00	3.98	0.00
phytohemagglutinin	0.00	1.45	2.53
CDKN1B	0.00	0.00	3.94
ATN1	0.00	2.36	1.55
CYP51A1	0.00	3.88	0.00
CYP26A1	0.00	1.63	2.23
tazemetostat	0.00	3.77	0.00
SP2509	0.00	3.70	0.00
CLPP	0.00	1.66	2.02
cadmium	0.00	1.66	2.02
PPARGC1A	0.00	3.61	0.00
sertindole	0.00	1.50	2.11
ethionine	0.00	3.55	0.00
TARDBP	0.00	3.54	0.00
USP8	0.00	0.00	3.54
FOXO4	0.00	3.50	0.00
TSC2	0.00	3.49	0.00
phytol	0.00	1.41	2.01
IL1B	0.00	1.62	1.76
eflornithine	0.00	3.35	0.00
CLDN7	0.00	3.34	0.00

poly rI:rC-RNA	0.00	2.00	1.32
Akt	0.00	1.91	1.40
nocodazole	0.00	1.44	1.86
nimesulide	0.00	0.00	3.30
IGF2	0.00	1.93	1.36
Congo Red	0.00	1.33	1.93
EIF3M	0.00	1.33	1.93
CYP26B1	0.00	1.33	1.93
MYCL	0.00	3.23	0.00
PAX3	0.00	0.00	3.22
ESRRG	0.00	0.00	3.22
KDM5A	0.00	1.66	1.55
2-bromoethylamine	0.00	3.21	0.00
SLC2A4	0.00	1.85	1.35
CRHR2	0.00	1.85	1.35
Pkg	0.00	1.85	1.35
taxifolin	0.00	0.00	3.20
LCP2	0.00	3.17	0.00
AKT1	0.00	3.16	0.00
cyclophosphamide	0.00	0.00	3.15
ERK1/2	0.00	1.43	1.64
Zn2+	0.00	0.00	3.07
Am 580	0.00	3.05	0.00
cycloheximide	0.00	0.00	3.05
pirinixic acid	0.00	3.03	0.00
cyclosporin A	0.00	2.99	0.00
RPS15	0.00	2.99	0.00
CD24	0.00	0.00	2.90
glucosylceramide	0.00	2.89	0.00

SNED1	0.00	2.89	0.00
phenylbutazone	0.00	2.88	0.00
IFNA2	0.00	0.00	2.86
SH3TC2	0.00	2.81	0.00
ferulic acid	0.00	0.00	2.80
LDL	0.00	2.78	0.00
U0126	0.00	2.76	0.00
SP3	0.00	2.76	0.00
MW-III-36C	0.00	0.00	2.71
CALHM1	0.00	0.00	2.71
diflunisal	0.00	0.00	2.71
SHC3	0.00	0.00	2.71
CRB2	0.00	0.00	2.71
STMN2	0.00	0.00	2.71
ACOT8	0.00	0.00	2.71
LY2811376	0.00	0.00	2.71
RTN1	0.00	0.00	2.71
soluble gamma-secretase modulator 41	0.00	0.00	2.71
PK 11195	0.00	0.00	2.71
RS86	0.00	0.00	2.71
N6-methyl-(R)-roscovitine	0.00	0.00	2.71
donepezil	0.00	0.00	2.71
soluble gamma-secretase modulator 49	0.00	0.00	2.71
JIP1/2/3	0.00	0.00	2.71
acetylcholinesterase inhibitor	0.00	0.00	2.71
ENTPD7	0.00	0.00	2.71
RGL1	0.00	0.00	2.71
PAK3	0.00	0.00	2.71
PPP1R9B	0.00	0.00	2.71

SKI-213271	0.00	0.00	2.71
bapineuzumab	0.00	0.00	2.71
GSAP	0.00	0.00	2.71
BTA-EG4	0.00	0.00	2.71
ECE	0.00	0.00	2.71
BACE2	0.00	0.00	2.71
IC261	0.00	0.00	2.71
KLC1	0.00	0.00	2.71
SKI-190986	0.00	0.00	2.71
sphingosine kinase inhibitor V	0.00	0.00	2.71
ARF3	0.00	0.00	2.71
AP4E1	0.00	0.00	2.71
iso-alpha acid	0.00	0.00	2.71
CLN5	0.00	0.00	2.71
ABCA2	0.00	0.00	2.71
TOM1	0.00	0.00	2.71
4-hydroxybutanoic acid	0.00	0.00	2.71
MC622	0.00	0.00	2.71
soluble gamma-secretase modulator 46	0.00	0.00	2.71
NECAB3	0.00	0.00	2.71
pinacidil	0.00	0.00	2.71
ITM2C	0.00	0.00	2.71
QPCT	0.00	0.00	2.71
infigratinib	0.00	0.00	2.71
MEDI-547	0.00	0.00	2.71
CS-1	0.00	0.00	2.71
CRANAD-17	0.00	0.00	2.71
EG443	0.00	0.00	2.71
FBXL20	0.00	0.00	2.71

CHF 5074	0.00	0.00	2.71
MC55w21	0.00	0.00	2.71
HM13	0.00	0.00	2.71
APBA2	0.00	0.00	2.71
MC55w10	0.00	0.00	2.71
CNTNAP1	0.00	0.00	2.71
ECE2	0.00	0.00	2.71
aleplasinin	0.00	0.00	2.71
ARCN1	0.00	0.00	2.71
D-4476	0.00	0.00	2.71
ginsenoside Rg3	0.00	0.00	2.71
FBXL2	0.00	0.00	2.71
SERPINH1	0.00	2.66	0.00
EIF3A	0.00	2.66	0.00
STK17A	0.00	2.66	0.00
mir-1	0.00	2.66	0.00
TWIST1	0.00	2.66	0.00
RNA polymerase II	0.00	0.00	2.66
CG	0.00	0.00	2.64
CREB1	0.00	2.64	0.00
TCF4	0.00	2.63	0.00
FOS	0.00	2.61	0.00
rasagiline	0.00	0.00	2.60
22(R)-hydroxycholesterol	0.00	0.00	2.57
LINC01139	0.00	2.57	0.00
amiodarone	0.00	2.54	0.00
GSN	0.00	2.48	0.00
ASAH1	0.00	2.47	0.00
HNRNPH1	0.00	0.00	2.45

HDL-cholesterol	0.00	2.44	0.00
paclitaxel	0.00	2.43	0.00
sildenafil	0.00	0.00	2.41
ATP7B	0.00	2.41	0.00
trandolapril	0.00	0.00	2.41
SPON1	0.00	0.00	2.41
SLC26A4-AS1	0.00	0.00	2.41
RER1	0.00	0.00	2.41
NAT8B	0.00	0.00	2.41
NAT8	0.00	0.00	2.41
SORCS1	0.00	0.00	2.41
meclofenamic acid	0.00	0.00	2.41
CIB1	0.00	0.00	2.41
NGB	0.00	0.00	2.41
SNRPA	0.00	0.00	2.41
SLC9A6	0.00	0.00	2.41
SLC11A2	0.00	0.00	2.41
MTHFR	0.00	0.00	2.41
PICALM	0.00	0.00	2.41
Z-IL-CHO	0.00	0.00	2.41
fenoprofen	0.00	0.00	2.41
RTN3	0.00	0.00	2.41
RTN2	0.00	0.00	2.41
ECE1	0.00	0.00	2.41
IDE	0.00	0.00	2.41
mir-644	0.00	0.00	2.41
ZNF326	0.00	0.00	2.41
APBA1	0.00	0.00	2.41
T-type Calcium Channel	0.00	0.00	2.41

INK4	0.00	0.00	2.41
ITM2B	0.00	0.00	2.41
IFITM3	0.00	0.00	2.41
necrostatin-1s	0.00	0.00	2.41
BACE1-AS	0.00	0.00	2.41
SORT1	0.00	2.41	0.00
lysophosphatidylcholine	0.00	2.40	0.00
TIMP3	0.00	0.00	2.35
MAOA	0.00	2.34	0.00
SUZ12	0.00	2.33	0.00
IRGM	0.00	0.00	2.31
RTN4	0.00	0.00	2.31
Z-LLL-CHO	0.00	0.00	2.31
5-azacytidine	0.00	0.00	2.30
RIPK1	0.00	0.00	2.30
NPC1	0.00	2.27	0.00
COL9A1	0.00	2.27	0.00
SAT1	0.00	2.27	0.00
methylprednisolone	0.00	2.27	0.00
ESR2	0.00	2.25	0.00
CCND1	0.00	2.24	0.00
Beta Secretase	0.00	0.00	2.23
HSPA4	0.00	0.00	2.23
E64	0.00	0.00	2.23
VDAC1	0.00	0.00	2.23
CSNK1E	0.00	0.00	2.23
tretinoin tocoferil	0.00	0.00	2.23
mir-346	0.00	0.00	2.23
Ly6a (includes others)	0.00	0.00	2.23

SNRNP70	0.00	0.00	2.23
3K3A-APC protein	0.00	0.00	2.23
WASF1	0.00	0.00	2.23
oleuropein aglycone	0.00	0.00	2.23
opaganib	0.00	0.00	2.23
mir-153	0.00	0.00	2.23
arundic acid	0.00	0.00	2.23
CDKN1A	0.00	2.22	0.00
IGFBP7	0.00	2.21	0.00
aldesleukin	0.00	2.21	0.00
HIC1	0.00	0.00	2.19
triamcinolone acetonide	0.00	2.19	0.00
Mek	0.00	2.18	0.00
FOXO3	0.00	2.16	0.00
tunicamycin	0.00	2.16	0.00
JUN	0.00	2.15	0.00
pioglitazone	0.00	0.00	2.14
capsaicin	0.00	0.00	2.14
tributyrin	0.00	0.00	2.14
fulvestrant	0.00	2.13	0.00
mir-210	0.00	2.12	0.00
NRIP1	0.00	0.00	2.11
RHO	0.00	0.00	2.11
cytarabine	0.00	0.00	2.11
SNX17	0.00	0.00	2.11
APH-1	0.00	0.00	2.11
ZDHHC21	0.00	0.00	2.11
GGA1	0.00	0.00	2.11
KLK6	0.00	0.00	2.11

GGA3	0.00	0.00	2.11
cromolyn	0.00	0.00	2.11
tetrahydrocurcumin	0.00	0.00	2.11
TTR	0.00	0.00	2.11
mir-298	0.00	0.00	2.11
VPS26A	0.00	0.00	2.11
leucine-2-alanine enkephalin	0.00	0.00	2.11
phosphoramidon	0.00	0.00	2.11
D-2-amino-5-phosphonovaleric acid	0.00	0.00	2.11
DHCR24	0.00	0.00	2.11
ACP1	0.00	0.00	2.11
AP2A1	0.00	0.00	2.11
MME	0.00	0.00	2.11
LAPTM4B	0.00	0.00	2.11
mir-147	0.00	0.00	2.11
RNASEH1	0.00	0.00	2.11
ANGPT2	0.00	2.10	0.00
Smad2/3-Smad4	0.00	2.10	0.00
trovafloxacin	0.00	0.00	2.10
ETF1	0.00	2.10	0.00
PRELID1	0.00	2.10	0.00
mir-675	0.00	2.10	0.00
azide	0.00	2.10	0.00
CFD	0.00	2.10	0.00
3-tert-butyl-4-hydroxyanisole	0.00	2.10	0.00
CFI	0.00	2.10	0.00
nafoxidine	0.00	2.10	0.00
PI16	0.00	2.10	0.00
Triton X-100	0.00	2.10	0.00

mir-1285	0.00	2.10	0.00
ASB13	0.00	2.10	0.00
TLL1	0.00	2.10	0.00
RAF1	0.00	2.09	0.00
RGS2	0.00	2.09	0.00
FASN	0.00	0.00	2.09
MAP2K5	0.00	2.09	0.00
CD46	0.00	2.05	0.00
ESR1	0.00	2.05	0.00
triacylglycerol	0.00	0.00	2.01
atenolol	0.00	0.00	2.01
MPO	0.00	0.00	2.01
DNM1	0.00	0.00	2.01
mini-GAGR	0.00	0.00	2.01
DDX21	0.00	0.00	2.01
lansoprazole	0.00	0.00	2.01
IgG2b	0.00	0.00	2.01
ZC3H10	0.00	0.00	2.01
SORL1	0.00	0.00	2.01
LGMN	0.00	0.00	2.01
spiperone	0.00	0.00	2.01
WZ-4002	0.00	0.00	2.01
SMPD3	0.00	0.00	2.01
HK2	0.00	0.00	2.01
Cr6+	0.00	0.00	2.01
SGMS1	0.00	0.00	2.01
SNX27	0.00	0.00	2.01
PROM1	0.00	2.01	0.00
DAG1	0.00	2.01	0.00

FGF21	0.00	2.00	0.00
APOA1	0.00	1.98	0.00
FAS	0.00	1.97	0.00
doxorubicin	0.00	1.97	0.00
IAPP	0.00	1.96	0.00
epigallocatechin-gallate	0.00	0.00	1.95
mir-204	0.00	1.94	0.00
zinc	0.00	0.00	1.94
PRKAA1	0.00	1.93	0.00
(-)-arctigenin	0.00	0.00	1.93
GSK690693	0.00	0.00	1.93
aurintricarboxylic acid	0.00	0.00	1.93
RGFP966	0.00	0.00	1.93
13-hydroxyoctadecadienoic acid	0.00	0.00	1.93
furosemide	0.00	0.00	1.93
AATF	0.00	0.00	1.93
USF1	0.00	0.00	1.93
mir-15	0.00	0.00	1.93
diethylstilbestrol	0.00	1.91	0.00
prednisolone	0.00	0.00	1.91
cholesterol	0.00	1.90	0.00
GNA15	0.00	1.90	0.00
KIF3A	0.00	1.88	0.00
IL1A	0.00	0.00	1.88
D-glucose	0.00	0.00	1.87
RTN4R	0.00	0.00	1.86
antisense oligonucleotide	0.00	0.00	1.86
mir-296	0.00	0.00	1.86
DVL1	0.00	0.00	1.86

rutin	0.00	0.00	1.86
ST6GALNAC1	0.00	0.00	1.86
TNKS	0.00	0.00	1.86
PT-2385	0.00	0.00	1.86
2-hydroxyestradiol	0.00	0.00	1.86
EHT-1864	0.00	0.00	1.86
PSENEN	0.00	0.00	1.86
3,5-dihydroxyphenylglycine	0.00	0.00	1.86
SOAT1	0.00	0.00	1.86
phorbol esters	0.00	0.00	1.86
RELA	0.00	0.00	1.85
trans-hydroxytamoxifen	0.00	1.83	0.00
OTX2	0.00	1.82	0.00
sunitinib	0.00	1.82	0.00
2-(4-amino-1-isopropyl-1H-pyrazolo[3,4-d]pyrimidin-3-yl)-1H-indol-5-ol	0.00	1.82	0.00
diosgenin	0.00	1.81	0.00
ganglioside GM1	0.00	0.00	1.81
TRPC4AP	0.00	0.00	1.81
raclopride	0.00	0.00	1.81
pyrophosphate	0.00	0.00	1.81
alpha-tocopherol succinate	0.00	0.00	1.81
L-type Calcium Channel	0.00	0.00	1.81
CXCR1	0.00	0.00	1.81
motexafin gadolinium	0.00	0.00	1.81
TTN	0.00	0.00	1.81
protocatechuic acid	0.00	0.00	1.81
cinnamon powder	0.00	0.00	1.81
GRK5	0.00	0.00	1.81
FBXO2	0.00	0.00	1.81

CD33	0.00	0.00	1.81
EPHA4	0.00	0.00	1.81
MRE11	0.00	0.00	1.81
TSH	0.00	1.81	0.00
SPTLC1	0.00	1.80	0.00
EGFL6	0.00	1.80	0.00
EIF3H	0.00	1.80	0.00
HPS1	0.00	1.80	0.00
lanreotide	0.00	1.80	0.00
FRZB	0.00	1.80	0.00
ADAMTS13	0.00	1.80	0.00
gliclazide	0.00	1.80	0.00
PLEKHA2	0.00	1.80	0.00
Rab11	0.00	1.80	0.00
SRRT	0.00	1.80	0.00
glucose oxidase	0.00	1.80	0.00
COMP	0.00	1.80	0.00
8-aminoadenosine	0.00	1.80	0.00
PX 478	0.00	1.80	0.00
DRP2	0.00	1.80	0.00
MLIP	0.00	1.80	0.00
PLEKHA1	0.00	1.80	0.00
BAZ1A	0.00	1.80	0.00
PRSS3	0.00	1.80	0.00
4-nitrobenzoic acid	0.00	1.80	0.00
indotecan	0.00	1.80	0.00
NOXO1	0.00	1.80	0.00
COL11A1	0.00	1.80	0.00
UC2288	0.00	1.80	0.00

STK38L	0.00	1.80	0.00
RPLP2	0.00	1.80	0.00
4-hydroxytamoxifen	0.00	1.80	0.00
lenalidomide	0.00	1.78	0.00
HEXIM1	0.00	1.78	0.00
phosphate	0.00	0.00	1.77
racemic flurbiprofen	0.00	0.00	1.76
Ighg2b	0.00	0.00	1.76
BIN1	0.00	0.00	1.76
SLC30A3	0.00	0.00	1.76
APH1A	0.00	0.00	1.76
mir-455	0.00	0.00	1.76
RFXAP	0.00	0.00	1.76
dantrolene	0.00	0.00	1.76
DNM3OS	0.00	0.00	1.76
BCKDK	0.00	0.00	1.76
pentazocine	0.00	0.00	1.76
SPDEF	0.00	1.75	0.00
PPARG	0.00	0.00	1.74
LIPE	0.00	1.74	0.00
bromobenzene	0.00	1.74	0.00
OGT	0.00	0.00	1.73
PLAU	0.00	1.72	0.00
Mapk	0.00	0.00	1.72
tanespimycin	0.00	1.72	0.00
JUN/JUNB/JUND	0.00	1.71	0.00
CTSS	0.00	1.71	0.00
K-252	0.00	1.71	0.00
ABCA7	0.00	0.00	1.71

N-chlorotaurine	0.00	0.00	1.71
Cd33	0.00	0.00	1.71
TAPI-1	0.00	0.00	1.71
RELN	0.00	0.00	1.71
FRMD6	0.00	0.00	1.71
calcium chloride	0.00	0.00	1.71
oxadiazon	0.00	0.00	1.71
PTCD1	0.00	0.00	1.71
acitretin	0.00	0.00	1.71
oleoylethanolamide	0.00	0.00	1.71
GDNF	0.00	1.71	0.00
TEAD1	0.00	1.71	0.00
NFKB1	0.00	0.00	1.70
KDM8	0.00	1.69	0.00
KDM3B	0.00	1.69	0.00
sterol	0.00	1.68	0.00
PLA2R1	0.00	1.68	0.00
mir-10	0.00	0.00	1.68
L-triiodothyronine	0.00	0.00	1.68
Brd4	0.00	1.67	0.00
MTF1	0.00	0.00	1.67
nandrolone	0.00	0.00	1.67
4-hydroxyestradiol-17beta	0.00	0.00	1.67
zileuton	0.00	0.00	1.67
Gcn5l	0.00	0.00	1.67
clioquinol	0.00	0.00	1.67
ATP7A	0.00	0.00	1.67
Cu2+	0.00	0.00	1.67
lidocaine	0.00	0.00	1.67

Fcor	0.00	0.00	1.67
cigarette smoke	0.00	1.66	0.00
VEGFA	0.00	0.00	1.66
CHADL	0.00	1.66	0.00
MDM4	0.00	1.66	0.00
tetracycline	0.00	1.64	0.00
ADAM12	0.00	1.64	0.00
Hif1	0.00	1.64	0.00
RXRA	0.00	0.00	1.64
CST3	0.00	0.00	1.63
AFAP1-AS1	0.00	0.00	1.63
naringin	0.00	0.00	1.63
PAWR	0.00	0.00	1.63
KPT-9274	0.00	0.00	1.63
BBP-398	0.00	0.00	1.63
WWC1	0.00	0.00	1.63
Fe2+	0.00	0.00	1.63
BACE1	0.00	0.00	1.63
nicardipine	0.00	0.00	1.63
(-)-epicatechin gallate	0.00	0.00	1.63
HSF4	0.00	0.00	1.63
LGALS3BP	0.00	0.00	1.63
SERPINA3	0.00	0.00	1.63
FLZ	0.00	0.00	1.63
LONP1	0.00	1.63	0.00
COP1	0.00	1.63	0.00
AS1842856	0.00	1.63	0.00
BCYRN1	0.00	1.63	0.00
ADAMTS18	0.00	1.63	0.00

FOXC1	0.00	0.00	1.63
AMPK	0.00	0.00	1.63
Tardbp	0.00	1.63	0.00
PPP1R3C	0.00	1.63	0.00
RBM5-AS1	0.00	1.63	0.00
ethyl-3-trifluoromethylbenzyl-alpha-ketoglutarate	0.00	1.63	0.00
epiallopregnanolone	0.00	1.63	0.00
SLC48A1	0.00	1.63	0.00
NC9	0.00	1.63	0.00
HOXB8	0.00	1.63	0.00
arginine butyrate	0.00	1.63	0.00
3-hydroxybutyrate arginate	0.00	1.63	0.00
Eotaxin	0.00	1.63	0.00
ZNF219	0.00	1.63	0.00
BMP1	0.00	1.63	0.00
GLUD1	0.00	1.63	0.00
EEF1D	0.00	1.63	0.00
TMOD1	0.00	1.63	0.00
norcantharidin	0.00	1.63	0.00
Lycium barbarum polysaccharides	0.00	1.63	0.00
ZSCAN10	0.00	1.63	0.00
GPD1L	0.00	1.63	0.00
C20-D3-vitamin A	0.00	1.63	0.00
OTUB2	0.00	1.63	0.00
ATF7IP	0.00	1.63	0.00
N-butyryl arginine	0.00	1.63	0.00
isoleucine	0.00	1.63	0.00
GW3965	0.00	0.00	1.62
camptothecin	0.00	1.61	0.00

ZBTB48	0.00	1.60	0.00
selumetinib	0.00	1.60	0.00
methylene blue	0.00	0.00	1.60
ATXN3	0.00	0.00	1.60
HPSE	0.00	0.00	1.60
ladostigil	0.00	0.00	1.60
B4GALNT1	0.00	0.00	1.60
L1CAM	0.00	0.00	1.60
GNB3	0.00	0.00	1.60
RUNX2	0.00	0.00	1.59
IL13	0.00	1.59	0.00
SP110	0.00	1.58	0.00
HMOX1	0.00	0.00	1.58
SMARCA5	0.00	0.00	1.58
TRPM2	0.00	1.58	0.00
MXD1	0.00	1.57	0.00
lipopolysaccharide	0.00	0.00	1.57
STOX1	0.00	0.00	1.57
TRPV1	0.00	0.00	1.57
SGPP1	0.00	0.00	1.57
LCOR	0.00	0.00	1.57
D-tubocurarine	0.00	0.00	1.57
Perm1	0.00	0.00	1.57
exisulind	0.00	0.00	1.57
growth factor	0.00	0.00	1.57
FH	0.00	0.00	1.57
beta-1,3-glucan	0.00	0.00	1.57
PPP3CA	0.00	1.56	0.00
PTHLH	0.00	1.56	0.00

IRF2	0.00	0.00	1.55
sodium tungstate	0.00	1.55	0.00
CR1L	0.00	1.55	0.00
ICMT	0.00	1.55	0.00
ACOX1	0.00	1.54	0.00
SIRT7	0.00	0.00	1.54
L-685,458	0.00	0.00	1.54
monophosphoryl lipid A	0.00	0.00	1.54
YARS2	0.00	0.00	1.54
aloxistatin	0.00	0.00	1.54
GTF2I	0.00	0.00	1.54
calpeptin	0.00	0.00	1.54
RFX5	0.00	0.00	1.54
DIRAS3	0.00	0.00	1.54
APBB1	0.00	0.00	1.54
SERTAD2	0.00	0.00	1.54
CLCN5	0.00	0.00	1.54
SIAH2	0.00	0.00	1.54
24-hydroxycholesterol	0.00	0.00	1.54
TERT	0.00	1.53	0.00
ERN1	0.00	1.53	0.00
L-glutamic acid	0.00	0.00	1.53
MAPK7	0.00	1.53	0.00
CEBPA	0.00	1.53	0.00
bardoxolone	0.00	1.53	0.00
Calcineurin A	0.00	1.53	0.00
GLIS2	0.00	1.53	0.00
IFT88	0.00	1.53	0.00
ADORA2A	0.00	0.00	1.52

tretinoin	0.00	1.52	0.00
IFT57	0.00	0.00	1.51
cystamine	0.00	0.00	1.51
copper	0.00	0.00	1.51
MAPK8IP3	0.00	0.00	1.51
caffeic acid	0.00	0.00	1.51
MAPK10	0.00	0.00	1.51
epoprostenol	0.00	0.00	1.51
farnesyl pyrophosphate	0.00	0.00	1.51
AQP1	0.00	0.00	1.51
GAST	0.00	1.51	0.00
NFKBIA	0.00	1.50	0.00
GR-MD-02	0.00	1.50	0.00
tirapazamine	0.00	1.50	0.00
RPL35A	0.00	1.50	0.00
RPS5	0.00	1.50	0.00
firtecan pegol	0.00	1.50	0.00
CASP14	0.00	1.50	0.00
proanthocyanidin derivative	0.00	1.50	0.00
CC8490	0.00	1.50	0.00
GNG13	0.00	1.50	0.00
RPL12	0.00	1.50	0.00
RPS18	0.00	1.50	0.00
TAOK2	0.00	1.50	0.00
phenformin	0.00	1.50	0.00
MIR129	0.00	1.50	0.00
PWWP2A-ROS1	0.00	1.50	0.00
CIL56	0.00	1.50	0.00
S100A2	0.00	1.50	0.00

6-dimethylaminopurine	0.00	1.50	0.00
GNG7	0.00	1.50	0.00
cathepsin L inhibitor	0.00	1.50	0.00
SLAMF7	0.00	1.50	0.00
13(S)-hydroxyoctadecadienoic acid	0.00	1.50	0.00
nabumetone	0.00	1.50	0.00
ruthenium red	0.00	1.50	0.00
thymeleatoxin	0.00	1.50	0.00
ribociclib	0.00	1.50	0.00
NCF2	0.00	1.50	0.00
TRIM65	0.00	1.50	0.00
TAN 67	0.00	1.50	0.00
ITPR	0.00	1.50	0.00
AMELX	0.00	1.50	0.00
ABCC9	0.00	1.50	0.00
DCC	0.00	1.50	0.00
ANKH	0.00	1.50	0.00
glabridin	0.00	1.50	0.00
NBR2	0.00	1.50	0.00
PHLDA1	0.00	1.50	0.00
Ap2	0.00	1.50	0.00
choline	0.00	1.50	0.00
IRF8	0.00	0.00	1.49
IL4	0.00	1.49	0.00
SDC1	0.00	0.00	1.48
pCPT-cAMP	0.00	0.00	1.48
leupeptin	0.00	0.00	1.48
mir-137	0.00	0.00	1.48
ABCC8	0.00	0.00	1.48

ZDHHC7	0.00	0.00	1.48
TNK1	0.00	0.00	1.48
leukotriene C4	0.00	0.00	1.48
doxifluridine	0.00	0.00	1.48
losartan potassium	0.00	0.00	1.48
EGF	0.00	1.48	0.00
SFPQ	0.00	1.48	0.00
L-arginine	0.00	1.48	0.00
GSR	0.00	1.48	0.00
26s Proteasome	0.00	1.48	0.00
atorvastatin	0.00	1.48	0.00
APOE	0.00	0.00	1.47
HNRNPA2B1	0.00	0.00	1.47
NR3C2	0.00	0.00	1.47
NCOA3	0.00	1.47	0.00
AGN194204	0.00	1.46	0.00
S100B	0.00	0.00	1.46
Endothelin	0.00	0.00	1.46
vinorelbine	0.00	0.00	1.46
ATP2A2	0.00	0.00	1.46
8-(4-chlorophenylthio)-guanosine-3', 5'-cyclic monophosphate	0.00	0.00	1.46
mir-515	0.00	0.00	1.46
PGR	0.00	1.46	0.00
diclofenac	0.00	1.46	0.00
halofuginone	0.00	0.00	1.45
TGM2	0.00	1.45	0.00
PPARA	0.00	1.44	0.00
NFE2L1	0.00	1.44	0.00
eprenetapopt	0.00	1.44	0.00

IGHM	0.00	1.44	0.00
ISLR	0.00	1.44	0.00
L-carnitine	0.00	0.00	1.44
27-hydroxycholesterol	0.00	0.00	1.44
leuprolide	0.00	0.00	1.44
triflusal	0.00	0.00	1.44
NUMB	0.00	0.00	1.44
DPP-23	0.00	0.00	1.44
EGOT	0.00	0.00	1.44
CREM	0.00	1.43	0.00
hydrocortisone	0.00	0.00	1.42
STAT1	0.00	0.00	1.42
6-hydroxydopamine	0.00	1.42	0.00
Nr1h	0.00	0.00	1.42
NPM1	0.00	1.42	0.00
MED30	0.00	0.00	1.41
Ncoa-Nr1i2-Rxra	0.00	0.00	1.41
HNRNPA1	0.00	0.00	1.41
betaine	0.00	0.00	1.41
leptomycin B	0.00	0.00	1.41
AURKB	0.00	0.00	1.41
pirfenidone	0.00	0.00	1.41
alitretinoin	0.00	0.00	1.41
RAB23	0.00	1.41	0.00
H19	0.00	1.41	0.00
methylamine	0.00	1.41	0.00
mir-489	0.00	1.41	0.00
SMARCC2	0.00	1.41	0.00
VGLL4	0.00	1.41	0.00

LSP1	0.00	1.41	0.00
CDR2	0.00	1.41	0.00
ACSL6	0.00	1.41	0.00
cinnamyl-3,4-dihydroxy-alpha-cyanocinnamate	0.00	1.41	0.00
hydroxycitric acid	0.00	1.41	0.00
RPS12	0.00	1.41	0.00
BLOC1S6	0.00	1.41	0.00
RPS11	0.00	1.41	0.00
GH2	0.00	1.41	0.00
PDCL	0.00	1.41	0.00
Mst/krs	0.00	1.41	0.00
HCG18	0.00	1.41	0.00
LOC100506098	0.00	1.41	0.00
valproic acid	0.00	1.41	0.00
tetraethylammonium	0.00	1.40	0.00
NR1D1	0.00	1.40	0.00
H89	0.00	0.00	1.39
NLRC5	0.00	0.00	1.39
GF 120918	0.00	0.00	1.39
PER1	0.00	0.00	1.39
ST8SIA1	0.00	0.00	1.39
ADM2	0.00	0.00	1.39
CYP2E1	0.00	0.00	1.39
pilocarpine	0.00	0.00	1.39
T3-TR-RXR	0.00	1.38	0.00
NORAD	0.00	1.38	0.00
ABL1	0.00	1.38	0.00
PC-SPES	0.00	1.37	0.00
ADRB1	0.00	0.00	1.37

edaravone	0.00	0.00	1.37
MAPK8IP1	0.00	0.00	1.37
ADIPOR1	0.00	0.00	1.37
NOX1	0.00	0.00	1.37
Abcb1b	0.00	0.00	1.37
zinc sulfate	0.00	0.00	1.37
TCF7L2	0.00	1.37	0.00
APC	0.00	0.00	1.37
epicatechin	0.00	1.36	0.00
levodopa	0.00	1.36	0.00
PCGEM1	0.00	1.36	0.00
TAZ	0.00	0.00	1.36
HFE	0.00	0.00	1.35
GAS5	0.00	0.00	1.35
KDM4A	0.00	0.00	1.35
EIF4G1	0.00	0.00	1.35
SPHK2	0.00	0.00	1.35
NFE2	0.00	0.00	1.35
genistein	0.00	1.35	0.00
methotrexate	0.00	1.34	0.00
retinoid	0.00	1.34	0.00
WNT7A	0.00	0.00	1.34
vanillin	0.00	0.00	1.34
TGFB1I1	0.00	0.00	1.34
PLD1	0.00	0.00	1.34
shikonin	0.00	0.00	1.34
TINCR	0.00	0.00	1.34
ammonium chloride	0.00	0.00	1.34
LCAT	0.00	0.00	1.34

SAFB2	0.00	0.00	1.34
paroxetine	0.00	0.00	1.34
Hmgb2 (includes others)	0.00	1.33	0.00
GCN2iA	0.00	1.33	0.00
Msx3	0.00	1.33	0.00
Snhg20	0.00	1.33	0.00
CDH13	0.00	1.33	0.00
lestaurtinib	0.00	1.33	0.00
CYP3A	0.00	1.33	0.00
CG-200745	0.00	1.33	0.00
GNMT	0.00	1.33	0.00
CLEC4M	0.00	1.33	0.00
conduritol epoxide	0.00	1.33	0.00
zonisamide	0.00	1.33	0.00
dec-RRLL-cmk	0.00	1.33	0.00
DNMT3L	0.00	1.33	0.00
Gm35986	0.00	1.33	0.00
CPXM1	0.00	1.33	0.00
guanosine triphosphate	0.00	1.33	0.00
DHX36	0.00	1.33	0.00
SSPN	0.00	1.33	0.00
STK38	0.00	1.33	0.00
goralatide	0.00	1.33	0.00
PTH	0.00	0.00	1.33
DNMT3B	0.00	0.00	1.33
TXNRD1	0.00	1.32	0.00
dopamine	0.00	0.00	1.32
norepinephrine	0.00	0.00	1.32
ILK	0.00	1.32	0.00

TNC	0.00	1.32	0.00
4-phenylbutyric acid	0.00	1.32	0.00
calpain	0.00	0.00	1.32
mir-154	0.00	0.00	1.32
LRPAP1	0.00	0.00	1.32
BTG2	0.00	0.00	1.32
raloxifene	0.00	1.31	0.00
MRTFB	0.00	1.31	0.00
tacrolimus	0.00	1.31	0.00
EPAS1	0.00	1.30	0.00
lipid A	0.00	1.30	0.00
HBEGF	0.00	1.30	0.00
beta-carotene	0.00	1.30	0.00
SPRY1	0.00	0.00	1.30
immethridine	0.00	0.00	1.30
SGPL1	0.00	0.00	1.30
ATXN1	0.00	0.00	1.30
ACLY	0.00	0.00	1.30

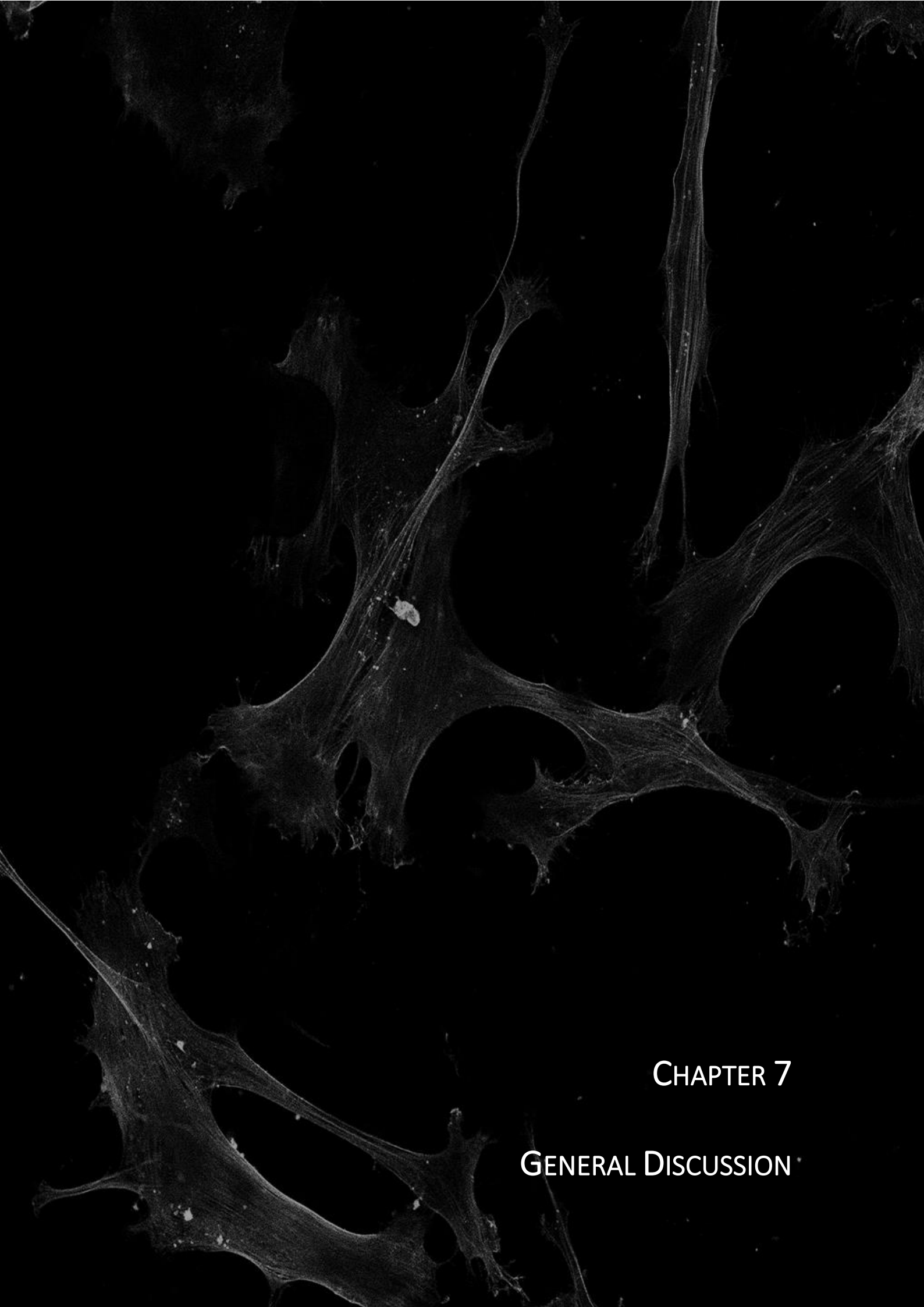

CHAPTER 7

GENERAL DISCUSSION

CHAPTER 7

GENERAL DISCUSSION

The present doctoral thesis is based on the need to develop better biomaterials for bone regeneration and improve current *in vitro* methods. A material needs to present specific characteristics for bone substitution, such as good bulk and mechanical properties and biocompatibility. Even though Ti and its alloys present good mechanical strength and biocompatibility, they are relatively bioinert, and surface modifications are needed to provide these materials with specific features needed for certain clinical applications. The sol-gel process is one of many techniques that allows this surface modification combined and controllably releasing bioactive compounds. Additionally, the difficulties translating *in vitro* results into *in vivo* effects have increased the need to develop better assays capable of predicting patient outcomes. One potent tool to describe the interactions between cells/tissues and materials is proteomics. The characterization of the adsorbed proteins onto a surface or the cell protein expression profile is a viable alternative to overcome the obstacles of the traditional *in vitro* methods.

With these general aims, the experimental design of this thesis consisted of developing different sol-gel coatings doped with selected bioactive agents, *in vitro* characterization with osteoblasts and macrophages cell cultures, description of protein adsorption patterns of said materials, study of the proteomic profile study of osteoblasts exposed to the material with the best *in vitro* response, and correlation between the *in vitro* and proteomic results to define biomarkers for bone regeneration.

The bioactive agents chosen were melatonin (MLT), zinc (Zn), magnesium (Mg), and calcium (Ca). This selection was based on bibliographic research, taking into consideration their effects on bone regenerative processes. MLT has been linked to osteoblast proliferation and differentiation stimulation and bone formation, while Zn is essential in stimulating osteogenesis and mineralization and suppressing osteoclast differentiation. Mg has a comprehensive battery of functions in maintaining normal cell homeostasis, incorporating the hydroxyapatite structure, mineral metabolism, and osteoblast function regulation.

All materials were successfully developed. The addition of each element did not affect the final crosslinking of the sol-gel network, and a controlled degradation and release was obtained. MLT

(**Chapter 2**) increased *RUNX2* and *BMP2* gene expression in 10MTL, but it did not improve ALP activity. No differences were found in the inflammatory response, regardless the MLT concentration. Regarding protein adsorption, MLT doped coatings presented less affinity to proteins related to the complement pathway (CO7, IC1, CO5, CO8A, and CO9), and the affinity to proteins associated with coagulation and angiogenesis (A2GL and PLMN) was also dependent on the MLT concentration. Similarly, Zn (**Chapter 3**) increased the gene expression of *ALP*, *TGF-β*, and *RUNX2* but did not improve ALP activity. The inflammatory response was Zn-dependent. The proteomic analysis showed that Zn increased the adsorption of proteins that regulate the immune reaction (*e.g.*, VTNC, IC1, FHR1, CLUS, and KAIN) and decreased the adsorption of CATB, which is associated with chronic inflammation. In addition, proteins with osteogenic function presented a higher affinity to the materials containing Zn. In **Chapter 4**, Mg-doped materials augmented the expression of osteogenic genes and the ALP activity while reducing TNF-α secretion and increasing anti-inflammatory genes expression. The cells cultured on these materials showed higher cell surface area and integrin gene expression. Mg-doped coatings also presented more affinity with immune-system regulatory proteins (CLUS, IC1, CFAH, and VTNC), proteins related to tissue regeneration (VTNC and CYTA), and cell adhesion (DSG1, FILA2, and DESP).

Then, to improve Mg-doped materials *in vitro* responses via the activation of coagulation, Ca was added to the materials (**Chapter 5**). Ca is one of the most important bone elements and is essential to its structure and metabolism. The concentration of 0.5 wt% of Ca was selected based on previous works by our group. *In vitro* assays showed that the osteogenic response and cell adhesion depended on Mg incorporated into the material. Also, the mixture led to an increment of TNF-α and TGF-β secretion by macrophages. The analysis of protein adsorption revealed that CaMg coatings generally adsorbed more proteins associated with the regulation of inflammatory responses (*e.g.*, ALBU, CLUS, HPT, HPTR, A1AG1, and A1AG2) and cell adhesion (DSG1, DESP, FBLN1, and ZA2G). However, these materials presented less affinity with proteins related to tissue regeneration processes and coagulation (*e.g.,* FA9, FA10, FA11, and FA12). These results showed that ions' interaction in mixtures depends on each ion amount added to the mix and not a simple sum of properties.

The best material (MT1.5Mg) was selected based on previously described results for the characterization of the proteomic profile of HOb exposed to the material (**Chapter 6**). Comparisons between MT and MT1.5Mg allowed comprehending the effects of Mg on the protein expression at three time points (1, 3, and 7 days). MT1.5Mg mainly regulated pathways of early osteoblast differentiation, insulin metabolism, cell adhesion, and oxidative stress. It was

possible to correlate the results obtained here with the ones from Chapter 4. For example, the effects observed on osteogenic gene expression can be related to pathways such as PI3K/AKT, mTOR, and ERK/MAPK. At the same time, the increment of cell adhesion may be explained by the regulation of integrin and FAK signaling and the actin cytoskeleton. With this, it was possible to understand that the action of Mg on osteogenesis and cell adhesion is rather complex by affecting multiple signaling pathways and regulating the expression of several proteins associated with these processes.

Considering the general results obtained, it was possible to correlate the properties of these bioactive agents with *in vitro* results and protein adsorption patterns. Generally, materials with better osteogenic potential (Zn and Mg) presented a higher affinity with proteins associated with regenerative processes, such as VTNC. As it was verified in the materials CaMg, a greater inflammatory response by macrophages was usually accompanied with higher affinity with complement proteins (*e.g.*, CO6, CO5, CO4B, CO4B, and CO9), and acute inflammatory responses (*e.g.*, A1AG1, A1AG2, and AACT). On the other hand, the regulation of macrophage response was correlated with the adsorption of proteins regulatory of inflammation (*e.g.*, CLUS, ALBU, IC1, VTNC) or a lower affinity of the material to complement proteins. Also, specific proteins that can explain the well-known effects of these materials on bone regeneration were found. For example, Zn-doped coatings showed lower affinity to CATB, an enzyme involved in the NF-κB activation, which is essential for osteoclast activation and can clarify Zn effects on osteoclastogenesis. The higher affinity of Mg and CaMg coatings to proteins associated with cell adhesion (*e.g.*, DSG1 and DESP) can explain the Mg effects on cell adhesion and expression of proteins necessary for cell adhesion, such as integrins. Moreover, the analysis of HOb protein expression profiles also shed light on the complex cellular mechanisms involved in the regulation of osteogenesis and cell adhesion by Mg.

The results achieved allowed detecting a characteristic protein adsorption pattern associated with osteogenic responses. The addition of different bioactive agents onto the sol-gel coatings led to the adsorption of specific proteins that can explain the *in vitro* responses verified or well-known effects of these molecules. The application of proteomics can be a powerful technique in the characterization of biomaterials allowing the improvement of current *in vitro* methods.

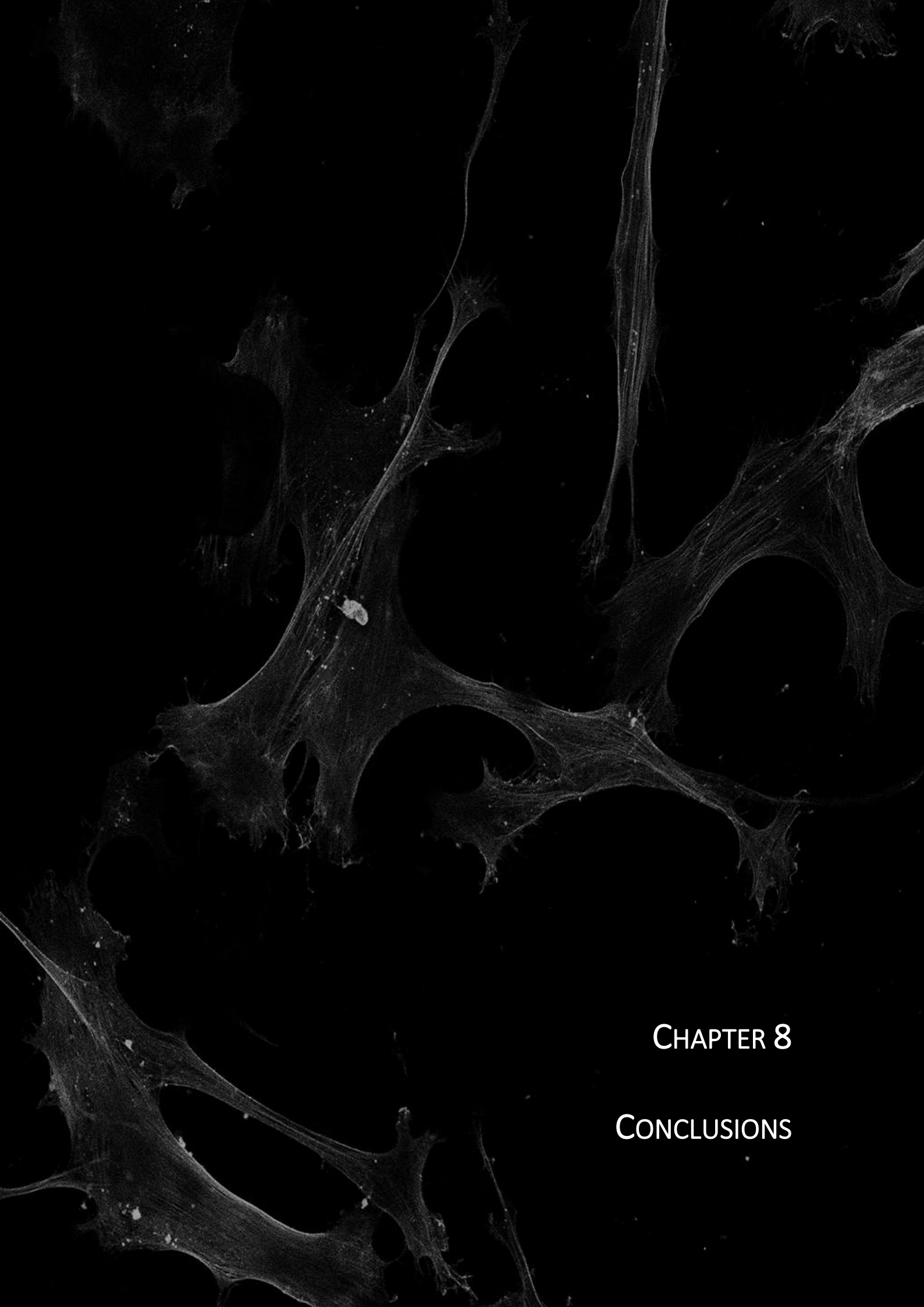

CHAPTER 8

CONCLUSIONS

CHAPTER 8

CONCLUSIONS

The studies presented on this doctoral thesis allow obtaining the following partial conclusions:

- In Chapter 2, MLT presented effects on the induction of osteogenic gene expression at the highest percentage, even though it did not improve cell proliferation and ALP activity. The proteomic analysis showed differences in the adsorption of proteins associated with the complement pathway, coagulation, and angiogenesis, indicating an effect of MLT in these pathways in a dose-response manner.
- In Chapter 3, Zn increased the osteogenic gene expression, while the inflammatory response was dependent on the amount of Zn incorporated into the material. The proteomic analysis revealed that Zn increased the adsorption of proteins that regulate of the immune reaction (*e.g.*, VTNC, IC1, FHR1, CLUS, and KAIN) and decreased the adsorption of CATB, which is associated with chronic inflammation. In addition, proteins with osteogenic function presented a higher affinity to the materials containing Zn.
- In Chapter 4, Mg-doped materials reduced inflammatory TNF-α secretion and increment of anti-inflammatory genes expression while increasing adsorption of immune-system regulatory proteins. The Mg-doped materials also showed a higher affinity to the proteins related to cell adhesion and the cells seeded on them exhibited an increment in the cell surface area and integrin gene expression. Also, Mg augmented the expression of osteogenic genes and the ALP activity, and these samples presented a higher affinity with proteins related to tissue regeneration.
- In Chapter 5, the CaMg materials generally presented higher affinity for complement proteins (*e.g.*, CO6, CO5, CO4B, CO4B, and CO9), and acute inflammatory responses (*e.g.*, A1AG1, A1AG2, and AACT) in a Mg dose-response manner. However, when compared to Ca, CaMg adsorbed more proteins associated with the regulation of inflammatory responses and showed a reduced affinity for proteins associated with inflammation. Additionally, CaMg mixtures generally adsorbed more proteins related to cell adhesion, and cell area increased in a Mg-dependent way. All the materials presented a lower affinity to proteins related to tissue regeneration processes. At the same time, the *in vitro* assays showed that the amount of Mg modulated the ALP activity and osteogenic gene expression.

- In Chapter 6, the analysis for protein expression profiles of osteoblasts seeded onto MT1.5Mg showed regulation by the material of pathways of early osteoblast differentiation, insulin metabolism, cell adhesion, and oxidative stress. MT1.5Mg upregulated several proteins associated with osteogenesis (CO3A1, IGFBP3, and MK01) and significantly affected the expression of myosins (MYO5A, MYO9B, MYL3, and MYLK) and integrins (ITA5, ITB5, and ITA6). In addition, CDC42 and MXRA8, important promotors of cell adhesion, were found upregulated by MT1.5Mg. In contrast, components of the anti-oxidant system (PRDX2, SOD, CATA, and GTSO1) were downregulated.

With this, the general conclusions of this doctoral thesis are:

- The sol-gel technique allowed obtaining release vehicles of MLT and ions and the modification of Ti surfaces.
- The specific proteins adsorbed by the coating of a material are related to the cellular responses of cells seeded onto this surface. Materials with higher osteogenic potential had greater affinity with VTNC. Considering inflammation, the adsorption of CLUS, IC1, CFAH, and VTNC was accompanied by the regulation of inflammation *in vitro*. In specific cases, Zn-doped coatings presented lower affinity with CATB, which may explain its known effects on osteoclastogenesis. On the other hand, Mg-doped coatings adsorbed proteins associated with cell adhesion while increasing the cell area of osteoblasts growing onto these surfaces.
- When cells grow on a material, the surface composition of this material affects multiple cellular pathways. The characterization of the proteomic profile of osteoblasts seeded onto MT1.5Mg showed that the effects of the material on the cell are rather complex, affecting the whole cellular machinery. Osteogenesis and cell adhesion modulation by Mg seem to come from an overall effect rather than on single processes.
- Proteomics presents an excellent potential for biomaterial characterization, either by characterizing proteins adsorbed onto the material surface or by studying the proteomic profiles of cells exposed to the material, allowing the identification of specific markers associated with certain cellular responses. However, more studies applying proteomics in the biomaterials field are needed to better comprehend the *in vitro* responses induced by the materials and improve their design.

CONCLUSIONES

Los estudios presentados en esta tesis doctoral permiten obtener las siguientes conclusiones parciales:

- En el Capítulo 2, MLT mostró los mayores efectos sobre la inducción de la expresión génica osteogénica, aunque no mejoró la proliferación celular ni la actividad ALP. El análisis proteómico mostró diferencias en la adsorción de proteínas asociadas con la vía del complemento, la coagulación y la angiogénesis, lo que indica un efecto dosis-respuesta de la MLT.
- En el Capítulo 3, el Zn aumentó la expresión de los genes osteogénicos, mientras que la respuesta inflamatoria dependió de la cantidad de Zn incorporada al material. El análisis proteómico reveló que el Zn aumentó la adsorción de proteínas reguladoras de la reacción inmune (p.ej., VTNC, IC1, FHR1, CLUS y KAIN) y disminuyó la adsorción de CATB, que está asociada con inflamación crónica. Además, las proteínas con función osteogénica presentaron mayor afinidad por los materiales con Zn.
- En el Capítulo 4, los materiales dopados con Mg redujeron la secreción de citocinas inflamatorias y el incremento de la expresión de genes antiinflamatorios. Simultáneamente, estos recubrimientos aumentaron la adsorción de proteínas reguladoras del sistema inmunológico. Los materiales dopados con Mg también mostraron una mayor afinidad por las proteínas relacionadas con la adhesión celular y se verificó un incremento en el área de superficie celular y la expresión génica de integrinas. Además, la presencia de Mg aumentó la expresión de genes osteogénicos, la actividad ALP y la mayor afinidad por proteínas relacionadas con la regeneración tisular.
- En el Capítulo 5, los materiales de CaMg generalmente presentaron mayor afinidad por las proteínas del complemento (p.ej., CO6, CO5, CO4B, CO4B y CO9) y respuestas inflamatorias agudas (p.ej., A1AG1, A1AG2 y AACT) en una dosis-respuesta de Mg conducta. Sin embargo, en comparación con el Ca, el CaMg adsorbió más proteínas asociadas con la regulación de las respuestas inflamatorias y mostró una afinidad reducida por las proteínas asociadas con la inflamación. Además, las mezclas de CaMg generalmente adsorbieron más proteínas relacionadas con la adhesión celular y el área celular aumentó de manera dependiente del Mg. Todos los materiales presentaron una menor afinidad por las proteínas relacionadas con los procesos de regeneración tisular.

Al mismo tiempo, los ensayos in vitro mostraron que la cantidad de Mg modulaba la actividad ALP y la expresión del gen osteogénico.

- En el Capítulo 6, el análisis de los perfiles de expresión de proteínas de los osteoblastos sembrados en MT1.5Mg mostró la regulación de las vías de diferenciación temprana de los osteoblastos, el metabolismo de la insulina, la adhesión celular y la oxidación del material. MT1.5Mg incrementó varias proteínas asociadas con la osteogénesis (CO3A1, IGFBP3, MK01) y afectó significativamente la expresión de miosinas (MYO5A, MYO9B, MYL3, MYLK) e integrinas (ITA5, ITB5, ITA6). Además, se encontró que Cdc42 y MXRA8, importantes promotores de la adhesión celular estaban regulados positivamente por MT1.5Mg. Sin embargo, el sistema antioxidante (PRDX2, SOD, CATA, GTSO1) fue regulado negativamente.

De este modo, las conclusiones generales que pueden extraerse del trabajo experimental presentado son:

- La técnica sol-gel permitió la obtención de vehículos de liberación de MLT e iones y la modificación de superficies de Ti.
- Las proteínas específicas adsorbidas por el recubrimiento de un material están relacionadas con las respuestas celulares de las células sembradas en esta superficie. Los materiales con mayor potencial osteogénico tuvieron mayor afinidad por VTNC. Considerando las respuestas inflamatorias, la adsorción de CLUS, IC1, CFAH y VTNC estuvo acompañada de la regulación de la inflamación *in vitro*. En algunos casos concretos, los recubrimientos dopados con Zn presentaron menor afinidad con CATB, lo que puede explicar sus efectos conocidos sobre la osteoclastogénesis. Por otro lado, los recubrimientos dopados con Mg adsorbieron proteínas asociadas con la adhesión celular a la vez que aumentó el área celular de los osteoblastos que crecieron sobre estas superficies.
- Cuando las células crecen en un material, la composición de la superficie de este material afecta a múltiples vías celulares. La caracterización del perfil proteómico de los osteoblastos sembrados en MT1.5Mg mostró que los efectos del material en la célula son bastante complejos, afectando a toda la maquinaria celular. La osteogénesis y la modulación de la adhesión celular por Mg parecen provenir de un efecto general más que de procesos únicos.
- La proteómica presenta un excelente potencial para la caracterización de biomateriales, ya sea caracterizando proteínas adsorbidas en la superficie del material o estudiando los perfiles proteómicos de las células expuestas al material, permitiendo la

identificación de marcadores específicos asociados a determinadas respuestas celulares. Sin embargo, se necesitan más estudios que apliquen la proteómica en el campo de los biomateriales para comprender mejor las respuestas *in vitro* inducidas por los materiales y mejorar su diseño.

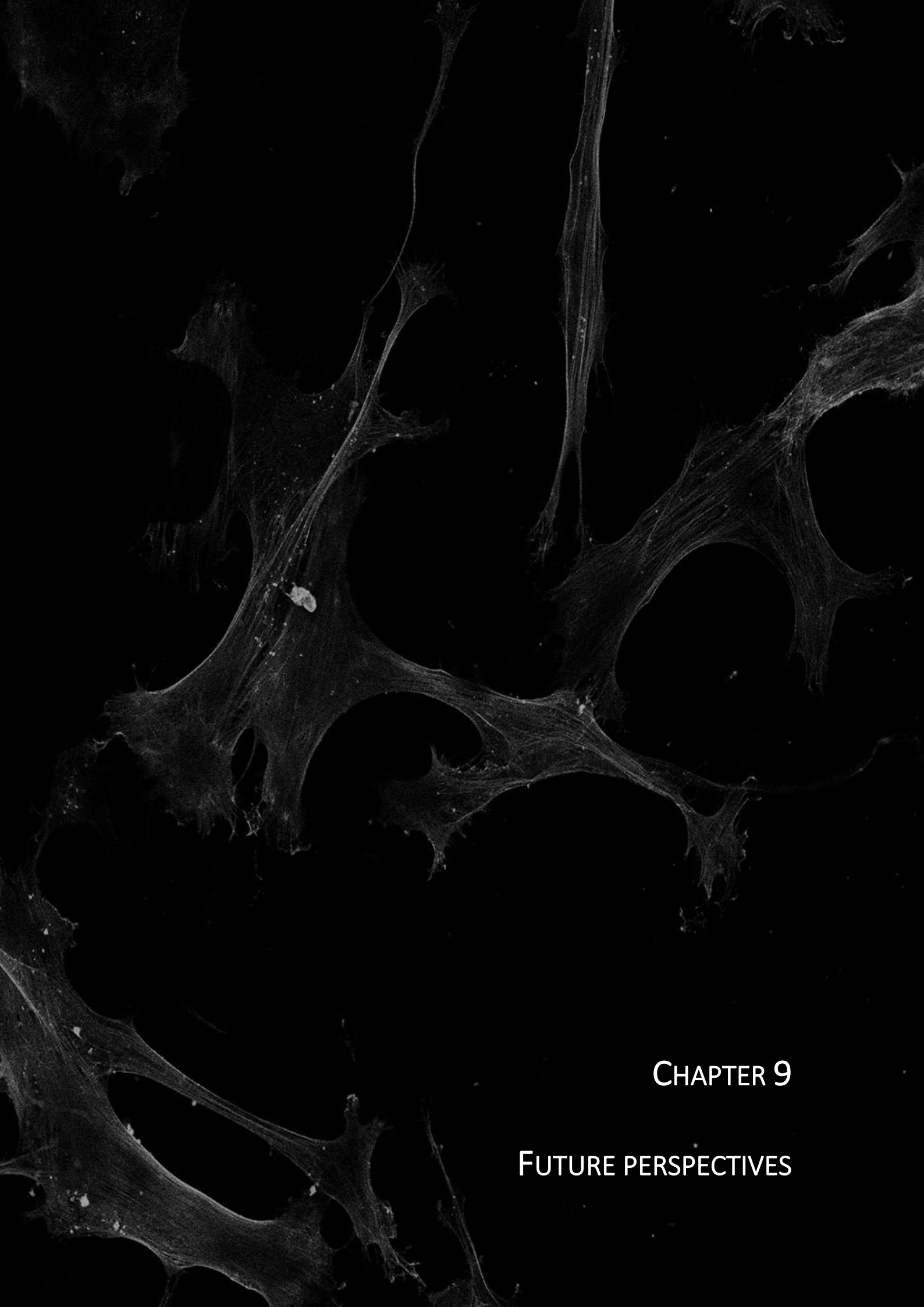

CHAPTER 9

FUTURE PERSPECTIVES

CHAPTER 9

FUTURE PERSPECTIVES

The results presented in this doctoral thesis raise several questions that need further investigation, both for the development of new sol-gel materials and application of proteomics in biomaterial characterization.

Designing new sol-gel coatings with other bioactive molecules, such as boron, copper, and BMPs, may be exciting not only from the biomaterial development standpoint, but can also help optimize our current proteomic assays by identifying clusters of proteins associated with the already described properties of these molecules.

Considering the potentialities of profiling protein expression by cells, assays with longer time points, other cell lines, such as macrophages, and co-culture systems will optimize the current *in vitro* assays and filter newly developed materials. In fact, in the context of the international research stay as a PhD student at Helmholtz-Zentrum Hereon (Germany), *in vitro* studies with macrophages, osteoblasts, and co-culture of macrophages/osteoblasts seeded onto Ti, MT, and MT1.5Mg were performed. This work consisted of the characterization of cell responses with PCR, ELISA, confocal microscopy, and assessment of protein expression with LC-MS/MS. The results are currently being analyzed at Universitat Jaume I and CIC bioGUNE. Moreover, adding more incubation times in the assays with human serum will help understand the dynamics of protein adsorption (Vroman effect). Previously, our group studied this phenomenon in Ti surface modified by calcium deposited after incubation with human serum at three different time points. We found differences in the specific adhered proteins and their quantity over the assay time. Thus, applying this type of assays to other materials will allow a better characterization of the materials developed.

Also, the characterization of these materials and others that we may develop with different cell lines, such as fibroblasts or HUVEC, will new give insights into how they affect angiogenesis and soft tissue regeneration, which are processes key for certain clinical applications, such as dental implants.

Finally, with the results obtained from *in vitro* assays and proteomic characterization, the materials with the best potential will be selected for New Zealand rabbit condyle testing. Their ability to improve implant osseointegration *in vivo* will be evaluated. Furthermore, applying

proteomics to *in vivo* studies also presents an interesting future line of research. With this, it will be possible to comprehend better the complex mechanisms behind the body's response to material implementation. Also, conducting *in vivo* trials at several time points (*e.g.*, one and three weeks after implant surgery) will give a broader insight into tissue regeneration processes.

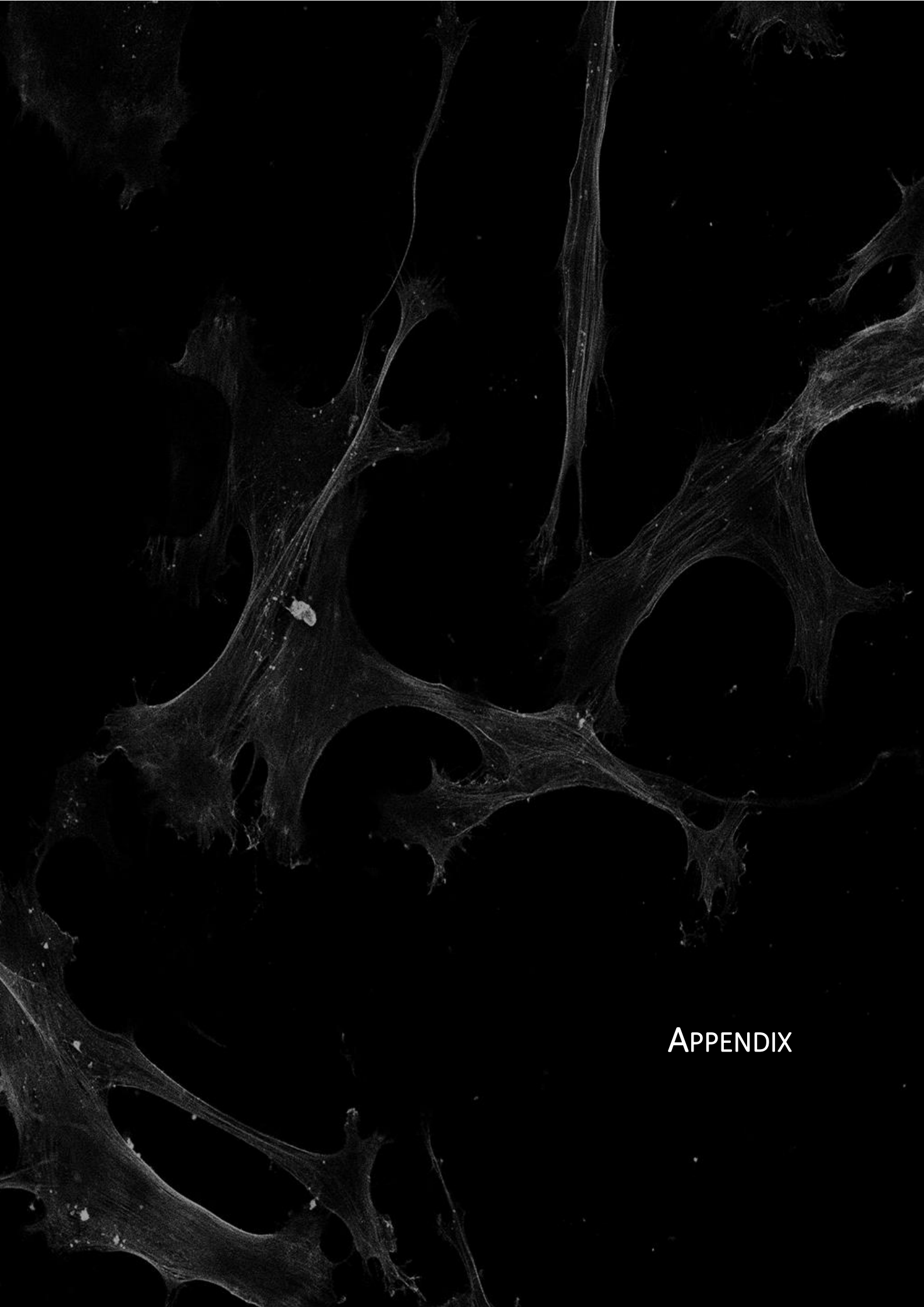

Appendix

I. LIST OF PUBLICATIONS

The list below details the works published in indexed international journals, which are the result of the experimental work carried out during the PhD period:

1. F. Romero-Gavilán; **A. Cerqueira*** *et al.* (2021). Protein adsorption/desorption dynamics on Ca-enriched titanium surfaces: biological implications. JBIC Journal of Biological Inorganic Chemistry, 26(6), 715-726. **Equal contribution*
2. **A. Cerqueira**; *et al.* (2021). Zinc-Doped Sol-gel Coating for Bone Tissue Regeneration: Protein Adsorption and Cellular Responses. eCM Periodical, 2021, Collection 1; 2021 ScSB Abstracts (page P17)
3. **A. Cerqueira**; *et al.* (2021). Correlation Between Proteomics, Macrophage Polarization, and Oxidative Stress in Biomaterials. eCM Periodical, 2021, Collection 1; 2021 ScSB Abstracts (page P48)
4. **A. Cerqueira**; *et* al. (2021). Evaluation of the inflammatory responses to sol–gel coatings with distinct biocompatibility levels. Journal of Biomedical Materials Research Part A.
5. **A. Cerqueira**; *et al.* (2021). Characterization of magnesium doped sol-gel biomaterial for bone tissue regeneration: The effect of Mg ion in protein adsorption. MATERIALS SCIENCE & ENGINEERING C- Materials for Biological Applications. 121, pp. 111839.
6. E. Anitua; **A. Cerqueira**; *et al.* (2021). Influence of calcium ion-modified implant surfaces in protein adsorption and implant integration. International Journal of Implant Dentistry. 7:32.
7. **A. Cerqueira**; F. Romero-Gavilán*; *et al.* (2021). Bioactive zinc-doped sol-gel coating modulates protein adsorption patterns and *in vitro* cell responses. MATERIALS SCIENCE & ENGINEERING C- Materials for Biological Applications. 121, pp. 111839. **Equal contribution*
8. **A. Cerqueira**; *et al.* (2020). Biomaterial biocompatibility: the correlation between the adsorption of complement proteins and macrophage polarization. eCM Periodical. Collection 1; 2020 TERMIS EU Abstracts (page 40)
9. F. Romero-Gavilán; **A. Cerqueira**; *et al.* (2020). Proteomic characterization of calcium-doped sol-gel coatings. eCM Periodical. Collection 1; 2020 TERMIS EU Abstracts (page 67).
10. **A. Cerqueira**; *et al.* (2020). Proteomic and *in vitro* evaluation of Ca-containing sol-gel coatings. Clinical Oral Implants Research, 31, 80-80.

11. F. Romero-Gavilán; **A. Cerqueira**; *et al.* (2020). Gradual complement protein adsorption and macrophage polarization: inflammation & dental implants. Clinical Oral Implants Research, 31, 107-107.

12. **A. Cerqueira**; *et al.* (2020). A possible use of melatonin in the dental field: Protein adsorption and *in vitro* cell response on coated titanium. MATERIALS SCIENCE & ENGINEERING C- Materials for Biological Applications. 116, pp. 1 - 10.

13. F. Romero-Gavilán; J. Carlos-Almeida; **A. Cerqueira**; *et al.* (2020). Sol-gel coatings made using methyl-modified alkoxysilanes: The balance between protection and bioactivation. PROGRESS IN ORGANIC COATINGS. 147, pp. 1 - 10.

14. F. Romero-Gavilán; N. Araújo-Gomes; **A. Cerqueira**; *et al.* (2019). Proteomic analysis of calcium-enriched sol–gel biomaterials. JOURNAL OF BIOLOGICAL INORGANIC CHEMISTRY. 24, pp. 563 - 574.

II. FIRST PAGE OF THE PUBLISHED ARTICLES PRESENTED AS THESIS RESULTS

CHAPTER 2

Materials Science & Engineering C 116 (2020) 111262

Contents lists available at ScienceDirect

Materials Science & Engineering C

journal homepage: www.elsevier.com/locate/msec

A possible use of melatonin in the dental field: Protein adsorption and *in vitro* cell response on coated titanium

Andreia Cerqueira[a], Francisco Romero-Gavilán[a,*], Nuno Araújo-Gomes[b], Iñaki García-Arnáez[c], Cristina Martinez-Ramos[d], Seda Ozturan[e], Mikel Azkargorta[f], Félix Elortza[f], Mariló Gurruchaga[c], Julio Suay[a], Isabel Goñi[c]

[a] Department of Industrial Systems Engineering and Design, Universitat Jaume I, Av. Vicent Sos Baynat s/n, 12071 Castellón de la Plana, Spain
[b] Department of Developmental Bioengineering, University of Twente, Faculty of Science and Technology, 7522LW Enschede, the Netherlands
[c] Facultad de Ciencias Químicas, Universidad del País Vasco, P. M. de Lardizábal, 3, 20018 San Sebastián, Spain
[d] Center for Biomaterials and Tissue Engineering, Universitat Politècnica de Valencia, Camino de Vera, s/n, 46022 Valencia, Spain
[e] Department of Periodontology, Faculty of Dentristy, Istambul Medeniyet University, Istanbul, Turkey
[f] Proteomics Platform, CIC bioGUNE, CIBERehd, ProteoRed-ISCIII, Bizkaia Science and Technology Park, 48160 Derio, Spain

ARTICLE INFO

Keywords:
Osseointegration
Hybrid sol-gel
Inflammation
Proteomics
Coating
N-acetyl-5-metoxy-tryptamine

ABSTRACT

Melatonin (MLT) is widely known for regulating the circadian cycles and has been studied for its role in bone regeneration and inflammation. Its application as a coating for dental implants can condition the local micro-environment, affecting protein deposition on its surface and the cellular and tissue response. Using sol-gel coatings as a release vehicle for MLT, the aim of this work was to assess the potential of this molecule in improving the osseointegration and inflammatory responses of a titanium substrate. The materials obtained were physicochemically characterized (scanning electron microscopy, contact angle, roughness, Fourier-transform infrared spectroscopy, nuclear magnetic resonance, Si release, MLT liberation, and degradation) and studied *in vitro* with MC3T3-E1 osteoblastic cells and RAW264.7 macrophage cells. Although MLT application led to an increased gene expression of RUNX2 and BMP2 in 10MTL, it did not improve ALP activity. On the other hand, MLT-enriched sol-gel materials presented potential effects in the adsorption of proteins related to inflammation, coagulation and angiogenesis pathways depending on the dosage used. Using LC-MS/MS, protein adsorption patterns were studied after incubation with human serum. Proteins related to the complement systems (CO7, IC1, CO5, CO8A, and CO9) were less adsorbed in materials with MLT; on the other hand, proteins with functions in the coagulation and angiogenesis pathways, such as A2GL and PLMN, showed a significant adsorption pattern.

CHAPTER 3

Materials Science & Engineering C 121 (2021) 111839

Contents lists available at ScienceDirect

Materials Science & Engineering C

journal homepage: www.elsevier.com/locate/msec

Bioactive zinc-doped sol-gel coating modulates protein adsorption patterns and in vitro cell responses

A. Cerqueira [a,1], F. Romero-Gavilán [a,*,1], I. García-Arnáez [b], C. Martinez-Ramos [c], S. Ozturan [d], I. Iloro [e], M. Azkargorta [e], F. Elortza [e], R. Izquierdo [a], M. Gurruchaga [b], I. Goñi [b], J. Suay [a]

[a] Department of Industrial Systems Engineering and Design, Universitat Jaume I, Av. Vicent Sos Baynat s/n, 12071 Castellón de la Plana, Spain
[b] Departament of Science and Technology of Polymers, Universidad del País Vasco, P. M. de Lardizábal, 3, 20018 San Sebastián, Spain
[c] Center for Biomaterials and Tissue Engineering, Universitat Politècnica de Valencia, Camino de Vera, s/n, 46022, Valencia, Spain
[d] Department of Periodontology, Faculty of Dentristy, Istanbul Medeniyet University, Istanbul, Turkey
[e] Proteomics Platform, CIC bioGUNE, Basque Research and Technology Alliance (BRTA), CIBERehd, ProteoRed-ISCIII, Bizkaia Science and Technology Park, 48160 Derio, Spain

ARTICLE INFO

Keywords:
Proteomics
Bioinorganic chemistry
Biomaterials
Bone regeneration
Hybrids

ABSTRACT

Zinc is an essential element with an important role in stimulating the osteogenesis and mineralization and suppressing osteoclast differentiation. In this study, new bioactive $ZnCl_2$-doped sol-gel materials were designed to be applied as coatings onto titanium. The biomaterials were physicochemically characterized and the cellular responses evaluated in vitro using MC3T3-E1 osteoblasts and RAW264.7 macrophages. The effect of Zn on the adsorption of human serum proteins onto the material surface was evaluated through nLC-MS/MS. The incorporation of Zn did not affect the crosslinking of the sol-gel network. A controlled Zn^{2+} release was obtained, reaching values below 10 ppm after 21 days. The materials were no cytotoxic and lead to increased gene expression of ALP, TGF-β, and RUNX2 in the osteoblasts. In macrophages, an increase of IL-1β, TGF-β, and IL-4 gene expression was accompanied by a reduced TNF-α liberation. Proteomic results showed changes in the adsorption patterns of proteins associated with immunological, coagulative, and regenerative functions, in a Zn dose-dependent manner. The variations in protein adsorption might lead to the downregulation of the NF-κB pathway, thus explain the observed biological effects of Zn incorporation into biomaterials. Overall, these coatings demonstrated their potential to promote bone tissue regeneration.

CHAPTER 4

Materials Science & Engineering C 125 (2021) 112114

Contents lists available at ScienceDirect

Materials Science & Engineering C

journal homepage: www.elsevier.com/locate/msec

Characterization of magnesium doped sol-gel biomaterial for bone tissue regeneration: The effect of Mg ion in protein adsorption

Andreia Cerqueira [a], Francisco Romero-Gavilán [a,*], Iñaki García-Arnáez [b], Cristina Martinez-Ramos [c], Seda Ozturan [d], Raúl Izquierdo [a], Mikel Azkargorta [e], Félix Elortza [e], Mariló Gurruchaga [b], Julio Suay [a], Isabel Goñi [b]

[a] Department of Industrial Systems Engineering and Design, Universitat Jaume I, Av. Vicent Sos Baynat s/n, 12071 Castellón de la Plana, Spain
[b] Departament of Science and Technology of Polymers, Universidad del País Vasco, P. M. de Lardizábal, 3, 20018 San Sebastián, Spain
[c] Center for Biomaterials and Tissue Engineering, Universitat Politècnica de Valencia, Camino de Vera, s/n, 46022 Valencia, Spain
[d] Department of Periodontology, Faculty of Dentistry, Istanbul Medeniyet University, Dumlupınar D100 Karayolu, 98, 34720 Istanbul, Turkey
[e] Proteomics Platform, CIC bioGUNE, Basque Research and Technology Alliance (BRTA), CIBERehd, ProteoRed-ISCIII, Bizkaia Science and Technology Park, 48160 Derio, Spain

ARTICLE INFO

Keywords:
Mg^{2+}
Biomedical applications
Osseointegration
Proteomics
Hybrids
Integrins

ABSTRACT

Magnesium is the fourth most abundant element in the human body with a wide battery of functions in the maintenance of normal cell homeostasis. In the bone, this element incorporates in the hydroxyapatite structure and it takes part in mineral metabolism and regulates osteoclast functions. In this study, sol-gel materials with increasing concentrations of $MgCl_2$ (0.5, 1, and 1.5%) were synthesized and applied onto Ti surfaces as coatings. The materials were first physicochemically characterized. *In vitro* responses were examined using the MC3T3-E1 osteoblastic cells and RAW264.7 macrophages. Human serum protein adsorption was evaluated employing nLC-MS/MS. The incorporation of Mg did not affect the crosslinking of the sol-gel network, and a controlled release of Mg was observed; it was not cytotoxic at any of the tested concentrations. The cytoskeleton arrangement of MC3T3-E1 cells cultured on the Mg-doped materials changed in comparison with controls; the cells became more elongated, with protruded lamellipodia and increased cell surface. The expression of integrins (ITGA5 and ITGB1) was boosted by Mg-coatings. The ALP activity and expression of TGF-β, OSX and RUNX2 genes were also increased. In RAW264.7 cells, TNF-α secretion was reduced, while TGF-β and IL-4 expression rose. These changes correlated with the altered protein adsorption patterns. The Mg-doped coatings showed increased adsorption of anti-inflammatory (CLUS, IC1, CFAH, and VTNC), cell adhesion (DSG1, FILA2, and DESP) and tissue regeneration (VTNC and CYTA) proteins. This integrated approach to biomaterial characterization revealed the potential of Mg in bone tissue regeneration.

III. WORK PRESENTED AT CONFERENCES

The list below details the works presented at conferences, which are the result of the experimental work, carried out during the PhD period:

1. J. Suay; F. Romero-Gavilán; **A. Cerqueira**; *et al.* (2021). Zinc-modified sol-gel coating: proteomic and *in vitro* study. Poster presented at TERMIS2021. Online format due to COVID-19.
2. **A. Cerqueira**; *et al.* (2021). Sol-gel coatings with Ca-Mg mixtures for titanium implants: effect on bone tissue regeneration. Poster presented at 30th Annual Scientific Meeting of the European Association for Osseointegration (EAO 2021). Online format due to COVID-19.
3. **A. Cerqueira**; *et al*. (2021). The effect of magnesium on protein adsorption in biomaterials for bone tissue regeneration. Oral presentation at European Society for Biomaterials 2021. Online format due to COVID-19.
4. F. Romero-Gavilán; **A. Cerqueira**; *et al.* (2021). The effect of Zn ions in protein adsorption and cell responses. Poster presented at European Society for Biomaterials 2021. Online format due to COVID-19.
5. **A. Cerqueira**; *et al.* (2021). Zinc-Doped Sol-gel Coating for Bone Tissue Regeneration: Protein Adsorption and Cellular Responses. Poster presented at Scandinavian Society for Biomaterials 2021. Online format due to COVID-19.
6. **A. Cerqueira**; *et al*. (2021). Correlation Between Proteomics, Macrophage Polarization, and Oxidative Stress in Biomaterials. Poster presented at Scandinavian Society for Biomaterials 2021. Online format due to COVID-19.
7. F. Romero-Gavilán; **A. Cerqueira**; *et al.* (2020). Identification of protein biomarkers through the design of biomaterials with specific biological functions. Oral presentation at 11th World Biomaterials Congress (WBC2020). Online format due to COVID-19.
8. **A. Cerqueira**; *et al.* (2020). Proteomic and *in vitro* evaluation of Ca-containing sol-gel coatings. Poster presented at 29th Annual Scientific Meeting of the European Association for Osseointegration (EAO 2020). Online format due to COVID-19.
9. F. Romero-Gavilán; **A. Cerqueira**; *et al.* (2020). Gradual complement protein adsorption and macrophage polarization: inflammation & dental implants. Poster presented at 29th Annual Scientific Meeting of the European Association for Osseointegration (EAO 2020). Online format due to COVID-19.

10. F. Romero-Gavilán; **A. Cerqueira**; *et al.* (2020). Proteomic characterization of calcium doped sol-gel coatings. Poster presented at TERMIS2020. Online format due to COVID-19.

11. **A. Cerqueira**; F. Romero-Gavilán; *et al.* (2020). Biomaterial biocompatibility: the correlation between the adsorption of complement proteins and macrophage polarization. Poster presented at TERMIS2020. Online format due to COVID-19.

12. I. García-Arnáez; N. Araújo-Gomes; F. Romero-Gavilán; **A. Cerqueira**; *et al.* (2019). Strontium-enriched sol-gel coatings for highly osteoregenerative biomaterials development. Poster presented at European Society of Biomaterials Congress (ESB). Dresden, Germany.

IV. LIST OF ABBREVIATIONS AND ACRONYMS

GENERAL

^{29}Si-NMR	Solid-state silicon nuclear magnetic resonance spectroscopy
2-Propanol	Isopropanol
AISI	American Iron and Steel Institute
Akt	Protein kinase b
ALP	Alkaline phosphatase
ANOVA	One-way analysis of variance
ATP	Adenosine triphosphate
ATR	Attenuated total reflection system
BCA	Bicinchoninic acid
bFGF	Basic fibroblast growth factor
BGLAP/OCN	Osteocalcin
BMDSC	Bone-marrow-derived stem cell
BMP	Bone morphogenetic protein
BMSC	Bone marrow mesenchymal stem cell
BMU	Basic multicellular unit
BSP	Bone sialoprotein
C	Centigrade
cAMP	Cyclic adenosine 3',5'-monophosphate
cDNA	Complementary DNA
cm	Centimeter
Col1A1	Collagen type I alpha 1
COX	Cyclooxygenase
COX	Cyclooxygenase
CP-MAS	Cross-polarization magic-angle spinning
CREB	cAMP response element-binding protein
CVD	Chemical vapor deposition
DAMP	Damage-associated molecular pattern
DAPI	4’,6-diamidino-2-phenylindole
DAVID	Database for annotation, visualization and integrated discovery
DMEM	Dulbecco's Modified Eagle Medium
DNA	Deoxyribonucleic acid
DPBS	Dulbecco’s phosphate-buffered saline
DTT	Dithiothreitol
ECM	Extracellular matrix
EGR2	Early growth response protein 2
eIF4	Eukaryotic initiation factor 4F
ERK	Extracellular signal-regulated kinase
FA	Focal adhesion
FAK	Focal adhesion kinase
FBS	Fetal bovine serum
FGF	Fibroblast growth factors
FTIR	Fourier Transform Infrared Spectroscopy
g	Gram
GADPH	Glyceraldehyde phosphate dehydrogenase
GF	Growth factors
GP6	Platelet glycoprotein VI
GPTMS	3-glycidoxypropyltrimethoxysilane

h Hour

HBDC Human bone-derived cell

HDL High-density lipoprotein

hFOB1.19 Human fetal osteoblastic cell

hMSC Human mesenchymal stem cell

HOb Human osteoblasts

ICP-MS Inductively coupled plasma mass spectrometry

IFN Interferon

IGF Insulin-like growth factor

IGF Insulin-like growth factors

IL Interleukin

iNOS Nitric oxide synthases

Integrin-linked kinase ILK

IPA Ingenuity® Pathway Analysis

ITGA5 Integrin-α5

ITGB1 Integrin-β1

JNK c-Jun N-terminal cinase

L Liter

LC-MS/MS Liquid chromatography with tandem mass spectrometry

M Molar

MAC Membrane attack complex

MAP Molecule Activity Prediction

MAPK Mitogen-activated protein kinase

MC3T3-E1 Mouse calvaria osteosarcoma

MCP Monocyte chemoattractant protein

Mg Milligram

MIP Macrophage inflammatory protein

mL Milliliter

MLT Melatonin; N-acetyl-5-metoxy-tryptamine

mM Millimolar

MSC Mesenchymal stem cell

MTMOS Methyltrimetoxisilane

mTOR Mechanistic target of rapamycin

NF-κB Nuclear factor kappa-light-chain-enhancer of activated B cell

NF-κB Nuclear factor kappa-light-chain-enhancer of activated B cells

nLC-MS/MS Nano-scale liquid chromatographic tandem mass spectrometry

NO Nitric oxide

OPG Osteoprotegerin

OPN Osteopontin

OSX/SP7 Osterix

PAK p21-activated kinase

PANTHER Protein analysis through evolutionary relationship

PCR Polymerase chain reaction

PDGF Platelet-derived growth factor

PDGF Platelet-derived growth factors

PDMS Polydimethylsiloxane

PI3K Phosphoinositide 3-kinase

PKA cAMP-dependent protein kinase

p-nitrophenylphosphate *p*-NPP

PVD Physical vapor deposition

PVD Physical vapor deposition

qRT-PCR Quantitative real-time PCR

Ra	Roughness
RANK	Receptor activator of nuclear factor kappa-B
RANKL	Receptor Activator of NF-κB Ligand
RANTES	Chemokine (C-C motif) ligand 5
RAW 264.7	Mouse murine macrophage
RNA	Ribonucleic acid
RUNX2	Runt-related transcription factor 2
s	Second
SAE	Sandblasted acid-etched
SBF	Simulated body fluid
SD	Standard deviation
SDS	Sodium dodecyl sulfate
SE	Standard error
SEM	Scanning electron microscopy
TEAB	Triethylammonium bicarbonate buffer
TEOS	Tetraethylorthosilane
TGF	Transforming growth factor
Ti	Titanium
TNF	Tumor necrosis factor
TRAP	Tartrate-resistant acid phosphatase
UV	Ultraviolet
VEGF	Vascular endothelial growth factor
XRD	X-ray diffraction analysis
µL	Microliter
µM	Micromolar

CHEMICAL NOMENCLATURE

Ag	Silver
B	Boron
C	Carbon
Ca	Calcium
$Ca_{10}(PO_4)_6(OH)_2$	Hydroxyapatite
$CaCl_2$	Calcium chloride
CH_3	Methyl
CO	Carbon monoxide
CO_2	Carbon dioxide
H	Hydrogen
H_2O	Water
HCl	Hydrochloric acid
HNO_3	Nitric acid
Mg	Magnesium
$MgCl_2$	Magnesium chloride
N	Nitrogen
OH	Hydroxide
R	Radical
Si	Silicon
Sr	Strontium
Zn	Zinc
$ZnCl_2$	Zinc chloride

PROTEIN NOMENCLATURE

A2GL Leucine-rich alpha-2-glycoprotein

1433S 14-3-3 protein sigma

2A5D Serine/threonine-protein phosphatase 2A 56 kDa regulatory subunit delta isoform

A1AG1 Alpha-1-acid glycoprotein 1

A1AG2 Alpha-1-acid glycoprotein 2

A1AT Alpha-1-antitrypsin

A1BG Alpha-1B-glycoprotein

A2MG Alpha-2-macroglobulin

AACT Alpha-1-antichymotrypsin

ADSV Adseverin

ALBU Serum albumin

ALDOA Fructose-bisphosphate aldolase A

ANT3 Antithrombin-III

APMAP Adipocyte plasma membrane-associated protein

APOA1 Apolipoprotein A-I

APOA2 Apolipoprotein A-II

APOA4 Apolipoprotein A-IV

APOC2 Apolipoprotein C-II

APOC3 Apolipoprotein C-III

APOC4 Apolipoprotein C-IV

APOE Apolipoprotein E

APOF Apolipoprotein F

APOH Beta-2-glycoprotein 1

APOL1 Apolipoprotein L1

APOM Apolipoprotein M

ARHG2 Rho guanine nucleotide exchange factor 2

ATPA ATP synthase subunit alpha. mitochondrial

BLMH Bleomycin hydrolase

C1QC Complement C1q subcomponent subunit C

C1S Complement C1s subcomponent

C4BPA C4b-binding protein alpha chain

CAD13 Cadherin-13

CAN1 Calpain-1 catalytic subunit

CASPE Caspase-14

CATA Catalase

CATB Cathepsin B

CBPB2 Carboxypeptidase B2

CDC42 Cell division control protein 42 homolog

CEMIP Cell migration-inducing and hyaluronan-binding protein

CERU Ceruloplasmin

CFAH Complement factor H

CLUS Clusterin

CO1A1 Collagen alpha-1(I) chain

CO2A1 Collagen alpha-1 (II)

CO3 Complement C3

CO3A1 Collagen alpha-1 (III)

CO4A Complement C4-A

CO4A2 Collagen alpha-2 (IV)

CO4B Complement C4-B

CO5 Complement C5

CO5A2 Collagen alpha-2(V)

CO6 Complement component C6

CO7 Complement component C7

CO7A1 Collagen alpha-1(VII) chain

CO8A Complement component C8 alpha chain

CO8B Complement component C8 beta chain

CO9 Complement component C9

COMP Cartilage oligomeric matrix protein

CRP C-reactive protein

CSK22 Casein kinase II subunit alpha

CUL1 Cullin-1

CXCL7 Platelet basic protein

CYTA Cystatin-A

DCD Dermcidin

DEF3 Neutrophil defensin 3

DESP Desmoplakin

DR9C7 Short-chain dehydrogenase/reductase family 9C member 7

DSG1 Desmoglein-1

EF1A3 Putative elongation factor 1-alpha-like 3

EIF3M Eukaryotic initiation factor 3

ENOA Alpha-enolase

F13B Coagulation factor XIII B chain

FA10 Coagulation factor X

FA11 Coagulation factor XI

FA12 Coagulation factor XII

FA5 Coagulation factor V

FA9 Coagulation factor IX

FBLI1 Filamin-binding LIM protein 1

FBLN1 Fibulin-1

FCN2 Ficolin-2

FHR1 Complement factor H-related protein 1

FHR5 Complement factor H-related protein 5

FILA2 Filaggrin-2

G3P Glyceraldehyde-3-phosphate dehydrogenase

GBB1 Guanine nucleotide-binding protein G(I)/G(S)/G(T) subunit beta-1

GELS Gelsolin

GPX1 Glutathione peroxidase 1

GSDMA Gasdermin-A

GSTO1 Glutathione S-transferase omega-1

H90B2 Putative heat shock protein HSP 90-beta 2

HABP2 Hyaluronan-binding protein 2

HBA Hemoglobin subunit alpha

HBB Hemoglobin subunit beta

HEMO Hemopexin

HEP2 Heparin cofactor 2

HORN Hornerin

HPT Haptoglobin

HPTR Haptoglobin-related protein

HRG Histidine-rich glycoprotein

HSP7C Heat shock cognate 71 kDa protein

HV118 Immunoglobulin heavy variable 1-18

HV551 Immunoglobulin heavy variable 5-51

IBP3 Insulin-like growth factor binding protein-3

IBP4 Insulin-like growth factor-binding protein 4

IC1 Plasma protease C1 inhibitor

IGHA2 Ig alpha-2 chain C region

IGHG2 Immunoglobulin heavy constant gamma 2

IGHG4 Immunoglobulin heavy constant gamma 4

IGHM Immunoglobulin heavy constant mu

IGJ Immunoglobulin J chain

IGKC Immunoglobulin kappa constant

IPSP Plasma serine protease inhibitor

ITA5 Integrin-α5

ITA6 Integrin-α6

ITB5 Integrin-β5

ITIH1 Inter-alpha-trypsin inhibitor heavy chain H1

ITIH2 Inter-alpha-trypsin inhibitor heavy chain H2

ITIH4 Inter-alpha-trypsin inhibitor heavy chain H4

K1109 Uncharacterized protein KIAA1109

KAIN Kallistatin

KCRM Creatine kinase M-type

KLKB1 Plasma kallikrein

KNG1 Kininogen-1

KV106 Immunoglobulin kappa variable 1-6 O

KV127 Immunoglobulin kappa variable 1-27

KV320 Immunoglobulin kappa variable 3-20

KVD40 Immunoglobulin kappa variable 2D-40

LAC3 Ig lambda-3 chain C regions

LEG3 Galectin-3

LG3BP Galectin-3-binding protein

LPXN Leupaxin

LTBP2 Latent-transforming growth factor beta-binding protein 2

MA7D1 MAP7 domain-containing protein 1

MASP2 Mannan-binding lectin serine protease 2

MASP2 Mannan-binding lectin serine protease 2

MK01 Extracellular signal-regulated kinase MAPK 1

MXRA8 Matrix remodeling-associated protein 8

MYL3 Myosin light chain 3

MYLK Myosin light chain kinase

MYO5A Myosin-Va

MYO9B Myosin-IXb

PAIP1 Polyadenylate-binding protein-interacting protein 1

PAXI Paxillin

PCDGL Protocadherin gamma-C4

PCOC1 Procollagen C-endopeptidase enhancer 1

PF4V Platelet factor 4 variant

PGK1 Phosphoglycerate kinase 1

PI4KA Phosphatidylinositol 4-kinase alpha

PIGR Polymeric immunoglobulin receptor

PIP Prolactin-inducible protein

PKP1 Plakophilin-1

PLAK Junction plakoglobin

PLCB4 1-phosphatidylinositol 4,5-bisphosphate phosphodiesterase beta-4

PLCG1 1-phosphatidylinositol 4,5-bisphosphate phosphodiesterase gamma-1 O

PLEC Plectin

PLF4 Platelet factor 4

PLMN Plasminogen

PON1 Serum paraoxonase/arylesterase 1

PP1B Serine/threonine-protein phosphatase PP1-beta catalytic subunit

PRDX1 Peroxiredoxin-1

PRDX2 Peroxiredoxin-2

PRG4 Proteoglycan 4

PROC Vitamin K-dependent protein C

PROS Vitamin K-dependent protein S

PSA3 Proteasome subunit alpha type-3

PSA6 Proteasome subunit alpha type-6

PSA7 Proteasome subunit alpha type-7

PSME2 Proteasome activator complex subunit 2

PTN1 Tyrosine-protein phosphatase non-receptor type 11

RAB10 Ras-related protein Rab-10

RAB35 Ras-related protein Rab-35

RAB9A Ras-related protein Rab-9A

RALB Ras-related protein Ral-B

RALB Ras-related protein Ral-B

RHOG Rho-related GTP-binding protein RhoG

RS13 40S ribosomal protein S13

SAA1 Serum amyloid A-1 protein

SAA4 Serum amyloid A-4 protein

SAMP Serum amyloid P-component

SEPP1 Selenoprotein P

SODM Superoxide dismutase

SPB12 Serpin B12

SPB3 Serpin B3

ST38L Serine/threonine-protein kinase 38-like

STK24 Serine/threonine-protein kinase 24

TBA1B Tubulin alpha-1B chain

TES Testin

TGM1 Protein-glutamine gamma-glutamyltransferase K

TGM3 Protein-glutamine gamma-glutamyltransferase E

THRB Prothrombin

TITIN Titin

TRFE Serotransferrin

TRY1 Trypsin-1

TSK Tsukushin

UBB Polyubiquitin-B

UCRI Cytochrome b-c1 complex subunit Rieske

VASP Vasodilator-stimulated phosphoprotein

VIME Vimentin

VNN2 Vascular non-inflammatory molecule 2

VTDB Vitamin D-binding protein

VTNC Vitronectin

YKT6 Synaptobrevin homolog YKT6

ZA2G Zinc-alpha-2-glycoprotein

ZPI Protein Z-dependent protease inhibitor

V. LIST OF FIGURES

CHAPTER 1

CHAPTER 2

Figure 2.8. PANTHER diagram of the pathways associated with the proteins differentially adherent to MLT enriched coatings in comparison with 70M30T without MLT.

CHAPTER 3

Figure 3.1. Graphical abstract of the paper "Bioactive zinc-doped sol-gel coating modulates protein adsorption patterns and *in vitro* cell responses"

Figure 3.2. SEM microphotograph of SAE-Ti (a), MT (b), MT0.5Zn (c), MT1Zn (d) and MT1.5Zn (e). Scale bar, 10 μm.

Figure 3.3. ^{29}Si MAS-NMR (a) and FTIR (b) spectra of sol-gel networks MT, 0.5MTZn, MT1Zn, and MT1.5Zn.

Figure 3.4. The arithmetic average of roughness (Ra; a) and contact angle (WCA; b). Results are shown as mean ± SE. The asterisks ($p \leq 0.05$ (*) and $p \leq 0.001$ (***)) indicate the statistical significance of differences between the materials with and without Zn (MT).

Figure 3.5. Hydrolytic degradation (a) and Zn^{2+} release kinetics (b) for the MT sol-gels doped with $ZnCl_2$. Bars indicate standard errors.

Figure 3.6. MC3T3-E1 (a) cell proliferation after 1, 3, and 7 days and (b) ALP activity after 7 and 14 days. Results are shown as mean ± SE. The asterisks ($p \leq 0.05$ (*) and $p \leq 0.001$ (***)) indicate statistically significant differences between the materials with Zn and the coating without Zn (MT).

Figure 3.7. Gene expression of (a) ALP, (b) TGFβ, (c) iNOS, (d) RUNX2, (e) RANKL, and (f) RANK in MC3T3-E1 cells at 7 and 14 days of assay. Results are shown as mean ± SE. The asterisks ($p \leq 0.05$ (*), $p \leq 0.01$ (**), and $p \leq 0.001$ (***)) indicate statistically significant IL differences between the materials with Zn and the coating without Zn (MT). Data were normalized to blank wells (without any material) using the $2^{-\Delta\Delta Ct}$ method.

Figure 3.8. Gene expression of (a) TNFα, (b) IL-1β, (c) TGF-β, and (d) IL-4, and (e) TNF-α cytokine liberation in RAW264.7 cells at 2 and 4 days of assay. Results are shown as mean ± SE. The asterisks ($p \leq 0.05$ (*), $p \leq 0.01$ (**), and $p \leq 0.001$ (***)) indicate statistically significant differences between the materials with Zn and the coating without Zn (MT). Gene expression data were normalized to blank wells (without any material) using the $2^{-\Delta\Delta Ct}$ method.

Figure 3.9. PANTHER functional classification of proteins differentially adsorbed onto the Zn-containing coatings in comparison with the control material MT. Proteins with $p \leq 0.05$ and

a ratio higher than 1.5 in either direction (UP – increased and DOWN – reduced) were considered differentially adsorbed.

Supplementary figure 3.1. MC3T3-E1 cellular viability when exposed to the materials in study. A cellular viability below 70% indicates that the material is cytotoxic. Results are shown as mean ± SE.

CHAPTER 4

Figure 4.1. Graphical abstract of the paper "Characterization of magnesium doped sol-gel biomaterial for bone tissue regeneration: the effect of Mg ion in protein adsorption"

Figure 4.2. (a) FT-IR, (b) ^{29}Si-NMR and (c) XRD spectra of the studied sol-gel networks.

Figure 4.3. SEM microphotographs of (a) Ti, (b) MT, (c) MT0.5Mg, (d) MT1Mg, (e) MT1.5Mg and (f) enlarged areas of MT1Mg and MT1.5Mg coatings. Scale bars: (a-e) 10 and (f) 1 µm. Roughness Ra (g) and contact angle (WCA; h) are also displayed. Results are shown as means ± SE. The asterisks ($p \leq 0.05$ (*) and $p \leq 0.001$ (***)) indicate significant differences between MT and Mg-doped MT.

Figure 4.4. Release kinetics of Mg^{2+} ions (a) and hydrolytic degradation (b) of the sol-gel coatings enriched with $MgCl_2$. Bars indicate standard errors.

Figure 4.5. Fluorescent confocal images of cytoskeleton arrangement of MC3T3-E1 on (a) Ti, (b) MT, (c) MT0.5Mg, (d) MT1Mg and (e) MT1.5Mg and (f) area of the cells adhered to the materials (f). Actin filaments were stained with phalloidin (green), and nuclei were stained with DAPI (blue). Scale bar: 10 µm. ALP activity (g) of MC3T3-E1 cells at 7 and 14 days. Results are shown as means ± SE. The asterisks ($p \leq 0.05$ (*), $p \leq 0.01$ (**), and $p \leq 0.001$ (***)) indicate statistically significant differences between MT and Mg-doped MT.

Figure 4.6. ELISA results for (a) TGF-β and (b) TNF-α for RAW264.7 cultures at 2 and 4 days. Data are shown as means ± SE. The asterisks ($p \leq 0.05$ (*) and $p \leq 0.001$ (***)) indicate statistically significant differences between MT and Mg-doped MT.

Figure 4.7. Gene expression of (a) alkaline phosphatase (ALP), (b) transforming growth factor (TGF-β), (c) osterix (OSX), (d) runt-related transcription factor 2 (RUNX2), (e) α5-integrin (ITGA5), and (f) β1-integrin (ITGB1) in MC3T3-E1 cultures at 7 and 14 days. Gene expression was normalized to blank wells (without any material) using the $2^{-\Delta\Delta Ct}$ method. Results are shown as means ± SE. The asterisks ($p \leq 0.05$ (*), $p \leq 0.01$ (**), and $p \leq 0.001$ (***)) indicate statistically significant differences between MT and Mg-doped MT.

Figure 4.8. Gene expression of (a) interleukin (IL)-6, (b) tumor necrosis factor (TNF)-α, (c) transforming growth factor (TGF)-β, and (d) IL-4 in RAW264.7 macrophages after 2 and 4 days of culture. Gene expression was normalized to blank wells (without any material) using the $2^{-\Delta\Delta Ct}$ method. Results are shown as means ± SE. The asterisks ($p \leq 0.05$ (*), $p \leq 0.01$ (**), and $p \leq 0.001$ (***)) indicate statistically significant differences between MT and Mg-doped MT.

Figure 4.9. PANTHER diagram of biological functions and pathways associated with the proteins differentially adhering to Mg-enriched coatings in comparison with MT (without Mg).

Supplementary Figure 4.1. Cross-cut test results (a) and thickness measurements (b). Results are shown as means ± SE.

CHAPTER 5

Figure 5.1. Graphical abstract of the paper "The effect of calcium-magnesium mixtures in sol-gel coatings for bone tissue regeneration"

Figure 5.2. (a) ^{29}Si-NMR, (b) FT-IR spectra, and (c) XRD of the obtained sol-gel materials.

Figure 5.3. Contact angle (WCA; a) and roughness (Ra; b) results. Data are shown as mean ± SD. The asterisk (*) indicates differences between MT and the ion doped-coatings and the rhombus (◆) indicates differences between the Ca-doped and the CaMg-doped materials. SEM microphotograph of (c) Ti, (d) MT, (e) Ca, (f) Ca0.5Mg, (g) Ca1Mg, (h) Ca1.5Mg, and (e'-h') extended images. Scale bars: (c-h) 10 and (e'-h') 1 µm.

Figure 5.4. Hydrolytic degradation (a); Mg^{2+} (b) and Ca^{2+} (c) ion kinetic release for developed the sol-gel coatings. Data are shown as mean ± SE.

Figure 5.5. Fluorescent confocal images of cytoskeleton arrangement of MC3T3-E1 on (a) Ti, (b) MT, (c) Ca, (d) Ca0.5Mg, (e) Ca1Mg, (f) Ca1.5Mg, and (g) area of the cells adhered to the materials. Actin was stained with phalloidin (green) and nuclei were stained with DAPI (blue). Scale bar: 10 µm. ALP activity (h) in MC3T3-E1 at 7 and 14 days. Results are shown as mean ± SE. The asterisk (*) indicates differences between MT and the ion doped-coatings and the rhombus (◆) indicates differences between the Ca-doped and the CaMg-doped materials.

Figure 5.6. Cytokine secretion quantification through ELISA of (a) TGF-β and (b) TNF-α in RAW264.7 at 2 and 4 days. Results are shown as mean ± SE. The asterisk (*) indicates differences between MT and the ion doped-coatings and the rhombus (◆) indicates differences between the Ca-doped and the CaMg-doped materials.

Figure 5.7. Relative gene expression of (a) alkaline phosphatase (ALP), (b) transcription factor SP7/osterix, (c) transforming growth factor (TGF)-β and (d) runt-related transcription factor 2 (RUNX2) on MC3T3-E1 at 7 and 14 days. Data were normalized in relation to blank (wells without any material) with the $2^{-\Delta\Delta Ct}$ method. Results are shown as mean ± SE. The asterisk (*) indicates differences between MT and the ion doped-coatings and the rhombus (◆) indicates differences between the Ca-doped and the CaMg-doped materials.

Figure 5.8. Relative gene expression of (a) tumor necrosis factor (TNF)-α, (b) interleukin (IL) 1-β**,** (c) transforming growth factor (TGF)-β and (d) IL-10 on RAW264.7 at 2 and 4 days. Data were normalized in relation to blank (wells without any material) with the $2^{-\Delta\Delta Ct}$ method. Results are shown as mean ± SE. The asterisk (*) indicates differences between MT and the ion doped-coatings and the rhombus (◆) indicates differences between the Ca-doped and the CaMg-doped materials.

Figure 5.9. Normalized protein abundance of proteins associated with coagulation - (a) histidine-rich glycoprotein (HRG), (b) serpin B12 (SBP12), (c) plasminogen (PLMN), (d) hemoglobin subunit alpha, (e) coagulation factor XII (FA12) –, immune responses - (f) C-reactive protein (CRP)**,** (g) complement component C8 beta chain (CO8B), bleomycin hydrolase (BLMH) -, and cell adhesion – (i) junction plakoglobin (PLAK). Results are shown as mean ± SE. The asterisk (*) indicates differences between MT and the ion doped-coatings and the rhombus (◆) indicates differences between the Ca-doped and the CaMg-doped materials.

CHAPTER 6

Figure 6.1. Graphical abstract of the paper "The complexity of the Mg-biomaterials effects on the entire osteoblastic machinery: a proteomic study"

Figure 6.2. Biological processes of HOb cells regulated by MT1.5Mg at 1, 3, and 7 days.

Figure 6.3. Protein classes associated with the proteins differentially expressed by Hob cells seeded onto MT1.5Mg at 1, 3, and 7 days.

Figure 6.4. Heat map of pathways associated with (A) osteogenesis, (B) cell-matrix and focal adhesion, and (C) oxidative stress expressed by HOb seeded onto MT1.5Mg at 1, 3, and 7 days. Pathways were considered significantly regulated when -log(*p*-value) > 1.3.

Figure 6.5. Network analysis from IPA® for associations among molecules associated with collagen(s), TFGB1, IGF1, and binding of osteoblasts of the proteins obtained from HOb seeded on MT1.5Mg after 1 day of assay. Upregulated proteins are found in red, while downregulated

are found in green. Orange lines indicate *predicted activation*; blue lines indicate *predicted inhibition*; yellow lines indicate *findings inconsistent with state of downstream molecule*; grey lines indicate *effect not predicted*.

Figure 6.6. RICTOR predicted activity from IPA® on HOb seeded on MT1.5Mg at 1 day. Molecules with *predicted activation* are found in orange, while downregulated proteins are found in green. Blue lines indicate *predicted inhibition*; yellow lines indicate *findings inconsistent with state of downstream molecule*; grey lines indicate *effect not predicted*.

VI. LIST OF TABLES

Supplementary Table 4.2. Progenesis comparative analysis of proteins differentially adsorbed onto $MgCl_2$ enriched coatings (MT0.5Mg, MT1Mg, and MT1.5Mg) in respect to MT.

CHAPTER 5

Table 5.1. Nomenclature of the designed sol-gel materials with the respective amounts of $CaCl_2$ and $MgCl_2$. The mass percentages were calculated concerning the total amount of alkoxysilane.

Table 5.2. Summary of the proteins differentially adsorbed onto the sol-gel materials doped with Ca and CaMg associated with relevant biological processes (immune response, cell adhesion, tissue regeneration, and coagulation).

Supplementary Table 5.1. Targets studied in MC3T3-E1 osteoblasts and RAW264.7 macrophages.

Supplementary Table 5.2. Progenesis comparative analysis between the proteins identified onto the CaMg materials with respect to the control treatment without ions. Proteins with ANOVA $p < 0.05$ (yellow) and a ratio higher than 1.5 in either direction was considered as significantly different. Proteins with increased affinity to coatings doped with the ion mixtures in comparison to MT are marked in red, while those with reduced affinity appear in green.

Supplementary Table 5.3. Progenesis comparative analysis between the proteins identified onto the CaMg materials with respect to the Ca coatings. Proteins with ANOVA $p < 0.05$ (yellow) and a ratio higher than 1.5 in either direction was considered as significantly different. Proteins with increased affinity to coatings doped with CaMg in comparison to Ca are marked in red, while those with reduced affinity appear in green.

CHAPTER 6

Table 6.1. Upstream regulators determined by IPA® on MT1.5Mg. The molecules were considered significantly regulated when -log(*p*-value) > 1.3.

Table 6.2. Proteins differentially expressed on MT1.5Mg with functions in osteogenesis, cell-matrix and focal adhesion, and oxidative stress. Proteins with $p \leq 0.05$ and a ratio higher than 1.5 in either direction (UP: increased and DOWN: reduced) were considered significant.

Supplementary table 6.1. Progenesis comparative analysis between the proteins identified onto MT1.5Mg with respect to MT at 1 day *in vitro*. Proteins were considered differentially expressed when the ratio was higher than 1.5 in either direction and *p* value < 0.05. Proteins overexpressed in MT1.5Mg are marked in red, while those under expressed are marked in green.

Supplementary table 6.2. Progenesis comparative analysis between the proteins identified onto MT1.5Mg with respect to MT at 3 days *in vitro*. Proteins were considered differentially expressed when the ratio was higher than 1.5 in either direction and *p* value < 0.05. Proteins overexpressed in MT1.5Mg are marked in red, while those under expressed are marked in green.

Supplementary table 6.3. Progenesis comparative analysis between the proteins identified onto MT1.5Mg with respect to MT at 7 days *in vitro*. Proteins were considered differentially expressed when the ratio was higher than 1.5 in either direction and *p* value < 0.05. Proteins overexpressed in MT1.5Mg are marked in red, while those under expressed are marked in green.

Supplementary table 6.4. Upstream regulators determined by IPA® on MT1.5Mg. The molecules were considered significantly regulated when -log(*p*-value) > 1.3.